# Baryonic processes in the large scale structuring of the Universe

Jean-Baptiste Durrive

NNT: 2016 SACLS 346

# Thèse de doctorat
de
l'Université Paris-Saclay
préparée à
l'Université Paris-Sud

au sein de l'Institut d'Astrophysique Spatiale, Orsay

Ecole doctorale N° 576
(Particules, Hadrons, Énergie et Noyau: Instrumentation, Image, Cosmos et Simulations)

Spécialité de doctorat: Astroparticules et Cosmologie

par

**M. DURRIVE Jean-Baptiste**

## Baryonic processes in the large scale structuring of the Universe

Thèse présentée et soutenue à Orsay, le 13 Octobre 2016.

Composition du Jury :

| | | |
|---|---|---|
| Dr. Boulanger François | Institut d'Astrophysique Spatiale | Président |
| Pr. Combes Françoise | Observatoire de Paris LERMA & Collège de France | Rapportrice |
| Dr. Ferrière Katia | Institut de Recherche en Astrophysique et Planétologie | Rapportrice |
| Pr. Joyce Michael | Laboratoire de Physique Nucléaire et de Hautes Energies | Examinateur |
| Pr. Zaroubi Saleem | Kapteyn Astronomical Institute<br>Faculty of Mathematics & Natural Sciences | Examinateur |
| Dr. Langer Mathieu | Institut d'Astrophysique Spatiale | Directeur de thèse |

# Remerciements

Rédiger cette section est assez frustrant, parce qu'il est impossible d'être exhaustif, et donc nécessairement je vais être injustement incomplet. J'ai hésité à me lancer dans la rédaction d'un long texte pour essayer de rendre 'hommage' à un maximum de personnes, mais finalement je me contenterai de rester très général, sans liste précise de noms, pour éviter de donner une impression de hierarchisation ou de faire des omissions qui ne seraient pas représentatives mais simplement dues au fait que je ne peux pas me rappeler de tout précisément à l'heure où j'écris ces lignes. J'ai eu l'occasion de rencontrer beaucoup de gens ces dernières années. J'ai eu énormément de plaisir à interagir avec eux, et je suis sincèrement très reconnaissant du temps qu'ils m'ont consacré, alors que ça n'était pas toujours évident. Je mise sur le fait que les gens concernés se reconnaîtront ici.

Un mot plus précis tout de même sur mon laboratoire d'accueil. En plus des trois années à plein temps en tant que doctorant, j'ai en fait cotoyé l'IAS dès ma L3, donc presque six années au final. Je tenais à souligner combien il est agréable d'y travailler, car il y règne un esprit d'équipe, un respect entre tous les membres du laboratoire (scientifiques ou non), et un subtil compromis entre travail sérieux et ambiance détendue. Ces lignes peuvent sembler un peu vagues, mais, je vous l'assure, il y a en dessous de ces mots un très grand nombre d'anecdotes qui justifient leur présence ici. Pour tout de même citer un exemple concret qui me semble très représentatif, je mentionnerai juste les réunions appelées 'Welcome Back' qui ont été mises en place lors de mes années de thèse. Nous nous réunissions une fois par semaine, thésards, stagiaires, post-docs et permanents, pour discuter de sciences, au sens large, et de façon informelle autour d'un café (ou de choses plus inhabituelles, souvent asiatiques). Mais surtout, il n'y avait pas d'objectif précis à atteindre, il ne s'agissait pas d'être productif ou innovant. L'idée était d'être véritablement guidé par la curiosité, 'tout simplement'. Cela paraît en effet 'simple', mais pourtant il me semble que rares sont ceux qui prennent effectivement le temps de faire ce genre de choses. Nous sommes trop souvent aveuglés par l'urgence des dates limites, par les objectifs à court termes, et divers types de pressions nous emportent dans des directions que nous ne souhaitions pas emprunter initialement. Tout cela nous fait oublier les raisons pour lesquelles nous travaillons avec tant d'efforts, voire de sacrifices. Ces pauses étaient l'occasion de se rappeler collectivement nos motivations fondamentales, celles qui nous poussent à nous engager dans la recherche. Aussi, nous avons souvent trop tendance à avoir peur de faire des erreurs, à essayer de dissimuler nos lacunes et ne pas poser de questions 'naïves'. Or ces réunions étaient l'occasion de dépasser ces bloquages et de nous (ré)apprendre à raisonner sereinement. Je remercie en particulier Mathieu et Julien, qui ont vraiment toujours pris le temps d'y participer, de chercher à démystifier certains domaines obscurs à nous autres 'petits jeunes', d'avoir toujours cherché à répondre à nos questions tout en ayant la modestie d'admettre leur ignorance sur certains aspects, de nous encourager à en poser d'autres et d'insister pour que nous prenions le temps de faire cette pause. Je tenais à souligner tout cela, car je pense qu'une telle ambiance n'est pas une chose acquise définitivement, mais qui doit se maintenir activement, et cela nécessite d'avoir conscience de son importance. J'invite et souhaite donc que tout le monde continue de faire en sorte que cela perdure, afin que les générations suivantes puissent profiter d'expériences similaires à la mienne.

Je remercie aussi particulièrement Marty et Mathieu pour nos projets scientifiques annexes à nos thèses respectives et pour nos débats de sociétés (réelles et imaginaires). Merci aussi au jury pour sa participation et pour avoir lu aussi attentivement le manuscrit et nourrit des discussions aussi constructives pendant, et même bien après, la soutenance. Et bien sûr je remercie ma famille pour tout son soutient, et en particulier pour avoir développé ma curiosité, ce qui rend libre, heureux et donne une raison d'être.

# Contents

# Chapter 1

# Introduction

The dynamics of the Universe is vertiginous, thanks to the ranges of length and time scales involved. This fact is pleasing in itself, but the sky becomes even more attractive when probed in the light of physics. Indeed, it is intellectually very satisfying, and methodologically very convenient, that the governing equations are *scale independent* (see for instance Goedbloed & Poedts, 2004). This property reduces an a priori Herculean task to a humanly tractable one, by reducing the analysis to essentially a dozen of dimensionless parameters, namely Mach, Reynolds, Knudsen, etc., numbers. The richness of the overall dynamics then simply corresponds to the various possible regimes. Scale invariance is also the essence of analogies. Many a priori unrelated processes and phenomena turn out to have surprisingly similar intrinsic behaviours, and topics from a priori completely disconnected fields may turn out to have so much in common that comparison with one another brings precious insight. Finally, together with orders of magnitude which highlight the gist of complex phenomena, this fact, in some sense, brings closer to us these unreachable objects we are interested in, by returning their dynamics back to our intuition.

In the present chapter I will introduce the context which my work falls into, and present the two problematics I will focus on: the origin of cosmological magnetic fields in part I, and gravitational fragmentation of stratified structures in part II. The next chapter will also be introductory, but a bit more technical. There, I will present the formal tools I will use in order to address those two physics questions.

## 1.1 Global cosmological model: some elements

The current Standard Model of Cosmology is called the ΛCDM model and is illustrated in figure 1.1. For detailed introductions to it see e.g. Peebles (1993), Dodelson (2003) or Bernardeau (2007). It is based on the theory of General Relativity, i.e. the fundamental equations governing the dynamics are the Einstein Equations, linking the geometry of space-time (its metric) to its content (energy-momentum tensor). Furthermore, measurements of the Cosmic Microwave Background (see for instance Planck Collaboration, 2015a, for an overview of some of the latest results of the Planck mission) indicate that the Universe was highly isotropic and homogeneous at its early stages of evolution, and galaxy surveys show that it is still the case statistically speaking on its largest scales, as discussed in figure 1.2. Guided by these observations, the Standard Model is based on the Cosmological Principle which consists in assuming that the Universe is isotropic and homogeneous. Consequently, the relevant metric to describe the geometry of space-time at cosmological scales is the simplest (non trivial) one, namely the Friedmann-Lemaître-Roberston-Walker metric. This metric contains only one degree of freedom, the scale factor $a$, which provides the model with expansion and contraction, as it appears in the link $\vec{r}(t) = a(t)\vec{x}$ between physical $\vec{r}$ and comoving coordinates $\vec{x}$. The other direct consequence of this principle is that the energy-momentum tensor describing the matter content of the Universe in the Einstein Equations has the form $T^{\mu}{}_{\nu} = \mathrm{diag}(-\rho, P, P, P)$, where $\rho$ is the energy density and $P$ the pressure. In this framework, the Einstein equations reduce to the so-called Friedmann equations,

$$\begin{cases} H^2 = \dfrac{8\pi G}{3}\rho + \frac{\Lambda}{3} \\ \dot{\rho} + 3H(\rho + P) = 0, \end{cases} \tag{1.1}$$

where $H \equiv \frac{\dot{a}}{a}$ is the Hubble parameter, $G$ the gravitational constant and $\Lambda$ the cosmological constant. Note that here natural units are used, such that $c = 1$, and the global spatial curvature is neglected, as its measured value is very close to, and still compatible with, zero (e.g. Planck Collaboration, 2015b). The fluids considered in the model are: (i) Radiation, a term which in fact refers to all relativistic material, essentially photons and light neutrinos, (ii) Dark Energy, a fluid required in the model to account for the observed acceleration of the expansion and which corresponds to the cosmological constant $\Lambda$, (iii) and matter, itself composed of two parts, namely the usual matter we experience daily, called baryonic in reference to the baryons of the Standard Model of Particle Physics which represent the bulk of inertia of ordinary matter, and another type of matter baptized Dark Matter which turns out to be five times more abundant than baryonic matter

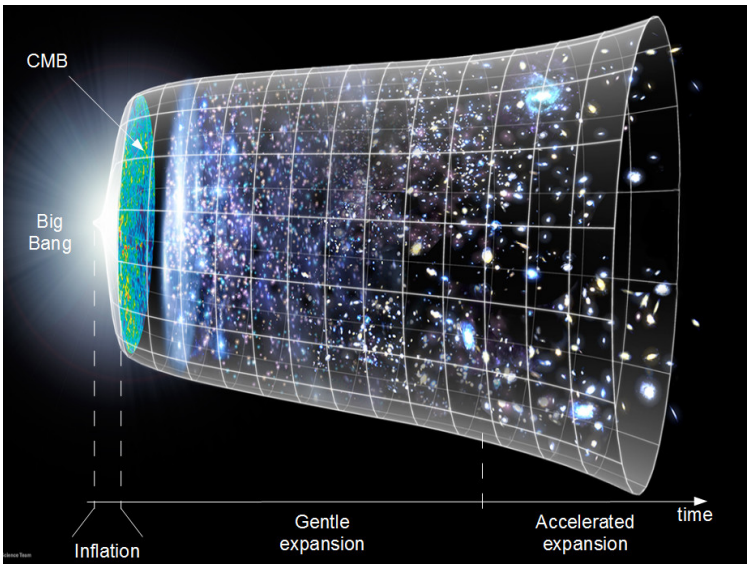


Figure 1.1: Artist view of the history of the Universe, with emphasis on the global expansion. Initially in a hot dense plasma state, the Universe became neutral after Recombination, an event that essentially coincided with the release of the Cosmic Microwave Background (CMB). It reached an ionized state again as the first stars and galaxies were born. This transition is called Cosmic Reionization. It then evolved by gravitational instability to become the structured Universe we know today. Adapted from NASA/WMAP Science Team.

(e.g. Planck Collaboration, 2015b). It is called dark because it does not interact electromagnetically and is thus invisible. The numerous observations requiring its existence are based on its gravitational effects (gravitational lensing, rotation curves of galaxies, structure formation, etc.). Also, in the Cosmological Standard Model, it is referred to as cold (hence the C in ΛCDM) in the sense that it is non-relativistic.

Each of the fluids can be characterized by its equation of state $P = w\rho$, with a corresponding value of $w$: $w = 1/3$ for radiation, $w = -1$ for the Cosmological Constant (i.e. a negative pressure fluid...), and $w = 0$ for cold matter, i.e. a pressureless fluid. Note however that this pressureless approximation for Dark Matter is valid only as long as Dark Matter particles are free-streaming, i.e. that flows of such particles do not cross each other significantly, which is the case on the largest cosmological length and time scales. Indeed, an important property of Dark Matter is that it is collisionless, so that its analysis in full generality is quite complicated because effective fluid approaches are scarcely appropriate and kinetic theory is in principle required. Numerically, it is in general treated through $N$-body simulations (e.g. Springel et al., 2005) but there are attempts considering collisionless hydrodynamics (e.g. Mitchell et al., 2013). For treaties on collisionless dynamics see e.g. Binney & Tremaine (2008) and Fridman & Polyachenko (1984a,b).

This equation of state is an additional information which closes the system of equations (1.1), thus fully constraining $a(t)$, i.e. we can obtain the *expansion history* of the Universe as a function of its constituents by solving this system. But rather than discussing precisely the solutions, let us instead reformulate the equations as follows. The first Friedmann equation above may be written as an energy budget

$$\sum_i \Omega_i = 1 \tag{1.2}$$

where the density parameters are defined as $\Omega_i \equiv \rho_i/\rho_c$ with $\rho_i(z)$ the density of the fluid $i$ and the density $\rho_c(z) \equiv 3H^2/(8\pi G)$, called the critical density, is taken as reference at each redshift. The second equation in (1.1) shows that fluids of different nature are not subject to the expansion in the same way since the equation for the evolution of $\rho$ depends on $P$, and thus on the equation of state, and on the Hubble parameter, i.e. on the expansion. The outcome is that the energy densities of the various fluids in the Universe vary differently with redshift i.e. with time, since redshift is used as a measure of time in Cosmology. Therefore, their relative proportions vary as the Universe evolves, with $\Omega_{\rm radiation} \propto (1+z)^4$, $\Omega_{\rm matter} \propto (1+z)^3$ and $\Omega_\Lambda$ constant. It then turns out that radiation first dominated the energy content (at redshifts above roughly 3600), then matter dominated ($0.4 < z < 3600$), and since $z = 0.4$ the Universe has been in a Dark Energy dominated era.

Finally, note that our need to incorporate the Dark Matter and Dark Energy components in the Standard Model may in fact be, at least in part, the manifestation of our current misunderstanding of the fundamental laws of nature at cosmological scales. The Standard Model assumes that General Relativity is the relevant law for gravity, but many alternative theories of gravity are under investigation. For more information on extensions of Standard Cosmology, see e.g. Peter & Uzan (2013). But while the fundamental nature of some

of its constituents remains unclear to this day, it should be stressed that the Standard Model manages to account for an impressive amount of a priori independent observations with astonishingly few parameters.

## 1.2 Cosmological chronology: some key moments

The above model is also relevant to a structured Universe, provided we consider large enough scales at which the Universe is statistically homogeneous and isotropic (e.g. Hogg et al., 2005; Alonso et al., 2015). But when considering scales below roughly a hundred megaparsec and after Recombination, this model only provides us with a global dynamical framework in which matter structures itself gravitationally. Let us review briefly chronologically some of the milestones of the processes that occurred during its evolution, focusing on what will be useful for the present manuscript.

**Primordial Universe** At its very beginning, the Universe was in the state of an extremely hot and dense plasma. It underwent a fulgurant expansion called Inflation. Inflation was first introduced in order to try and understand how the Universe could be as homogeneous and isotropic as observed today: How can extremely distant places in the Universe be causally connected (hence homogeneity) if not even light had the time to travel such distances? Inflation is a mechanism which solves this so-called horizon problem, as well as two additional ones, the flatness and monopole problems. Inflation lasted typically $10^{-33}$ seconds, after which the expansion gentled, as indicated in figure 1.1.

Photons were coupled to matter through Thomson scattering as long as the interaction rate was higher than the expansion rate given by the Hubble parameter $H$. But as the Universe expanded, this condition ceased to be satisfied, and photons decoupled from matter: their mean free path increased greatly, becoming larger than the size of the Universe at that time. Since then, they have been essentially free-streaming, and we now detect them, almost intact, showing us an image of the early Universe: this relic radiation is called the Cosmic Microwave Background (CMB). A bit later, as the energy of photons decreased due to expansion, the reaction $H + \gamma \leftrightarrow p + e^-$ which prevented bound systems of protons with electrons to form, ceased to be at equilibrium. The Universe became essentially neutral. This period of transition, called Recombination, occurred when the Universe was roughly 380 000 years old (see Planck Collaboration, 2015b, for the latest measurements of the Recombination time).

This key transition constitutes a convenient milestone for categorizing studies in Cosmology, into those dedicated to the Primordial Universe, and those dedicated to its subsequent evolution, namely the Post-Recombination Universe. The present manuscript belongs to the latter category, so that the state of the Universe at Recombination will be regarded as our *initial condition*.

**Emergence of the cosmic web** Hence, at Recombination, the Universe was starless. It was composed of Dark Matter and primordial gas, essentially Hydrogen (76%) and Helium (24%). Because during the Primordial Universe era baryons were tightly coupled to photons, their distribution remained very homogeneous, so that at Recombination their typical density fluctuations were only of $\delta\rho/\rho \sim 10^{-5}$ (rms). Dark Matter however, which decoupled much earlier, had already started evolving under its own gravity and was thus already somewhat inhomogeneously distributed. Since Dark Matter dominates the matter content of the Universe, the primordial gas fell into the Dark Matter gravitational potential wells already formed at these early times (see Tseliakhovich & Hirata, 2010; Fialkov, 2014, for an account of the effects of the relative velocity between Dark Matter and baryons).

Let us just recall the formulation of the well-known Jeans instability criterion in the simplest case of linear inhomogeneities in an otherwise homogeneous, static background (for details, see for instance Lequeux et al., 2005). Combining the linearized equations of local mass and momentum conservation with the linearized Poisson equation, and developing the perturbations onto plane-waves, it is straightforward (see also section 7.1.1) to show that the dispersion relation relating the angular frequency $\omega$ to the scales $k$ is

$$\omega^2 = c_a^2 k^2 - 4\pi G \rho_{\text{mean}}, \tag{1.3}$$

where $\rho_{\text{mean}}$ is the mean density and $c_a$ the speed of sound. The Jeans criterion for instability is $\omega^2 < 0$, meaning that gravitational collapse overcomes the counteracting effect of pressure gradients, in which case the density of initially overdense regions grows exponentially. In an expanding background, the formal expression of the dispersion relation is left unchanged, except that $k$ must be replaced by $k/a(t)$ where $k$ this time is the comoving wave-number and $a(t)$ the time dependent scale factor. As a result, the initial growth of overdense regions is slower than exponential, as the expansion plays essentially the role of a time dependent damping term (see for instance Peacock, 1999). Consider now an initial, ellipsoidal overdensity so that we may distinguish three principal axes. Without expansion, it can be shown that, due to gravitational collapse, such an overdensity contracts first along the shortest axis, then along the second shortest and finally along the longest. From this picture, we may understand that the overdensity first becomes a sheet (collapse in the first direction), then a filament (second direction) and then a node or halo (third collapse). In an expanding background, this series of events is modified only insofar as each given direction first decouples

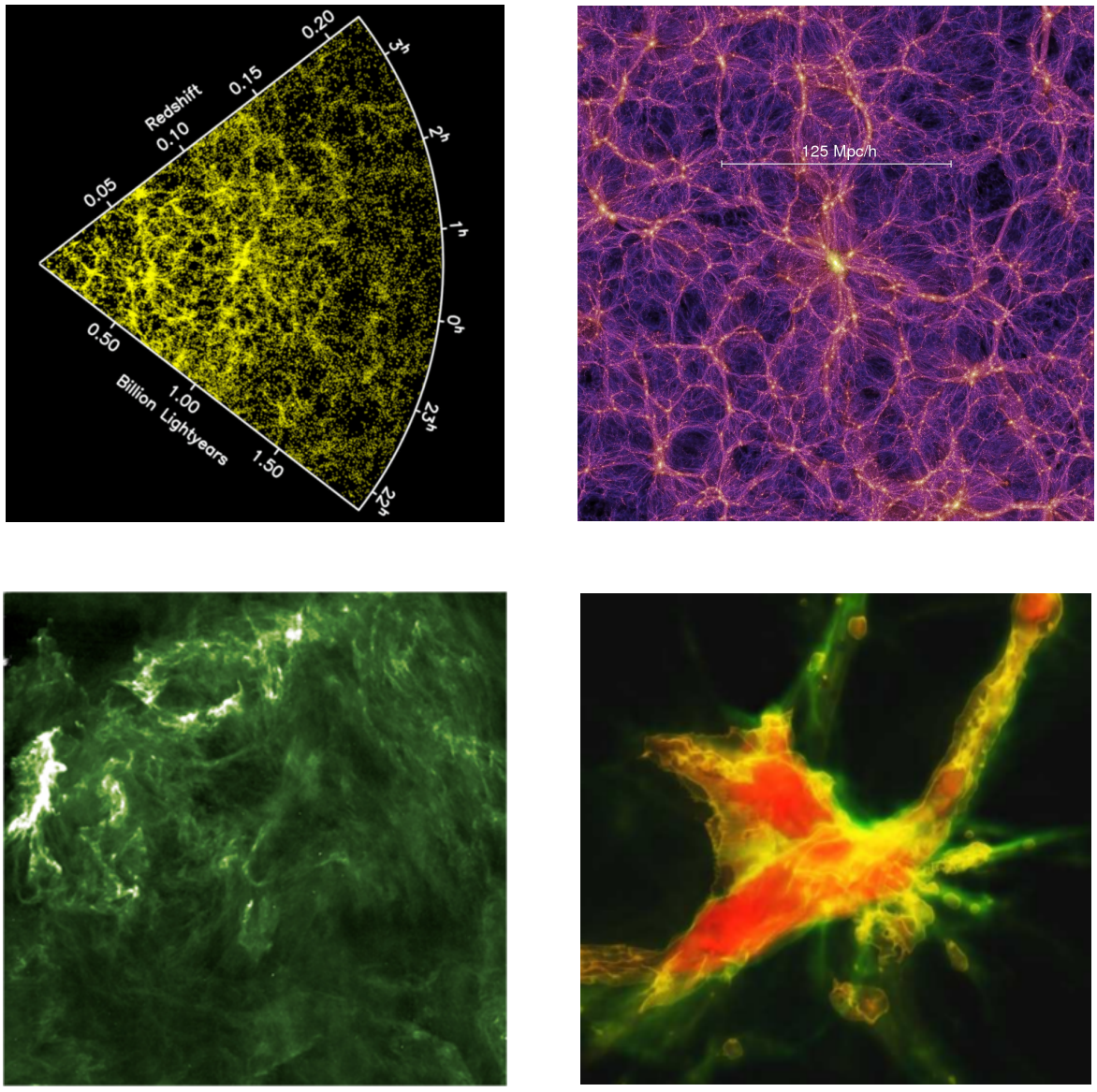


Figure 1.2: Both observations and theoretical arguments indicate that (self-gravitating) filamentary and planar structures are present at all scales and at all times in the Universe. Top left: (*Observations*) Galaxy surveys (here the 2dF Galaxy Redshift Survey – Percival et al., 2001; Cole et al., 2005) clearly exhibit a filamentary distribution of galaxies, though at the largest scales, this distribution may be considered as homogeneous and isotropic statistically speaking (e.g. Hogg et al., 2005; Alonso et al., 2015). Top right: (*Simulations*) The cosmic web: At cosmological scales (a few hundreds of Mpc are shown here), matter in the Universe is distributed in a filamentary way (shown in this *Millenium* simulation is Dark Matter only – Springel et al., 2005). Bottom left: (*Observations*) Filamentary structures are ubiquitous in the ISM (here a *Herschel*-SPIRE 250 $\mu$m map of the Polaris flare – Miville-Deschênes et al., 2010). Bottom right: (*Simulations*) A forming galaxy ten billion years ago: a filamentary structure appears also at those scales (a hundred of kpc are shown here) and those epochs (from Greif et al., 2008). Note that magnetic fields most probably played an important role at those scales.

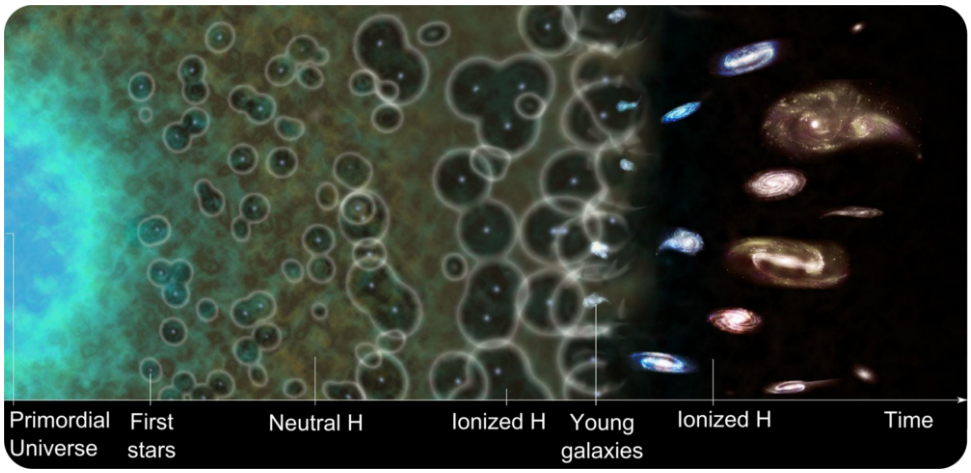


Figure 1.3: Another sketch of the history of the Universe (crédit: NASA/CXC/M. Weiss), with emphasis on the evolution of baryons during the Epoch of Reionization. Once large enough non-linear halos are assembled by gravitational collapse, first stars and galaxies begin to form, ionizing progressively back the intergalactic gas, creating bubbles of HII (cf. Loeb & Furlanetto, 2013). Those cosmological Strömgren spheres will play a major role in the magnetogenesis mechanism detailed in part I.

from the global expansion, an event called 'turn-around' (cf. Sheth et al., 2001). The interested reader may consult Angrick & Bartelmann (2010), and references therein, who bridge the linear onset of tri-axial Jeans instability with the later non-linear, virialized stages of resulting sheets, filaments and halos.

But where do initial density perturbations come from? In the paradigm prevailing today, they originate in quantum fluctuations of the inflaton field that are stretched to macroscopic scales during inflation (e.g. Lyth & Liddle, 2009). Indeed, as confirmed by the most recent measurements of the CMB anisotropies, we may understand that inflation seeds the universe with perturbations at all scales, with a nearly scale-invariant power-spectrum (e.g. Planck Collaboration, 2015b). With such initial conditions, it has been understood that structure formation proceeds in a hierachical way, essentially bottom-up (i.e. small structures collapse first, see Mo et al., 2010, for instance). Thus, combining the bottom-up hierarchy with the sequential triaxial collapse of anisotropic fluctuations, it is natural to expect a coexistence of cosmic sheets, filaments and halos, as already demonstrated by Zeldovich (1970, see also Shen et al., 2006, for theoretical aspects of the statistics of these structures). Thus, in essence, the outcome of these processes is that gravitational collapse naturally produces a filamentary topology, which accounts for the overall topology of the cosmic web on the largest scales, revealed both by numerical simulations and observations (e.g. Klypin & Shandarin, 1983; Van de Weygaert & Bond, 2008; Klar & Mücket, 2010; Eckert et al., 2015; Gheller et al., 2015). Note that sheets and filaments of matter appear in many other Astrophysical contexts too. In the interstellar medium (ISM) of galaxies for instance (cf. figure 1.2), the sheet-like and filamentary structure of giant molecular clouds has been known for a long time. There, it actually results from the conspiring action of gravity, supernova explosions, thermal instability, cloud-cloud collisions, turbulence and magnetic fields (e.g. Schneider & Elmegreen, 1979; Bally et al., 1987; Mizuno et al., 1995; Hartmann, 2002; Myers, 2009; Pudritz & Kevlahan, 2013; André et al., 2014; André, 2015; Federrath, 2016; Kalberla et al., 2016). Finally, in the cosmological context, it is important to keep in mind that sheets, filaments and nodes exist not only in the present day cosmic web, but are already present also at high redshifts, from protogalactic to cosmological scales (see figures 1.2 and 1.4), while the Universe is only leaving its Dark Ages during Reionization.

**The Epoch of Reionization** As the first collapsed objects became dense enough to initiate nuclear reactions in their core, the first stars, called Population III, were born. The era during which the Universe did not contain any luminous sources, called the *Dark Ages*, lasted roughly 100 Myrs, and the epoch at which the first stars switched-on is prettily called *Cosmic Dawn*. Population III stars were chemically pristine since they formed from a chemically poor gas, and are even called 'metal-free' [1]. They were most likely very massive (hundreds of solar masses, see e.g. Bromm, 2013) and very short lived (lifetimes of the order of one megayear). The second generation of stars formed from a gas that had been enriched by the chemical elements left over by the explosive death of the first generation of stars (see for instance Schneider, 2012). The properties of these stars, such as their lifetimes and spectra, are thus different so that they were baptized Population II stars. Assemblies of such stars are often called protogalaxies, primordial galaxies or first galaxies. In this hierarchical scenario, the most massive Dark Matter halos formed later, so that we expect the most luminous sources, namely quasars, resulting from the formation of super massive black holes to have formed only late in this chronology. These sources (Population III stars, protogalaxies and quasars) emitted photons

[1] The terminology 'metal' in Astrophysics is used for all elements heavier than Helium

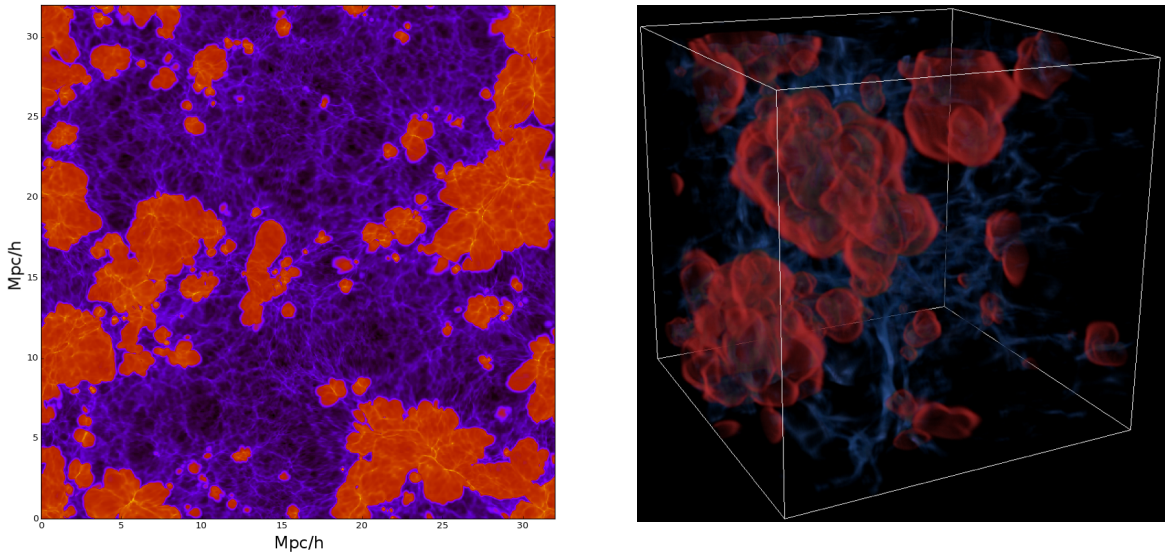


Figure 1.4: View of the Universe as the first galaxies formed (redshift $z = 11$), resulting from a cosmological simulation using the EMMA numerical code (Aubert et al., 2015). Left: Gas temperature distribution. Red areas are fully ionized gas at $10^4$ K, the Strömgren spheres, while the blue corresponds to neutral Hydrogen at 10 K in the IGM. Right: Three-dimensional view, with the same color coding. (Image credit: D. Aubert & N. Deparis, Observatoire de Strasbourg.)

of energy above the ionization threshold of Hydrogen and Helium, thus ionizing the neutral medium in their vicinity. The ionized region formed around an ionizing source is called a *Strömgren sphere*, or HII region. For details on their formation and evolution see e.g. Shu (1992) or Lequeux et al. (2005), and Furlanetto et al. (2004) for details specific to the cosmological context. Little by little, as the number of sources formed increased and the Strömgren spheres grew and percolated, the ionized fraction of the intergalactic medium (IGM) increased, until at some point the Universe became fully ionized. This transition from a neutral to an ionized state is called Cosmic Reionization because the Universe was in an ionized state for the second time. The period from Cosmic Dawn to Cosmic Reionization is called the *Epoch of Reionization* (EoR), and lasted typically 800 Myrs (see Planck Collaboration, 2016, for the latest contraints on the EoR deduced from CMB measurements). Figure 1.3 is an artist illustration of the aforementioned sequence of events, putting emphasis on the percolation of Strömgren spheres. The physics of Reionization is extremely rich and interesting, and for more details, the reader is invited to consult Loeb & Furlanetto (2013), or its digest, pocket version Loeb (2010). But for now, just to get a bit more realistic view of what these events were like at a given epoch, let us look at the results of some numerical simulations. Figure 1.4 corresponds to two snapshots from a cosmological simulation of the EoR using the EMMA code (Aubert et al., 2015). They show baryons in the Universe at redshift $z = 11$, i.e. it is a view of a slice of figure 1.3 at roughly 400 Myrs after the Big-Bang. Looking at figure 1.4, note two facts that will be of great importance for the works presented in this manuscript, notably chapter 3: (i) the so-called Strömgren spheres, in red in this figure, are not truly spherically symmetric, even before starting to overlap with neighboring HII regions, and (ii) the IGM, in blue in this figure, is not homogeneous, but very clumpy. Both properties will play a major role in part I of this manuscript.

## 1.3 Focus on two Problematics

The above section introduced the global cosmological context. Within its frame, we are now going to focus on two specific aspects.

**The Origin of Cosmological Magnetic Fields** The origin of cosmological magnetic fields is a major open question in Cosmology. Indeed, as we will see in a moment, not only do we know that galaxies and galaxy clusters possess significant magnetic fields, both at present and in the remote universe, but also recent high energy gamma ray observations suggest that a substantial fraction of the entire present day intergalactic space may be actually magnetized. Numerous mechanisms for generating such magnetic fields at cosmological scales have been proposed, operating mainly in the primordial Universe. However, post-recombination mechanisms based on well established physics exist too. Establishing the origin of cosmological magnetic fields is a major challenge for observational Astrophysics that will be tackled notably with the forthcoming Square Kilometre Array (see the chapters on cosmic magnetism, pp. 371-597, of Bourke et al., 2015, for instance). In part

I of this manuscript, after a brief review of cosmological magnetogenesis models in general, I will focus on a particular one, of astrophysical nature. As we have recalled above, during the so-called Cosmic Dawn, the first luminous sources photoionized the neutral IGM surrounding them. I will show where, under what conditions and up to what strengths, this process may have generated magnetic fields on intergalactic scales, thus contributing to the magnetization of the Universe before, and alongside structure formation.

**Fragmentation in the Cosmic Web** As we have seen, based on joint observational and theoretical arguments, we are brought to the conclusion that matter in the Universe is distributed in a web-like manner, with sheets and filamentary structures connecting nodes or halos at almost all scales and epochs. I have not mentioned it yet but cosmological simulations suggest that, on cosmological scales, these nodes are supplied with matter, baryonic and dark, flowing along the filaments, and that part of this accretion occurs intermittently (e.g. Kereš et al., 2009; Dekel et al., 2009b,a; Sánchez Almeida et al., 2014). This suggests that denser clumps of matter might form not only within the nodes of the cosmic web, but also in either voids, walls or filaments. It is fair to mention that, as has been pointed out, a fraction of the clumps may be of artificial origin due to numerical effects that are inherent to classical Smooth Particle Hydrodynamics numerical codes (see Hobbs et al., 2013; Nelson et al., 2013, for a discussion), and less present in simulations based on moving mesh techniques (cf. Springel, 2010). However, the rest of the clumps most probably has a true physical origin (Hobbs et al., 2016). While the so-called Lyman-$\alpha$ forest appearing in the spectra of distant quasars is interpreted as being due to intervening cosmic filaments (cf. for instance Chapter 7, *Galaxy formation physics*, by T. Abel, G. Bryan and R. Teyssier in Chabrier, 2009), the state, smooth or fragmented, of the IGM gas on the largest scales of the cosmic web is still observationally poorly known, except perhaps in a few specific cases on intermediate scales (e.g. the gas bridges between cluster pairs revealed by the Plank mission – Planck Collaboration, 2013). Detecting this gas and determining its dynamical state belongs to the major objectives of both the Square Kilometre Array (e.g. Bourke et al., 2015, p. 695) and the Athena mission of the European Space Agency (Nandra et al., 2014).

Are the clumps in filaments and cosmic walls observed in cosmological numerical simulations solely the product of the growth of primordial overdensities? Are these gas clumps always subtended by collapsed Dark Matter haloes, or is it possible that baryon fragments form and grow thanks to sub-grid gravitational instabilities? As we will see, this actually raises the general following question, relevant not only to the cosmic web: **How does gravitational instability occur in stratified media?** My motivation in part II has been to answer this question and investigate to which extent the clumps in cosmological sheets and filaments may have formed in situ through gravitational instability.

Before diving into the depth of each problematic, let us begin by recalling some of the key physical ingredients that underlie them both.

# Chapter 2

# Tools

Baryonic matter in the Universe, apart from extremely rare exceptions like planets and us, is in the *plasma state*[1], not necessarily but possibly magnetized. The good and fascinating news is that the laws governing plasma physics are *scale invariant* (see e.g. Goedbloed & Poedts, 2004). Plasma physics developed, understood and experimented with in laboratories, is thus an essential tool for Astrophysicists and Cosmologists. It is particularly essential for me, because I am directly interested in the question of the origin and evolution of cosmological magnetic fields. But also, generally speaking, it is often very fruitful to learn from another field what the relevant methods are. In section 7.2 and beyond, I will give an example of this fact, as I will explore gravitational fragmentation, without considering magnetic fields (yet), in the lines of studies performed in the plasma literature. But finally, I must add that in fact plasma physics is worth studying for its own intrinsic beauty. More precisely, my personal interest in it comes from the fact that it is a field of physics which is both very intuitive, because we are familiar, to some extent, with the quantities involved, and yet, the more we study plasmas, the more we discover that they may be extremely surprising and rich of subtleties. I also enjoy the fact that we can (in general) visualize the phenomena at play, and make the link between the equations and what we see, which is far less evident in fields like quantum and particle physics for instance.

Let us then consider that baryonic matter in the Universe is a plasma, which is largely driven by *gravity*, and in particular by its own gravitation. Therefore, to understand the Universe, it is crucial to master as well as possible the formal tools to describe self-gravitating plasmas, i.e. magnetic fields *and* gravity. To this day, the most general theoretical framework to describe gravity, and thus to model the Universe, is that of General Relativity. However, for the questions I will address in this manuscript, the relevant range of parameters is such that my study does not require this general framework. Indeed, although the distances considered here are essentially cosmological, typically of the order of one Mpc, they remain small compared to the curvature of the Universe. Even to consider the expansion of the Universe, a Newtonian approach, complemented with the use of the scale factor and comoving coordinates, is perfectly relevant. Also, densities are small enough to only weakly curved space-time (no black hole physics for instance) and velocities are small compared to the speed of light so that we neither need to consider gravitational waves nor any special relativistic effect (as opposed to studies of AGN jets for instance). This study will thus be conducted using Newtonian dynamics.

Which approach are we going to adopt here? Due to their intrinsic limitations, numerical simulations are not able to capture fully the breadth of time and length scales involved in structure formation, especially in diluted, numerically under-sampled regions of space. The analytical approach, adopted here, is crucial for understanding fully the underlying physics, and is complementary to numerical simulations. Finally, just like the personal reason why I am focusing on plasma physics evoked above, choosing the analytical approach is also worth for the sheer pleasure of it.

## 2.1 Electromagnetism

Any vector field, that vanishes suitably quickly at infinity, is entirely determined by its divergence and curl[2]. The divergence and curl of the electric and magnetic fields are determined in a coupled manner, constituting Maxwell's equations for electromagnetism. In Gaussian (CGS) units, they read

$$\begin{cases} \vec{\nabla} \times \vec{E} = -\frac{1}{c}\partial_t \vec{B} & \text{(Maxwell-Faraday)} \\ \vec{\nabla} \times \vec{B} = \frac{1}{c}\partial_t \vec{E} + \frac{4\pi}{c}\vec{J} & \text{(Maxwell-Ampère)} \\ \vec{\nabla} \cdot \vec{E} = 4\pi\rho_q & \text{(Maxwell-Gauss)} \\ \vec{\nabla} \cdot \vec{B} = 0 & \text{(No Magnetic Monopoles)} \end{cases} \tag{2.1}$$

[1] Throughout my manuscript, I take the liberty to use the term plasma loosely to designate interchangeably ionized and neutral fluids except, of course, in cases where the ionization state is essential.

[2] For additional details, see for instance the following discussion by Kirk T. McDonald on the Helmholtz decomposition: http://puhep1.princeton.edu/~kirkmcd/examples/helmholtz.pdf.

while in SI units, they read

$$\begin{cases} \vec{\nabla} \times \vec{E} = -\partial_t \vec{B} & \text{(Maxwell-Faraday)} \\ \vec{\nabla} \times \vec{B} = \frac{1}{c^2}\partial_t \vec{E} + \mu_0 \vec{J} & \text{(Maxwell-Ampère)} \\ \vec{\nabla} \cdot \vec{E} = \frac{\rho_q}{\epsilon_0} & \text{(Maxwell-Gauss)} \\ \vec{\nabla} \cdot \vec{B} = 0 & \text{(No Magnetic Monopoles)} \end{cases} \tag{2.2}$$

where $\vec{J}$ is the total current density and $\rho_q$ the total charge density. The fundamental constants $\mu_0, \epsilon_0$ and $c$ are linked by $\mu_0\epsilon_0 = \frac{1}{c^2}$. Note that my main plasma physics reference during the first part of my Ph.D. has been Krall & Trivelpiece (1973) who privilege Gaussian units, while later it has been Goedbloed & Poedts (2004) and Goedbloed et al. (2010) who work in SI units. This is the reason why my work on magnetogenesis, presented in part I, is formulated in Gaussian units, while the part mentioning magnetic fields in my work on gravitational fragmentation, in part II, is formulated in SI units. This should not be a difficulty for the reader since the equations are the same, up to multiplicative constants. As a reminder, as far as charge density, electric and magnetic fields are concerned we have

$$\rho_{\mathrm{q,cgs}} = \frac{\rho_{\mathrm{q,SI}}}{\sqrt{4\pi\epsilon_0}}, \quad \vec{E}_{\mathrm{cgs}} = \sqrt{4\pi\epsilon_0}\vec{E}_{\mathrm{SI}}, \quad \vec{B}_{\mathrm{cgs}} = \sqrt{\frac{4\pi}{\mu_0}}\vec{B}_{\mathrm{SI}}. \tag{2.3}$$

The four equations (2.1) or (2.2) do not have the same nature: The two relations governing the curl of $\vec{E}$ and $\vec{B}$ are dynamical, corresponding to evolution equations, while those on the divergences should be seen as initial conditions. Indeed, taking the divergence of the Maxwell-Ampère and Maxwell-Faraday equations, together with the local charge conservation equation $\vec{\nabla} \cdot \vec{J} + \partial_t \rho_q = 0$, gives (in SI units)

$$\begin{cases} \partial_t \left( \vec{\nabla} \cdot \vec{E} - \frac{\rho_q}{\epsilon_0} \right) = 0, \\ \partial_t \left( \vec{\nabla} \cdot \vec{B} \right) = 0. \end{cases} \tag{2.4}$$

Hence, due to charge conservation, if the Maxwell-Gauss equation is satisfied initially, then it remains so during the whole evolution, and similarly for $\vec{\nabla} \cdot \vec{B} = 0$. In that sense they constitute initial conditions for the evolution equations Maxwell-Faraday and Maxwell-Ampère.

In the non relativistic limit, displacement currents, corresponding to the term $c^{-1}\partial_t \vec{E}$, are negligible, so that in this manuscript we will neglect this term. The resulting set of equations is usually called 'Pre-Maxwell equations', because historically the displacement current term was introduced by J. C. Maxwell to ensure local charge conservation.

While the electromagnetic field may propagate in vacuum ($\rho_q = 0$ and $\vec{J} = \vec{0}$), we are interested in electric and magnetic fields evolving with matter. The quantities $\rho_q$ and $\vec{J}$ acting as sources in the above Maxwell equations are themselves governed by fluid equations in which $\vec{E}$ and $\vec{B}$ intervene. All these equations together constitute the MHD equations, describing the complex intertwining of matter and electromagnetic fields, and that we shall now have a look at.

## 2.2 Magneto-Fluid dynamics

I want to introduce the ideal MHD equations from a rather fundamental description, that of kinetic theory, because it will be the starting point of part I, but also because it is intellectually satisfying to have an idea of their fundamental origin rather than simply admiting them. However, the derivation presented below is a straight-to-the-point one. I omit a certain number of details that are, in my opinion, very important to be clear about the meaning and validity of the equations that we are dealing with, but that are unnecessary to expose here. For a precise discussion of the present implicit averages and unmentioned assumptions see for instance the very good chapters 2 and 3 of Krall & Trivelpiece (1973).

**From orbit, to kinetic, to fluid** Consider a collection of particles of various species, hereafter tagged by a symbol $\alpha$, and characterized by their charge $q_\alpha$ and mass $m_\alpha$. They are for example electrons or protons. The equation of motion of each of these charged, non-relativistic particles evolving in an electric field $\vec{E}$, magnetic field $\vec{B}$ and gravitational potential $\phi$, is given by Newton's second law (Gaussian units)

$$\frac{d\vec{v}}{dt} = \frac{q_\alpha}{m_\alpha}\left( \vec{E} + \frac{\vec{v} \times \vec{B}}{c} \right) - \vec{\nabla}\phi. \tag{2.5}$$

This many-body description, in which the motion of every single particle is taken into account, is in general not tractable. However, in the vast majority of situations, it is in fact not necessary for answering our questions. Indeed, because we are interested in systems with extremely large numbers of particles, say of the

order of the Avogadro number, a statistical description of the system, in terms of macroscopic variables (like density, temperature, pressure, etc.), is perfectly relevant and sufficient. It is however good to keep in mind that by our choice of description, we are leaving behind some information, so that some plasma properties and phenomena are absent in the formalism we will adopt here.

The study of the trajectory of a single isolated charged particle is called *orbit theory* and is well understood. The difficulty comes from the fact that a plasma is a collection of a large number of *interacting* particles. Collective effects are well described statistically. The point is to partition the system into volumes that are large enough to neglect statistical fluctuations due to the discreteness of the particles they contain and treat the medium as a continuum, but small enough to use differential calculus and talk about fluid elements. In *kinetic theory*, the information on both the (probable) number of particles and their velocity distribution is retained by working with the distribution function $f_\alpha(t,\vec{r},\vec{v})$. By definition, the probable number of particles of type $\alpha$ at position $\vec{r}$ with velocity $\vec{v}$ in the volume element $d^3\vec{r}d^3\vec{v}$ is equal to $f_\alpha(t,\vec{r},\vec{v})d\vec{r}d\vec{v}$. Note that volume elements in this description are six-dimensional since points are described in the six-dimensional space $(\vec{r},\vec{v})$ called phase space. Liouville's theorem states that in the absence of binary interactions between particles, density in phase space is constant in time ($\frac{df_\alpha}{dt}=0$). Now collisions, for instance, modify the distribution function because it is a process that changes the velocity of particles. The evolution of $f_\alpha$ is governed by the following equation

$$\frac{df_\alpha}{dt} = \partial_t f_\alpha|_s\,, \tag{2.6}$$

which we will refer to as the Boltzmann equation. On the right hand side, the source term is usually the term modeling collisions, but this term corresponds to any process which sources the distribution function. For example in chapter 3, we will model photoionization processes as a source term in this equation since it also modifies the velocity of particles, and in fact modifies the number of particles too. Now, in the six-dimensional phase space, by definition of the total time derivative, we have

$$\frac{df_\alpha(t,\vec{r},\vec{v})}{dt} \equiv \partial_t f_\alpha + \frac{d\vec{r}}{dt}.\frac{\partial f_\alpha}{\partial \vec{r}} + \frac{d\vec{v}}{dt}\cdot\frac{\partial f_\alpha}{\partial \vec{v}} \tag{2.7}$$

so that, using Newton's second law (2.5) for each species $\alpha$, the Boltzmann equation may be explicited as

$$\partial_t f_\alpha + \vec{v}.\frac{\partial f_\alpha}{\partial \vec{r}} + \left[\frac{q_\alpha}{m_\alpha}\left(\vec{E}+\frac{\vec{v}\times\vec{B}}{c}\right) - \vec{\nabla}\phi\right]\cdot\frac{\partial f_\alpha}{\partial \vec{v}} = \partial_t f_\alpha|_s\,. \tag{2.8}$$

This equation contains a lot of information, and often too much for our purposes. The *fluid description* consists in leaving behind the information about the whole distribution of velocities, by averaging, inside each volume element, on the velocity variable. This is called the fluid reduction, because we are reducing the amount of information carried in the equations we are manipulating.

Now, since we are dealing with a system containing various species $\alpha$, we may reduce the kinetic description to a fluid one, for *each* of these species. Doing so consists in working with

$$\begin{cases} n_\alpha = \int f_\alpha d^3\vec{v} \\ \vec{V}_\alpha = \frac{1}{n_\alpha}\int \vec{v} f_\alpha d^3\vec{v} \\ P_\alpha = m_\alpha \int \left(\vec{V}_\alpha - \vec{v}\right)\left(\vec{V}_\alpha - \vec{v}\right) f_\alpha d^3\vec{v} \end{cases} \tag{2.9}$$

which are respectively the number density, the velocity and the pressure tensor of species $\alpha$. These are called macroscopic quantities, because we are now only considering the averaged velocity $\vec{V}_\alpha$ inside each volume element rather than the microscopic details of the distribution of velocities carried by the full distribution function. To derive the equations governing these quantities, one has to evaluate the various moments (i.e. first multiply the equation by powers of $\vec{v}$ and then integrate over the entire velocity space) of the Boltzmann equation. This means evaluating

$$\int g_i \left[\frac{df_\alpha}{dt} - \partial_t f_\alpha|_s\right] d^3\vec{v} = 0 \tag{2.10}$$

where for instance the first three moments are

$$\begin{array}{ll} g_0 = 1 & 0^{\text{th}} \text{ moment: mass conservation} \\ g_1 = m_\alpha \vec{v} & 1^{\text{st}} \text{ moment: momentum conservation} \\ g_2 = \frac{1}{2}m_\alpha v^2 & 2^{\text{nd}} \text{ moment: energy conservation} \end{array} \tag{2.11}$$

and yield respectively the mass, the momentum and the energy conservation equations of species $\alpha$. The system is then described as multiple interacting fluids. This description is thus called the *multi-fluid description*.

Keeping track of the individual properties of each species is not always necessary, and despite the existence of multiple components, the description is often further reduced to a *mono-fluid* description. This consists in working in the center-of-mass with the quantities

$$\begin{cases} \rho = \Sigma_\alpha n_\alpha m_\alpha \\ \vec{V} = \frac{1}{\rho}\Sigma_\alpha n_\alpha m_\alpha \vec{V}_\alpha \\ P = \Sigma_\alpha m_\alpha \int \left(\vec{V} - \vec{v}\right)\left(\vec{V} - \vec{v}\right) f_\alpha d^3\vec{v} \end{cases} \tag{2.12}$$

being respectively the mass density, the center-of-mass velocity and the total center-of-mass pressure tensor in the one-fluid. With the above information, one may write the fluid equations in full generality. However, as far as the fluid equations are concerned, in part II we will not manipulate them in full generality, as exposed in Krall & Trivelpiece (1973) for instance, but in the ideal MHD limit. For example, pressure is described by the above tensor, but when viscosity is small, as we shall assume in this manuscript, it becomes diagonal and proportional to the scalar pressure: $P = pI$ where $I$ is the identity tensor. The starting point in part I however, will be the very general Boltzmann equation (2.8).

The zeroth moment gives the mass conservation equation

$$\partial_t \rho + \vec{\nabla} \cdot (\rho \vec{v}) = 0. \tag{2.13}$$

As its name suggests, this equation simply states that mass is conserved: In a given volume element, if the amount of matter varies ($\partial_t \rho$), it necessarily comes from the imbalance of the incoming and outcoming matter (formally: the divergence operator) from neighboring volume elements (there is no source term here).

The first moment gives the following momentum conservation

$$\rho \frac{d\vec{v}}{dt} = \rho \left(\partial_t \vec{v} + \vec{v} \cdot \vec{\nabla}\vec{v}\right) = -\vec{\nabla} p + \vec{j} \times \vec{B} - \rho \vec{\nabla}\phi. \tag{2.14}$$

This corresponds to Newton's second law for a fluid element of the mono-fluid. It stems from Newton's law on single particles (2.5), but is fundamentally different from it: We are now considering fluid elements, so that quantities are per unit volume (mass and current densities), the concept of pressure arises due to the collection of particles, and also the acceleration is now either Lagrangian ($\frac{d\vec{v}}{dt}$, evaluated while moving with the fluid) or Eulerian ($\partial_t \vec{v}$, evaluated at a fixed position). By order of appearance, the terms on the far right hand side correspond to the force (density) due to pressure gradients, to the Lorentz force and finally to the gravitational force.

**Ohm's law and induction equation** From these equations, we may derive an extremely important relation, namely the equation governing the current density in the plasma, called Ohm's law. I defer its presentation in full generality to section 3.2.2, where it will be at the center of the discussion. For now, let us admit here its simplest form (cf. e.g. Shu, 1992)

$$\vec{J} = \sigma(\vec{E} + \vec{v} \times \vec{B}), \tag{2.15}$$

where $\sigma$ is the conductivity. Plugging it into Ampère's law, we obtain the equation governing the evolution of the magnetic field, called the induction equation

$$\partial_t \vec{B} = \vec{\nabla} \times \left(\vec{v} \times \vec{B}\right) + \eta \Delta \vec{B}. \tag{2.16}$$

The first term is the convective term, resulting from the interaction between the fluid and the magnetic field, and $\eta = (\sigma\mu_0)^{-1}$ is the magnetic diffusivity, assumed to be a constant. How efficient is magnetic diffusion in the cosmological context? Consider the diffusive limit, in which the convective term is negligible. Then $\vec{B}$ obeys a diffusion equation. In terms of orders of magnitude it reads $\frac{1}{t_D} \sim \frac{\eta}{L^2}$, where $t_D$ is a characteristic timescale and $L$ a characteristic length scale of this diffusion. Since cosmic magnetic fields are spread on the largest scales of the Universe, we can try and estimate how much time it would take a magnetic field created at some point to reach such scales by simple diffusion. Taking for $L$ the Hubble radius $\frac{c}{H_0} \sim 4 \times 10^{18}$ m and characterizing the intergalactic medium by a typical magnetic diffusivity of $\eta \sim 10^{-6}$ $\Omega$.m, we obtain a diffusion time of the order

$$t_D \sim \frac{L^2}{\eta} \sim 10^{31} \text{ years}, \tag{2.17}$$

which is much more than the age of the Universe of $t_H \sim 10^{10}$ years. This means that due to the high conductivity (small $\eta$) of the intergalactic medium and the large scales involved, once a magnetic field is created somewhere, it does not diffuse. We say that it is 'frozen' into matter. Therefore, in the rest of this manuscript, we will not take this diffusion term into account.

So how does $\vec{B}$ evolve with the expansion of the Universe? Let us look at a simple example: Consider a sphere of plasma of radius $r$ undergoing a uniform and isotropic contraction. Since the $\vec{B}$ field is frozen into

matter, by mass conservation in this volume and flux conservation through its surface, we have that $\rho r^3$ and $Br^2$ are constant (cf. e.g. Kulsrud, 2005). Thus

$$\frac{B}{\rho^{\frac{2}{3}}} = \text{constant}, \tag{2.18}$$

and in the Standard Model of Cosmology $\rho \propto a^{-3}$ (cf. chapter 1) so that

$$B \propto a^{-2} \tag{2.19}$$

that is $B \propto (1+z)^2$. This evolution of $\vec{B}$ is called the adiabatic dilution and is valid only for the largest scales since it is derived in the FLRW homogeneous and isotropic framework.

**Higher moments: A need for Closure** The zeroth moment of the Boltzmann equation (2.8) yields a relation (mass conservation) between the zeroth moment of the distribution function (density) and the first moment (velocity). The first moment of the Boltzmann equation yields a relation (momentum conservation) between the zeroth, the first, and the second moment (pressure) of the distribution function. The second moment of the Boltzmann equation yields a relation (energy conservation) between the zeroth, first, second and third moment (heat flux) of the distribution function. The pattern that emerges turns out to be general: The equation governing the $n^{\text{th}}$ moment always contains the $(n+1)^{\text{th}}$ moment too. This is problematic because it means that the resulting system of equations is never closed this way. Everytime we add an equation, we add a new variable. Hence, rather than pursuing taking higher and higher moments, the usual procedure consists in stopping at the equation on the second moment, because only the three first moments have a simple physical interpretation, and to close the system with an additional equation, other than the following moment, dictated by physical arguments. This additional equation is called a *closure relation*. The choice of this relation strongly impacts the relevance and domain of validity of the model. In that sense, there are as many fluid models as closure relations. In this manuscript we will consider a classical model, namely that of polytropic fluids, which is interesting for its large domain of validity. Let us now see where it comes from.

## 2.3 Thermodynamics

In this manuscript, the choice of closure relations is as follows. In the most general case, pressure and density are related by an equation of state, corresponding to a relation of the form $p = p(\rho, s)$ or $p = p(\rho, T)$, where $s$ and $T$ are respectively the specific entropy (entropy per unit mass) and the temperature. Now, let us consider that baryons form a fluid that is an *ideal gas*, i.e. such that

$$p = \frac{\rho k_B T}{m} \tag{2.20}$$

where $m$ is the mass of a single particle, $T$ is the temperature and $k_B$ is Boltzmann's constant. A first simple case corresponds to that of an isothermal fluid, for which temperature is uniform. Then

$$p = \kappa \rho \tag{2.21}$$

where $\kappa = \frac{k_B T}{m}$ is spatially constant. More generally, one can show (cf. appendix F.2 of Binney & Tremaine, 2008) that for an ideal gas the specific entropy $s$ is linked to the number $q$ of internal degrees of freedom of the particles by the relation

$$s = \frac{k_B}{m} \ln\left(\frac{T^{(q+3)/2}}{\rho}\right) + \text{ constant}. \tag{2.22}$$

This relation brings in another interesting special case, namely the case in which the entropy is uniform (isentropic fluid). Then

$$\rho \propto T^{(q+3)/2} = T^{\frac{1}{\gamma-1}} \tag{2.23}$$

where

$$\gamma = \frac{q+5}{q+3} \tag{2.24}$$

is called the polytropic exponent. Combining this with (2.20), we obtain the following *polytropic* equation of state

$$p = \kappa \rho^\gamma \tag{2.25}$$

where $\kappa$ is a constant that depends on the specific entropy. We see from (2.21) that the isothermal equation of state corresponds to that of a polytrope with $\gamma = 1$.

Note that in these cases the equation of state is of the form $p = p(\rho)$. A fluid having this property is said to be barotropic. In fact, for a non magnetized fluid to be at rest in a gravitational field (which will be the

case of study in chapter 6), it must necessarily be barotropic. Indeed, the hydrostatic equilibrium, marked with the subscripts 0, is then given by equation (2.14) with vanishing velocity and magnetic field, that is

$$\vec{\nabla} p_0 + \rho_0 \vec{\nabla} \phi_0 = \vec{0}. \tag{2.26}$$

Taking the curl of this relation gives $\vec{\nabla} \times (\rho_0^{-1} \vec{\nabla} p_0) = \vec{0}$ and thus at every position we have

$$\vec{\nabla} \rho_0 \times \vec{\nabla} p_0 = \vec{0}. \tag{2.27}$$

This means that the gradient of density and the gradient of pressure are aligned everywhere, which implies that surfaces of constant density need to coincide with surfaces of constant pressure for a static solution to exist. Therefore, an unmagnetized fluid at rest in a gravitational field necessarily satisfies $p_0 = p_0(\rho_0)$, i.e. is barotropic.

It is thus particularly natural to consider a polytropic equation of state for the equilibrium. However the choice of equation of state, used as closure relation here, for the *out of equilibrium* fluid, is not evident. As we will see in section 9.2, when studying the evolution of perturbations in a fluid, depending on the timescales of evolution of the perturbations, there may or may not be time for heat transfer to happen. The relevant closure relation for the perturbed fluid may then differ from that of the equilibrium fluid. This difference gives rise to buoyancy, and thus to g-modes (using the stellar physics terminology) and convection. This stresses the importance of the choice of closure. Except in section 9.2 devoted to it, we will in this manuscript deliberately switch-off convection by considering equation (2.25), both for the equilibrium state and for out of equilibrium perturbations.

## 2.4 Gravitation

As far as gravity is concerned, in the Cosmology and Astrophysics literature, equilibrium states are generally discussed in terms of gravitational potentials ($\Phi$) rather than in terms of gravitational accelerations ($\vec{g}$). We usually say that 'baryons fall in the potential wells induced by Dark Matter' for instance. However, as we will discuss in section 7.1.3, in this manuscript I will describe perturbations in terms of forces, rather than in terms of energies and potentials. In that sense $\vec{g}$ will turn out to be a more natural variable to discuss perturbations. Hence, I will here use both $\Phi$ and $\vec{g}$, though in essence both descriptions contain the same information, since one is (minus) the gradient of the other

$$\vec{g} = -\vec{\nabla} \Phi. \tag{2.28}$$

Note that because of this definition, the vector field $\vec{g}$ is irrotational

$$\vec{\nabla} \times \vec{g} = \vec{0}. \tag{2.29}$$

As we will see in section 8.2, the linearized version of this constraint will be a key ingredient in our study. The gravitational acceleration $\vec{g}$ is governed by

$$\vec{\nabla} \cdot \vec{g} = -4\pi G \rho \tag{2.30}$$

so that, with definition (2.28), the gravitational potential $\Phi$ is governed by

$$\Delta \Phi = 4\pi G \rho \tag{2.31}$$

where $G$ is Newton's constant. These equations are called *Poisson equation*, respectively for the gravitational acceleration and for the gravitational potential. Physically, the form of equation (2.31) is very meaningful. Indeed, Newtonian gravity corresponds to a double limit of Einstein's theory of General Relativity: the weak field and non-relativistic limits. More precisely (cf. e.g. Barrau & Grain, 2011), linearizing Einstein's field equations around a flat space-time (weak field) results in a wave equation, sourced by the energy content of the Universe[3]. This propagation of space-time perturbations corresponds to gravitational waves, which travel at the speed of light because it is governed by the d'Alembert operator $c^{-2}\partial_t^2 - \Delta$. Then, when taking the non-relativistic limit, corresponding formally to an infinite speed of light, the d'Alembert operator makes way to the Laplace operator that appears in (2.31). In other words, equation (2.31) states that gravity is instantaneous in the Newtonian regime considered here. Finally, note that it is common to find in the literature an opposite choice of sign in the definition of $\phi$ and $\vec{g}$ and thus in Poisson equations (e.g. Goldreich & Lynden-Bell, 1965; İbanoğlu, 2000). The convention-independent quantity is the sign of the gravitational force term in the momentum conservation.

[3]The right hand side of (2.31) is the 'residue' of this source term once the non-relativistic limit is taken in addition.

## 2.5 Self-gravitating magnetized structures

Gathering the material introduced above, we may state that the set of equations governing the dynamics of a self-gravitating ideal polytropic magnetized fluid reads

$$\boxed{\begin{cases} \partial_t \rho + \vec{\nabla} \cdot (\rho \vec{v}) = 0 & \text{(Mass conservation)} \\ \rho \left( \partial_t \vec{v} + \vec{v} \cdot \vec{\nabla} \vec{v} \right) = -\vec{\nabla} p + \vec{j} \times \vec{B} - \rho \vec{\nabla} \phi & \text{(Momentum Conservation)} \\ \vec{j} = \frac{1}{\mu_0} \vec{\nabla} \times \vec{B} & \text{(Maxwell-Ampère's)} \\ p = \kappa \rho^\gamma & \text{(Polytrope)} \\ \partial_t \vec{B} = \vec{\nabla} \times \left( \vec{v} \times \vec{B} \right) & \text{(Induction Equation)} \\ \Delta \phi = 4 \pi G \rho & \text{(Poisson Equation)} \end{cases}} \tag{2.32}$$

This is our starting point, from which we are going to do the two following things.

First, there is one other absolutely crucial ingredient for the Astrophysical and Cosmological context that I have not mentioned so far: *Radiation*. Radiation is of course essential to probe the Universe because it is the main element we can directly collect and analyze, but it also plays, in many situations, an important dynamical role. The most evident ones are radiation pressure, and heating or cooling, by evacuating energy through radiative processes. But in the first part of this manuscript, I will reveal a more subtle role radiation may play: It can generate magnetic fields! Formally speaking, I will expose how a radiation field may modify the induction equation in the system (2.32) above, by acting as a source term in the Vlasov equation (2.8) and thus as a source term in the induction equation.

Second, in the Universe everything moves, rotates, merges, accretes, etc. Nothing is at rest. Therefore, structures are permanently subject to perturbations which either make them *oscillate* or, under some circumstances, expose them to *instabilities*. Apprehending precisely how, when and where instabilities may occur is a key to understand the shaping of the Universe. The second part of this manuscript is thus dedicated to studying how sensitive structures are to the perturbations they are subject to, i.e. how instabilities may develop. Formally speaking, we will linearize the set of equations (2.32) and perform a normal mode analysis, in the light of the so-called spectral theory.

# Part I

# Generation of Cosmological Magnetic Fields

Magnetic fields are ubiquitous in the Universe. They are present at all scales and all epochs (cf. section 3.1.1). Yet, it is still unclear where, when and how precisely they were generated. This part of the manuscript is dedicated to the question of the origin of cosmic magnetic fields on large scales which is still an open, and major, problem of Astrophysics and Cosmology. In chapter 3 we will first see that in the history of the Universe, many environments have been favorable to the generation of magnetic fields. After a brief overview of the various magnetogenesis models proposed in the literature so far, I will focus on a particular mechanism, of astrophysical nature, which was first suggested by Langer et al. (2005), and the physics of which I developed thoroughly in Durrive & Langer (2015). Then in chapter 4, I will present a detailed model that I have developed, together with M. Langer, H. Tashiro and N. Sugiyama, to estimate the level at which this mechanism contributed to the magnetization of the Universe before, and alongside early luminous structure formation. Finally, in chapter 5, I will show preliminary results of an investigation I am conducting with D. Aubert based on cosmological numerical simulations, which complements the aforementioned analytical works.

# Chapter 3

# Magnetogenesis by Photoionization

## 3.1 Magnetic Fields and their generation

Dark Matter and Dark Energy are exciting to explore, but we still know, all in all, very little of the physics of these exotic constituents of the Universe. On the contrary, there is a component in the Universe that we know is also omnipresent, of which we know the physics very well, and yet that remains puzzling for cosmologists: cosmological magnetic fields.

### 3.1.1 Magnetic Fields in the Universe

**Magnetic fields are ubiquitous** Indeed, magnetic fields are ubiquitous in the Universe. Their stunningly wide length and strength ranges basically follow the simple rule that the larger the scale, the weaker the strength (e.g. Vallée, 1990, 2011). For instance magnetars are the most magnetized objects with $10^{15}$ G[1], while normal stars typically contain 1 G fields. In the interstellar medium, several $10^{-6}$ G are usual at kpc scales, and $10^{-6}$ G in clusters of galaxies at the Mpc scale. Finally, the largest structures such as cosmological filaments may have some $10^{-10}$ G fields and as we shall see below, cosmological voids may host $10^{-16}$ G magnetic fields. For a review of the observational aspects of large scale magnetic fields, see Ryu et al. (2011) for instance.

The detection and measurement of extra-terrestrial magnetic fields has been an ongoing, flourishing activity since the end of the 19th century (following the suggestion of Zeeman, 1897) and the beginning of the 20th century. For instance, Hale (1908) was the first to confirm observationally the existence of extra-terrestrial magnetic fields by observing sun-spots. Much progress has been made since, and it is nowadays well known that magnetic fields play a major role in the evolution of our Sun (cf. the 11 years cycle, e.g. Priest, 2014) and in the formation and evolution of stars in general (e.g. Petit et al., 2014). Since these pioneering observations, various techniques have been developed, based on fundamental physical effects, such as the Zeeman effect, synchrotron emission, Faraday rotation and polarization of optical starlight. For a clear presentation of these techniques and methods, see Widrow (2002) for instance.

All those techniques have allowed us to detect magnetic fields, and measure their strengths, not only in our galaxy (Haverkorn, 2015, and references therein), but also in extragalactic structures on large scales (Kronberg, 1994). It is striking that magnetic fields were found in all the galaxies probed. What is more, in most of the observed galaxies, the magnetic field has a spiral structure which is often observed not only in spiral galaxies (as in M51, see figure 3.1), but in almost every galaxy, even in ring, flocculent and irregular galaxies (Fletcher, 2010; Beck, 2011). This feature hints at a mechanism, of the dynamo type, which would be responsible for the organisation of the $B$-field lines on galactic scales (Brandenburg & Subramanian, 2005). Moreover, the strength measured is of the order of a few tens of $\mu$G, such that magnetic fields are actually dynamically important in galaxies: the energy density they represent is typically $\rho_{\rm mag} = \frac{B^2}{8\pi} \sim 1$ eV cm$^{-3}$ since for instance $B \sim 5\mu$G in the Milky Way at the scale of the spiral arms (see figure 3.1 showing a map of the magnetic field in the Milky Way deduced from the Planck satellite data). Such energy densities are essentially of the same order of magnitude as those of other components: cosmic rays, and thermal and turbulent gas motions. Remarkably, fields with similar strengths are detected not only in galaxies of our neighbourhood, but also in distant, early galaxies (e.g. Bernet et al., 2008). This implies that such strong magnetic fields were already present in cosmic structures when the Universe was less than half its present age. This puts a severe constraint on the generation and evolution mechanisms within cosmic structures.

Similar observations have allowed one to detect magnetic fields in larger structures, namely in clusters of galaxies (for reviews, see Carilli & Taylor, 2002; Govoni & Feretti, 2004; Feretti et al., 2012; Brüggen, 2013). Microgauss fields have thus been measured which, in most cases, are rather turbulent on scales ranging from a few hundreds of parsecs up to tens of kiloparsecs (Feretti et al., 2012). In some clusters, however, magnetic

[1] 1 Gauss = $10^{-4}$ Tesla.

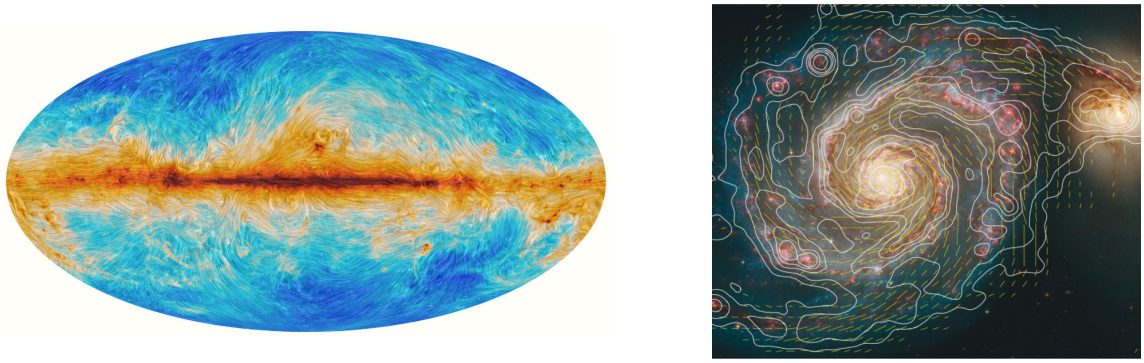

Figure 3.1: Left: Magnetic field in our Galaxy (credit: ESA & Planck collaboration). The colour scale represents the total intensity of dust emission, revealing the structure of interstellar clouds in the Milky Way. The texture is based on measurements of the direction of the polarized light emitted by the dust, which in turn indicates the orientation of the magnetic field. Right: Magnetic field in galaxy M51 (Fletcher et al., 2011).

fields appear to possess a regular component, coherent on scales reaching 400 kpc, associated with intra-cluster filamentary radio relics (Govoni et al., 2005). On yet larger scales, those of the cosmic web, it is fair to say that magnetic fields remain observationally largely elusive. While hints of substantial magnetization (at the 2 $\mu$G level) along the filamentary region at the south-west of the Coma cluster have been reported (Bonafede et al., 2013), a clear detection of $B$-fields on the scales of the cosmic web has yet to be claimed. As I mentioned in chapter 1, for that we might have to wait for the SKA to be operational. So far, only a few indirect constraints are available in the literature as we will see below.

**Cosmological magnetic fields** Dense regions are highly magnetized and therefore seem like the place to look for information on magnetic fields. However, they are also highly turbulent, so that magnetic fields have lost their initial properties (e.g. Dolag et al., 2002). In order to probe the origin of those fields, it is therefore on the contrary more appropriate to look at the less turbulent Intergalactic Medium, where magnetic fields were less processed and hopefully remained in their primitive configuration. But how strong are such cosmological magnetic fields? To this day observations lead to the following upper and lower bounds.

*Upper bounds.* Wasserman (1978) and Kim et al. (1996) studied the effect of a background magnetic field, present at Recombination, on the subsequent structure formation. They assessed the effect on the velocity and density fields of matter. Fluctuations in the magnetic field induce fluctuations in the velocity and matter fields through the Lorentz force. Hence they modify the spectrum of density perturbations, generating additional power at small scales. Therefore a magnetic field increases the number of collapsing objects and thus of forming stars, so that its presence makes the Epoch of Reonization finish earlier. The magnetic field at Recombination therefore could not have been too strong, namely not stronger than $10^{-9}$ G, otherwise too many stars would have been formed to be consistent with our knowledge of the Reionization epoch. Note however that further investigations were performed, and no consensus has been reached yet. Indeed, for instance Tashiro & Sugiyama (2006) confirmed, through analytical considerations, that strong enough primordial fields indeed enhance early star formation, but recently Marinacci et al. (2015), using ideal magnetohydrodynamic cosmological numerical simulations, claimed that they on the contrary lead to a suppression of the cosmic star formation efficiency. They interpret this suppression as due to the additional pressure in gaseous structures arising from the magnetic field, and we may also expect magnetic tension to have a similar effect. An upper limit was also inferred based on the idea that strong magnetic seeds in the early universe would leave imprints on the Cosmic Microwave Background (CMB). A primordial magnetic field induces scalar, vector and tensor perturbations in the metric, leading to both temperature anisotropies and polarization signals. Precise calculations with comparison to CMB data (for example Shaw & Lewis, 2012; Planck Collaboration, 2015c) give the typical limit $B \leq 10^{-9}$ G. Faraday Rotation measurements towards distant quasars give the same upper limit assuming a maximal field reversal scale of 1 Mpc (Kronberg, 1994).

*Lower bounds.* With only upper bounds, measurements are still compatible with zero. Fortunately, a *lower limit*, and thus an evidence of non zero magnetic fields at cosmological scales, was announced a few years ago. It was made possible through high energy gamma-ray observations, with the space telescope Fermi and ground based telescope HESS (High Energy Spectroscopic System) data (Neronov & Vovk, 2010; Taylor et al., 2011; Takahashi et al., 2012). More precisely, gamma-rays with energies of the order of, or greater than the TeV emitted by blazars interact with the diffuse extragalactic background light (i.e. the radiation of extragalactic origin that fills the Universe, of which the CMB), creating electron-positron pairs in intergalactic space. These pairs interact via Inverse Compton scattering with CMB photons, and Neronov & Vovk (2010) show that typical 5 TeV electrons from blazars scatter typical $6 \times 10^{-4}$ eV CMB photons at about 90 GeV. Therefore a secondary cascade of gamma-rays appears. In the presence of magnetic fields, the

electrons and positrons trajectories are altered, making the cascade emission signal to appear as extended around the primary source. Thus the source size appears different from the point spread function of the telescope if the magnetic field in the intergalactic medium is non zero. What is more, the stronger the intergalactic magnetic field, the stronger the damping of the high energy gamma ray flux measured in the telescope. Combining both information, the authors of Neronov & Vovk (2010) were able to put a lower limit on the strengths of fields at large scales: $10^{-17}\mathrm{G} \leq B$ over distances of about 80 Mpc. Note that this measurement was made only for three blazars in the recent Universe (redshift $z \sim 0.18$) because known blazars are rare. The objective is therefore to have more and more measurements by using other sources (e.g. AGNs) with the same method. We could thus obtain information on cosmological magnetic fields in more directions, and even have an observational angular power spectrum of cosmic magnetic fields i.e. on the whole sky.

Now, in addition to the gamma-ray telescopes, LOFAR (LOw Frequency ARray) and SKA (Square Kilometre Array) are two radio-telescopes for which cosmic magnetism is one of the 'Key Science Projects', meaning that it is one of the main motivations for which the instruments are built for. LOFAR is an interferometric array of radio telescopes ($10 - 240$ MHz) with more than 20 000 antennas distributed mainly in the Netherlands but also across Europe, in countries including Germany, France, the UK, and Sweden. It reaches a resolution equivalent to a 1000 km diameter telescope. SKA will be a set of thousands of linked radio wave receptors (50 MHz - 14 GHz) located in Australia and South Africa. It is expected to be operational around 2020 (phase 1). It will reach a resolution equivalent to a larger than 3000 km diameter telescope. Finally, as we will see in the next section, seed magnetic fields were generated on cosmological scales during the EoR. Although weak (of the order of $10^{-19}$ G) and very remote, the strengths of the seeds produced, together with their specific spatial configuration, could actually also be revealed directly through the recently proposed probe of magnetic fields in the EoR detailed by Venumadhav et al. (2014), although large coherence lengths of the magnetic fields might be mandatory.

As a result, even though they are far from new in human knowledge, magnetic fields are becoming a new observable in Cosmology (they have been even proposed as key ingredients for the detection and study of the cosmic web itself, see Vazza et al., 2015) and it is timely to focus on the subject of their origin and cosmological evolution. But interpreting these data remains very problematic and it is crucial to know as precisely as possible where and how these fields may have appeared. On the theoretical side this question has been tackled very early, with studies dating from the late 1950s (Hoyle & Ireland, 1960). Many different approaches have been proposed as we will see right below. But despite all this work, their origin is still one of the greatest question of modern Cosmology.

### 3.1.2 Brief Overview of Magnetogenesis Models in Cosmology & Astrophysics

The possibility that the Universe has been born magnetized cannot be dismissed a priori. But as an answer to the question of the origin of magnetic fields, it is a somewhat unsatisfactory solution. So the question is still open: When and how did they appear? The thing we know, as mentioned in the previous section, is that if they had appeared with strengths of the order of what they have today, structure formation history would have been totally different from what we observe. Hence the current paradigm is that they are the result of the amplification of weak seeds by adiabatic compression (since the fields are 'frozen-in') and dynamo effects during structure formation, and were maintained by dynamos later on. The current concensus is that seeds of only $10^{-22}$ to $10^{-12}$ G are required to reach the observed $\mu$G fields (e.g. Widrow et al., 2012; Durrer & Neronov, 2013). But when, where and how were these seeds generated? A plethora of models has been proposed, and since the constraints are not very strong yet, it is difficult to exclude most models while, at the same time, no model is entirely satisfactory. They are all problematic to some degree. Also, several of these mechanisms most probably happened together. One important question is thus to compare them and evaluate when and where one may have dominated over the others.

It is usual to divide these numerous mechanisms into two broad classes, based on the same distinction as in the chronology in chapter 1, namely Primordial Universe mechanisms and Post-Recombination ones.

**Primordial Universe** The literature on primordial mechanisms is vast. For reviews see e.g. Grasso & Rubinstein (2001), Widrow et al. (2012), Durrer & Neronov (2013) and Subramanian (2016). These mechanisms can be divided in three classes.

(i) *Inflation.* A major idea of inflation is to interpret the current matter density field of the Universe as stemming from quantum fluctuations of the primordial matter fields. This mechanism is very successful at accounting for observations of the statistical distributions of large scale cosmic structures (galaxies and galaxy clusters). It is therefore tempting to follow the same idea and propose that current magnetic fields originate in quantum fluctuations of the primordial electromagnetic field. Indeed how can magnetic fields be so wide-spread at such scales as suggested by the gamma-ray telescopes? This is why looking at seeds generated during inflation is a seducing idea. This approach has been considered and the result is puzzling: The fields generated have extremely small strengths, far too small to account for what we see today. Only mechanisms with physics beyond the Standard Model such as string theory or non standard physics such

as massive photons predict large enough magnetic strengths. Unfortunately, globally the predicted seed strengths range from $10^{-65}$ to $10^{-9}$G and depend very strongly on the details of the models. Thus magnetic field generation during inflation is far from generic. Note that the need to require new physics is interesting since the detection of cosmological magnetic fields could then constitute a new probe of exotic physics if other origins, as those mentioned below, are ruled out.

(ii) *Electroweak and Quark-Hadron phase transitions.* If not generated as early as in the inflation epoch, the fields may have been generated later in the primordial Universe, through mechanisms based on rather well established High Energy Physics: in the hot primordial plasma, the W and Z bosons and photons were interchangeable until temperature decreased enough for these bosons to become distinct. The weak and electromagnetic forces became then separate forces. This transition is called the Electroweak phase transition. Another paramount transition occured later on in the cooling primordial plasma: initially the temperature was so high that quarks could not form bound systems, but once the temperature decreased enough, quarks were able to cluster into hadrons. This transition is called the Quark-Hadron phase transition. Both phase transitions involved the release of huge amounts of energy and involved the acceleration of charged particles, e.g. at the boundaries between true and false vacua. Important currents and electromotive forces may then have appeared thus inducing magnetic field seeds. Detailed calculations showed that indeed strong fields certainly arose then, but only at horizon scales (the maximum distance a light ray could have traveled since the Big Bang at that time) which were extremely small, making it difficult for these fields to account for magnetic fields at present cosmological scales. Those mechanisms are however not discarded, because of possible inverse turbulent cascades. In (magneto)hydrodynamics, a (magnetic) direct 'cascade' is a process which transfers (magnetic) energy from large scales to small scales. In the study of cosmological magnetic fields, the inverse process is of great importance as many mechanisms can generate magnetic fields on small scales. An inverse cascade may then bring the generated fields to larger scales. Relying on magnetic helicity, in the context of the primordial Universe, it is still unclear whether such processes may or may not have been efficient enough.

(iii) *Before and at Recombination.* Towards the end of the radiation era, before and at recombination, magnetic fields were also generated, via vorticity in the primordial plasma. E. R. Harrison (1970) was the first to state this clearly. Electrons and protons in rotating plasma blobs interact with the background radiation through Compton scattering. However the cross section of this interaction is much larger for electrons than for protons, so that a charge separation and thus an electric field, is induced. Because the blob has a differential rotation, this electric field is rotational and thus induces a magnetic field in turn. Since then, many studies have refined the calculations, resulting in field strengths that are very weak compared to other mechanisms, namely of up to $B \sim 5 \times 10^{-24}$ G on Mpc scales at $z = 1100$ (Fenu et al., 2011; Saga et al., 2015).

**Post-recombination** For reviews including material on post-recombination mechanisms, see e.g. Widrow (2002), Kulsrud & Zweibel (2008), Ryu et al. (2011), and Widrow et al. (2012). In the post-recombination Universe, we can distinguish four possibilities.

(i) *Thermal (Biermann) battery.* This mechanism relies on the fact that when thermal pressure gradients are not aligned with electronic density gradients, electric fields of non-zero curl appear, thus inducing magnetic fields by Faraday's law (2.1). More precisely, as described in Xu et al. (2008), the Biermann battery appears as a source term in the induction equation (2.16). Namely neglecting the diffusion of the magnetic field we have (we will derive this Biermann term in the next section)

$$\partial_t \vec{B} = \vec{\nabla} \times \left( \vec{v} \times \vec{B} \right) + \frac{c \vec{\nabla} p_e \times \vec{\nabla} n_e}{n_e^2 e}, \tag{3.1}$$

where $n_e$ is the electron density and $p_e$ the electron pressure linked to temperature by the ideal gas law $p_e = n_e k_B T_e$ which is why this is also called a thermal battery. This mechanism was originally proposed by L. Biermann in 1950 to generate magnetic fields in stars in which the misalignment of density and pressure gradients of the electronic fluid stems from the differential rotation (Biermann, 1950; Kemp, 1982). This idea was later applied in the cosmological context in two ways. Firstly, during structure formation motions are very turbulent, and shocks at cosmological scales are ubiquitous (Ryu et al., 2003). Works like those of Pudritz & Silk (1989) and Kulsrud et al. (1997) showed that seeds of strengths $B \sim 10^{-20}$ to $10^{-18}$ G on protogalactic scales could thus emerge in the cosmic web. Secondly, magnetic fields at cosmological scales have been generated through the Biermann battery during the Epoch of Reionization (EoR), at the contact of ionization fronts from the first luminous objects with matter overdensities. This was first investigated analytically with simple estimates by Subramanian et al. (1994) and later numerically by Gnedin et al. (2000). In the latter paper, the authors present two typical situations in which temperature and density gradients are not aligned, cf. figure 3.2. The first one, which occurs essentially in the first stages of EoR, comes from the fact that as stars form in dense neutral clouds, pressure builds up and at some point the hot and ionized gas breaks out from the protogalaxy. This break out does not occur isotropically but rather in the way depicted in the left of figure 3.2. In the moderate density regime (overdensity $\delta \leq 10$) temperature

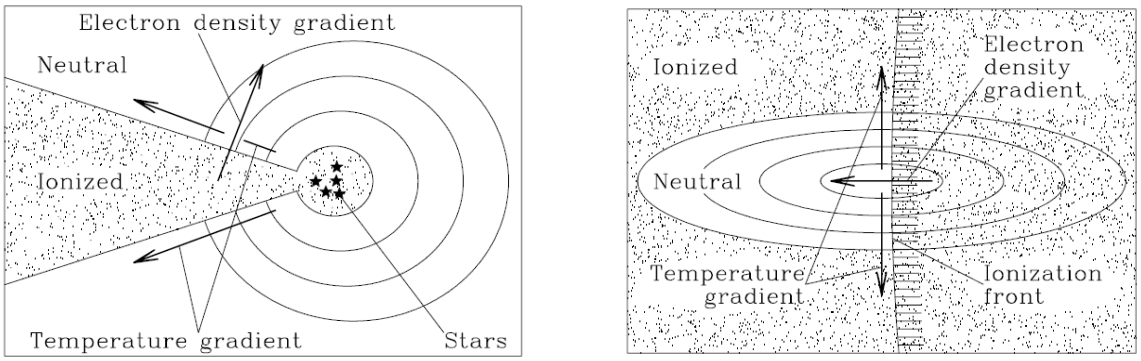


Figure 3.2: Two typical situations occuring during EoR in which temperature and density gradients are misaligned, thus generating magnetic field through the Biermann battery, as presented in Gnedin et al. (2000). Left: The breakout of ionization fronts from protogalaxies. Right: The propagation of ionization fronts through high-density neutral clumps or filaments.

correlates with density, so that in such neutral overdense regions, the temperature gradients are radial, like the density gradient. But at the same time, the ionization front breaking out is by definition the transition between a fully ionized and fully neutral medium, so that as highlighted in the figure, the geometry of the situation is such that the electron density gradient is on the contrary orthoradial. Therefore, the condition for the Biermann battery to operate is maximally efficient in this situation. The second situation, depicted on the right of figure 3.2, corresponds to an ionized front passing through a neutral clump or filament. This may occur all along the EoR, and even later, once ionized bubbles have overlapped but neutral clumps remain because they are dense enough for recombinations to counterbalance ionizations (recombination time decreases with density). As before, temperature gradients are radial, but now electron density gradients are horizontal (for a vertical ionization front as in the figure) so that both are misaligned and a magnetic field is generated. The fields are generated on relatively large scales but the strengths are of the same order as in the cosmological shocks mentioned above. Some dynamo effect is thus required to amplify them.

(ii) *Plasma instabilities.* Plasma instabilities such as the Weibel instability (Weibel, 1959) can create magnetic field seeds with high strengths, reaching for example $10^{-7}$ G, but only on small plasma scales. However, this process may occur in large volumes, such as in galaxy cluster shocks (Schlickeiser & Shukla, 2003; Medvedev et al., 2006). It hence requires some inverse cascade to account for the coherence of fields on large scales. Fields up to $10^{-16}$ G on kpc scales could arise in tens of Myrs, provided fields on smaller scales do not saturate the instability (Ryu et al., 2011).

(iii) *Momentum transfer from photons.* The interaction of photons with matter may induce magnetic fields through two processes, namely Thomson scattering and photoionization. Given the mass dependence of the Thomson cross section $\sigma_T \propto m^{-2}$, electrons are more accelerated than protons by photons, thus inducing electric fields, which acquire non-zero curl thanks to inhomogeneities or turbulence, thus inducing magnetic fields. As mentioned previously, some explored the possibility that this happened at Recombination, but resulting in strengths too weak to be a dominant mechanism. At Reionization however, matter distribution is much more inhomogeneous, making it a promising period for the creation of seeds by momentum transfer from photons to electrons. In protogalaxies, field of typically $B \sim 10^{-18}$ G on protogalactic scales could be reached (Mishustin & Ruzmaĭkin, 1972; Langer et al., 2003; Chuzhoy, 2004). The role of photoionizations during EoR has been explored around first stars by Silk & Langer (2006) and Shiromoto et al. (2014) for instance, and in the whole intergalactic medium by Langer et al. (2005), Ando et al. (2010) and Durrive & Langer (2015), and the next section is dedicated to it. Note that Doi & Susa (2011) examined the relative importance of this photoionization mechanism and the Biermann battery in numerical simulations of the neighbourhood of an ionizing super-massive star. In their study, they focus on the situation across an ionization front, in which a self-shielded, neutral, $\delta \simeq 10^2 - 10^3$ over-density defines very sharp and strong gradients in the temperature and electronic density fields. Such a situation could indeed occur within Strömgren spheres of the very first luminous sources. Under those conditions, they concluded that the Biermann battery dominates by one order of magnitude. In Langer et al. (2005) and Durrive & Langer (2015), mild, neutral over-densities way outside the Strömgren regions of stronger, long-lived ionizing sources, are considered. In such contexts, the Biermann battery may not be effective, be it for purely geometrical reasons, as argued in Durrive & Langer (2015), and the major advantage of the photoionization mechanism is that the whole intergalactic medium is premagnetized, i.e. magnetic seeds are generated almost everywhere.

(iv) *Outflows.* So far we have presupposed that the magnetic fields in the IGM today have been generated *in situ*, while in fact a fraction of it may have been generated inside structures and only then somehow reached less dense regions. As we have seen in chapter 2, diffusion is absolutely inefficient in the cosmological context. A possibly very efficient process however are outflows, i.e. they were expelled into the IGM. We may distinguish three typical cases. Firstly, the most powerful outflows one may think of are those from

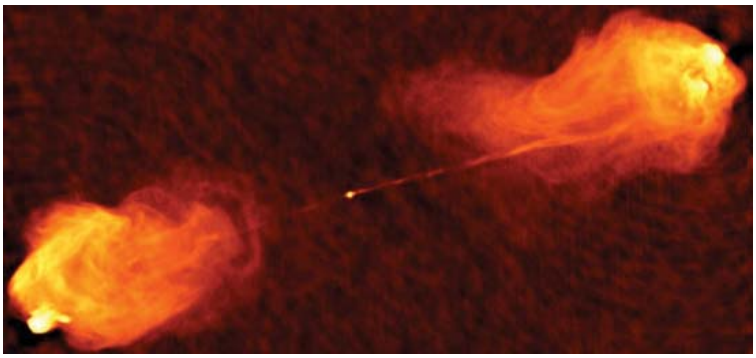

Figure 3.3: VLA image at 5GHz of the hyper-active radio galaxy Cygnus A (credit: NRAO/AUI & R. Perley) showing jets that inject magnetized plasma, deposited in giant radio lobes, into the IGM. Note that the jets extend over dozens of kpc here (Carilli & Barthel, 1996), and may reach distances of the Mpc order in other AGNs.

AGNs (Rees, 1987; Daly & Loeb, 1990; Ensslin et al., 1997), cf. figure 3.3, but those sources are relatively rare, so that their efficiency to globally magnetize the IGM is not necessarily great. Authors like Furlanetto & Loeb (2001) have estimated that by $z \sim 3$ some 5-20 % of the IGM may be 'polluted' by $B \sim 10^{-9}$ G with correlation lengths of the order of the radio lobe size, namely of the Mpc. Secondly, galactic winds from galaxies inside clusters may also contribute. This was investigated for example by Kronberg et al. (1999), Bertone et al. (2006) and Donnert et al. (2009). They claim that magnetic fields of $10^{-12}$ G to $10^{-8}$ G strengths may have been spread in most of the IGM with correlation lengths of the order of one kpc. However, such results strongly depend on the prescriptions of galactic winds. This is one example of situations which underlines the importance of gaining precision in the modeling of 'small scale' phenomena in order to better constrain and understand what happens on larger scales. Thirdly, as far as galactic winds are concerned, it is most natural to think of galaxies inside structures, but in the context of cosmological magnetic fields, winds from void galaxies are well situated to be of interest, as first pointed out by Beck et al. (2013). In this work, the authors consider cosmic ray driven winds, through Bohm diffusion. The relevance of this choice of diffusion process is still under debate in the community. They perform a simple estimate for a typical void and conclude that fields of up to $10^{-15}$ G may be spread in voids. But the authors themselves qualify their result as a 'highly speculative' estimate because of the crudeness of their assumptions. This idea deserves a more thorough inspection, and authors like Ramond & Langer started digging further in this direction by investigating rigorously the transport of plasma in expanding voids due to the global expansion of the Universe in the general relativistic frame (Ramond, 2015).

## 3.2 Intergalactic Magnetogenesis by Photoionization from the First Luminous Sources

In 2005, an astrophysical mechanism generating intergalactic magnetic fields during the EoR based on photoionization was introduced by Langer et al. (2005). I will now present my contribution to this work: I explored in depth and in detail the physics of the mechanism, notably by deriving the expression of the generated magnetic field from first principles, and exhibited the characteristic length scales of the problem.

This mechanism is particularly interesting in the cosmological context because, as we shall see, it naturally induces magnetic fields on large scales, because the driver is high energy photons (UV and X) which have long mean free paths, and on early stages of structure formation, namely as long as a significant fraction of the IGM was neutral. This contrasts with mechanisms based on the Biermann battery (cosmological shocks or propagating ionization fronts, cf. section 3.1.2) which generate fields essentially in high density environments.

In this section, I will summarize the ideas I proposed, the steps I followed and the results I obtained. For the details of the calculations, I invite the reader to consult the article Durrive & Langer (2015), attached in section 3.2.4, that this work led to.

### 3.2.1 Intuitively

**The mechanism** According to the Standard Model of Cosmology, the first stars, galaxies and quasars formed in neutral pristine gas during the first billion years of the history of the Universe. As they radiated, they photoionized their surroundings, and formed around them fully ionized regions, called Strömgren spheres or HII regions. More precisely, the structure of these regions is the result of the competition between ionization and recombination processes. The radius of a Strömgren sphere is defined as the distance from

the source at which the ionization and recombination rates are equal. Within this distance, photoionizations dominate and the inside of the sphere is considered as fully ionized. On the contrary, far from the source recombinations dominate so that the medium remains essentially neutral. However, photoionizations at the exterior of Strömgren spheres do occur. Indeed, the mean free path of photons goes as the cube of their energy ($\lambda_{\text{mfp}} \propto \nu^3$), so that UV and X photons travel, and may photoionize, far beyond the Strömgren radius. The ionizations giving rise to the HII region itself are essentially achieved by photons with energies close to the Hydrogen ionization threshold. Now, from Maxwell-Faraday equation $\partial_t \vec{B} = -c\vec{\nabla} \times \vec{E}$, we know that the requirement for a magnetic field to be generated is the existence of a process that induces a *rotational electric field*, and as detailed in figure 3.4, a clumpy intergalactic medium and anisotropic Strömgren spheres are sufficient to fulfill this requirement. In realistic configurations, this lack of symmetry in the IGM and Strömgren spheres is evident, as we can see for example in the results of numerical simulations 1.4, so that magnetic fields *must* have been generated by this mechanism.

**A mechanism of cosmological interest** This mechanism is relevant for Cosmology obviously because it takes place during the remote times of first star formation, but also because it generates fields on cosmological scales. Indeed, the driving process is photoionization, so that an obvious length scale of the problem is the mean free path of photons, which depends on their energy but also on the density of the medium in which photons propagate, and thus on the epoch at which they where emitted. Table 3.1 shows orders of magnitude of these values in the relevant ranges of redshift and for typical values of energy of the emitted photons. These values are indeed of cosmological interest and, as shown in section 3.2.4, are of the same order of magntitude as the intersource distance of the sources that emit them. In other words, this mechanism can potentially magnetize the whole IGM all along the Epoch of Reionization.

What is more, as explained in figure 3.4, the heart of the mechanism is that inhomogeneities in the IGM and the anisotropy of Strömgren spheres make the absorption along adjacent lines of sight different, yielding the required curl in the electric field generated by photoionizations. The key point is that if at some distance from the source adjacent lines of sight are differentiated, then, in the vast majority of cases, they will remain as such and thus magnetic field will be generated at this point and all the way beyond it. This is the reason why, as we will see in the precise calculations below, the magnetized areas generated look like shadows behind inhomogeneities. This mechanism thus naturally generates fields on large scales.

Finally, this mechanism is interesting for Cosmology because it occurs so early in the history of the Universe, when the first sources are only forming. This may impact the subsequent formation of the following generation of stars, which then form in pre-magnetized regions. It is thus important to assess in full detail the strength of the fields generated by this mechanism, which is the purpose of the following.

### 3.2.2 Formally

We are now going to model a source, emitting photons radially, which is surrounded by the IGM, a multi-component plasma. Throughout this chapter and the next one, the usual spherical coordinates $(r, \theta, \varphi)$ will be used, the source being at the origin.

**Procedure** Formally speaking, the idea to model this mechanism is to think back at what the photoionization process consist in. Consider a volume element crossed through by photons emitted by a source. Some photoionizations occur, which not only increase the number of free electrons in the volume element, but free them with a velocity that depends on the energy of the incident photon. Therefore, photoionization modifies both the number density *and the velocity distribution* of electrons in the volume element. Fundamentally this process therefore requires to be modeled through a *kinetic description* of the plasma and of the radiation field. However, Maxwell's equations (2.1) governing the electromagnetic field are macroscopic. Therefore, once we have modeled photoionization at the kinetic level, our task will be to reduce the description to a

| $z$ | $\ell_{\nu_0}$(kpc) | $\ell_{4\nu_0}$(kpc) | $\ell_{10\nu_0}$(kpc) |
|---|---|---|---|
| 30 | 0.0073 | 0.47 | 7.3 |
| 15 | 0.053 | 3.4 | 53 |
| 10 | 0.16 | 11 | 160 |
| 6 | 0.64 | 41 | 640 |

Table 3.1: Orders of magnitude of mean free paths $\ell_\nu \equiv (\bar{n}\sigma_\nu)^{-1}$ (where $\bar{n}(z)$ is the mean gas density of the Universe at redshift $z$ and $\sigma_\nu$ is the photoionization cross section) of photons of frequency $\nu = \nu_0, 4\nu_0$ and $10\nu_0$ at various redshifts during the EoR. These frequencies correspond respectively to the ionization threshold and two typical frequencies of the sources present at EoR, cf. section 3.2.4 for more details.

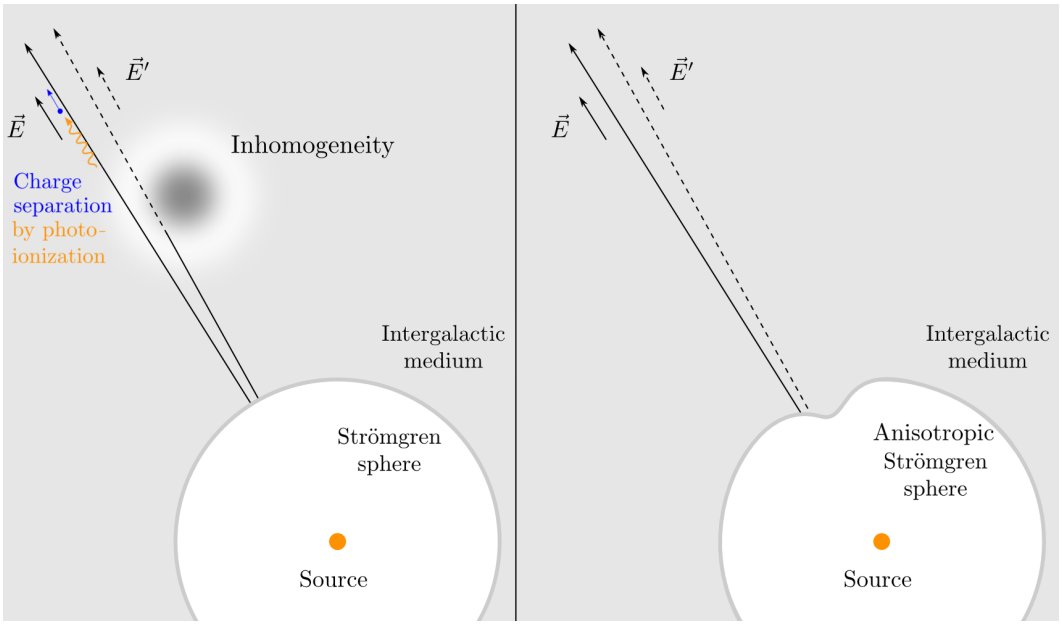


Figure 3.4: Illustration of the mechanism. Left: A luminous source emits photons beyond its Strömgren sphere (white area) into the surrounding globally neutral IGM (gray area). The continuous arrow starting from the edge of the Strömgren sphere to the upper left corner of the figure represents a given line of sight. All along this line of sight, photoionizations occur, one of which is represented in the picture. Each of these photoionizations induces a charge separation which gives rise to an electric field. Because these photoionizations occur continuously and steadily, the electric field is sustained. Now, if the IGM is perfectly homogeneous and the Strömgren sphere spherically symmetric, then all the lines of sight would be equivalent, and the resulting electric field would be curl-free. However, if an overdense region is present in the IGM, it differentiates adjacent lines of sight because the absorption along each of them differs. The electric field then has a non vanishing curl and a magnetic field thus emerges. This is schematically represented in the figure by a second line of sight half continuous half dashed, along which the photoionizations induce an electric field locally equal to $\vec{E}'$ different from the value $\vec{E}$ of its neighboring volume elements. Right: A second configuration favorable to the generation of intergalactic magnetic fields by photoionization is when the Strömgren sphere is anisotropic, even in a homogeneous IGM, because again the key is to differentiate lines of sight. Note that the field is thus naturally generated on large scales, since once two lines of sight differ, they remain different as we keep moving away from the source.

macroscopic one, as presented in chapter 2. But which are the macroscopic quantities we need to compute? Our aim is to compute the magnetic field. To do so, we need to find the equation governing it, which is called the induction equation, and as we will see the induction equation can be obtained by taking the curl of the equation governing the current density $\vec{J}$ in the plasma, which is the Ohm's law.

We will thus proceed as follows: From a kinetic description of the IGM and of the radiation field emitted by the source, we will derive Ohm's law, the curl of which will lead us to the induction equation (3.15) below. This relation contains an additional term compared to the one usually presented and manipulated in the Cosmology literature, namely the term due to photoionizations. For clarity, let me decompose this derivation in four steps.

**Step 1: Describing the fields** Let us adopt a kinetic description of the fields involved.

The radiation field of astrophysical ionizing sources is usually described in terms of the specific spectral density $I_\nu$, which corresponds to the distribution function of photons, with the information on the norm of the momentum given by $\nu$ and its direction by the unit vector $\hat{k} \equiv \vec{k}/k$. For details on the definition of this quantity, see for example Shu (1991) or Rybicki & Lightman (1986). In principle, one should solve the complete radiative transfer equation governing the evolution of $I_\nu$ to get an explicit expression of it, but for our purpose, it is sufficient to consider the following solution to this equation (Shu, 1991):

$$I_\nu(t, \vec{r}, \hat{k}) = L_\nu \, \frac{e^{-\tau_\nu}}{4\pi r^2} \, \delta(\hat{k} - \hat{r}), \tag{3.2}$$

where $L_\nu$ is the spectral luminosity density of the source, $\hat{r}$ is the radial unit vector, $n_{\rm HI}$ the Hydrogen density and

$$\tau_\nu = \sigma_\nu \int_0^r n_{\rm HI} dr \tag{3.3}$$

is the optical depth with $\sigma_\nu$ the photoionization cross section. The $\delta(\hat{k} - \hat{r})$ factor accounts for the fact that the source emits radially and $\frac{1}{4\pi r^2}$ corresponds to the geometric dilution.

The matter fields relevant here are those composing the IGM. Cosmological recombination was an incomplete process: during the Dark Ages, a tiny non zero ionization fraction remained in the IGM. The free electrons and ions from this plasma are usually called residual electrons and residual ions. In addition to them, photoionizations liberate new electrons and ions. In the article of section 3.2.4, we thus consider five different species composing the IGM, namely:

$$\alpha = \begin{cases} 1 : \text{residual electrons;} \\ 2 : \text{residual ions;} \\ 3 : \text{photoionization electrons;} \\ 4 : \text{photoionization ions;} \\ 5 : \text{neutrals.} \end{cases}$$

Each of these matter fields is characterized by its distribution function $f_\alpha$. Each $f_\alpha$ is governed by the following generalized Vlasov equation:

$$\frac{df_\alpha}{dt} = \partial_t f_\alpha|_c + \partial_t f_\alpha|_s \, . \tag{3.4}$$

This is equation (2.8) presented in chapter 2, where now I have decomposed the source term of the right hand side in two parts: the first term corresponds to collisions and the second is the source term due to photoionizations that we are going to explicit in expression (3.13) below. This is in essence the most important equation because this is where the photoionization process is modeled.

**Step 2: Ohm's law** In terms of the quantities defined in the multifluid description of section 2.2, the total current density is simply the sum of the current density of all species, i.e. $\vec{J} = \Sigma \vec{J}_\alpha$ where $\vec{J}_\alpha = q_\alpha n_\alpha \vec{V}_\alpha$. Now since we are delving back into the kinetic description here, this should be rewritten as

$$\vec{J} = \sum_\alpha q_\alpha \int \vec{v} f_\alpha d^3\vec{v}. \tag{3.5}$$

Therefore, we see that it is by taking the first moment of (3.4) weighted by $q_\alpha$, and summing over all species that we may get the equation governing $\vec{J}$. This yields the following generalized Ohm's law:

$$\begin{aligned} &\partial_t \vec{J} + \left(\vec{V}.\vec{\nabla}\right)\vec{J} + \left(\vec{\nabla}\cdot\vec{J}\right)\vec{V} - \vec{V}\vec{V}\cdot\vec{\nabla}\rho \\ &= \Sigma_\alpha \tfrac{q_\alpha^2 n_\alpha}{m_\alpha}\left(\vec{E} + \tfrac{\vec{V}_\alpha \times \vec{B}}{c}\right) - \vec{P} + \vec{C} + \underbrace{\Sigma_\alpha \frac{q_\alpha}{m_\alpha}\dot{\vec{p}}_\alpha}_{\substack{\text{momentum} \\ \text{transfer}}} \end{aligned} \tag{3.6}$$

where the important quantity for the present discussion is the last term, given by

$$\dot{\vec{p}}_\alpha \equiv \int m_\alpha \vec{v}\, \partial_t f_\alpha|_s \, d^3\vec{v}, \tag{3.7}$$

which corresponds to the momentum transfer from photons to species $\alpha$. There is no need to explicit the expressions of the pressure term $\vec{P}$ and the collision term $\vec{C}$ for the present discussion. They can be found in section 3.2.4.

Now, given that we are looking for fields that are initially vanishing and will remain small, we may linearize the full equation (3.6). Then, in the article of section 3.2.4, we justify in detail, estimating each term with orders of magnitude, that given the cosmological length scales and timescales of interest (tens of kpc and tens of Myrs), a certain number of terms may be neglected, so that the relevant expression of the above generalized Ohm's law for our purpose is the simple expression

$$\boxed{\begin{array}{c} \vec{0} = -qn_e\vec{E} - \vec{\nabla}p_e + \dot{\vec{p}}_{\rm pe} \\ \text{where} \quad \dot{\vec{p}}_{\rm pe} = \displaystyle\int m_e\vec{v}\, \partial_t f_{\rm pe}|_s \, d^3\vec{v} \end{array}} \tag{3.8}$$

(Simplified Ohm's Law)

where 'pe' stands for photoionization electrons. Note that delving into this amount of detail in the modeling is not only a way of deriving rigorously the term due to photoionization in the induction equation, but is also the opportunity to reveal interesting subtleties. For instance, as detailed in the article below, $n_e$ in (3.8) is the *total* number density of electrons, while the source term $\dot{\vec{p}}_{\rm pe}$ is due to the newly freed electrons from photoionization only, and the pressure term is due to residual electrons only. Also, we may now interpret the source term $\dot{\vec{p}}_{\rm pe}$ naturally as follows: $\partial_t f_{\rm pe}|_s \, d^3\vec{v}\, d^3\vec{r}\, dt$ is the number of photoelectrons generated in a volume element $d^3\vec{r}$ during $dt$, appearing with momentum $m_e\vec{v}$. Thus $\dot{\vec{p}}_{\rm pe}\, d^3\vec{r}\, dt$ represents the total electron momentum appearing in a volume $d^3\vec{r}$ during $dt$, so that $\dot{\vec{p}}_{\rm pe}$ is a momentum density generation rate. While equation (3.6) has been correctly described many times as a close analogue to Newton's second law, we can see here, however, that the term $\dot{\vec{p}}_{\rm pe}$ is not, in essence, a force density, but a *source* of momentum.

**Step 3: The source term $\dot{\vec{p}}_{\rm pe}$** We still have to explicit this source term as a function of the parameters of the problem. Microscopically, a fraction $f_{\rm mt}$ of the momentum of the incident photon is transferred to the freed electron during photoionization, which may be rewritten as

$$m_e\vec{v} = f_{\rm mt}(\nu)\frac{h\nu}{c}\hat{r}, \tag{3.9}$$

where $f_{\rm mt}$ is frequency dependent, given by Sommerfeld & Schur (1930):

$$f_{\rm mt}(\nu) = \frac{8}{5}\frac{\nu-\nu_0}{\nu}, \tag{3.10}$$

for $\nu > \nu_0$. Note that this fraction may be larger than one, in which case the ions recoil.

Now, by definition $\partial_t f_e|_s \, d^3\vec{v}d^3\vec{r}dt$ is equal to the number of photoelectrons of speed $v$ in direction $\hat{v}$ generated at a position $\vec{r}$ at a time $t$. Since we consider Hydrogen only, each photoionization produces only one electron. This number is thus equal to the number of photoionizations due to photons of frequency $\nu$ in direction $\hat{k} = \hat{v}$ where $\nu$ satisfies (3.9). Finally, consider a simple projectile-target model, in which particles of type A, with density $n_A$ and velocity $v_A$, are incident on particles of type B at rest with density $n_B$. The cross section of the interaction bewteen A and B particles is $\sigma$. Then the number of reactions per unit time and unit volume is given by $n_A v_A n_B \sigma$. In that spirit, we have that the photoionization rate density is the product of the number density of incident photons, the velocity of incident photons, the number density of target Hydrogen atoms and the cross section, so that

$$\partial_t f_e|_s \, d^3\vec{v}d^3\vec{r}dt = \left[n_\gamma^{\rm inc} d\nu d\Omega\right] c\sigma_\nu n_{\rm HI} d^3\vec{r}dt \tag{3.11}$$

where the number density of incident photons of frequency $\nu$ with direction $\hat{k}$ at $\vec{r}$ at time $t$ is

$$n_\gamma^{\rm inc}(t,\vec{r},\hat{k},\nu) = \frac{I_\nu/c}{h\nu} \tag{3.12}$$

by definition of the monochromatic specific intensity. Therefore we model the source term in the expression (3.8) by

$$\partial_t f_e|_s \, d^3\vec{v} = \frac{I_\nu\sigma_\nu}{h\nu} n_{\rm HI} d\nu d\Omega. \tag{3.13}$$

This relation describes the photoionization process at the microscopic level. Plugging it, together with (3.9), into the expression of $\dot{\vec{p}}_{\rm pe}$ in (3.8), we obtain

$$\boxed{\dot{\vec{p}}_{\rm pe} = \frac{n_{\rm HI}}{c}\int_{\nu_0}^{\infty} f_{\rm mt}(\nu)\sigma_\nu L_\nu \frac{e^{-\tau_\nu}}{4\pi r^2} d\nu\ \hat{r}} \tag{3.14}$$

(Macroscopic Source Term)

where $\nu_0$ is the Hydrogen ionization threshold.

**Step 4: Induction equation and Generated Field** The induction equation is then given by the curl of (3.8) with expression (3.14), and may be written, using Faraday's law, as

$$\boxed{\partial_t \vec{B} = \underbrace{-\frac{c}{e}\frac{\vec{\nabla} n_e}{n_e^2} \times \vec{\nabla} p_e}_{\text{Biermann}} + \underbrace{\frac{c}{e n_e}\left[\frac{\vec{\nabla} n_e}{n_e} \times \dot{\vec{p}}_{\rm pe} - \vec{\nabla} \times \dot{\vec{p}}_{\rm pe}\right]}_{\text{Photoionization}}}. \tag{3.15}$$

(Induction Equation)

The first term on the right hand side is the usual Biermann battery term present in the induction equation (3.1), and the two additional terms are due to photoionization. The Biermann term will be discussed in the next section and will not be considered here otherwise. Then integrating (3.15), the magnetic field at time $t$ and position $\vec{r}$ may be written as a sum of two contributions:

$$\boxed{\vec{B}(t,\vec{r}) = \vec{B}_{\rm local} + \vec{B}_{\rm global}} \tag{3.16}$$

(Generated Magnetic Field)

where the 'local' term is

$$\vec{B}_{\rm local} = \int_0^t F^{\rm int}_{\rm local} \vec{F}^{\rm geom}_{\rm local}\ dt \tag{3.17}$$

$$F^{\rm int}_{\rm local} = \frac{1}{q x_e^2}\frac{1}{4\pi r^2}\int_{\nu_0}^{\infty} f_{\rm mt}\sigma_\nu L_\nu e^{-\tau_\nu} d\nu \tag{3.18}$$

$$\vec{F}^{\rm geom}_{\rm local} = \vec{\nabla} x_e \times \hat{r} \tag{3.19}$$

and the 'global' (because it contains an integration over space) term

$$\vec{B}_{\rm global} = \int_0^t F^{\rm int}_{\rm global} \vec{F}^{\rm geom}_{\rm global}\ dt \tag{3.20}$$

$$F^{\rm int}_{\rm global} = \frac{1}{q x_e}\frac{1}{4\pi r^2}\int_{\nu_0}^{\infty} f_{\rm mt}\sigma_\nu^2 L_\nu e^{-\tau_\nu} d\nu \tag{3.21}$$

$$\vec{F}^{\rm geom}_{\rm global} = \vec{\nabla}\left(\int_{r_s}^{r} n_{\rm HI} dr\right) \times \hat{r}. \tag{3.22}$$

where $x_e = \frac{n_e}{n_{\rm HI}}$ is the total electron fraction.

Formally, $\vec{B}_{\rm local}$ and $\vec{B}_{\rm global}$ are both products of two terms, integrated over time: an 'interaction' term $F^{\rm int}$ and a 'geometric' term $\vec{F}^{\rm geom}$. The interaction term characterizes the impact of the source at a time $t$ and a position $\vec{r}$, as it includes the absorption, geometric dilution, the photoionization cross section and the fraction of momentum transferred from photons to electrons. The geometric term however is independent of the properties of the ionizing source and dictates how favorable the spatial configuration of the IGM is for the generation of magnetic field.

Indeed, the $\vec{F}^{\rm geom}_{\rm global}$ term is *precisely* the formal expression of the requirement we have been intuiting in figure 3.4: the cross product shows that what matters are the non radial gradients (i.e. differences between lines of sight) of the column density $\int n_{\rm HI} dr$ (this corresponds to the situation on the left of figure 3.4) or the anisotropy of the Strömgren sphere, because the lower boundary of the integral is $r_s$, which gives rise to a non zero term when $r_s$ has an angular dependence (when the configuration is spherically symmetric, $n_{\rm HI}$ and $r_s$ are functions of $r$ only, so the gradient in $\vec{F}^{\rm geom}_{\rm global}$ is purely radial and thus vanishes due to the cross product). Also, the integration over space translates the fact that if at some distance two adjacent lines of sight differ, they will in general remain different further away from the source. For this reason the global term generates magnetic fields on large distances. Therefore, behind an inhomogeneity, some magnetic field is generated from this global term even if the medium is homogeneous there, and is only attenuated by geometric flux dilution, absorption and the $1/r$ factor from the gradient.

We will consider a homogeneous Reionization scenario and suppose that the ionization contrast vanishes, meaning that the ionization fraction $x_e$ is uniform, so that $\vec{\nabla} x_e$ will be neglected in the following analysis, and we will focus on the $\vec{B}_{\rm global}$ term.

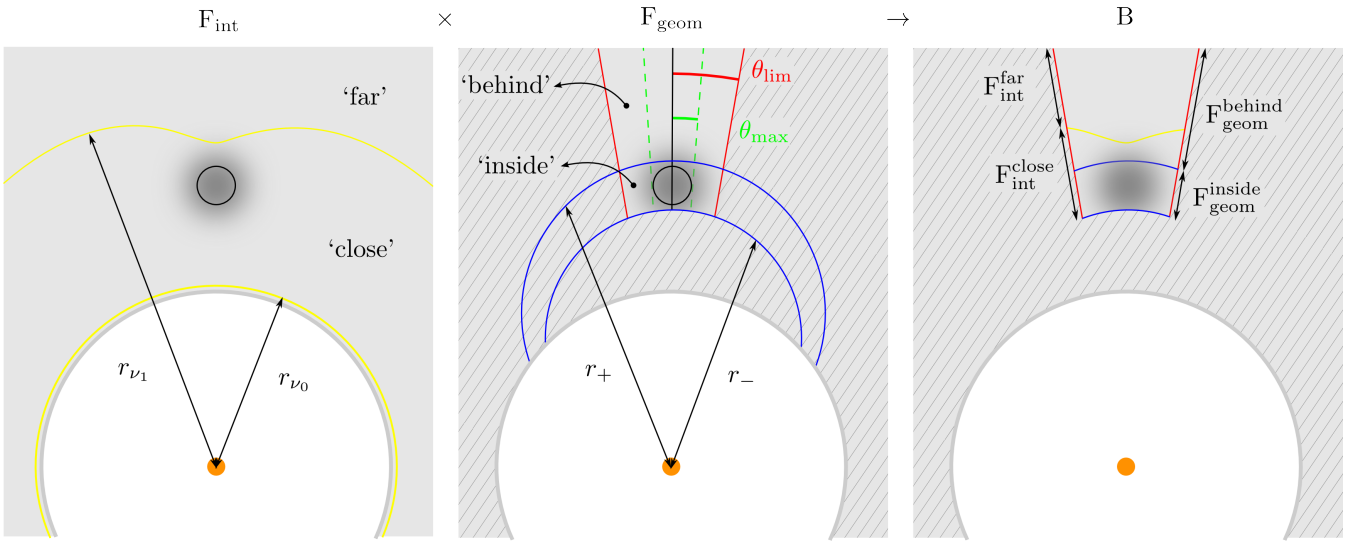


Figure 3.5: Left panel: Magnetic fields may be generated significantly only through inhomogeneities that are 'close enough' to the source for the number of photoionizations to be large enough. Middle panel: Magnetic fields may be generated significantly only where the gradients in the inhomogeneity are large enough and adequately oriented with respect to the direction of incident photons for the overall electric field to be rotational. Right: Magnetic fields are generated in areas in which the constraints described in the left and middle panels are obeyed simultaneously. Hatching indicates regions where the strengths are weakest. See section 3.2.4 for details.

### 3.2.3 Exploring $\vec{B}_{\rm global}$

Let us now explore in detail the term $\vec{B}_{\rm global}$. More precisely, in this section and the next chapter, we will focus, by considering *spherically symmetric* Strömgren spheres by taking $r_s = $ constant, on the contribution in the 'global' term of inhomogeneity in the Hydrogen density ($n_{\rm HI}(\vec{r})$) due to the clumpiness of the Intergalactic medium. The contribution of the anisotropy of the Strömgren sphere ($r_s(\vec{r})$) is something that I am still currently exploring through a numerical approach, and its discussion is deferred to chapter 5. Like in the previous section, I will here summarize the ideas, steps and results of my work. For the details of the calculations, see section 3.2.4.

**Gaussian inhomogeneities** The general expression (3.20) is valid for any density distribution $n_{\rm HI}$, and needless to say that, even by considering $r_s$ as a constant, revealing the characteristic length scales of the transverse part of the gradient of the integral along the line of sight of a general density field is definitely not obvious. Therefore, in order to understand what are the relevant length scales of the problem, I have considered a simple density profile of expression

$$n_{\rm HI}(\vec{r}) = \bar{n}\left(1 + \delta_0 \exp\left(-\frac{(\vec{r}-\vec{D})^2}{2\sigma^2}\right)\right), \tag{3.23}$$

i.e. a homogeneous background containing a Gaussian inhomogeneity of width $\sigma$ and height $\delta_0$, centered at position $\vec{D}$ from the source. The advantage of such a profile is that it constitutes a simple but non trivial model, in the sense that it is characterized by three simple scales ($D$, $\sigma$ and $\delta_0$) and significantly eases calculations, giving access to closed analytical forms, but at the same time it does not present singularities or discontinuities like a top hat profile does at its edge or a profile with a central cusp. Expression (3.23) thus constitutes an interesting toy model which brings to light the essence of the mechanism at once and awakens our intuition for more realistic configurations.

**Identifying the areas of interest** As we have seen, the total expression (3.20) is the product of two contributions, the interaction term and the geometric term. As illustrated in figure 3.5, I have analyzed them separately, by determining their respective characteristic zones.

(i) The interaction term (left panel of figure 3.5) expresses the following. Photons emitted by the source first travel through the Strömgren sphere, in which they have a very low probability of interacting. On the contrary, starting from the edge of the sphere, photons of frequency $\nu$ have a mean free path noted $\ell_\nu$ due to their interaction with the IGM. The most energetic photons of the source, of frequency noted $\nu_1$, are those which may travel furthest. It is thus natural that the magnetic field generation by this mechanism is drastically reduced beyond the distance $r_s + \ell_{\nu_1}$, since few photons reach that far. In the next chapter, I will

call the *'interaction zone'* this shell, of thickness $\ell_{\nu_1}$, around the Strömgren sphere in which the interactions between the source and the IGM is significant.

(ii) The geometric term (middle panel of figure 3.5) is independent of the source, and delimits the area in which the density distribution fulfills the requirement for the electric field to be rotational due to the shape of the inhomogeneity. For the Gaussian profile (3.23) of width $\sigma$ and at distance $D$, the magnetic field is significantly generated only inside the cone[2] of aperture angle

$$\theta_{\text{lim}} = \arcsin\left(\frac{3\sqrt{3}}{2}\frac{\sigma}{D}\right) \tag{3.24}$$

and that the highest values are reached close[3] to the central region of the inhomogeneity (area 'inside' in figure 3.5) with a powerlaw decrease behind that region (area 'behind' in figure 3.5).

These results are very interesting because they enable us to summarize very simply and grasp the properties of the distribution of the fields generated, while they are in essence very complex, given the full equation (3.20). And indeed, this will be the key to computing analytically the statistical properties of such generated fields in chapter 4, since these simple areas will be the only information we will keep to obtain efficient estimates.

**Numerical applications in the Cosmological context** We now have a good grasp of the spatial distribution of the magnetic field corresponding to formula (3.20), but what are the typical numerical values of the strengths resulting from it? We know that the Epoch of Reionization is a very complex era, in which many complicated processes occurred simultaneously, so that to this day there is no simple model which would provide us with the spectrum, the power and the distribution of the various sources present in the Universe during this era, as a function of redshift. Therefore, in the same spirit as with the Gaussian profile above, we are going to consider a very simple model of EoR to explore the range of values reached for $|\vec{B}|$ through this mechanism, and though simple, it will be very enlightening.

Based on our understanding of the EoR briefly presented in section 1.2, let us decompose this epoch into three stages, considering that in each of these redshift ranges a particular type of source dominates, namely

(i) $30 < z < 20$: Clusters of Population III stars (clusters of 'first stars'),

(ii) $20 < z < 10$: Clusters of Population II stars ('first galaxies'),

(iii) $10 < z < 6$: Quasars.

The $z > 30$ epoch corresponds to Dark Ages in which no luminous source is formed yet, and for redshifts below 6 the Universe is fully ionized so that our mechanism ceases to operate. These three types of sources are modeled by powerlaw spectra, i.e. their monochromatic luminosity is of the form

$$L_\nu = L_0\left(\frac{\nu}{\nu_0}\right)^\alpha \quad \text{for } \nu_0 \leq \nu \leq \nu_1, \tag{3.25}$$

and they differ by their value of the spectral index $\alpha$, the cut-off frequency $\nu_1$, and the normalization $L_0$ which accounts for the intrinsic power of the source. Population III star clusters have a very flat spectrum with a cut-off frequency such that they emit only up to UV photons, and they are not very powerful sources. Quasars on the contrary, emit high energy photons (UV and X) and are very powerful. First galaxies are intermediate sources with respect to these two extreme cases. One should keep in mind that the spectra at these epochs are still rather poorly constrained, but the values chosen here (see section 3.2.4) should be typical, and also the tendencies revealed below remain valid independently of the precise numerical values.

As detailed in section 3.2.4, I have performed numerical applications in which I made the various parameters entering the problem vary, namely the properties of the inhomogeneity (position $D$, height $\delta_0$ and width $\sigma$) with various types of sources (spectral index $\alpha$, intrinsic power $L_0$, and cut-off frequency $\nu_1$) at various epochs (redshift $z$). The take home messages are the following.

- Typical strengths are summarized in table 3.2. Naïvely, one would expect the strength of the generated field to be all the more important that the source is powerful, because it then emits more photons, inducing more photoionizations in the IGM. But one should not forget that the more powerful the source, the larger its Strömgren radius, so that photons are all the more *diluted* before reaching the IGM and photoionizing it. For this reason, sources which generate the magnetic fields with the largest strengths on the largest distances are intermediate sources, which constitute *a compromise between photoionizing power and geometric dilution*. In this simple Reionization model, first stars generate large strengths but on small scales (i.e. close to their Strömgren spheres), while quasars generate small strengths but on large scales. *First galaxies* constitute the aforementioned compromise.

[2] Recall that the illustrations of figure 3.5 are axially symmetric about the vertical axis joining the center of the source and the center of the inhomogeneity.

[3] At radius $r = D$ and angle $\theta_{\text{max}} = \arcsin\left(\frac{\sigma}{D}\right)$.

| Source | Redshift | Log $\lvert B\rvert$ (Gauss) | Distance from the ionization front (kpc) |
|---|---|---|---|
| Pop III | 30 | $-19$ | 0.3 |
| | | $-21$ | 1 |
| | 20 | $-19$ | 0.5 |
| | | $-21$ | 1 |
| Primordial galaxy | 20 | $-20$ | 10 |
| | | $-22$ | 15 |
| | 10 | $-21$ | 30 |
| | | $-22$ | 100 |
| Quasar | 10 | $-21$ | 300 |
| | | $-22$ | 1000 |
| | 6 | $-22$ | 500 |
| | | $-23$ | 1500 |

Table 3.2: Typical values obtained through this mechanism in a cosmologically relevant numerical application. The first column corresponds to the various types of sources considered to be dominant at the epochs denoted in the second column. The third column shows the typical strengths of the magnetic fields generated at the distances away from the Strömgren sphere shown in the fourth column. These strengths and distances correspond to the typical values obtained by varying the different properties of the inhomogeneities.

- An additional ingredient has to be taken into account: the environment, i.e. the density of the IGM at the epoch at which the sources evolve, and the abundance of such sources (mean intersource distance). In that respect too, first galaxies constitute an interesting balance. Indeed, first stars appear early (high redshifts), so that they evolve in a dense IGM which is mostly neutral. This favors photoionizations and thus magnetic field generation, but because they are not very powerful, the distances they can magnetize are small compared to their typical intersource distance so that they magnetize only a small fraction of the IGM. Quasars on the contrary, magnetize distances comparable or greater than their mean intersource distance, despite their scarcity, but since they appear towards the end of Reionization, the Hydrogen density is lowered by the global expansion and the IGM has already been partly ionized by the preexisting sources so that their environment prevents them from generating magnetic fields optimally. In that sense, *first galaxies*, which appear at an intermediate epoch and magnetize distances of the order of their separation, constitute another interesting compromise.

- Magnetic fields of higher strengths and on larger distances are generated in *underdense regions*. Indeed, the same process occurs in underdense regions as in overdense ones because what matters to make the electric field rotational are density *gradients*, but in voids photons have longer mean free paths since they are less absorbed, and thus more photoionizations occur further from the sources. Void regions extend the 'interaction zone' of the sources.

- In the absolute, the numerical values of table 3.2 may seem unreasonably small. But as we have seen in section 3.1.2, these values are typical of magnetogenesis models of the cosmological context. Among the numerous magnetogenesis mechanisms of cosmological interest, the relevant one to directly compare the present mechanism with, is the Biermann battery. Indeed, they operate at the same epochs, and often in the same places simultaneously, as one can see in formula (3.15). We must therefore assess when and where one mechanism dominates the other. Their careful comparison was beyond the scope of the paper I am reviewing here, but at the end of the article we put forward arguments advocating that while the Biermann term is most certainly dominant close to the Strömgren sphere, the photoionization mechanism should dominate far from the source where the temperature is low and has large gradients. This particularity is precisely what makes this mechanism interesting when it comes to generating magnetic fields on large cosmological scales.

### 3.2.4 Article

Monthly Notices of the ROYAL ASTRONOMICAL SOCIETY
MNRAS **453,** 345–356 (2015) doi:10.1093/mnras/stv1578

# Intergalactic magnetogenesis at Cosmic Dawn by photoionization

J.-B. Durrive[1,2]★ and M. Langer[1,2]

[1]*Institut d'Astrophysique Spatiale, Bâtiment 121, Univ. Paris-Sud, UMR8617, Orsay, F-91405, France*
[2]*CNRS, Orsay, F-91405, France*

Accepted 2015 July 13. Received 2015 June 11; in original form 2015 April 1

**ABSTRACT**

We present a detailed analysis of an astrophysical mechanism that generates cosmological magnetic fields during the Epoch of Reionization. It is based on the photoionization of the intergalactic medium by the first sources formed in the Universe. First the induction equation is derived, then the characteristic length and time-scales of the mechanism are identified, and finally numerical applications are carried out for first stars, primordial galaxies and distant powerful quasars. In these simple examples, the strength of the generated magnetic fields varies between the order of $10^{-23}$ G on hundreds of kiloparsecs and $10^{-19}$ G on hundreds of parsecs in the neutral intergalactic medium between the Strömgren spheres of the sources. Thus, this mechanism contributes to the premagnetization of the whole Universe before large-scale structures are in place. It operates with any ionizing source, at any time during the Epoch of Reionization. Finally, the generated fields possess a characteristic spatial configuration which may help discriminate these seeds from those produced by different mechanisms.

**Key words:** magnetic fields – intergalactic medium – cosmology: theory – dark ages, reionization, first stars – large-scale structure of Universe.

## 1 INTRODUCTION

The origin of cosmological magnetic fields is a major open question in cosmology. Recent high-energy gamma-ray observations suggest that a substantial fraction, if not the whole, of the intergalactic space is magnetized (e.g. Neronov & Vovk 2010). The current paradigm to account for the existence of such cosmological magnetic fields states that a first mechanism, or several mechanisms combined, generated large-scale magnetic fields but of very weak strengths (so-called seed fields) that were amplified later on, during structure formation, essentially through turbulence (see e.g. Brandenburg & Subramanian 2005; Ryu et al. 2011; Widrow et al. 2011, and references therein). Numerous mechanisms for generating magnetic fields on cosmological scales have been proposed, operating mainly in the primordial Universe, during inflation or the electroweak and quark-hadron phase transitions (e.g. Grasso & Rubinstein 2000; Widrow 2002; Kandus, Kunze & Tsagas 2011, and references therein). However, mechanisms operating in the radiation-dominated era (Harrison 1970; Zakharov & Anikanov 1992) or during recombination (e.g. Berezhiani & Dolgov 2004; Takahashi, Ichiki & Sugiyama 2008; Fenu, Pitrou & Maartens 2011), requiring some level of vorticity (possibly re-generated at the second order in perturbations), have also been proposed. Finally, astrophysical processes operating after recombination, capable of generating magnetic fields of cosmological interest, have been investigated too. They include the well-known Biermann battery, due to a thermal electromotive force, that was first introduced in the context of stars (Biermann 1950) and later successfully considered in cosmological contexts such as structure formation (Pudritz & Silk 1989; Kulsrud et al. 1997; Xu et al. 2008) and the propagation of ionization fronts (Subramanian, Narasimha & Chitre 1994; Gnedin, Ferrara & Zweibel 2000) during Cosmological Reionization. Collision-less shocks in cosmology are also potentially capable of generating magnetic fields by triggering plasma instabilities (e.g. Medvedev, Silva & Kamionkowski 2006; Coroniti 2014) as are return currents induced by cosmic rays (Miniati & Bell 2011). Note that large-scale magnetic fields may actually have been created within galaxies and then transported into the intergalactic medium (IGM) by powerful winds and/or jets (Kronberg, Lesch & Hopp 1999; Furlanetto & Loeb 2001; Beck et al. 2013). Globally, the level at which all these mechanisms may have contributed to the magnetization of the IGM is still an open question (for recent reviews, see e.g. Widrow et al. 2011; Durrer & Neronov 2013; Subramanian 2015) to which future observations with radio interferometers will bring essential pieces of answer (e.g. Bonafede et al. 2015).

Revisiting Langer, Aghanim & Puget (2005), we present here a detailed analysis of an astrophysical mechanism, based on the photoionization of the IGM, bound to have operated during the first billion years of the Universe. Ando, Doi & Susa (2010) and Doi & Susa (2011) explored numerically the same mechanism and compared it to the Biermann battery. However, in their analysis, they focused on the competition between these two mechanisms at the boundaries of self-shielded, essentially neutral clumps embedded

★ E-mail: jdurrive@ias.u-psud.fr

inside the H II regions of individual first stars. In these conditions, they found that the Biermann battery produces stronger magnetic fields than the radiation effects, on hundreds of parsecs scales. Here, we analytically study this mechanism, relying on the momentum transfer from ionizing photons to electrons, on large scales, way outside the Strömgren spheres of clusters of Population III stars, primordial galaxies and quasars.

In this paper, in Section 2 we introduce the mechanism in full generality. Then, in Section 3, we obtain a simplified order of magnitude estimate of the magnetic field strength as well as convenient, although approximate, scaling relations. In Section 4, we analyse in full details the expression obtained in Section 2, apply it to the context of the Epoch of Reionization (EoR) and obtain numerical values of the magnetic fields generated in the IGM by the first luminous sources. Finally, Section 5 is dedicated to a discussion where a comparison with the Biermann battery is also included.

## 2 THE MECHANISM

### 2.1 Presentation

The first sources in the Universe switched on in an essentially neutral IGM, mostly made of hydrogen, below redshifts of 30 (e.g. Loeb & Furlanetto 2013). As they radiated, the sources formed fully ionized regions around them, called Strömgren spheres, created mainly by photons just above the ionization threshold of 13.6 eV. However, higher energy photons were able to escape the Strömgren spheres and propagate deeper into the IGM, because the photoionization mean-free path is proportional to the cube of their energy. As pointed out by Langer et al. (2005), these photons transferred their momentum to electrons in the surrounding, otherwise neutral medium, and thus generated radial currents. These currents were in turn able to induce large-scale magnetic fields, provided the corresponding electric fields were rotational. This condition was actually satisfied thanks to the anisotropic absorption of the radiation due to the inhomogeneities of the neutral IGM.

Formally speaking, the ionization process is described microscopically as a perturbation of the distribution function of electrons. The description is then reduced to a macroscopic monofluid description to get a generalized Ohm's law, the rotational of which leads to the induction equation (Section 2.2). The general expression for the generated magnetic field thus obtained is then examined in a simple model of the cosmological context we are interested in, using power-law spectra for the sources and Gaussian profiles to model the clumpiness of the IGM. This allows us to identify the characteristic properties (characteristic length scales, typical strengths generated and field lines) of the regions that are significantly magnetized (Section 4.3), and then to obtain numerical estimates of these photogenerated magnetic fields (Section 4.4).

### 2.2 Formalism

#### *2.2.1 Fields*

In the non-relativistic limit, displacement currents are negligible, so we consider the following Maxwell's equations:

$$\nabla \times \boldsymbol{B} = \frac{4\pi}{c}\boldsymbol{J} \qquad \nabla \cdot \boldsymbol{B} = 0$$
$$\nabla \times \boldsymbol{E} = -\frac{1}{c}\partial_t \boldsymbol{B} \qquad \nabla \cdot \boldsymbol{E} = \rho$$

where $\boldsymbol{J}$ is the total current density and $\rho$ the total charge density. We will take $\rho = 0$ since the characteristic length scales of the problem are much larger than the Debye length, of the order of the kilometre here. Initially the current, the electric field and the magnetic field are null since we are interested in their ab initio generation.

Cosmological recombination was an incomplete process: during the Dark Ages, a tiny non-zero ionization fraction remained in the IGM. We will call residual electrons and residual ions the free electrons and ions from this plasma. As sources switched on, they photoionized their surroundings thus liberating new electrons and ions. As we will see, it is instructive to consider separately these two types of charged species. Hence we will consider five different species, namely:

$$\alpha = \begin{cases} 1: \text{ residual electrons;} \\ 2: \text{ residual ions;} \\ 3: \text{ photoionization electrons;} \\ 4: \text{ photoionization ions;} \\ 5: \text{ neutrals.} \end{cases}$$

Each of these matter fields is characterized by its distribution function $f_\alpha$. Each $f_\alpha$ is governed by the following generalized Vlasov equation:

$$\partial_t f_\alpha + \boldsymbol{v} \cdot \frac{\partial f_\alpha}{\partial \boldsymbol{r}} + \frac{q_\alpha}{m_\alpha}\left(\boldsymbol{E} + \frac{\boldsymbol{v}\times\boldsymbol{B}}{c}\right)\cdot\frac{\partial f_\alpha}{\partial \boldsymbol{v}} = \partial_t f_\alpha|_{\rm c} + \partial_t f_\alpha|_{\rm s}\,, \tag{1}$$

where $q_\alpha$ is the charge of species $\alpha$ and $m_\alpha$ its mass. On the right hand side, the first term is the usual collision term and the second is the source term due to photoionizations that is detailed in Appendix A.

Astrophysical ionizing sources are characterized by their specific spectral density $I_\nu$. In principle one should solve the complete radiative transfer equation governing the evolution of $I_\nu$, but for our purpose it is enough to consider the following solution to this equation:

$$I_\nu(t, \boldsymbol{r}, \hat{k}) = L_\nu \frac{\mathrm{e}^{-\tau_\nu}}{4\pi r^2}\delta(\hat{k} - \hat{r}), \tag{2}$$

where $L_\nu$ is the spectral luminosity density of the source and $\tau_\nu = \sigma_\nu \int_0^r n_{\rm H\,I}\mathrm{d}r$ is the optical depth with $\sigma_\nu$ the photoionization cross-section. The $\delta(\hat{k} - \hat{r})$ factor accounts for the fact that the source emits radially and $\frac{1}{4\pi r^2}$ corresponds to the geometric dilution.

#### *2.2.2 Induction equation*

This kinetic description is convenient to build the right-hand-side of equation (1), but it contains much more information than needed since we are looking for the macroscopic and summed over all species quantity $\boldsymbol{J}$ appearing in Maxwell's equations. Thus we reduce our description to that of a monofluid (cf. Krall & Trivelpiece 1973, and appendix B) and get the following equation governing $\boldsymbol{J}$, the generalized Ohm's law:

$$\partial_t \boldsymbol{J} + (\boldsymbol{V}\cdot\nabla)\boldsymbol{J} + (\nabla\cdot\boldsymbol{J})\boldsymbol{V} - \boldsymbol{V}\boldsymbol{V}\cdot\nabla\rho = \Sigma_\alpha \frac{q_\alpha^2 n_\alpha}{m_\alpha}\left(\boldsymbol{E} + \frac{V_\alpha \times B}{c}\right) - \boldsymbol{P} + \boldsymbol{C} + \Sigma_\alpha \frac{q_\alpha}{m_\alpha}\dot{\boldsymbol{p}}_\alpha \tag{3}$$

where

$$\dot{\boldsymbol{p}}_\alpha \equiv \int m_\alpha \boldsymbol{v}\ \partial_t f_\alpha|_{\rm s}\,\mathrm{d}^3\boldsymbol{v} \tag{4}$$

and the other terms are detailed in Appendix B. The last term of equation (3) corresponds to the momentum transfer from photons to electrons.

In this paper, we are interested in the generation of magnetic fields in a cosmological context. The typical gradient scales $L$ correspond to the size of matter inhomogeneities in the high-redshift IGM. To get an idea, we can consider $L \sim 10$ kpc. Further, as shown in Langer et al. (2005), on the very short initial times typical of the plasma time-scales, the generated strengths of the fields are negligible, and the next characteristic time is set by the lifetime of the source, typically from 1 to 100 Myr during Reionization. Therefore, when needed, we will take $T \sim 10$ Myr as a typical time-scale. Finally, during Reionization the typical residual electron density is $n_\mathrm{e} \sim 2 \times 10^{-4} \bar{n} = 4 \times 10^{-8}$ cm$^{-3}$ at $z = 9$ (e.g. Seager, Sasselov & Scott 2000). We will use these values in the following order of magnitude estimates.

The general expression (3) may then be simplified as follows.

(i) The time variation of $\boldsymbol{J}$ is completely negligible here. Indeed, combining Maxwell's equations yields $\frac{E}{J} \sim \frac{L^2}{c^2 T}$ so that:

$$\left| \frac{\frac{q^2 n_\mathrm{e}}{m_\mathrm{e}} \boldsymbol{E}}{\partial_t \boldsymbol{J}} \right| \sim \frac{q^2 n_\mathrm{e}}{m_\mathrm{e} c^2} L^2 \sim 10^{25} \gg 1 \tag{5}$$

where $q$ is the elementary charge.

(ii) Since displacement currents are neglected, $\boldsymbol{J}$ has a rotational form from Maxwell's equations, so $\nabla \cdot \boldsymbol{J} = 0$ here.

(iii) Starting from zero, $\boldsymbol{J}$, $\boldsymbol{E}$, and $\boldsymbol{B}$ are first-order terms initially and we can therefore linearize equation (3). Note that the generated magnetic field strengths will be small enough for this linearization to remain valid during the time-scales of interest.

(iv) Fluids with protons are assumed to move slowly. Thus $\boldsymbol{V}_\alpha$ for ionic species are first-order terms. Since $\boldsymbol{J}$ and $\boldsymbol{B}$ are also of first order and $m_\mathrm{e} \ll m_i$, the second term on the right-hand side of (3) is a second-order term and is neglected.

(v) For the pressure term, we assume the $\nabla \cdot \boldsymbol{P}_\alpha^\mathrm{CM}$ for protonic species ($\alpha = 2$, 4, and 5) is small due to their large inertia. For residual electrons, we neglect viscosity effects ensuring an isotropic pressure tensor. Photoelectrons, however, are generated radially, thus introducing a small anisotropy, but we neglect this with respect to the pressure gradients of residual electrons. Hence:

$$\boldsymbol{P} = -\frac{q}{m_\mathrm{e}} \nabla p_\mathrm{e}, \tag{6}$$

where $p_\mathrm{e}$ is the residual electron pressure.

(vi) For the collision term, numerous types of collisions could in principle be considered given all the species involved. However, it would prove unnecessary since all the collision frequencies are far too small and therefore the associated time-scales far too large with respect to $T$. More precisely, taking the usual linear approximation $\boldsymbol{C} = \nu_\mathrm{c} \boldsymbol{J}$, where $\nu_\mathrm{c}$ is an averaged collision frequency, and comparing this term for example to the electric field in the plasma yields

$$\left| \frac{\boldsymbol{E}}{\frac{m_\mathrm{e}}{q^2 n_\mathrm{e}} \boldsymbol{C}} \right| \sim \frac{q^2 n_\mathrm{e}}{m_\mathrm{e}} \frac{L^2}{c^2} \frac{\nu_\mathrm{c}^{-1}}{T} \sim 3 \times 10^{14} \left( \frac{\nu_\mathrm{c}}{10^{-4} \mathrm{Hz}} \right)^{-1}. \tag{7}$$

Since typical values for collision frequencies hardly exceed $10^{-4}$ Hz, this ratio is always huge.

(vii) In the last term of equation (3), the dominant and essential contribution comes from the momentum exchange between ionizing photons and photoelectrons. Other contributions are negligible because of the large inertia of protons and neutrals, and the Thomson scattering cross-section which is many orders of magnitude smaller than the photoionization cross-section. This last term therefore reduces to

$$\dot{\boldsymbol{p}}_\mathrm{pe} = \int m_\mathrm{e} \boldsymbol{v} \, \partial_t f_\mathrm{pe} \big|_\mathrm{s} \, \mathrm{d}^3 \boldsymbol{v} \tag{8}$$

where 'pe' stands for photoelectrons. This expression may be interpreted as follows: $\partial_t f_\mathrm{pe} \big|_\mathrm{s} \, \mathrm{d}^3 \boldsymbol{v} \, \mathrm{d}^3 \boldsymbol{r} \, \mathrm{d}t$ is the number of photoelectrons generated in a volume element $\mathrm{d}^3 \boldsymbol{r}$ during $\mathrm{d}t$, appearing with momentum $m_\mathrm{e} \boldsymbol{v}$. Thus $\dot{\boldsymbol{p}}_\mathrm{pe} \, \mathrm{d}^3 \boldsymbol{r} \, \mathrm{d}t$ represents the total electron momentum appearing in a volume $\mathrm{d}^3 \boldsymbol{r}$ during $\mathrm{d}t$. Equation (8) is a momentum density generation rate. While equation (3) has been correctly described many times as a close analogue to Newton's second law, we stress, however, that the term (8) is not, in essence, a force density, but a *source* of momentum. Further, as detailed in Appendix A, expression (8) may be explicated as

$$\dot{\boldsymbol{p}}_\mathrm{pe} = \frac{n_\mathrm{H\,I}}{c} \int_{\nu_0}^{\infty} f_\mathrm{mt}(\nu) \sigma_\nu L_\nu \frac{\mathrm{e}^{-\tau_\nu}}{4\pi r^2} \mathrm{d}\nu \, \hat{r} \tag{9}$$

where $f_\mathrm{mt}$ is the fraction of momentum transferred from a photon to an electron in the photoionization process, and $\nu_0$ is the hydrogen ionization threshold.

Finally, under these assumptions, Ohm's law (3) simplifies to

$$\boldsymbol{0} = -q n_\mathrm{e} \boldsymbol{E} - \nabla p_\mathrm{e} + \dot{\boldsymbol{p}}_\mathrm{pe}. \tag{10}$$

Note that $n_\mathrm{e}$ is the total number density of electrons, but the source term $\dot{\boldsymbol{p}}_\mathrm{pe}$ is only due to the newly photoionized electrons, and the pressure term is only due to residual electrons. Furthermore, we emphasize again that this equation does not correspond to the balance of forces acting on single electrons (Ando et al. 2010; Doi & Susa 2011), but it rather expresses the readjustment of the electric field in the plasma in response to the apparition of new currents from photoelectrons.

The induction equation is then given by the curl of (10), and may be written, using Faraday's law, as

$$\partial_t \boldsymbol{B} = -\frac{c}{q} \frac{\nabla n_\mathrm{e}}{n_\mathrm{e}^2} \times \nabla p_\mathrm{e} + \frac{c}{q n_\mathrm{e}} \left( \frac{\nabla x_\mathrm{e}}{x_\mathrm{e}} \times \dot{\boldsymbol{p}}_\mathrm{pe} + \nabla \int_{r_\mathrm{s}}^{r} n_\mathrm{H\,I} \mathrm{d}r \times \dot{\boldsymbol{q}}_\mathrm{pe} \right) \tag{11}$$

where $x_\mathrm{e} = \frac{n_\mathrm{e}}{n_\mathrm{H\,I}}$ is the total electron fraction, and $\dot{\boldsymbol{q}}_\mathrm{pe}$ has the same expression as $\dot{\boldsymbol{p}}_\mathrm{pe}$ in (9) but with $\sigma_\nu^2$ instead of $\sigma_\nu$ in the integrand. The first term on the right-hand side is the usual Biermann battery term and the two additional terms are due to photoionization. The Biermann term will be discussed in Section 5 and will not be considered here otherwise. Then integrating (11), the magnetic field at time $t$ and position $\boldsymbol{r}$ may be written as a sum of two contributions:

$$\boldsymbol{B}(t, \boldsymbol{r}) = \boldsymbol{B}_\mathrm{local} + \boldsymbol{B}_\mathrm{global} \tag{12}$$

where the 'local' term is

$$\boldsymbol{B}_\mathrm{local} = \int_0^t F_\mathrm{local}^\mathrm{int} \boldsymbol{F}_\mathrm{local}^\mathrm{geom} \, \mathrm{d}t \tag{13}$$

$$F_\mathrm{local}^\mathrm{int} = \frac{1}{q x_\mathrm{e}^2} \frac{1}{4\pi r^2} \int_{\nu_0}^{\infty} f_\mathrm{mt} \sigma_\nu L_\nu \mathrm{e}^{-\tau_\nu} \mathrm{d}\nu \tag{14}$$

$$\boldsymbol{F}_\mathrm{local}^\mathrm{geom} = \nabla x_\mathrm{e} \times \hat{r} \tag{15}$$

and the 'global' term

$$\boldsymbol{B}_\mathrm{global} = \int_0^t F_\mathrm{global}^\mathrm{int} \boldsymbol{F}_\mathrm{global}^\mathrm{geom} \, \mathrm{d}t \tag{16}$$

$$F^{\rm int}_{\rm global} = \frac{1}{q x_{\rm e}} \frac{1}{4\pi r^2} \int_{\nu_0}^{\infty} f_{\rm mt} \sigma_\nu^2 L_\nu {\rm e}^{-\tau_\nu} {\rm d}\nu \tag{17}$$

$$\boldsymbol{F}^{\rm geom}_{\rm global} = \nabla \left( \int_{r_{\rm s}}^{r} n_{\rm H_I} {\rm d}r \right) \times \hat{r}. \tag{18}$$

Formally, $\boldsymbol{B}_{\rm local}$ and $\boldsymbol{B}_{\rm global}$ are both products of two terms, integrated over time: an 'interaction' term $F^{\rm int}$ and a 'geometric' term $\boldsymbol{F}^{\rm geom}$. The interaction term characterizes the impact of the source at a time $t$ and a position $\boldsymbol{r}$ as it includes the absorption, geometric dilution, the photoionization cross-section and the fraction of momentum transferred from photons to electrons. The geometric term determines whether gradients in the IGM are indeed non-radial as required, independently of the properties of the ionizing source.

Physically, one can interpret (12) in the following way. The charge separation induced by photoionizations generates an electric field in the plasma satisfying the equilibrium (10). For a magnetic field to grow out of it, the electric field must have a non-vanishing curl.

To see how this condition may be fulfilled, consider two adjacent volume elements at a given distance from the source. In both volume elements, the equilibrium (10) is satisfied and dictates the value of the electric field there. Forgetting about the pressure term in this discussion, we see that $\boldsymbol{E}$ depends on two things: the local density of electrons $n_{\rm e}$, and the local ability $\dot{\boldsymbol{p}}_{\rm pe}$ of the source to photoionize the medium. Thus, there are three ways for $\boldsymbol{E}$ to be different in the two volume elements: (i) they have the same $\dot{\boldsymbol{p}}_{\rm pe}$ but different $n_{\rm e}$; (ii) they have the same $n_{\rm e}$ but different $\dot{\boldsymbol{p}}_{\rm pe}$; and (iii) both $n_{\rm e}$ and $\dot{\boldsymbol{p}}_{\rm pe}$ are different. Situation (i) may occur if the electron density of the plasma is locally inhomogeneous. The resulting magnetic field is the local term (13). Situation (ii) occurs when the incident distribution of photons is inhomogeneous, that is when the radiation field is anisotropic. But since the source itself emits isotropically by assumption, the only origin of such anisotropies are inhomogeneities in the medium in which photons propagate, so that absorptions along adjacent lines of sight differ. Therefore, (ii) occurs due to non-radial gradients of the column densities, which gives rise to the global term (16). Finally, situation (iii) corresponds to the general case in which everything is inhomogeneous and yields the total magnetic field (12).

Note that if at some distance two adjacent lines of sight differ, they will in general remain different further away from the source. For this reason the global term generates magnetic fields on large distances. Therefore, behind an inhomogeneity, some magnetic field is generated from this global term even if the medium is homogeneous there, and is only attenuated by geometric flux dilution, absorption and the $1/r$ factor from the gradient.

## 3 ORDER OF MAGNITUDE

First, to get an intuition of the efficiency of this mechanism, let us provide a crude estimate of the reached magnetic strengths by evaluating expression (16) in the typical case of a primordial galaxy at $z = 10$. For this, as detailed in Sections 4.1 and 4.2, we consider the following parameters. We assume that the source has a Strömgren radius $r_{\rm s} \sim 48$ kpc, a spectral index $\alpha = -2$, a lifetime $t_{\rm s} = 100$ Myr, and a total UV luminosity $L^{\rm UV}_{\rm tot} = \int_{\nu_0}^{\infty} L_\nu {\rm d}\nu = 2.5 \times 10^7 {\rm L}_\odot$. At those epochs, the ionized fraction of the IGM is $x_{\rm e} \simeq 2 \times 10^{-4}$ while its mean density is $\bar{n} \simeq 2.5 \times 10^{-4}$ cm$^{-3}$. For the generation of electric fields possessing a curl, we consider that an inhomogeneity of amplitude $\delta_0 = 4$ is positioned at a distance $D \sim 1.3 r_{\rm s}$ from the source. For illustration, the magnetic field strength is evaluated at a distance $r = r_{\rm s} + \ell_{3\nu_0}$ from the source, where $\ell_{3\nu_0} = 27\,\ell_{\nu_0}$ is the mean-free path of photons of energy three times the hydrogen ionization threshold. Finally, the strength of the magnetic seed keeps on growing linearly in time as long as the momentum exchange process between photons and initially bound electrons is active. The photons we are interested in here being way above the hydrogen ionization threshold, they do not induce any significant expansion of the Strömgren sphere (see discussions on $t_{\rm rec}$ and $t_i$ in the next section), but instead propagate outside deep into the neutral IGM. Thus, the limiting time-scale for the process to operate is essentially the lifetime of the ionizing source $t_{\rm s}$.

To get a simple expression of (16), let us now take advantage of the strong dependence on $\nu$ in the optical depth to approximate absorption in the interaction term by a Heaviside function: ${\rm e}^{-\tau_\nu} \simeq \theta(\nu - \nu_{\rm c})$, where $\nu_{\rm c}$ is such that $\tau_{\nu_{\rm c}} = 1$. Then

$$\nu_{\rm c}(t, \boldsymbol{r}) = \nu_0 \left( \sigma_0 \int n_{\rm H_I} {\rm d}r \right)^{1/3} \simeq \nu_0 \left( \frac{r - r_{\rm s}}{\ell_{\nu_0}} \right)^{1/3}, \tag{19}$$

where the approximation assumes a homogeneous background. Considering in addition a power-law spectrum as in (22) on $[\nu_0, \infty]$ and using the fact that $r - r_{\rm s} \gg \ell_{\nu_0}$ yield

$$F^{\rm int}_{\rm global} \sim \frac{8}{35} \frac{\sigma_0^2 L^{\rm UV}_{\rm tot}}{q x_{\rm e}} \frac{1}{4\pi r^2} \left( \frac{r - r_{\rm s}}{\ell_{\nu_0}} \right)^{-7/3}. \tag{20}$$

Finally, to estimate the contribution of the geometrical term, we consider a spherical inhomogeneity of characteristic size $\sigma$ and amplitude $\delta_0$. Then $|\boldsymbol{F}^{\rm geom}_{\rm global}| = \frac{1}{r} \partial_\theta \int n_{\rm H_I} {\rm d}r$, where only the inhomogeneous part $\bar{n}\delta_0$ of the density matters, the angular variation is of the order of the angular diameter $\sigma/D$, and the integral along the line of sight is essentially the size of the inhomogeneity $\sigma$. Hence $|\boldsymbol{F}^{\rm geom}_{\rm global}| \sim \bar{n}\delta_0 \frac{D}{r}$. We may then plug in the numerical values mentioned above and get

$$|B| \sim 8 \times 10^{-20} {\rm G} \left( \frac{\delta_0}{4} \right) \left( \frac{L^{\rm UV}_{\rm tot}}{2.5 \times 10^7 {\rm L}_\odot} \right) \left( \frac{t_{\rm s}}{10^8\ {\rm yr}} \right). \tag{21}$$

This rapid estimate provides interesting information on the typical magnetic strength one might expect from this mechanism. In particular, it shows that momentum transfer from photons to electrons during Reionization is capable of producing fields with similar intensities as the usual thermal Biermann battery. However, the strength of the field strongly depends on the geometry and position of the inhomogeneity. Angularly, it is essentially governed by the geometrical term and radially by the interaction term, so that a strength of this order is reached only in specific regions.

Additionally, in accordance with intuition, expression (21) also shows that stronger gradients (i.e. larger inhomogeneities) will create stronger fields, and that longer-lived sources are better at creating stronger magnetic seed fields. Moreover, it indicates that the reached magnetic strength grows linearly with the UV luminosity of the ionizing source, suggesting that quasars may have produced stronger fields than faint primordial galaxies. However, the latter conclusion is actually incorrect. Indeed, as we detail below, the dependence on the physical parameters is more involved than what equation (21) suggests. For example, increasing the luminosity of the source increases not only the number of photons efficient at yielding a larger $B$, but also the number of photons at the hydrogen ionization threshold, leading to a bigger Strömgren sphere (though the dependency of $r_{\rm s}$ on $L^{\rm UV}_{\rm tot}$ is weak). Thus, in that case, the regions that get magnetized are actually more distant from the source, and the geometrical dilution of photons must be properly taken into account in order to get the correct estimate of $|B|$. Hence a careful and detailed analysis of (12) is necessary, which is the purpose of the following section.

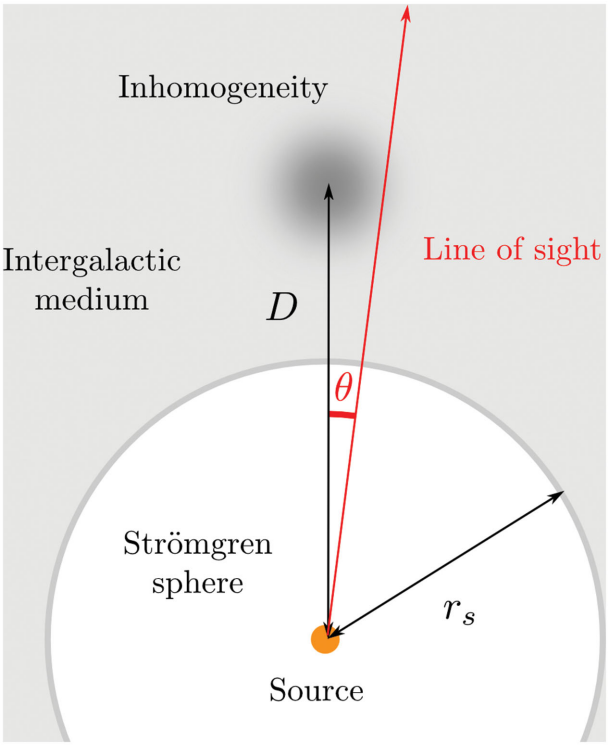


**Figure 1.** Representation of the modelled situation. A source forms a Strömgren sphere of radius $r_s$. An inhomogeneity in the IGM is situated at a distance $D$ from the source. All the graphs in this paper are plotted along the line of sight corresponding to $\theta = \theta_{\max}$ defined by equation (34).

## 4 APPLICATION AT COSMIC DAWN

The analytical formula of the magnetic field (12) we obtained is in principle applicable during Reionization in the vicinity of any ionizing source embedded in an arbitrarily inhomogeneous neutral medium. To gain further insight and obtain numerical estimates, we now apply this expression to some simple models, considering specific sources and a mildly non-linear inhomogeneity outside their Strömgren sphere, as represented in Fig. 1.

### 4.1 Sources of ionizing photons

We consider the three different types of sources that are believed to have driven Reionization: (clusters of) Population III stars, primordial galaxies, and high redshift quasars (QSOs). For simplicity, each source is characterized by a power-law luminosity, with normalization $L_0$ and spectral index $\alpha$ in a certain frequency range:

$$L_\nu = L_0 \left(\frac{\nu}{\nu_0}\right)^\alpha \text{ for } \nu \in [\nu_0, \nu_1] \tag{22}$$

where we will call $\nu_1$ the cut-off frequency. For quasars, we take $\alpha \sim -1.7$, $\nu_1 = 100\nu_0$ and a total luminosity of $10^{12}\mathrm{L}_\odot$ which fixes $L_0$ (e.g. Shang et al. 2011). Values for the other sources were based on the currently available synthetic spectra from the Yggdrasil model[1] (Zackrisson et al. 2011), which uses the Schaerer (2002) and Raiter, Schaerer & Fosbury (2010) single stellar populations for Population III stars, differing by their initial mass functions (IMF). We used the PopIII.1 model for Population III clusters, a zero-metallicity population with an extremely top-heavy IMF (50–500 $\mathrm{M}_\odot$, Salpeter slope), from which we obtained $\alpha \sim -0.3$, $\nu_1 = 4\nu_0$ and $L_0 = 10^{20}$ erg s$^{-1}$ Hz$^{-1}$. For primordial galaxies we considered Population II stars with a Kroupa IMF and metallicity $Z \in [0.0004, 0.008]$, which yields $\alpha \sim -2$, $\nu_1 = 4\nu_0$ and $L_0 = 3 \times 10^{25}$ erg s$^{-1}$ Hz$^{-1}$. In practice, we checked that our results do not depend on metallicity. From Martini (2004), we assumed quasars to live about 100 Myr. For Pop III clusters and first galaxies, we considered constant star formation rates for 100 Myr.

For simplicity the Strömgren spheres of the sources are taken spherically symmetric. In reality, they are far from symmetric, exhibiting often a 'butterfly' shape in numerical simulations (e.g. Ciardi et al. 2001), so that $r_\mathrm{s} = r_\mathrm{s}(\theta, \varphi)$ in principle. In this case, the lower boundary of the integral defining the column density in equation (18) varies spatially. In this first approach we neglect these angular variations. The magnitude of the radius of Strömgren spheres depends on whether the recombination rate is sufficient to reach the steady state. The recombination time-scale is $t_\mathrm{rec} = (\alpha_B \bar{n} C)^{-1}$, where $\bar{n}$ is the mean hydrogen density, $\alpha_\mathrm{B} = 2.6 \times 10^{-13}$ cm$^3$ s$^{-1}$ is the case B recombination coefficient at a gas temperature of $10^4$ K and $C(z)$ is the hydrogen clumping factor. This factor is still poorly constrained, and we adopt the fit $C(z) = 27.466 \exp(-0.114z + 0.001328z^2)$ obtained from simulations by Mellema et al. (2006). We note that the values of the clumping factor are somewhat sensitive to its definition (e.g. Finlator et al. 2012), but they remain of the same order of magnitude. In our redshift range, this yields $t_\mathrm{rec} \sim 10$ Myr while our sources live 100 Myr so, for simplicity, we considered the following expression of the Strömgren radius

$$r_\mathrm{s} = \left(\frac{3\dot{N}_\mathrm{ion}}{4\pi\alpha_B C \bar{n}_\mathrm{HI}^2}\right)^{1/3}, \tag{23}$$

where the rate of ionizing photons emitted by the source is $\dot{N}_\mathrm{ion} = \int_{\nu_0}^{\infty} \frac{L_\nu}{h\nu} \mathrm{d}\nu$. Finally, outside Strömgren spheres, Thomson scattering is negligible since in neutral regions its cross-section is by numerous orders of magnitude smaller than that of photoionization.

### 4.2 Intergalactic medium

For simplicity, we neglect the contribution of the first helium ionization and we consider a homogeneous Reionization scenario. We thus suppose that the ionization contrast $\delta_x$ vanishes, meaning that the ionization fraction $x_\mathrm{e}$ is uniform, so that $\nabla x_\mathrm{e} = \mathbf{0}$. In the rest of the paper, we will therefore focus only on the global term in equation (12).

The dynamical behaviour of baryons in the IGM is governed by

$$\frac{\mathrm{d}n_\mathrm{e}}{\mathrm{d}t} = \Gamma_\mathrm{p} n_\mathrm{HI} - \alpha_B n_\mathrm{e}^2 = -\frac{\mathrm{d}n_\mathrm{HI}}{\mathrm{d}t} \tag{24}$$

where the photoionization rate at a distance $\boldsymbol{r}$ from the source is

$$\Gamma_\mathrm{p}(t, \boldsymbol{r}) = \frac{1}{4\pi r^2} \int_{\nu_0}^{\infty} \frac{\sigma_\nu}{h\nu} L_\nu \mathrm{e}^{-\tau_\nu} \mathrm{d}\nu. \tag{25}$$

Outside the Strömgren sphere, since recombinations are negligible, the variation time-scale of the densities $n_\mathrm{HI}$ and $n_\mathrm{e}$ is the ionization time-scale $t_i = \Gamma_\mathrm{p}^{-1}$, which depends on the distance from the source. These densities may be considered constant wherever $t_i/t_\mathrm{s}$ is smaller than one. The distance at which $t_i = t_\mathrm{s}$ is indicated by a vertical dashed line in Figs 4, 6 and 7. To the right of this line, the assumption of constant $n_\mathrm{HI}$ and $n_\mathrm{e}$ is perfectly safe. Between $r_\mathrm{s}$ and this distance, their variation is not negligible in principle, but note that this line lies, in the vast majority of cases, very close to the Strömgren

[1] http://www.astro.uu.se/~ez/

**Table 1.** Orders of magnitude of mean-free paths of photons of frequency $\nu = \nu_0$, $4\nu_0$ and $10\nu_0$ at various redshifts during the EoR.

| $z$ | $\ell_{\nu_0}$(kpc) | $\ell_{4\nu_0}$(kpc) | $\ell_{10\nu_0}$(kpc) |
|---|---|---|---|
| 30 | 0.0073 | 0.47 | 7.3 |
| 15 | 0.053 | 3.4 | 53 |
| 10 | 0.16 | 11 | 160 |
| 6 | 0.64 | 41 | 640 |

radius. Therefore, the assumption of constant $n_{\rm H\,I}$ and $n_{\rm e}$ does not significantly affect the values of the magnetic field beyond this line.

To model simply the inhomogeneous IGM in which the source is embedded, we consider an inhomogeneity next to the Strömgren sphere, centred at a position $\boldsymbol{D}$ from the source (cf. Fig. 1), with various profiles. The first simple profile consists in a Gaussian inhomogeneity

$$n_{\rm H\,I} = \bar{n}\left(1 + \delta_0 \mathrm{e}^{-\frac{(r-D)^2}{2\sigma^2}}\right), \tag{26}$$

which is an overdensity for $\delta_0 > 0$ and an underdensity for $-1 \leq \delta_0 < 0$. Such a Gaussian overdensity may result from gravitational instability, but inhomogeneities may also form through thermal instability, collecting the surrounding matter, in which case the overdensity is surrounded by an underdense region. Hence a second simple model of inhomogeneity, which we will call hereafter a 'Mexican hat' profile (MH), composed of two imbricated Gaussians, a small width overdensity $\delta_0^+ > 0$ inside an extended width underdensity $\delta_0^- < 0$:

$$n_{\rm H\,I} = \bar{n}\left(1 + \delta_0^+ \mathrm{e}^{-\frac{(r-D)^2}{2\sigma_+^2}} + \delta_0^- \mathrm{e}^{-\frac{(r-D)^2}{2\sigma_-^2}}\right). \tag{27}$$

Mass conservation $\int (n_{\rm H\,I} - \bar{n})\,\mathrm{d}^3 r = 0$ then gives the constraint $\delta_0^+\sigma_+ + \delta_0^-\sigma_- = 0$.

### 4.3 The global term

In order to analyse in detail expression (16) and explicit its characteristics, we now consider an inhomogeneity with a Gaussian profile together with a source with a power-law spectrum. Given the importance of the mean-free path of photons in this model, we recall some typical orders of magnitude in Table 1, for frequencies typical of the ionizing photons emitted by the sources participating to the EoR.

#### *4.3.1 The interaction term*

As we have seen in equation (16), the strength of the magnetic field depends on two criteria: the intensity of the interaction of photons at a given distance, quantified by $F_{\rm int}$, and on the geometry of the situation, quantified by $F_{\rm geom}$. Let us first focus on the former. For a power-law spectrum (22), with the change of variable $y = \tau_\nu$, the interaction term reads

$$F_{\rm int} = \xi(r)\left(\frac{\gamma(\frac{6-\alpha}{3},\tau_{\nu_1}) - \gamma(\frac{6-\alpha}{3},\tau_{\nu_0})}{\tau_{\nu_0}^{\frac{6-\alpha}{3}}} - \frac{\gamma(\frac{5-\alpha}{3},\tau_{\nu_1}) - \gamma(\frac{5-\alpha}{3},\tau_{\nu_0})}{\tau_{\nu_0}^{\frac{5-\alpha}{3}}}\right), \tag{28}$$

where $\gamma$ is the lower incomplete gamma function. To lighten the expressions we have set $\xi(r) \equiv \frac{1}{q x_{\rm e}} \frac{8}{5} \frac{1}{4\pi r^2} \frac{(\sigma_0)^2 L_0 \nu_0}{3}$ and dropped the 'global' exponent from now on.

Now define $r_{\nu_0}$ the distance from the source at which $\tau_{\nu_0} = 1$, and $r_{\nu_1}$ such that $\tau_{\nu_1} = 1$. Note that they roughly correspond to the mean-free paths $\ell_{\nu_i}$ from the Strömgren sphere, $r_{\nu_i} \sim r_{\rm s} + \ell_{\nu_i}$, with equality for $\delta_0 \ll 1$. Then, three regions may be defined in the interaction term (cf. left panel of Fig. 2) namely: 'very close' to ($r_{\rm s} \leq r \ll r_{\nu_0} \ll r_{\nu_1}$), 'close' to ($r_{\nu_0} \ll r \ll r_{\nu_1}$) and 'far' from ($r_{\nu_0} \ll r_{\nu_1} \ll r$) the Strömgren sphere. Given the smallness of $\ell_{\nu_0}$ (cf. Table 1), the 'very close' regime is not relevant for our purpose here as it lies within the width of the Strömgren radius.

In the 'close' region, the interaction term (28) simplifies to

$$F_{\rm int}^{\rm close} = \xi(r)\left(\frac{\Gamma\left(\frac{5-\alpha}{3}\right)}{\tau_{\nu_0}^{\frac{5-\alpha}{3}}} - \frac{\Gamma\left(\frac{6-\alpha}{3}\right)}{\tau_{\nu_0}^{\frac{6-\alpha}{3}}}\right) \tag{29}$$

while 'far' from the Strömgren sphere

$$F_{\rm int}^{\rm far} = \xi(r)\left(1 - \frac{\nu_0}{\nu_1}\right)\left(\frac{\nu_1}{\nu_0}\right)^{\alpha-5} \frac{\mathrm{e}^{-\tau_{\nu_1}}}{\tau_{\nu_1}}. \tag{30}$$

In other words, the source has a certain 'impact zone' (the 'close' region) inside which its ionizing photons are numerous enough to interact significantly. Outside this region, the strength of the field decreases exponentially.

#### *4.3.2 The geometric term*

Let us now focus on the second factor of expression (16). To see precisely what the requirement of a favourable geometrical condition consists of, let us consider the simple case of a Gaussian inhomogeneity (26). In spherical coordinates as in Fig. 1, the geometric term reads

$$F_{\rm geom} = -\frac{\sqrt{2}\sigma\bar{n}\delta_0}{r} F_1\left(\sin\theta\frac{D}{\sigma}\right) \times \left[F_2\left(\frac{r - \cos\theta D}{\sigma}\right) - F_2\left(\frac{r_{\rm s} - \cos\theta D}{\sigma}\right)\right] \tag{31}$$

where

$$F_1(x) \equiv \frac{x}{\sqrt{2}} \mathrm{e}^{-\frac{x^2}{2}} \tag{32}$$

and

$$F_2(x) \equiv \mathrm{e}^{-\frac{x^2}{2}} - \sqrt{\frac{\pi}{2}} \cos\theta \frac{D}{\sigma} \operatorname{erf}\left(\frac{x}{\sqrt{2}}\right). \tag{33}$$

As far as the angular dependence is concerned, it is dominated by the $F_1$ factor which is itself characterized by the two angles:

$$\theta_{\rm max} = \arcsin\left(\frac{\sigma}{D}\right) \tag{34}$$

$$\theta_{\rm lim} = \arcsin\left(\frac{3\sqrt{3}}{2}\frac{\sigma}{D}\right) \tag{35}$$

where $\theta_{\rm max}$ is the angle corresponding to the maximum of the function $F_1(\sin\theta\frac{D}{\sigma})$ and $\theta_{\rm lim}$ is the angle for which the tangent at the inflexion point goes to zero. For angles larger than $\theta_{\rm lim}$, the strength of the interaction term is very strongly decreasing so that we will only consider lines-of-sight such that $\theta \in [-\theta_{\rm lim}, \theta_{\rm lim}]$.

For the radial dependence, defining

$$r_\pm(\theta) = \cos\theta D \pm \sqrt{2}\sigma, \tag{36}$$

three regions may be distinguished (cf. central panel of Fig. 2) namely: 'in front of' ($r_{\rm s} \leq r \ll r_-$), 'inside' ($r_- \ll r \ll r_+$) and 'behind' ($r_+ \ll r$) the inhomogeneity. 'In front of' the inhomogeneity,

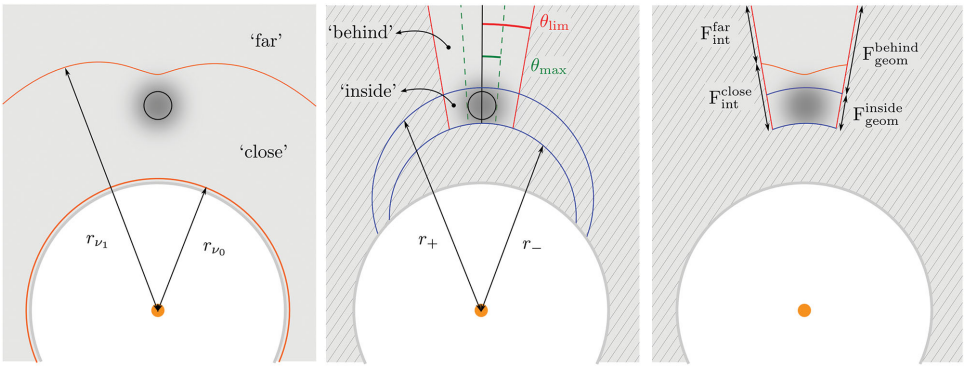


**Figure 2.** The properties of the magnetic field depend on whether the inhomogeneity is 'close' or 'far' from the Strömgren sphere ($r \ll r_{\nu_1}$ or $r_{\nu_1} \ll r$, left panel), and on whether we are considering the regions 'inside' or 'behind' the inhomogeneity ($r_- \ll r \ll r_+$ or $r_+ \ll r$, central panel). Thus, four different zones may be distinguished in which the magnetic field is the most significant (right panel). Hatching indicates regions where the strengths are weaker.

the two $F_2$ terms essentially cancel each other out, so that $\boldsymbol{B} \sim \boldsymbol{0}$ in this region. 'Inside' the geometric term simplifies to

$$F^{\rm inside}_{\rm geom} = \frac{\bar{n}\delta_0 D^2}{2\sigma^2} \mathrm{e}^{-\frac{(\sin\theta D)^2}{2\sigma^2}} \sin 2\theta \left(1 - \cos\theta \frac{D}{r} + \sqrt{\frac{\pi}{2}}\frac{\sigma}{r}\right), \quad (37)$$

while 'behind' the inhomogeneity

$$F^{\rm behind}_{\rm geom} = \bar{n}\delta_0 \sqrt{2\pi} \sin\theta \frac{D^2}{r\sigma} \mathrm{e}^{-\frac{(\sin\theta D)^2}{2\sigma^2}}. \quad (38)$$

In other words, this geometrical factor decreases the strength of the field exponentially above a certain angle $\theta_{\rm lim}$. It hence constraints the magnetic field to be generated only in the vicinity and behind inhomogeneities, within a domain in the shape of a shadow.

### 4.3.3 *Magnetized regions*

The result is that the field has a rather simple spatial distribution: it reaches its maximum strength in the vicinity of the inhomogeneity, roughly at $\theta = \theta_{\rm max}$ and $r = D$, and then decays with distance behind the inhomogeneity (cf. Fig. 3). More precisely, to a given source corresponds a given $r_{\nu_1}$ delimiting its 'close' and 'far' regions. Then the properties of the magnetic field generated around this source essentially depend on whether the surrounding inhomogeneities are inside the 'close' or 'far' regions as depicted on the right panel of Fig. 2.

Then we can see that if the inhomogeneity is close to the source ($D < r_{\nu_1}$), the strength reaches

$$B^{\rm inside}_{\rm close} = t\,\xi(D)\,\bar{n}\delta_0' \left[\Gamma\left(\frac{5-\alpha}{3}\right)\left(\frac{D - r_{\rm s} + \delta_0'\sigma}{\ell_{\nu_0}}\right)^{(\alpha-5)/3} - \Gamma\left(\frac{6-\alpha}{3}\right)\left(\frac{D - r_{\rm s} + \delta_0'\sigma}{\ell_{\nu_0}}\right)^{(\alpha-6)/3}\right], \quad (39)$$

while if it is far from it ($D > r_{\nu_1}$), it reaches

$$B^{\rm inside}_{\rm far} = t\,\xi(D)\,\bar{n}\delta_0' \left(1 - \frac{\nu_0}{\nu_1}\right)\left(\frac{\nu_0}{\nu_1}\right)^{5-\alpha} \frac{\exp\left(-\frac{D - r_{\rm s} + \delta_0'\sigma}{\ell_{\nu_1}}\right)}{\frac{D - r_{\rm s} + \delta_0'\sigma}{\ell_{\nu_1}}} \quad (40)$$

where $\delta_0' \equiv \sqrt{\frac{\pi}{2\mathrm{e}}}\delta_0$. Then after reaching these values, the field decays behind the inhomogeneity depending on the situation according to

$$B^{\rm behind}_{\rm close} \propto r^{-3}\left(\frac{r - r_{\rm s} + 2\delta_0'\sigma}{\ell_{\nu_0}}\right)^{\frac{\alpha-5}{3}} \quad (41)$$

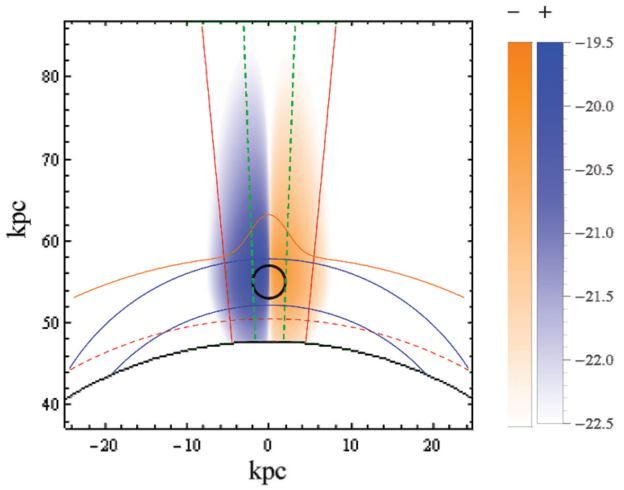


**Figure 3.** Typical field generated by an underdensity at $z = 10$ by a primordial galaxy. The thin black arc represents the edge of the Strömgren sphere. The thick black circle corresponds to the FWHM of the underdensity. The blue area corresponds to magnetic fields pointing towards the reader, orange in the opposite direction. Strength is indicated in gauss in logarithmic scale. Corresponding to the analytical decomposition explicated in Fig. 2, the continuous red lines show the $-\theta_{\rm lim}$ and $\theta_{\rm lim}$ directions, the dashed green lines correspond to the $-\theta_{\rm max}$ and $\theta_{\rm max}$ directions, the blue arcs indicate $r_-$ and $r_+$, and the continuous orange curve indicates $r_{\nu_1}$ ($\nu_1 = 4\nu_0$ here). The dashed red arc is the distance at which $t_i = t_{\rm s}$ (cf. text).

or

$$B^{\rm behind}_{\rm far} \propto r^{-3} \frac{\exp\left(-\frac{r - r_{\rm s} + 2\delta_0'\sigma}{\ell_{\nu_1}}\right)}{\frac{r - r_{\rm s} + 2\delta_0'\sigma}{\ell_{\nu_1}}}. \quad (42)$$

In these expressions we can see explicitly the role played by the amplitude of the inhomogeneity $\delta_0$. First of all, the sign of $B$ is given by the sign of $\delta_0$. Also, we can see that the strengths are larger in underdensities than in overdensities. Indeed, for negative $\delta_0$, $D - r_{\rm s} + \delta_0'\sigma$ is smaller than for a positive $\delta_0$. Expressions (39) and (40) thus yield larger values for a negative $\delta_0$ than a positive one. The same applies to expressions (41) and (42), showing that the fields will also be generated over larger distances in underdensities than in overdensities.

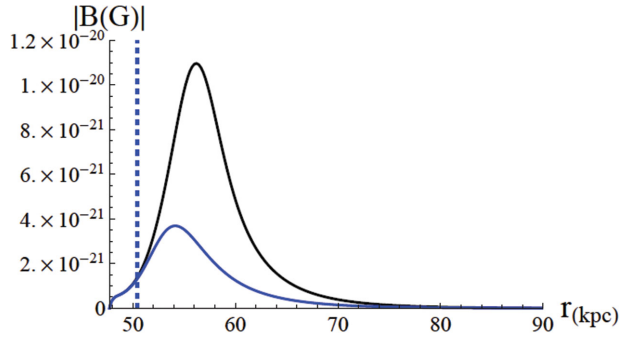


**Figure 4.** Magnetic field generated by a primordial galaxy, with two Gaussian inhomogeneities of same $|\delta_0|$, but with opposite signs (blue: positive; black: negative). We see that the mechanism is more efficient in underdense regions. Vertical dashed line indicates the distance at which $t_i = t_s$.

### 4.4 Sensitivity to physical parameters

Fig. 3 shows a typical result in the case of an underdensity, for a primordial galaxy at $z = 10$. The superimposed lines are separating the different regions studied in the above section. Interesting field strengths are produced in regions that span transversally the domain between $-\theta_{\rm lim}$ and $\theta_{\rm lim}$, and extend radially over a few $\ell_{4\nu_0}$ behind the inhomogeneity. In addition, the dashed red arc represents the distance corresponding to $t_i = t_s$, below which $n_{\rm H\,I}$ is overestimated as discussed in Section 4.2. The strength and scales reached by the generated field depend on many parameters: those characterizing the IGM ($D$, $\sigma$ or $\sigma_+$, $\delta_0$ or $\delta_0^+$ and $\bar{n}$), those characterizing the source ($L_0$, $\alpha$ and $\nu_1$), and the redshift $z$. In light of the above analytical expressions, we now make those parameters vary one by one in order to evaluate their importance.

#### 4.4.1 *Varying the properties of the inhomogeneity*

For simplicity all the configurations (source and inhomogeneity) considered here possess an axial symmetry (cf. Fig. 1). Therefore there are no orthoradial gradients along the symmetry axis, and thus the magnetic field vanishes in the $\theta = 0$ direction. For this reason, all the graphs presented here are plotted along the line of sight $\theta = \theta_{\rm max}$. Note also that all graphs start at $r = r_s$. Obviously, the larger $|\delta_0|$ the larger the gradients, and thus the higher the strengths generated in principle. On the other hand, large $\delta_0$ implies strong absorption in the case of an overdensity. So for example behind a very dense region, the field vanishes but is important at its edges. In the following, we consider pockets of neutral gas, not virialized, in the vicinity of an early isolated ionizing source. Therefore we consider $-1 \leq \delta_0 \lesssim 5$.

In Fig. 4 we plot the field generated in an overdensity and an underdensity, differing only by the sign of $\delta_0$. We see that the strength is higher and generated on larger scales in the underdensity case, which is due to the fact that there are more photons at a given distance than in the overdensity case. This was already noticed previously from expressions (39) to (42). In Fig. 5 we study the influence of the position and profile of the inhomogeneity for a given source. For illustrative purposes we take a QSO at redshift $z = 10$. On the left of the figure, the profile of the inhomogeneity ($\sigma$, $\delta_0$) is kept constant while its distance from the source $D$ is increased. We can see that the closer the inhomogeneity, the stronger the strength, which is natural since photons are absorbed and diluted as they travel away from the source. Also, for QSOs, $\ell_{\nu_1}$ is huge (cf. Table 1) so that we are always 'close' to the source and formulae $B_{\rm close}^{\rm inside}$ and $B_{\rm close}^{\rm behind}$ apply. We indeed recover the power-law asymptotic trend with distance of equation (41). In the central panel of Fig. 5, $D$ and $\delta_0$ are kept constant as $\sigma$ varies. The narrower the density profile, the greater the strength, since gradients are more important for narrow profiles. Note that because the term we are considering in equation (12) is global, once a non-radial gradient is formed, it generates magnetic fields along the entire line of sight. This is why the narrow profiles generate fields of stronger strengths on larger distances. Their angular extent about the symmetry axis is smaller though. The right panel of Fig. 5 has to be compared with its central panel: they correspond to the same study but with a MH profile instead of a Gaussian overdensity profile. We can see that the strengths are larger. This comes from the fact that photons in underdensities are less absorbed so that the flux of ionizing photons is more important within the overdensity than in the simply Gaussian overdensity case. This is all the more true than the width of the underdensity is important, which is why contrary to the Gaussian case, the wider the profile, the larger the strength for an MH profile. Also, since the field has opposite directions in underdense and overdense regions, the contributions from the underdensity and the overdensity composing the MH profile cancel out. This is why for such a profile, at some distance, the field changes sign. In the right panel of Fig. 5 we can see that this distance depends on the width of the MH.

In both Figs 5 and 6, when the inhomogeneity is very close to the Strömgren sphere, the strength reaches high values at the outer edge of the ionized region. This is because in our model we impose spherically symmetric ionized regions which intercepts the Gaussian profile of the inhomogeneity thus inducing non-radial gradients and a magnetic field. In more realistic situations, such border effects will indeed take place as the ionization front will be distorted at the contact of an inhomogeneity. A more precise study of such effects is left for future work.

Finally, expression (18) dictates the topology of the magnetic field. Field lines given by $\boldsymbol{B} \times \boldsymbol{dl} = \boldsymbol{0}$ in spherical coordinates with

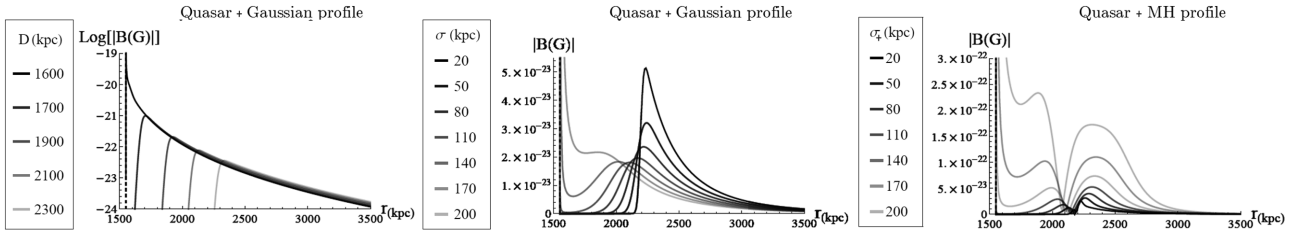


**Figure 5.** Magnetic field generated with various inhomogeneities, for a given source (here a quasar at $z = 10$). Left: Gaussian overdensity of fixed profile, varying distance. Middle: Gaussian overdensity at fixed position, varying its width $\sigma$. Right: MH profile at fixed position, varying its width $\sigma_+$. The lines corresponding to distances at which $t_i = t_s$ (cf. Section 4.2) are not visible here because for quasars the Strömgren sphere is so large that photons are very diluted as they reach $r_s$, and $t_i$ becomes much larger than $t_s$ already at the edge of the Strömgren sphere.

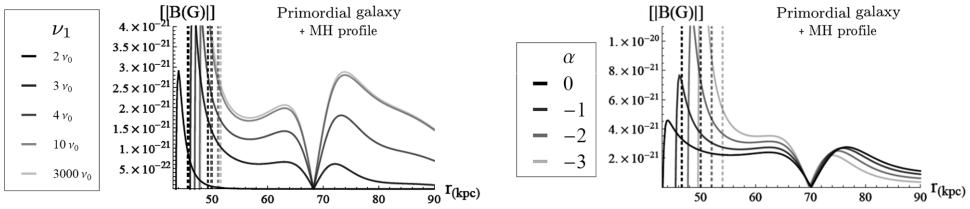


**Figure 6.** Magnetic field generated with various source properties, with a given MH inhomogeneity at a given position, at $z = 10$. Left: for a fixed power-law spectrum, we vary the cut-off frequency $\nu_1$. Right: for a fixed total luminosity, we vary the spectral index $\alpha$. Vertical dashed lines show the distances at which $t_i = t_s$.

$\boldsymbol{dl} = dr\,\hat{r} + rd\theta\,\hat{\theta} + r\sin\theta d\phi\,\hat{\phi}$ satisfy

$$dr = 0 \text{ and } \frac{\mathrm{d}\theta}{\mathrm{d}\varphi} = -\frac{\partial_\varphi \int n_{\mathrm{H\,I}}\mathrm{d}r}{\partial_\theta \int n_{\mathrm{H\,I}}\mathrm{d}r}. \quad (43)$$

Since $dr = 0$, field lines remain on spheres centred on the source. In the case of a $\varphi$-independent configuration, as in all the examples considered here, $d\theta = 0$ so the lines are circles around the axis of symmetry of the system. This is why in all the density plots of this paper the fields point perpendicularly to the plane of the plot. In a more general case the lines remain loops at given radii since $dr = 0$ but with a more complicated shape given by (43). Though, once formed, these fields will be processed by the velocity field of the IGM, their peculiar initial spatial configuration is interesting as it may help discriminate magnetic fields generated through this process from those generated by different mechanisms.

### 4.4.2 *Varying the properties of the source*

In Fig. 6 we choose a certain MH inhomogeneity, at $z = 10$, and vary the spectral index $\alpha$ and cut-off frequency $\nu_1$ of the source, here a primordial galaxy for illustration.

On the left of the figure, we make the cut-off frequency $\nu_1$ vary. We observe that above a certain value, the strength of the generated magnetic field has reached a plateau. For instance in the case shown, the field strength generated with $\nu_1 = 10\nu_0$ is almost identical to that generated with $\nu_1 = 3000\nu_0$. This is because $\ell_{10\nu_0}$ is larger than 50 kpc at $z = 10$, so photons of frequency above $10\nu_0$ do not interact significantly in the neighbourhood of the inhomogeneity. Also, far behind it they are too diluted to generate a significant magnetic field. This result underlines the following compromise: this mechanism requires photons of high enough energy to photoionize deep in the IGM to generate magnetic fields on large distances, but not too high either because of dilution [cf. equations (41) and (42)].

On the right of Fig. 6, we make the spectral index $\alpha$ vary. Since the total luminosity is fixed, harder spectra correspond to sources with fewer low-energy photons, which is why harder spectra generate weaker fields near the source, but stronger fields far from the source. Also, naturally, the harder the spectrum the further in the IGM the field is generated. However, we can see in this example that the strengths do not depend too strongly on the spectral index, only up to factors of 2. This can be seen in the analytical expressions of the previous section like equation (28), where $(\alpha - 5)/3$ and $(\alpha - 6)/3$, for the relevant values of $\alpha$, do not vary much with $\alpha$ and so $B$ does not either.

Finally, we consider various redshifts. Depending on the epoch, the type of ionizing sources and the properties of the IGM are different. For illustration, we decompose the EoR in three stages: PopIII star clusters for $z \in [30, 20]$, primordial galaxies for $z \in [20, 10]$ and quasars for $z \in [10, 6]$. Fig. 7 shows examples of field configurations obtained at $z = 20$ and $z = 10$, and Table 2 is a summary of the typical strengths obtained after varying the different parameters of the model. They allow us to identify the following trends. In the beginning of EoR, Population III clusters generate relatively high strengths ($\sim 10^{-19}$ G) but on relatively small scales (hundreds of parsecs), while on the contrary, at the end of EoR, quasars generate low strengths ($\sim 10^{-22}$ G) but on important scales (hundreds of kpc). First galaxies are somewhat in-between and generate $\sim 10^{-21}$ G on tens of kpc in the middle of the EoR. This may be interpreted as follows. Population III clusters are not very energetic so they form small Strömgren spheres and thus photons from the source are not too diluted as they reach the IGM. However, since they appear early in the EoR, $\bar{n}$ is large and thus the mean-free path of photons is small. Therefore, many photons photoionize and generate strong magnetic fields near the Strömgren sphere. On the contrary, quasars are very energetic and generate huge Strömgren spheres, so that photons from the source are very diluted as they reach the IGM. In addition since quasars appear late in EoR, the IGM is not very dense and the mean-free path of energetic photons is huge. Consequently the ionizing flux is relatively low and the generated magnetic field is weak, but extends on important scales.

## 5 DISCUSSION

The cases detailed above are idealized. In reality, as we have mentioned, Strömgren spheres are deformed, there is a full distribution of asymmetric inhomogeneities outside the H II regions, and ionizing sources may not be isolated. Taking all this into account would allow us in principle to compute the full magnetic power spectrum generated by photoionization. Furthermore, the IGM is dynamical and the weak turbulence associated with the mildly non-linear regime of structure formation on large scales will process the initial power spectrum of the magnetic field. A study of all these effects is beyond the scope of this paper and should be best addressed with dedicated numerical simulations.

As we have seen, an interesting feature of this mechanism is that it generates magnetic fields outside Strömgren spheres on distances of the order of a few $\ell_{\nu_1}$, or even larger in underdense regions. By comparing these distances to the half typical separation between Strömgren spheres, we may get an idea of the fraction of the Universe that may be magnetized by this mechanism. Let us first do so for Population III star clusters at $z = 20$. Considering they formed by molecular cooling in gas overdensities of mass $10^6\,\mathrm{M}_\odot$ (cf. Barkana & Loeb 2000), their half physical mean separation is roughly 10 kpc, estimated from the abundance of their $\sim 3\sigma$ parent haloes (Mo & White 2002). In addition, the radius of their Strömgren spheres is of the order of a fraction of kpc, and $\ell_{4\nu_0}$ is about one kpc large. Thus, it seems that these sources magnetize essentially on the outskirts of their Strömgren spheres, leaving an important fraction of the IGM unmagnetized. Consider now faint dwarf galaxies at $z = 15$, and quasars of $10^{12}\,\mathrm{L}_\odot$ at $z = 10$. Faint dwarf galaxies

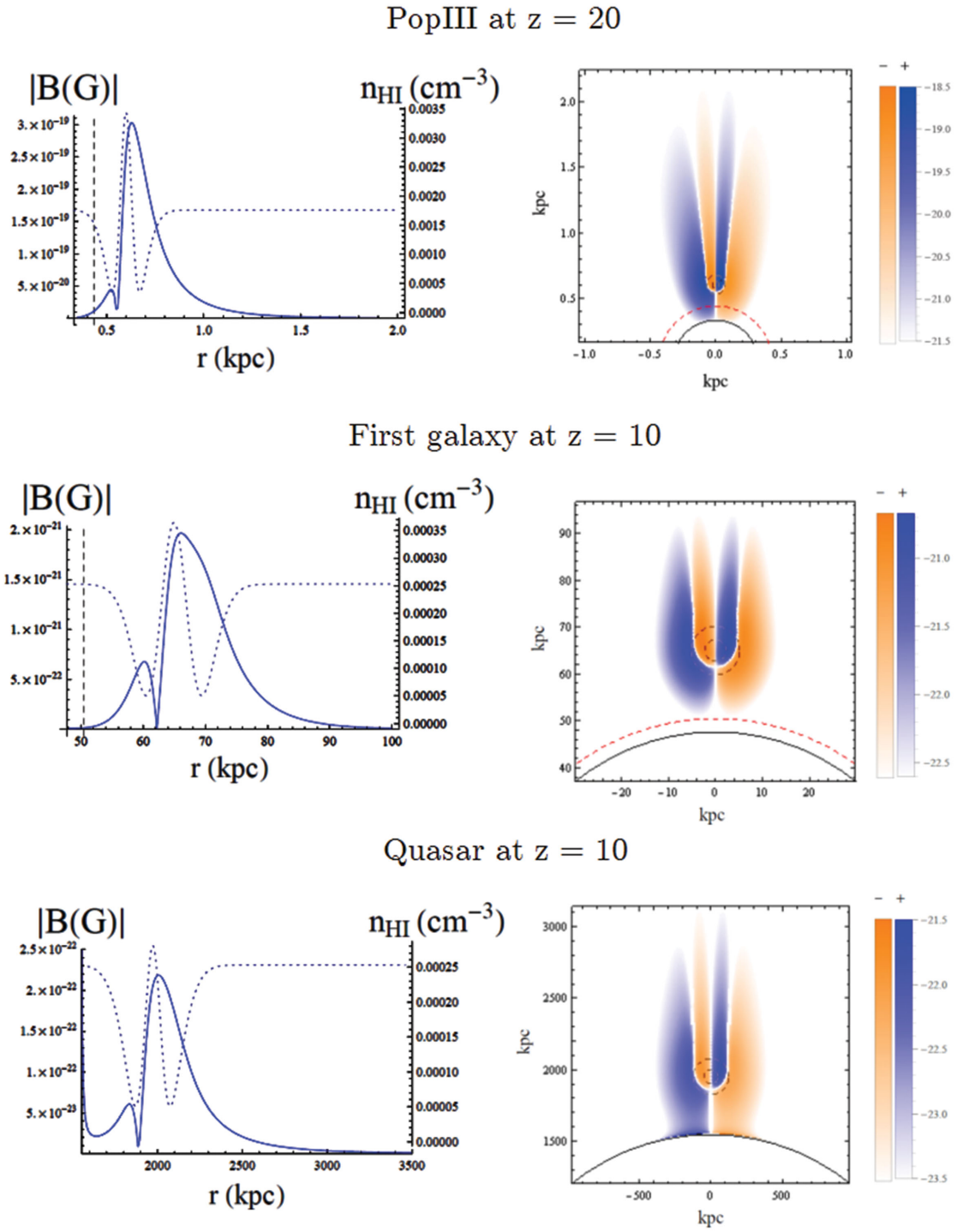


**Figure 7.** Examples of the field generated with MH inhomogeneities for each type of sources considered here. Left column: left $y$-axis and blue curves show the absolute value of the magnetic field strength. Vertical dashed lines indicate the distances at which $t_i = t_s$. Right $y$-axis and dotted lines show the inhomogeneity profiles. Right column: black line is the Strömgren sphere. Inner and outer dashed black circles correspond to $\sigma_+$ and $\sigma_-$ of the inhomogeneity, respectively. Blue areas correspond to magnetic field pointing towards the reader, orange in the opposite direction. Strengths are in gauss in logarithmic scale.

are the major candidate sources responsible for reionization (e.g. Bouwens et al. 2012; Wise et al. 2014). Assuming they are hosted in $10^8$ $M_\odot$ haloes, their half physical mean separation is a couple of tens of kpc. Their Strömgren radii are of the order of a few tens of kpc, and $\ell_{4\nu_0}$ is a couple of kpc large. Luminous quasars, on the other hand, are extremely rare at $z = 10$, which seems confirmed by the recent *Planck* results implying that the redshift of reionization, $z_{re} = 8.8$, is lower than previously thought (Planck Collaboration 2015). For illustration, considering they are hosted by $5\sigma$ haloes, their half physical mean separation is of a couple of Mpc. Their Strömgren spheres have radii of the order of the Mpc, and these sources have photons of large enough mean-free paths to magnetize in between these spheres. Therefore, these orders of magnitude are more favourable in the case of primordial galaxies and quasars than

**Table 2.** Third column shows the typical strengths generated at the distances away from the Strömgren sphere shown in the fourth column. These strengths are typical values obtained by varying the different properties of the inhomogeneities.

| Source | Redshift | Log\|$B$\| (G) | Distance from the ionization front (kpc) |
|---|---|---|---|
| Pop III | 30 | −19 | 0.3 |
| | | −21 | 1 |
| | 20 | −19 | 0.5 |
| | | −21 | 1 |
| Primordial galaxy | 20 | −20 | 10 |
| | | −22 | 15 |
| | 10 | −21 | 30 |
| | | −22 | 100 |
| Quasar | 10 | −21 | 300 |
| | | −22 | 1000 |
| | 6 | −22 | 500 |
| | | −23 | 1500 |

in the case of Population III star clusters, and suggest that these sources may have participated through this mechanism to the weak magnetization of an important fraction, if not the whole, of the IGM. Note that even the case of Population III star clusters is interesting, as these sources thus premagnetize the environment in which the next generation of stars and galaxies forms.

In this study we have focused on the photoionization term in the induction equation. An exact comparison of this term with the Biermann term is beyond the scope of this paper. We note that Doi & Susa (2011) examined their relative importance in numerical simulations of the neighbourhood of an ionizing super-massive star. In their study, they focus on the situation across an ionization front, in which a self-shielded, neutral, $\delta \simeq 10^2$–$10^3$ overdensity defines very sharp and strong gradients in the temperature and electronic density fields. Such a situation could indeed occur within Strömgren spheres of the very first luminous sources. Under those conditions, they concluded that the Biermann battery dominates by one order of magnitude. In our case, we considered mild, neutral over-densities way outside the Strömgren regions of stronger, long-lived ionizing sources. In such contexts, the Biermann battery may not be effective, be it for purely geometrical reasons. To see that, consider again equation (11), in which we have separated the global photoionizing contribution from the local contribution. It is the global contribution that creates magnetic fields in regions where the Biermann battery does not operate. Comparison of the two mechanisms is relevant only in regions where they coexist. For that purpose, it is convenient to note that equation (11) may be rewritten as

$$\partial_t \boldsymbol{B} = \frac{c}{e}\frac{\nabla n_\mathrm{e}}{n_\mathrm{e}^2} \times \left[-\nabla p_\mathrm{e} + \dot{\boldsymbol{p}}_\mathrm{pe}\right] - \frac{c}{e n_\mathrm{e}} \nabla \times \dot{\boldsymbol{p}}_\mathrm{pe}. \tag{44}$$

On the right hand side, the last part contains the full global term examined in this paper (cf. equation 16), and a contribution to the local term. The remaining contribution to the local term is contained in the $\dot{\boldsymbol{p}}_\mathrm{pe}$ present in the square brackets. In regions where the Biermann battery is efficient, i.e. where pressure and density gradients are not aligned, it is enough to compare $\dot{\boldsymbol{p}}_\mathrm{pe}$ to the pressure gradient. More precisely, since $\dot{\boldsymbol{p}}_\mathrm{pe}$ is always radial, their comparison makes sense only in cases where $-\nabla p_\mathrm{e}$ is radial too. Then, considering a perfect gas equation of state $p_\mathrm{e} = n_\mathrm{e} k_b T_\mathrm{e}$, their ratio yields typically

$$\left|\frac{\dot{\boldsymbol{p}}_\mathrm{pe}}{n_\mathrm{e} k_b \nabla T_\mathrm{e}}\right| \sim 13 \left(\frac{T_\mathrm{e}}{10\,\mathrm{K}}\right)^{-1} \left(\frac{L_\mathrm{g}}{10\,\mathrm{kpc}}\right) \tag{45}$$

where $L_\mathrm{g}$ is the typical scale of temperature gradients. For illustration, we have taken $\dot{p}_\mathrm{pe} = 3 \times 10^{-44}$ erg cm$^{-4}$, which is obtained at a rather remote distance of $2r_\mathrm{s} \sim 100$ kpc from a primordial galaxy at $z = 10$. Hence, in this case, the photoionization term dominates, even at a distance of $2r_\mathrm{s}$ at which photons are very diluted. Also note that, because the Biermann battery contribution is independent of the properties of the source, the ratio above scales linearly with the luminosity of the ionizing source.

The magnetogenesis mechanism examined here, based on the simple physics of momentum transfer from ionizing photons to photoelectrons, is therefore likely to have generated seed magnetic fields on cosmological scales during Reionization. Although weak and very remote, the strengths of the seeds produced, together with their specific spatial configuration, could actually be revealed directly through the recently proposed probe of magnetic fields in the EoR detailed by Venumadhav et al. (2014), although large coherence lengths of the magnetic fields might be mandatory.

## ACKNOWLEDGEMENTS

We would like to thank Nabila Aghanim and Katia Ferrière for stimulating discussions. J.-B. D. acknowledges financial support by the P2IO LabEx (ANR-10-LABX-0038) in the framework 'Investissements d'Avenir' (ANR-11-IDEX-0003-01) managed by the French National Research Agency (ANR).

## REFERENCES

Ando M., Doi K., Susa H., 2010, ApJ, 716, 1566
Barkana R., Loeb A., 2000, Phys. Rep., 349, 125
Beck A. M., Hanasz M., Lesch H., Remus R. S., Stasyszyn F. A., 2013, MNRAS, 429, L60
Berezhiani Z., Dolgov A. D., 2004, Astropart. Phys., 21, 59
Biermann L., 1950, Zeitschrift für Naturforschung A, 5, 65
Bonafede A. et al., 2015, Advancing Astrophysics with the Square Kilometre Array, PoS(AASKA14), 095
Bouwens R. J. et al., 2012, ApJ, 752, L5
Brandenburg A., Subramanian K., 2005, Phys. Rep., 417, 1
Ciardi B., Ferrara A., Marri S., Raimondo G., 2001, MNRAS, 324, 381
Coroniti F. V., 2014, ApJ, 780, 146
Doi K., Susa H., 2011, ApJ, 741, 93
Durrer R., Neronov A., 2013, A&AR, 21, 62
Fenu E., Pitrou C., Maartens R., 2011, MNRAS, 414, 2354
Finlator K., Oh S. P., Özel F., Davé R., 2012, MNRAS, 427, 2464
Furlanetto S. R., Loeb A., 2001, ApJ, 556, 619
Gnedin N. Y., Ferrara A., Zweibel E. G., 2000, ApJ, 539, 505
Grasso D., Rubinstein H. R., 2000, Phys. Rep., 348, 163
Harrison E. R., 1970, MNRAS, 147, 279
Kandus A., Kunze K. E., Tsagas C. G., 2011, Phys. Rep., 505, 1
Krall N. A., Trivelpiece A. W., 1973, Principles of Plasma Physics, International Series in Pure and Applied Physics. McGraw-Hill Kogakusha, Tokyo
Kronberg P. P., Lesch H., Hopp U., 1999, ApJ, 511, 56
Kulsrud R. M., Cen R., Ostriker J. P., Ryu D., 1997, ApJ, 480, 481
Langer M., Aghanim N., Puget J.-L., 2005, A&A, 443, 367
Loeb A., Furlanetto S. R., 2013, The First Galaxies in the Universe, Princeton Series in Astrophysics. Princeton University Press, Princeton
Martini P., 2004, in Ho L., ed., Coevolution of Black Holes and Galaxies: Volume 1, Carnegie Observatories Astrophysics Series. Cambridge University Press, Cambridge, p. 169

Medvedev M. V., Silva L. O., Kamionkowski M., 2006, ApJ, 642, L1
Mellema G., Iliev I. T., Pen U.-L., Shapiro P. R., 2006, MNRAS, 372, 679
Miniati F., Bell A. R., 2011, ApJ, 729, 73
Mo H. J., White S. D. M., 2002, MNRAS, 336, 112
Neronov A., Vovk I., 2010, Science, 328, 73
Planck Collaboration 2015, preprint (arXiv:1502.01582)
Pudritz R. E., Silk J., 1989, ApJ, 342, 650
Raiter A., Schaerer D., Fosbury R. A. E., 2010, A&A, 523, A64
Ryu D., Schleicher D. R. G., Treumann R. A., Tsagas C. G., Widrow L. M., 2011, Space Sci. Rev., 166, 1
Schaerer D., 2002, A&A, 382, 28
Seager S., Sasselov D. D., Scott D., 2000, ApJS, 128, 407
Shang Z. et al., 2011, ApJS, 196, 2
Sommerfeld A., Schur G., 1930, Annalen der Physik, 396, 409
Subramanian K., 2015, preprint (arXiv:1504.02311)
Subramanian K., Narasimha D., Chitre S. M., 1994, MNRAS, 271, L15
Takahashi K., Ichiki K., Sugiyama N., 2008, Phys. Rev. D, 77, 124028
Venumadhav T., Oklopčić A., Gluscevic V., Mishra A., Hirata C. M., 2014, preprint (arXiv:1410.2250)
Widrow L. M., 2002, Rev. Modern Phys., 74, 775
Widrow L. M., Ryu D., Schleicher D. R. G., Subramanian K., Tsagas C. G., Treumann R. A., 2011, Space Sci. Rev., 166, 37
Wise J. H., Demchenko V. G., Halicek M. T., Norman M. L., Turk M. J., Abel T., Smith B. D., 2014, MNRAS, 442, 2560
Xu H., O'Shea B. W., Collins D. C., Norman M. L., Li H., Li S., 2008, ApJ, 688, L57
Zackrisson E., Rydberg C. E., Schaerer D., Östlin G., Tuli M., 2011, ApJ, 13, 17
Zakharov A. V., Anikanov V. A., 1992, Soviet Phys. J., 35, 98

## APPENDIX A: MOMENTUM TRANSFER TERM

A fraction $f_{\rm mt}$ of the momentum of the incident photon is transferred to the freed electron during photoionization:

$$m_{\rm e}\boldsymbol{v} = f_{\rm mt}(\nu)\frac{h\nu}{c}\hat{\boldsymbol{r}}, \tag{A1}$$

where $f_{\rm mt}$ is frequency dependent (Sommerfeld & Schur 1930):

$$f_{\rm mt}(\nu) = \frac{8}{5}\frac{\nu-\nu_0}{\nu}. \tag{A2}$$

Note that this fraction may be larger than one, in which case the ions recoil.

Now, by definition $\partial_t f_{\rm e}|_{\rm s}\,{\rm d}^3\boldsymbol{v}{\rm d}^3\boldsymbol{r}{\rm d}t$ is equal to the number of photoelectrons of speed $v$ in direction $\hat{v}$ generated at a position $\boldsymbol{r}$ at a time $t$. Since we consider hydrogen only, each photoionization produces only one electron. This number is thus equal to the number of photoionizations due to photons of frequency $\nu$ in direction $\hat{k}=\hat{v}$ where $\nu$ satisfies (A1). Finally, since the photoionization rate density is the product of the number density of incident photons, the velocity of incident photons, the number density of target hydrogen atoms and the cross-section, we get

$$\partial_t f_{\rm e}|_{\rm s}\,{\rm d}^3\boldsymbol{v}{\rm d}^3\boldsymbol{r}{\rm d}t = \left[n_\gamma^{\rm inc}{\rm d}\nu{\rm d}\Omega\right] c\sigma_\nu n_{\rm H\,I}{\rm d}^3\boldsymbol{r}{\rm d}t \tag{A3}$$

where the number density of incident photons of frequency $\nu$ with direction $\hat{k}$ at $\boldsymbol{r}$ at time $t$ is

$$n_\gamma^{\rm inc}(t,\boldsymbol{r},\hat{k},\nu) = \frac{I_\nu/c}{h\nu} \tag{A4}$$

by definition of the monochromatic specific intensity. Therefore we model the source term microscopically in equation (1) by

$$\partial_t f_{\rm e}|_{\rm s}\,{\rm d}^3\boldsymbol{v} = \frac{I_\nu\sigma_\nu}{h\nu}n_{\rm H\,I}{\rm d}\nu{\rm d}\Omega, \tag{A5}$$

so that macroscopically we get from expression (9) from equation (8).

## APPENDIX B: NOTATIONS

In the multifluid description, macroscopic physical quantities are defined as

$$\begin{aligned}
n_\alpha &= \int f_\alpha {\rm d}^3\boldsymbol{v}\\
\boldsymbol{V}_\alpha &= \frac{1}{n_\alpha}\int \boldsymbol{v} f_\alpha {\rm d}^3\boldsymbol{v}\\
\boldsymbol{P}_\alpha &= m_\alpha\int (\boldsymbol{V}_\alpha-\boldsymbol{v})(\boldsymbol{V}_\alpha-\boldsymbol{v})\, f_\alpha {\rm d}^3\boldsymbol{v}\\
\boldsymbol{J}_\alpha &= q_\alpha n_\alpha \boldsymbol{V}_\alpha,
\end{aligned} \tag{B1}$$

respectively the number density, the velocity, the pressure tensor and the current density of species $\alpha$. This description is then reduced to a single fluid with

$$\begin{aligned}
\rho_m &= \Sigma_\alpha n_\alpha m_\alpha\\
\rho_q &= \Sigma_\alpha n_\alpha q_\alpha\\
\boldsymbol{V} &= \frac{\Sigma_\alpha n_\alpha m_\alpha \boldsymbol{V}_\alpha}{\Sigma_\alpha n_\alpha m_\alpha}\\
\boldsymbol{J} &= \Sigma_\alpha \boldsymbol{J}_\alpha\\
\boldsymbol{P} &= \Sigma_\alpha \boldsymbol{P}_\alpha^{\rm CM}\\
\boldsymbol{P}_\alpha^{\rm CM} &= m_\alpha\int (\boldsymbol{V}-\boldsymbol{v})(\boldsymbol{V}-\boldsymbol{v})\, f_\alpha {\rm d}^3\boldsymbol{v},
\end{aligned} \tag{B2}$$

respectively the mass density, the charge density, the centre-of-mass velocity, the current density and the total centre-of-mass pressure tensor in the one-fluid. Then, taking the first moment of (1) weighted by $q_\alpha$, and summing over all species, yields the generalized Ohm's law (3), with the additional notations:

$$\begin{aligned}
\boldsymbol{P} &\equiv \Sigma_\alpha \frac{q_\alpha}{m_\alpha}\nabla\cdot\boldsymbol{P}_\alpha^{\rm CM}\\
\boldsymbol{C} &\equiv \Sigma_\alpha q_\alpha \int \boldsymbol{v}\,\partial_t f_\alpha|_{\rm c}\,{\rm d}^3\boldsymbol{v}.
\end{aligned} \tag{B3}$$

This paper has been typeset from a TEX/LATEX file prepared by the author.

# Chapter 4

# Magnetogenesis Throughout the Epoch of Reionization

The mechanism detailed in the previous chapter operates around any source all along the Epoch of Reionization. So far we have computed the magnetic field generated around individual sources. Now, in order to evaluate the cosmological importance of this mechanism, we need to estimate the level at which the Universe is magnetized by this process. This naturally depends on the distribution of sources (the typical separation distance of their Strömgren spheres), their spectral properties, the epochs at which they appear and the distribution of inhomogeneities in the IGM. This is a work I am leading, in collaboration with M. Langer, H. Tashiro (Nagoya, Japan) and N. Sugiyama (Nagoya, Japan), with the provisional title 'Mean Energy Density of Photogenerated Magnetic Fields During EoR' (Durrive et al., 2016, to be submitted).

## 4.1 Procedure

There are many ways of evaluating the level to which the Universe is magnetized by a given mechanism. Here, we are going to derive what is probably the simplest criterion, namely we are going to *estimate the mean magnetic energy density injected in the IGM by all the sources radiating during the Epoch of Reionization*, with a simple model. However, we will see that even this simple approach already turns out to be involved due to the important number of elements one has to take into account. This will thus be a very good and necessary starting point for deeper explorations, as for example that mentioned in chapter 5.

**Procedure** As presented in the previous chapter, magnetic fields are generated inside and around overdense clouds in the IGM, but as we have seen, the exact formula derived for $\vec{B}$ is quite complicated. The key point is that we have however also identified the characteristic length scales of the problem, and we are thus able to model simply the magnetized area around a given overdensity. The second key element is that from the Standard Model of Cosmology, we have tools to estimate the statistical distribution of sources and overdensities in the Universe. Then, combining both informations, we may estimate the magnetic field generated by photoionization during the EoR.

More precisely, as illustrated in figure 4.1, using the so-called Press-Schechter formalism, we may compute analytically the mean comoving number density of DM halos of a given mass at a given redshift. And as we know, baryonic matter falls into the potential wells of DM, so that DM halos host baryons, both sources (stars, galaxies and quasars) and clouds (slightly overdense regions, making up the clumpiness of the IGM). We are thus going to distinguish between two types of DM halos: Baryons in 'large enough' mass DM halos have collapsed into luminous sources, while 'small enough' mass DM halos contain diffuse baryons constituting slightly overdense clouds. This way, we will have an estimate of the distribution of sources, and of the distribution of clouds around each source, all along the EoR.

We will thus proceed as follows: First, in section 4.2, we will model the magnetic field generated around one source, due to the presence of one cloud and then due to the presence of a distribution of clouds around it; then in section 4.3 we will estimate the global field generated by a distribution of such sources surrounded by clouds.

## 4.2 Around one source

### 4.2.1 One cloud

**A concise expression for $B$** In the previous chapter, we have explored the spatial distribution and typical numerical values of the magnetic field given by the very general formula (3.20). Even for a simple Gaussian inhomogeneity, these quantities are given by rather involved expressions, but we have extracted

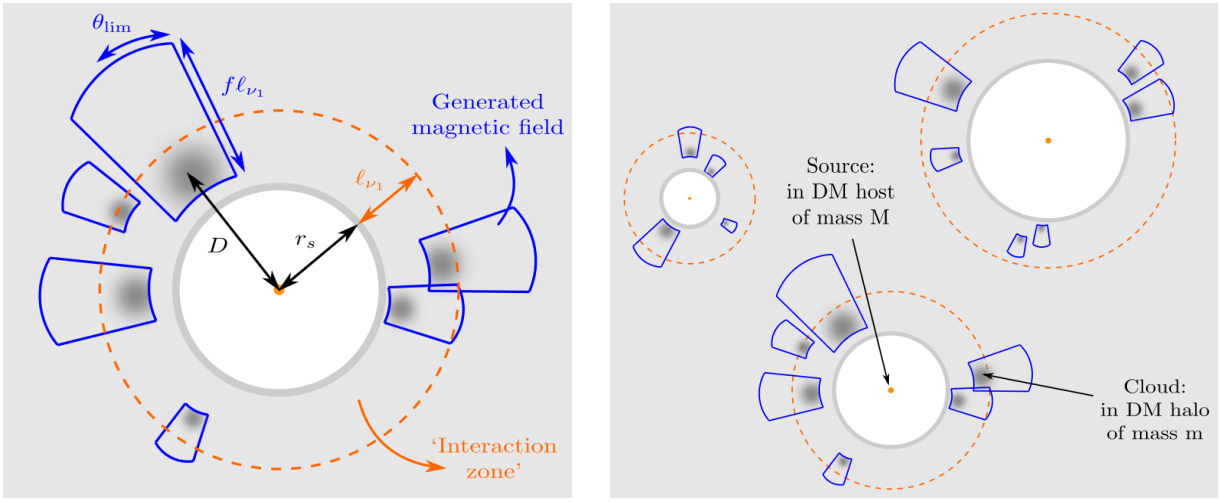


Figure 4.1: Illustration of the magnetic field generation during EoR. The dark gray spots are overdense clouds in the neutral IGM (the light gray region) close to sources of ionizing photons (the orange spots). The white regions represent the Strömgren sphere ($r \leq r_s$). Left panel: We may summarize the results of the thorough analysis of chapter 3 as follows: Only clouds between $r_s$ and $r_s + \ell_{\nu_1}$ (the orange dashed line, delimiting the 'interaction zone') contribute significantly to the magnetic field generation, and the fields are generated inside the blue frames with strengths well approximated by formula (4.1). Right panel: All along the EoR this mechanism operates around each source. The aim of this chapter is to compute the mean magnetic field generated by a distribution of sources, themselves surrounded by distribution of clouds as illustrated here.

from them the gist of information necessary for our purpose here by identifying the typical areas in which the field strength is significant. As illustrated on the left of figure 4.1, we are now going to keep only the following information: (i) Magnetic fields may be generated only by the clouds that are close enough to the source, i.e. that are within the 'interaction zone' defined as the shell of thickness $\ell_{\nu_1}$ around the Strömgren sphere, where $\ell_{\nu_1}$ is the mean free path of the energetic photons emitted by the source (of frequency $\nu_1$), and (ii) around a given cloud, characterized by $(\delta_0, \sigma)$ (cf. equation (3.23)), at distance $D$ from the source, some magnetic field is generated in the volume delimited by the blue frame in figure 4.1. More precisely, the magnetic field strength generated is well approximated by the following profile

$$B_{\sigma,\delta_0,D}(r,\theta,\varphi) = B_{\rm max}\left(\frac{r}{D}\right)^{-3}\left(\frac{r - r_s + \sqrt{2\pi/e}\,\delta_0\sigma}{D - r_s + \sqrt{2\pi/e}\,\delta_0\sigma}\right)^{\frac{\alpha-5}{3}} \tag{4.1}$$

where $B_{\rm max}$ is defined below. This expression should be multiplied by the following Heaviside step functions

$$\Theta(r - D)\Theta(r - r_s)\Theta(\theta_{\rm lim} - \theta)\Theta(D + f\ell_{\nu_1} - r) \tag{4.2}$$

to delimit the region in which $B$ is considered as non-negligible, corresponding to the blue frame surrounding each cloud in figure 4.1. Thus the field is azimuthally symmetric since there is no dependence on the angle $\varphi$, but only $\theta$, where the angle $\theta_{\rm lim}$ is given by (3.24). For $r < D$ the field is equal to zero, then at $r = D$ it reaches its maximum

$$B_{\rm max} = t_* \frac{1}{15}\sqrt{\frac{2}{\pi e}}\frac{\sigma_0^2 L_0 \nu_0}{q x_e D^2} n_{\rm HI}\delta_0 F(D,\sigma), \tag{4.3}$$

where $t_*$ is the lifetime of the hard photon emitting phase of the source, set to $t_* = 100$ Myr in our model, and $F(D,\sigma)$ is the coefficient representing the geometrical effects of the cloud

$$F(D,\sigma) = \Gamma\left(\frac{5-\alpha}{3}\right)\left(\frac{D - r_s + \sqrt{\pi/2e}\,\delta_0\sigma}{\ell_{\nu_0}}\right)^{(\alpha-5)/3} - \Gamma\left(\frac{6-\alpha}{3}\right)\left(\frac{D - r_s + \sqrt{\pi/2e}\,\delta_0\sigma}{\ell_{\nu_0}}\right)^{(\alpha-6)/3}. \tag{4.4}$$

For $r > D$ the strength decays as a powerlaw, where we introduce a cut-off distance $f\ell_{\nu_1}$, after which the field will be considered as negligible. The role of the factor $f$ is to let us control this cut-off, measuring it in units of the relevant scale $\ell_{\nu_1}$. We will discuss it further in the next chapter.

**Energy generated due to one cloud** The magnetic energy generated in the IMG due to one cloud is the sum of the magnetic energy density $\frac{B^2}{8\pi}$ (Gaussian units) over the whole volume in which the field is generated, that is

$$\boxed{E_{\sigma,\delta_0}(D) = \int_0^{\theta_{\rm lim}} d\theta \sin\theta \int_0^{2\pi} d\varphi \int_D^{D+f\ell_{\nu_1}} dr\; r^2 \frac{B^2_{\sigma,\delta_0,D}}{8\pi}} \tag{4.5}$$

where $B_{\sigma,\delta_0,D}$ is given by (4.1).

### 4.2.2 Distribution of clouds

Around one source, a distribution of clouds is present, each of them generating a field given by (4.5). As illustrated on the right of figure 4.1, let us consider a source contained in a DM host of mass $M$, and characterize the distribution of clouds surrounding it by the mass $m$ of their underlying dark matter halos. As suggested by the notations, we consider the mass $M$ to be larger than the masses $m$, since the baryons in the DM halos of mass $m$ are supposed not to have collapsed, while a luminous source is already formed in the host of mass $M$. Note also that to help avoiding confusion we call 'host' the DM overdensity of mass $M$ which hosts the source, and 'halos' the DM overdensities of mass $m$ containing the clouds.

By definition of the correlation function (Peebles, 1980), the probability of finding a DM halo of mass $m$ within a spherical shell of volume $4\pi D^2 dD$, at a distance $D$ from a host of mass $M$ is given by

$$d^2P(D,m|M) = \frac{dn_m}{dm}(1 + b_h(M)b_c(m)\zeta(D))\ 4\pi D^2 dD\ dm, \tag{4.6}$$

where $dn_m/dm$ is the mass function of halos. Its expression is given by the Press-Schechter formalism (Press & Schechter, 1974, see also Mo et al., 2010). The function $\zeta$ is the linear matter density correlation function, and two bias parameters, $b_h(M)$ and $b_c(m)$, are introduced, respectively for the host of mass $M$ and the halo of mass $m$, to represent the enhancement of these overdensity peaks with respect to the background mass overdensity (cf. Mo et al., 2010, for instance).

Clouds contained in halos of mass $m$ induce the generation of a magnetic energy $E_m(D)$ in the IGM, as discussed in the above section, and are distributed around hosts of mass $M$ according to (4.6). Summing up the contributions of all the clouds surrounding the source contained in the host of mass $M$, we may say that a source generates a magnetic energy

$$\boxed{E_M = \int_{r_s}^{r_s+\ell_{\nu_1}} \int_{m_{\min}}^{m_{\max}} E_m(D)\ d^2P(D,m|M)}. \tag{4.7}$$

(Energy Generated by One Source surrounded by a Distribution of Clouds)

The boundaries of the first integral express the fact that only the clouds inside the 'interaction zone' (cf. figure 4.1) generate significant magnetic fields. Let us now discuss the boundaries of the second integral, namely $m_{\min}$ and $m_{\max}$.

**A troublesome degeneracy?** In expression (4.5) the cloud is characterized by the couple of parameters $(\sigma, \delta_0)$, representing its characteristic size and central overdensity, because these are the *two* key parameters entering the magnetogenesis mechanism under consideration. Now, in this chapter we are aiming at computing the mean field generated by a typical cosmological distribution of such clouds using the Press-Schechter formalism. A difficulty arises from the fact that, in this formalism, overdensities are characterized by their mass only, i.e. by only *one* parameter. This degeneracy is somewhat troublesome because the value of the generated magnetic field depends on the details $(\sigma, \delta_0)$ of the clouds, and not just their mass.

**Parameters $\delta_0$ and $\sigma$: relevant ranges** As a halo of a given mass $m$ can contain a cloud of mass $m_c$ that can be either small and dense (small $\sigma$ but large $\delta_0$), or large and dilute (large $\sigma$ but small $\delta_0$), the first step to alleviate this difficulty is to discuss the relevant ranges for the parameters $\delta_0$ and $\sigma$.

The relevant values of $\delta_0$ are constrained by the absorption by the cloud of the energetic photons (of frequency $\nu_1$) emitted by the source. Indeed, totally opaque clouds cannot contribute efficiently to the magnetization of the IGM since no photon passes through them. More precisely, when light crosses a cloud modeled as a Gaussian overdensity $\delta_0$ of width $\sigma$ embedded in a background density $\bar{n}$, the radiation intensity behind the cloud is attenuated by a factor

$$\epsilon = e^{-\sigma_{\nu_1}\int n_{\mathrm{HI}} dr} \simeq e^{-\sigma_{\nu_1}\bar{n}(1+\delta_0)2\sigma} \tag{4.8}$$

with respect to the ambient radiation field. Using the fact that $\bar{n}\sigma_{\nu_1} = \frac{1}{\ell_{\nu_0}}\left(\frac{\nu_1}{\nu_0}\right)^{-3}$, we may invert relation (4.8) to get

$$1 + \delta_0 \simeq \frac{\ell_{\nu_0}}{2\sigma}\left(\frac{\nu_1}{\nu_0}\right)^3 \ln \epsilon^{-1}. \tag{4.9}$$

From this expression, we easily get estimates of the relevant parameter ranges. Indeed, consider for instance a cloud overdensity with $\delta_0 \simeq 5.5$. At a redshift of $z = 15$, we have shown that $\ell_{\nu_0} \simeq 0.05$ kpc (cf. table 3.1).

Considering $\nu_1 = 10\nu_0$ photons, a cloud size of $\sigma \simeq 5$ kpc gives $\epsilon \simeq 0.27$. Considering $\nu_1 = 4\nu_0$ photons, the same cloud suffices to bring the attenuation factor $\epsilon$ down to $1.5 \times 10^{-9}$. As expected, we see that clouds with larger overdensities $\delta_0$ need to be smaller in extent for them to be relevant to our mechanism.

On the other hand, larger overdensities correspond to halos that are more advanced in their evolution towards becoming fully non-linear structures that end up hosting luminous sources. Since we are interested here in starless clouds only, we cannot consider too large values of $\delta_0$. At the same time, too small values would correspond to tiny linear perturbations unable to provide the medium with significant enough anisotropies of the lines of sight from the central source of ionizing photons. Thus, a reasonable compromise is to consider, as we did, clouds with $\delta_0 \simeq 5.55$. Of course, this value is not chosen randomly, since it corresponds to the density contrast of a cloud at its turn-around, in the spherical collapse model, in a flat, matter dominated universe (see for instance Mo et al., 2010, p. 217).

Once $\delta_0$ is fixed, we just need to limit the range of the parameter $\sigma$. As we just saw, one upper bound is easily set by requiring that the resulting attenuation factor is not too small, i.e. the cloud is not totally opaque. Another upper bound is simply that, located at a distance $D$ from the source of ionizing photons, the width of a cloud cannot be larger than $D - r_s$, otherwise it would encroach on the Strömgren sphere of the source, which is not physical. Thus, in principle, when considering a distribution of clouds, we could consider widths between 0 and the minimum of these two upper bounds. However, we want to consider true clouds and not transient density fluctuations due to acoustic pressure waves in the IGM. Thus, the lower bound on $\sigma$ is actually set naturally by the Jeans length, which is also consistent with the fact that we consider cloud overdensities around their turn-around.

Finally, assuming that baryons occupy DM halos with the universal fraction, i.e. that the mass of the cloud $m_\mathrm{c}$ is linked to the mass of its parent DM halo $m$ by

$$m_\mathrm{c} = \frac{\Omega_b}{\Omega_m} m, \tag{4.10}$$

and using the fact that a cloud parameterized by $(\sigma, \delta_0)$ has a mass $m_\mathrm{c} \simeq \frac{4\pi}{3}\sigma^3 \bar{n}(1+\delta_0) m_\mathrm{p}$ ($m_\mathrm{p}$ is the proton mass), these considerations then translate in a straightforward manner in terms of the lower and upper bounds $m_\mathrm{min}$ and $m_\mathrm{max}$ in equation (4.5).

## 4.3 Magnetic Energy Density Generated in the IGM

Now that we know the magnetic field generated around an isolated source, in order to compute the field generated in the whole Universe, we need to take into account the cosmological context in which sources evolve. This will consist in three things. First, the sources are contained in hosts of mass $M$, and we will use the Press-Schechter formalism to estimate their statistical distribution, just like we did for the clouds. Second, we need to take into account the fact that among all the DM overdensities forming, not all of them contain sources and also in principle we need to model when (at which $z$) the sources form. We are going to choose a rate at which DM hosts 'switch on', i.e. in which a source forms, that makes our model consistent with an important observational constraint on EoR, namely the optical depth parameter deduced from the Planck data. Indeed, if too many hosts contain sources, then the EoR happens too fast compared to observations, and vice versa. Third, a shortcoming we need to remedy is that by simply summing up the contribution of the sources that appear, we are not taking into account the overlapping of the various Strömgren spheres, which is the very essence of EoR, and that is all the more important here that the present magnetogenesis model operates in the neutral regions only. Therefore, something must account for the fact that sources switching on early are isolated and thus indeed generate the energy computed in the previous section, but those appearing towards the end of the EoR hardly contribute to the magnetization of the IGM because not much of the neutral gas is left. In this work, we propose to circumvent these two last difficulties using the concept of ionization fraction of the IGM as follows.

### 4.3.1 Ionization of the IGM

Recall that one of the conclusions of chapter 3 is that in our simple model of EoR, the first galaxies constituted the best compromise with respect to the various constraints. We will thus for the present discussion consider as the sources of ionizing photons only first galaxies.

**Ionized Volume associated with DM hosts of mass $M$** Consider a dark matter halo of mass $M$. Assuming baryons occupy it with the universal fraction, it contains a mass $\frac{\Omega_b}{\Omega_m} M$ of baryons. However, not all this mass is converted into the stars constituting the hosted ionizing source, and we will call $f_*$ the fraction of baryons converted into stars. Now, the volume of the ionized bubble generated by the source is the volume of a sphere of radius equal to the Strömgren radius (e.g. Loeb & Furlanetto, 2013, and the

considerations of section 3.2.4)

$$r_s = \left( \frac{3\dot{N}_{\rm ion}}{4\pi\alpha_B C n_{\rm HI}^2} \right)^{1/3}, \tag{4.11}$$

where $\alpha_B$ is the case-B recombination coefficient ($\alpha_B = 2.6 \times 10^{-13}$ cm$^3$s$^{-1}$ at a gas temperature of $10^4$ K), $n_{\rm HI}$ is the neutral hydrogen number density in the IGM, and $C$ is the hydrogen clumping factor. The latter depends on the redshift and is still rather poorly constrained. We use the fitting function $C(z) = 27.466\exp(-0.114z + 0.001328z^2)$ obtained by Mellema et al. (2006). Finally, the rate at which the source emits ionizing photons is by definition $\dot{N}_{\rm ion} = \int_{\nu_0}^{\infty} \frac{L_\nu}{h\nu} d\nu$. Now using the results from the Yggdrasil model (Zackrisson et al., 2011, and additional ingredients like IMF and metallicity discussed in section 3.2.4), we find that for $10^6 M_\odot$ primordial galaxies, the spectral index is $\alpha \sim -2$, the cut-off frequency $\nu_1 \sim 4\nu_0$ and the normalisation $L_0 \sim 3 \times 10^{25}$ erg s$^{-1}$ Hz$^{-1}$. From this we find that the rate of ionizing photons emitted per baryons is $\dot{N}_\star = 60$ Myrs$^{-1}$, and since there are $f_* \frac{\Omega_b}{\Omega_m} \frac{M}{m_{\rm p}}$ baryons in the stars constituting our source, we find that the relevant rate at which ionizing photons are emitted is

$$\dot{N}_{\rm ion} = f_* f_{\rm esc} \dot{N}_\star \frac{\Omega_b}{\Omega_m} \frac{M}{m_p}, \tag{4.12}$$

where we add the factor $f_{\rm esc}$, the escape fraction, to account for the fact that only a fraction of the emitted photons may participate in the formation of the cosmological Strömgren sphere.

All in all, we will associate to DM halos of mass $M$ hosting sources an ionized volume given by

$$V_{\rm ion}(M) = \frac{f_* f_{\rm esc} \dot{N}_\star}{\alpha_B C n_{\rm HI}^2} \frac{\Omega_b}{\Omega_m} \frac{M}{m_p}, \tag{4.13}$$

where $\dot{N}_\star = 60$ Myrs$^{-1}$.

**Ionized fraction** Neglecting any residual neutral fraction within ionized bubbles and calling $g_{\rm gl}$ the rate at which sources switch-on in DM halos, the ionized fraction at time $t$, i.e. the volume filling factor of ionized bubbles, is given by

$$Q_i(t) = \int^t dt \int_{M_*} dM \; V_{\rm ion}(M) \; g_{\rm gl} \; \frac{dn_M}{dM}. \tag{4.14}$$

Indeed, $(dn_M/dM)\, dM$ is the comoving number density of DM halos of mass between $M$ and $M + dM$ (obtained using the Press-Schechter formalism), and each of these halos is weighed by the volume it ionizes when it contains a source thanks to the multiplication by $g_{\rm gl} V_{\rm ion}(M)$. The lower mass limit for hosting galaxies is set to $M_* = 10^8 M_\odot$, corresponding to halos massive enough for atomic cooling, and gas condensation to be effective with a pristine gas composition (e.g. Loeb & Furlanetto, 2013).

**Parameters consistent with data and simulations** A requirement is that our model of Reionization must be consistent with the observations and the simulations related to EoR. This will enable us to choose relevant numerical values for some of the free parameters of the model.

The parameters $f_*$ and $f_{\rm esc}$ are uncertain and depend both on redshift and the source of ionizing photons. For example, observations of galaxies at $z \sim 3$ by (Iwata et al., 2009) indicate an escape fraction of $f_{\rm esc} < 0.1$ while numerical simulations (Wise & Cen, 2009; Hayes et al., 2011; Wise et al., 2014) suggest that at high redshifts it can be larger than 0.1. Here the detail of $f_*$ and $f_{\rm esc}$ will not matter, the important point being the number of ionizing photons outside the source, be it because there are a lot of stars or because photons escape easily. Therefore we will combine these two parameters by defining the parameter $f_{\rm eff} \equiv f_* f_{\rm esc}$ and set $f_{\rm eff} = 10^{-3}$ in our fiducial model.

For the parameter $g_{\rm gl}$, we take it equal to zero at redshifts greater than 20, and $g_{\rm gl} = 1.5 \times 10^{-9}$ yr$^{-1}$ at $z \leq 20$, in order for our model with $f_{\rm eff} = 10^{-3}$ to be consistent with the measurements of the ionization fraction during EoR. In our model, this epoch ends at $z = 7$, as shown in the top left plot of figure 4.2. For consistency checks, we also computed the Thomson optical depth to the CMB, and as shown in the top right graph of the same figure, the Reionization model we have assumed is perfectly consistent with the Planck cosmological results published in 2015: $\tau = 0.066 \pm 0.016$ (Planck Collaboration, 2015b, and still very well within the error bars of the most recent result $\tau = 0.058 \pm 0.012$ released by the Planck Collaboration, 2016).

### 4.3.2 Distribution of sources

The expression (4.7) we derived in the previous section corresponds to the energy generated in the IGM by an *isolated* source, while in principle when taking a distribution of sources into consideration, we must take into account the fact that the various Strömgren spheres overlap. This is essential since our mechanism is efficient only in neutral regions, so that we expect its efficiency to decrease as Reionization progresses.

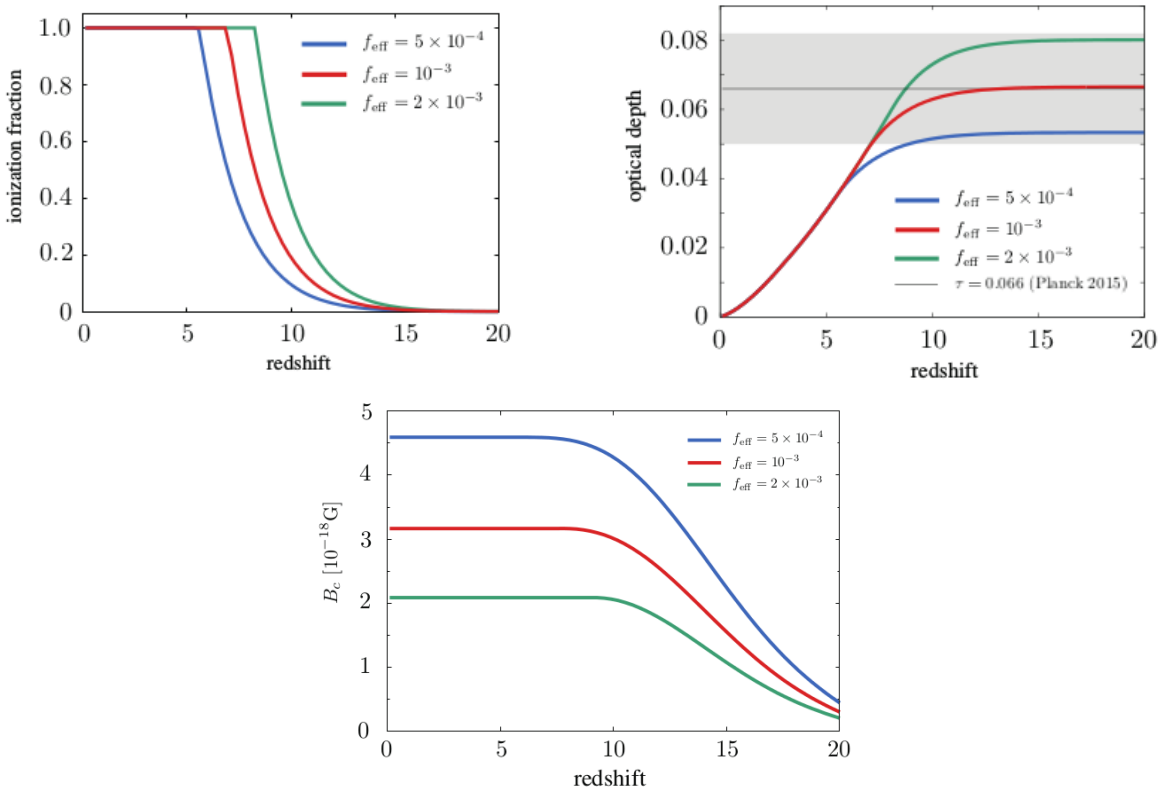


Figure 4.2: Evolution with redshift, for different reionization parameters, of the ionization fraction $Q_i$ (top left), of the integrated Thomson optical depth $\tau$ to the CMB (top right) and of the mean comoving magnetic field strength (bottom). The red, green and blue curves are for $f_{\rm eff} = 10^{-3},\ 2\times10^{-3},\ 0.5\times10^{-3}$, respectively. The spectral index of ionizing sources is set to $\alpha = -2$, corresponding to first galaxies.

Hence, we cannot simply add up the contribution of sources hosted in DM hosts with formula (4.7) without care, otherwise we would certainly overestimate the field generation. Instead, let us consider the following expression for the total comoving magnetic energy density present in the IGM at the time $t$:

$$\boxed{\frac{B_{\rm c}^2}{8\pi} = \int^t dt \frac{1-Q_i}{(1+z)^4} \int_{M_*} dM E_M\ g_{\rm gl}\ \frac{dn_M}{dM}}, \tag{4.15}$$

(Comoving Energy Density Generated during EoR)

where $B_{\rm c}(t)$ is the comoving strength of the magnetic field and $z$ is the redshift. First, similarly to what we did in expression (4.14) with $V_{\rm ion}(M)$, we weigh the number density of halos by $g_{\rm gl}$ so that once a source switches-on, we add its contribution, but at each timestep, we add the contribution only of the newly born sources as we should. Second, as we sum over time, we introduce a factor $1 - Q_i$ which reduces the amount of neutral Hydrogen in the model as time passes, consistently with the amount of sources switching-on since $Q_i$ is given by (4.14). And finally, the $(1 + z)^4$ factor comes from the fact that this formula corresponds to the comoving magnetic field, since adiabatic dilution by the expansion goes as $(1 + z)^2$ (cf chapter 2).

**Results** In Fig. 4.2, we plot the comoving strength of magnetic fields, $B_{\rm c}$, as a function of redshift, which tells the same information as the comoving energy density. The global trend is natural: as time passes, galaxies form and generate magnetic fields, i.e. convert some of their radiation energy into magnetic energy, which accumulates in the IGM, so that the curves raise with decreasing redshift. Once the Universe is totally ionized, the generation of magnetic fields stops. Green curves correspond to a Universe in which galaxies are 'strong', i.e. they emit ionizing photons at high rates (high $\dot{N}_{\rm ion}$, high $f_{\rm eff}$), either because stars are formed very efficiently (high $f_*$) or because photons are not trapped (high $f_{\rm esc}$). It is thus natural to see in figure 4.2 that they reionize the Universe faster than in the fiducial model (top left), and that in this case the optical depth is larger since more electrons are freed sooner (top right). The bottom plot of figure 4.2 may then come somewhat as a surprise, since it shows that the mean magnetic field generated in the Universe is weaker. But this surprise would originate in the same 'naïve' and incorrect intuition mentioned in section 3.2.3, namely that more powerful sources should generate stronger fields. In fact, we recover the idea that what matters in this mechanism is the compromise between having numerous photoionizations but in an extended neutral region. In this model where galaxies reionize the Universe fast, there is simply not enough

time for stronger magnetic field seeds to emerge, which explains why the green curve is below the others in the bottom plot of figure 4.2.

This model suggests that the Universe may be magnetized to the order of a few $10^{-18}$ G (comoving) thanks to photoionizations of the IGM all along the EoR. It is an interesting first approach to the problem and shows that the order of magnitude of the strength of the fields generated is not only important around isolated sources, but in a global context too. This approach also has the huge advantage of showing where the difficulties in the modeling are in view of a more refined approach, and it also gives us a valuable understanding of the various elements at play. However, it is clearly very simplistic in many aspects and may be improved in many ways. For example considering other sources than first galaxies as in chapter 3, we could derive the equivalent of the formula for the energy around an isolated source (4.7) but taking into account the possible vicinity of other sources. This would not be as straightforward as it seems, since we would need to assess properly the interaction between adjacent sources and about how the field is generated in and around clouds that are illuminated by multiple sources, is not obvious (e.g. how is the formula for the generated field modified when the radiation field is not unidirectional). Another improvement to take into account more precisely the spatial distribution of the generated field will be presented in section 5.2. Finally, now that we have a deep understanding of the mechanism and of its impact in the cosmological context thanks to analytical derivations, let us explore it further, in the following chapter, benefiting from numerical simulations of the EoR.

# Chapter 5

# Numerical approach

In parallel to the works presented in chapters 3 and 4, I have been exploring this magnetogenesis mechanism making use of the results of cosmological simulations. I am currently working in collaboration with D. Aubert (Strasbourg, France) and our work, introduced below, constitutes an article in preparation, with the provisional title 'Topological and Statistical Properties of Magnetic Field Seeds from Photoionization during Reionization' (Durrive & Aubert, 2016, in preparation).

## 5.1 Realistic shape of Strömgren spheres

**Exploring a contribution switched-off so far** Up to now, we have modeled our Strömgren spheres literally as 'spheres', i.e. spherically symmetric objects. However, as we have seen in chapter 1, it is clear from numerical simulations that realistic Strömgren spheres are highly anisotropic. This is important for our matters here because as we can see in the geometric term of the generated field, equation (3.22), an angular dependence of the Strömgren radius $r_s$ makes the gradient in that formula non radial and thus induces a non vanishing magnetic field. We anticipated this fact earlier in our intuitive discussion of chapter 3, as illustrated in the right of figure 3.4.

How significant will the generated field be? We can expect this contribution to be potentially very important, if not dominant, compared to the one studied so far due to the clumpiness of the IGM. Indeed, from the previous analysis, we know that the field is generated with the highest values and spans on the largest distances when the gradients are closest to the Strömgren sphere, since as we move away from the source, photons are absorbed and diluted making the mechanism less efficient. It is not obvious however which of the gradients in the IGM or of the shape of the Strömgren spheres are the greatest. We need to study precisely the importance of the geometry of the ionized regions around the sources.

While it has been enriching to pursue analytically in the previous chapters, it is interesting and important to also benefit from numerical tools to manipulate realistic configurations. D. Aubert and his collaborators (Aubert et al., 2015) developed an AMR code, named EMMA, simulating the EoR. This code includes collisionless dynamics, gas dynamics and radiative transfer in self-consistent simultaneous processing, so that the Strömgren spheres have realistic shapes. I use the Hydrogen density fields resulting from their simulations in formula (3.20). The difficulty to implement this formula is that we need to compute the gradient of the integral of the density, while the cube of data corresponding to $n_{\mathrm{HI}}$ is described using cartesian coordinates. Therefore, near the center, i.e. where the source is located, the sampling is very coarse so the gradient is badly defined, and since we are dealing with an integral quantity, the values far from the center are affected by the values computed near the center. In other words, errors accumulate. I developed a code bypassing this difficulty, and performed consistency tests, by recovering numerically the results derived analytically in chapter 3 with a spherical Strömgren sphere and a Gaussian inhomogeneity.

**An illustrative result** An example of a result is presented in figure 5.1, where the magnetic field generated around a galaxy at $z = 10$ is shown. In the left panel, the blue region corresponds to the Strömgren sphere, which has a realistic shape, and the green and yellow areas correspond to the clumpy IGM, with a realistic Hydrogen density distribution. In the right panel, the magnetic field in Gauss is shown. As expected, the field is strong all along the edge of the Strömgren sphere, and decreases with distance. In this example, the field strength reaches up to roughly $10^{-18}$ G, which is the order of magnitude obtained in chapter 3 when the Gaussian inhomogeneity was put very close to the ionization front ($D \sim r_s$). The Strömgren sphere acts like a collection of little Gaussian inhomogeneities. In this figure we can also perceive the footprint of the 'interaction zone'. Indeed, starting from the edge of the Strömgren sphere, the magnetic field may be roughly decomposed in three shells: the red in which $B$ is very strong, the green with intermediate values, and the blue in which the field is extremely weak. The green area corresponds to the 'interaction zone', in which photons are not too absorbed and diluted. Now, is the field generated *inside* the Strömgren sphere relevant? At this stage, this question remains open because formula (3.20), used to derive this map of magnetic field,

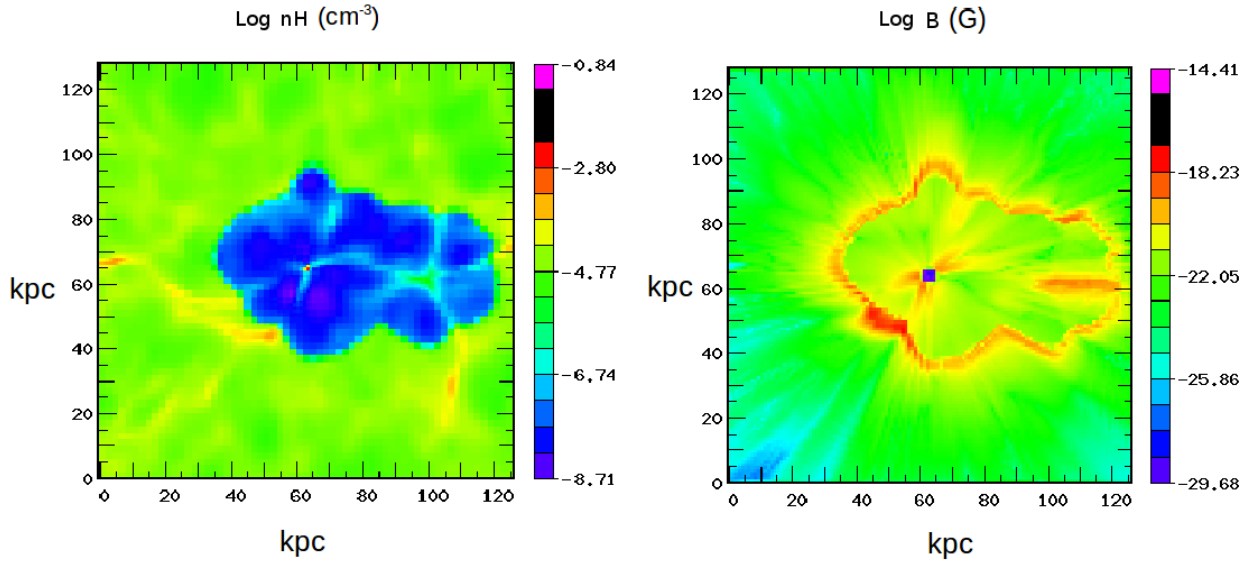


Figure 5.1: Left: Density field of neutral Hydrogen around a galaxy at $z = 10$ from a run of the EMMA cosmological simulation. The green areas are mostly neutral, while the blue constitute the fully ionized region, the Strömgren sphere, which is clearly not spherically symmetric. Right: Magnetic field generated through photoionizations using formula (3.20) with the density field of the left panel. See text for a discussion.

is valid in the mostly neutral region outside the Strömgren sphere, but I still have to check properly whether the assumptions made to lead to it may nevertheless be relevant inside it. But most importantly, these values do not influence much the values outside the sphere because the absorption inside is extremely small since the density of neutral gas there is extremely small.

Figure 5.1 confirms that this mechanism participates to the magnetization of an important fraction of the IGM, far from the sources. This is interesting in the prospect of the question of the origin of magnetic fields in voids, cf. chapter 1. But it is also interesting to see the outskirts of Strömgren spheres being magnetized, since this may have an impact on the formation of the next generation of stars. Indeed, even though of extremely weak strengths, as many works have already shown, they may be amplified very quickly and end up playing important dynamical roles. However, as discussed in chapter 3, in regions where electron density and temperature gradients are important, such as the edge of Strömgren spheres, the Biermann battery may be the dominant process Doi & Susa (2011). The key point and particularity of the present mechanism is that it may generate fields on large scales and far from the sources.

## 5.2 Statistical properties

A particularity of this magnetogenesis mechanism is that we have the full details of its generation. In primordial magnetogenesis models for instance, we have access only to statistical information, such as the power spectrum of the field. Here, we may refine the model endlessly to characterize the field. Two natural further steps in the modeling that we initiated in the above works are (i) taking the evolution of the Strömgren spheres into account and (ii) computing the magnetized volume fraction, as illustrated in figure 5.2, rather than simply the mean energy density generated. Indeed, sources generate magnetic fields of high strengths close to their Strömgren spheres and very weak further out. Therefore, at a given epoch, we expect a small fraction of the Universe to be highly magnetized, at strengths corresponding to those generated at the outskirts of the Strömgren spheres, and a weak magnetization of the whole Universe. In fact, recall (cf. figure 4.1) that in chapter 4 we introduced a factor $f$ to control the radial extent of the magnetized region around one cloud in our computation. Numerically, with the code that led us to figure 4.2, we observed that for $f$ typically greater than 2 the mean energy density did not vary anymore. This shows that the field is generated essentially inside or close to the clouds, showing the importance of assessing this more precisely, with a figure like 5.2. I have already done the calculations to estimate this analytically, in the same lines as for the mean energy density presented in the previous chapter. It will also be very enlightening to compare these analytical results with the numerical exploration I am currently undertaking using the outcomes of the EMMA code (Durrive & Aubert, 2016, in preparation).

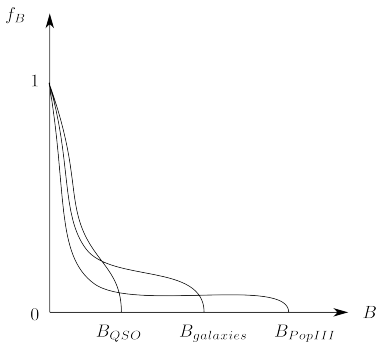


Figure 5.2: One possible improvement to the simple estimate of the mean energy density presented in chapter 4, is to compute the magnetized volume fraction for the three types of sources we are considering. This figure shows a sketch of the result we may expect from the outcomes of chapter 3: Population III star clusters generate fields of high strength but in small volumes of the Universe, while quasars do the opposite and galaxies have an intermediate behaviour. This result is within reach by modifying slightly the calculations of chapter 4.

# Part II

# Gravitational Fragmentation of the Cosmic Web

As discussed in chapter 1, matter in the Universe is distributed in a web-like structure. To describe it, three types of structures are distinguished, characterized by their geometry: Walls are planar structures, filaments are cylindrical, and nodes are spherical. This part of the manuscript is dedicated to studying the stability of walls and filaments of the cosmic web with respect to gravitational instability. In chapter 6 we will first study the various equilibria relevant to describe the cosmic web. Then chapter 7 will be an introduction to spectral theory as a tool to perform stability analyses, i.e. to study waves and instabilities in these equilibria. I will first present it in the context where I learnt it from, namely the plasma literature, and then present how I transported this tool to the context of gravitational instability. Chapter 8 will be dedicated to this in the planar case, relevant to study the stability of Cosmic Walls. Although this geometry is simple, the equations will turn out to be rather involved, so that this will also constitute a necessary preliminary step to the analysis of the cylindrical case, that of Cosmic Filaments, which includes additional effects due to curvature. This will be introduced in chapter 9, together with other ongoing works and prospects. I did this work in collaboration with M. Langer, and what is presented in chapter 8 will soon be published (Durrive & Langer, 2016, to be submitted).

# Chapter 6

# Equilibrium States of Cosmic Walls and Filaments

The aim of this chapter is to compute the important equilibrium quantities of various environments relevant to model the cosmic web, and that will constitute the equilibria that we will perturb in the following chapters. Since we are ultimately interested in the evolution of *perturbations*, we may at first consider too quickly a discussion of the *equilibrium state*, while in fact one should not underestimate its analysis. Indeed, as we will see later (section 8.2.4), equilibrium relations will be the key to simplifying and understanding the evolution of perturbations. References of historical importance on the equilibrium states of self-gravitating structures are, for planar structures Ledoux (1951), and for cylinders Ostriker (1964b). But for an extremely detailed study of polytropes (Lane-Emden equations, exact solutions and approximate solutions by the method of multiple scales, magnetopolytropes, distorted, relativistic, rotating, with background, expanding polytropes, etc) see Horedt (2004).

## 6.1 Governing Equations

In this study, we will consider static equilibrium states. Physically, the static assumption corresponds to considering equilibria such that the collapse and accretion are very slow, slower than the growth time of the perturbations. The extension to equilibria with flow will be discussed in chapter 10, and the outcome of it will be that flows make the analysis extremely involved and rich, but the essential features appear already in the static case. Hence, the set of equations governing the equilibrium quantities, denoted with a subscript 0, we are interested in here is the set (2.32) with vanishing velocity. Momentum conservation reads $-\vec{\nabla}p_0 + \vec{j}_0 \times \vec{B}_0 + \rho_0 \vec{g}_0 = \vec{0}$, where $p_0$, $\vec{j}_0$, $\vec{B}_0$, $\rho_0$ and $\vec{g}_0$ are respectively the equilibrium pressure, current density, magnetic field, density, and gravitational acceleration. However in the present chapter we are going to explicit only equilibria of unmagnetized fluids, relevant for the cosmological context in which magnetic fields are extremely weak. Momentum conservation thus reduces to the following hydrostatic equilibrium

$$\boxed{-\vec{\nabla}p_0 + \rho_0 \vec{g}_0 = \vec{0}} \tag{6.1}$$

(Hydrostatic equilibrium)

Physically, this relation states that the equilibrium density profile is such that pressure counterbalances gravity at every position. Note that as such, with only equation (6.1), $\vec{g}_0$ is not constrained. It may be due to an external structure, for example a planet attracting its atmosphere or a Dark Matter halo shaping the gravitational potential well in which a galaxy forms, but it may also be due to the structure itself. The latter case, of self-gravitating structures, is of great importance in the Astrophysical and Cosmological context. The field $\vec{g}_0$ has then to be computed self-consistently with (6.1), which is the purpose of the Poisson equation. As discussed in section 2.4, the equilibrium gravitational acceleration and potential are governed by

$$\boxed{\vec{\nabla} \cdot \vec{g}_0 = -\omega_0^2} \text{ or } \boxed{\Delta \Phi_0 = \omega_0^2} \tag{6.2}$$

(Equilibrium Poisson equation)

where both quantities are linked through $\vec{g}_0 = -\vec{\nabla}\Phi_0$, and where I define the extremely important frequency

$$\boxed{\omega_0^2 \equiv 4\pi G \rho_0} \tag{6.3}$$

(Characteristic Frequency for Gravitation)

which is position dependent for general density profiles.

As discussed in section 2.3, in order to have a closed set of equations defining fully the equilibrium state, we still need to add to (6.1) and (6.2) a relation between $p_0$ and $\rho_0$, and throughout the manuscript we will consider the dynamics of fluids with a polytropic equation of state

$$\boxed{p_0 = \kappa \rho_0^\gamma} \tag{6.4}$$

(Polytropic Equilibrium)

where $\gamma$ is the polytropic exponent, a constant given by the number of internal degrees of freedom of the particles the fluid is made of, as introduced in section 2.3. Note that in the literature, equilibrium states are more often described in terms of the polytropic index $n$ rather than the polytropic exponent $\gamma$, which is essentially the same since both are simply linked by

$$\gamma = 1 + 1/n. \tag{6.5}$$

The reason of this redundancy in notations is the following. The polytropic index $n$ is more natural to use when working on the equilibrium state, because it appears naturally in the Lane Emden equation that we shall see below (cf equation (6.23)), while working with the polytropic exponent $\gamma$ is more natural when discussing perturbations, because, as we shall see in section 9.2, a crucial point will be to compare how the equilibrium state and perturbations behave thermodynamically, corresponding to comparing their respective polytropic exponents $\gamma$ with $\gamma_{ad}$.

One of the most important quantities of the equilibrium state is the adiabatic speed of sound defined as $c_a \equiv \sqrt{\frac{\partial p_0}{\partial \rho_0}}$ where the derivative is taken at constant entropy. For a polytrope we have

$$c_a^2 = \gamma \frac{p_0}{\rho_0} = \kappa \gamma \rho_0^{\gamma - 1}. \tag{6.6}$$

An important point to notice is that since in general $\rho_0$ is a decreasing function of position (i.e. with distance from the center of the sphere, filament or slab), $c_a^2$ is decreasing too for $\gamma > 1$ but increasing for $\gamma < 1$. At the critical value $\gamma = 1$ the speed of sound is uniform, which corresponds to an isothermal atmosphere. I stress this property of the equilibrium state, anticipating our discussion on the behaviour of perturbations in stratified media. Indeed, we know that in an atmosphere with a non uniform temperature, the speed of sound varies with the position, so that wave fronts are distorted as they travel through the medium. This process gives rise to acoustic mirages and to the peculiar trajectories of p-modes in stars (cf the discussion around figure 7.1 below), which is the equivalent of the mirages occuring with light in deserts, on the sea or on the road, where temperature gradients induce position dependent refractive indices. Hence already from this fact we expect the system to be physically easier to interpret in the case of an isothermal atmosphere, but also mathematically it is clear that having $c_a^2$ a constant rather than a function will surely simplify greatly the analysis. For these reasons, in this manuscript, we will often focus on the case of isothermal atmospheres. As we will see when generalizing to arbitrary $\gamma$'s, both for the equilibrium and for perturbations, $\gamma = 1$ will clearly appear as a critical value, separating regimes of qualitatively different nature.

## 6.2 Uniform External Gravitational Acceleration

For starters, let us consider the simplest case: A plane stratified (in the $x$ direction) polytropic atmosphere in a uniform external gravitational field $\vec{g}_{\text{ext}} \equiv g_{\text{ext}} \hat{x}$. We will consider $g_{\text{ext}} < 0$, having in mind an upward $x$ direction. As we will see (sections 8.1.3 and 8.3.3) this model is important to rely on, to manipulate the tools to analyse perturbations with minimal mathematical complications, as well as to develop our physical intuition of the processes at play. But this model is also of physical interest per se: The self gravity of the atmosphere of a planet is completely negligible compared to the field in which it is embedded, so that this model is perfectly suited to analyse waves in planetary atmosphere for instance.

### a) Density

The hydrostatic equilibrium (6.1) then simply reads

$$p_0' = \rho_0 g_{\text{ext}}. \tag{6.7}$$

Note the use of the notation $g_{\text{ext}}$ rather than $g_0$ here: We will use $g_0$ in self-gravitating situations, requiring Poisson equation (6.2), while here $g_{\text{ext}}$ is a given quantity in the problem. Now together with the polytropic equation of state (6.4), the hydrostatic equilibrium yields:

**Non-isothermal fluid ($\gamma \neq 1$)** In this case

$$\left(\rho_0^{\gamma-1}\right)' = \frac{\gamma-1}{\kappa\gamma} g_{\rm ext}. \tag{6.8}$$

Now, for a clearer presentation and in particular to compare the various equilibria discussed in this section, let us work with dimensionless quantities. Define

$$\bar{\rho}(x) \equiv \frac{\rho_0(x)}{\rho_c} \text{ with } \rho_c \equiv \rho_0(0), \tag{6.9}$$

where the subscript $c$ is used here in anticipation of the self-gravitating cases for which $\rho_c$ will represent the central (at $x = 0$) value of the density and will be used extensively. Let us also adapt the length unit by working with

$$\bar{x} \equiv \frac{x}{L_\gamma} \text{ with } L_\gamma \equiv -\frac{1}{|\gamma-1|}\frac{c_a^2(0)}{g_{\rm ext}}. \tag{6.10}$$

The choice of sign comes from the fact that $g_{\rm ext} < 0$. Then the equation on $\rho_0$ becomes (now $'$ is $d/d\bar{x}$)

$$\left(\bar{\rho}^{\gamma-1}\right)' = \pm 1 \tag{6.11}$$

i.e. using the definition $\bar{\rho}(0) = 1$ to explicit the integration constant,

$$\boxed{\bar{\rho} = (1 \pm \bar{x})^{\frac{1}{\gamma-1}}} \tag{6.12}$$

with a plus sign for $\gamma < 1$ and a minus sign otherwise.

**Isothermal fluid ($\gamma = 1$)** In this case

$$\frac{\rho_0'}{\rho_0} = \frac{g_{\rm ext}}{\kappa}. \tag{6.13}$$

Now, let us still work with the dimensionless density $\bar{\rho}(x) \equiv \frac{\rho_0(x)}{\rho_c}$ but

$$\bar{x} \equiv \frac{x}{L_1} \text{ with } L_1 \equiv -\frac{c_a^2}{g_{\rm ext}}. \tag{6.14}$$

We have used the fact that, in this isothermal case, $\kappa$ is equal to $c_a^2$ (cf. relation (6.6)) and is a constant, so that there is no need to specify the position at which it is evaluated. Also, the choice of sign again comes from the fact that $g_{\rm ext} < 0$. Then the equation on the density becomes

$$(\ln\bar{\rho})' = -1 \tag{6.15}$$

so that, because $\bar{\rho}(0) = 1$, this state corresponds to an *exponential atmosphere*

$$\boxed{\bar{\rho} = e^{-\bar{x}}}. \tag{6.16}$$

We will come back to it several times in this manuscript, as a basis to build our understanding of more complex situations.

**b) Gravitational potential and acceleration**

By construction here

$$\vec{g}_0 = g_{\rm ext}\hat{x} \tag{6.17}$$

and since $\vec{g}_0 = -\vec{\nabla}\phi_0 = -\phi_0'\hat{x}$ we obtain

$$\phi_0(x) = -g_{\rm ext}x + \phi_c \tag{6.18}$$

where $\phi_c \equiv \phi_0(0)$.

## 6.3 Self-Gravitating Baryonic Structures

Let us now focus on self-gravitating systems: The gravitational acceleration in which the fluid is embedded is the one produced by its own density profile. In other words, we now include Poisson equation (6.2).

**a) Density**

The hydrostatic equilibrium (6.1) for a general polytrope (6.4) gives

$$\vec{g}_0 = \kappa\gamma\rho_0^{\gamma-2}\vec{\nabla}\rho_0. \tag{6.19}$$

Taking the divergence of this equation and using Poisson equation (6.2) yields the equation governing $\rho_0$.

**Non-isothermal fluid ($\gamma \neq 1$)** With dimensionless density $\bar{\rho} \equiv \frac{\rho_0}{\rho_c}$ this gives

$$\begin{cases} \Delta\left(\bar{\rho}^{\gamma-1}\right) + \dfrac{\bar{\rho}}{L_\gamma^2} = 0 & \text{for } \gamma > 1 \\ \Delta\left(\bar{\rho}^{\gamma-1}\right) - \dfrac{\bar{\rho}}{L_\gamma^2} = 0 & \text{for } \gamma < 1 \end{cases} \tag{6.20}$$

where

$$L_\gamma \equiv \sqrt{\frac{\kappa}{4\pi G}\frac{\gamma}{|\gamma-1|}\rho_c^{\gamma-2}}. \tag{6.21}$$

It is now natural (cf discussion around definition (6.5)) to put

$$\theta \equiv \bar{\rho}^{\gamma-1} \tag{6.22}$$

and to work with the polytropic index $n \equiv 1/(\gamma-1)$ to finally rewrite this as

$$\begin{cases} \Delta\theta + L_\gamma^{-2}\ \theta^n = 0 & \text{for } \gamma > 1 \\ \Delta\theta - L_\gamma^{-2}\ \theta^n = 0 & \text{for } \gamma < 1 \end{cases} \tag{6.23}$$

In the stellar literature, i.e. in spherical geometry, this is called a Lane-Emden equation. In the following, we will keep this terminology for other geometries too. Note that there is a qualitative change for $\gamma > 2$ and $< 2$: The characteristic length scale $L_\gamma$ in (6.21) is decreasing or increasing with $\rho_0(0)$ depending on that ordering. In particular, for $\gamma = 2$ the equation (6.31) does not depend on $\rho_0(0)$ at all anymore. In fact in that case the Lane-Emden equation is a simple harmonic oscillator so that the solutions are sine and cosine, which indeed do not present any envelop tending to zero at infinity.

**Isothermal fluid ($\gamma = 1$)** With now

$$\theta \equiv \ln\bar{\rho} \tag{6.24}$$

and

$$L_1 = \sqrt{\frac{\kappa}{4\pi G\rho_c}} \tag{6.25}$$

where here $\kappa$ is equal to $c_a^2$ since the fluid is isothermal, the same procedure yields

$$\Delta\theta + L_1^{-2}\ e^\theta = 0 \tag{6.26}$$

In mathematics this is called a Liouville equation, but as above, I will call Lane-Emden equation the equation governing $\theta$ (i.e. $\rho_0$) in all cases for simplicity. The isothermal case is particularly convenient as it presents very simple exact solutions. In planar geometry with $\bar{x} \equiv \frac{x}{L_1}$ we have

$$\boxed{\bar{\rho}(\bar{x}) = \cosh^{-2}\left(\frac{\bar{x}}{\sqrt{2}}\right)} \tag{6.27}$$

and in cylindrical geometry with $\bar{R} \equiv \frac{R}{L_1}$ we have

$$\boxed{\bar{\rho}(\bar{R}) = \left(1 + \frac{\bar{R}^2}{8}\right)^{-2}} \tag{6.28}$$

both chosen to have $\bar{\rho}(0)' = 0$ for simplicity.

Contrary to the uniform external acceleration case of section 6.2, the equation on $\rho_0$ for a self-gravitating fluid is of second order, therefore we need two boundary conditions to uniquely define the solution rather than one. In figure 6.1 we have considered density profiles flat at the center, namely such that

$$\bar{\rho}'(0) = 0 \tag{6.29}$$

which is reasonable physically, but it is a priori not necessary.

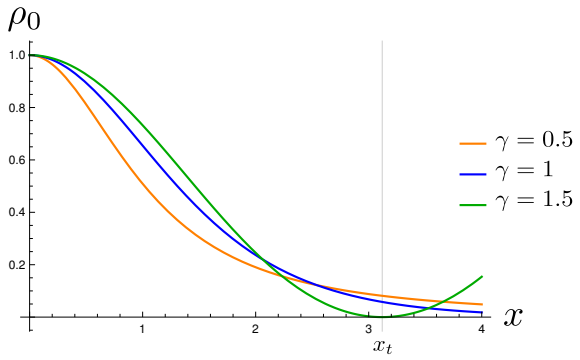


Figure 6.1: Profile $\rho_0(x)$ of a self-gravitating slab for various types of polytropes ($\gamma = 0.5$, $\gamma = 1$ and $\gamma = 1.5$) with $\rho(0)' = 0$. For $\gamma > 1$ the profile should be truncated. The vertical line indicates $x_t$ the position given by the thickness (6.37). The same plots for a cylindrical profile $\rho_0(R)$ are visually identical. In fact, the length scales $L_\gamma$ and $L_1$ are independent of the geometry considered, since they appear in equations (6.23) and (6.26) without expliciting the Laplacian operator.

**b) Gravitational potential and acceleration**

From relation (6.19) we obtain

$$\vec{g}_0 = -\vec{\nabla}\phi_0 \text{ where } \phi_0 = \begin{cases} \frac{\kappa\rho_c^{\gamma-1}\gamma}{\gamma-1}\left(1-\bar{\rho}^{\gamma-1}\right) + \phi_c & \text{for } \gamma \neq 1 \\ -\kappa \ln\bar{\rho} + \phi_c & \text{for } \gamma = 1 \end{cases} \tag{6.30}$$

where $\phi_c \equiv \phi_0(\vec{0})$ is the central value of the potential.

**c) Extent of the structure**

The density profiles of cylinders and slabs are finite in extent for $\gamma > 1$, while they are infinite otherwise and a thickness may be defined only by an arbitrary truncation. Determining the extent of the structure is crucial, because as we will see in the following chapters, the evolution of perturbations (the spectrum) strongly depends on the boundary conditions.

Let us now explicit the thickness in the planar geometry, since it is the case we will discuss the most in this manuscript. As mentionned, the following discussion is relevant only for $\gamma > 1$ where the finite extent exists. Then using the nondimensionalized position $\bar{x} \equiv x/L_\gamma$ (so $'$ here stands for $d/d\bar{x}$) where $L_\gamma$ is given by (6.21), the Lane-Emden equation (6.23) becomes

$$\theta'' + \theta^n = 0. \tag{6.31}$$

Multiplying this equation by $\theta'$ we may rewrite each term as a derivative, so that, integrating, we obtain

$$(\theta')^2 + \frac{2}{n+1}\theta^{n+1} = c_0 \tag{6.32}$$

where $c_0$ is a constant, chosen equal to the value of the left hand side at $x = 0$. Note that this relation provides us with the value of the derivative of the density at the edge of the slab, which can be a valuable information when discussing the boundary conditions. Now, since by definition $\theta(0) = 1$, we have

$$c_0 = (\theta_0')^2 + \frac{2}{n+1} \tag{6.33}$$

with $\theta_0' \equiv \theta'(x = 0)$. Since $\theta' \equiv \frac{d\theta}{d\bar{x}}$, equation (6.32) may be rewritten

$$\int_\theta^1 \frac{d\theta}{\sqrt{c_0 - \frac{2}{n+1}\theta^{n+1}}} = \pm\int_{\bar{x}}^0 d\bar{x} = \mp\,\bar{x} \tag{6.34}$$

where the fact that $\theta(\bar{x} = 0) = 1$ has been used. For the situations of interest $0 \leq \theta \leq 1$, so that the square root is well defined. With the change of variable $\varphi = \alpha\theta$ where $\alpha = (\frac{2}{(n+1)c_0})^{\frac{1}{n+1}}$, followed by a power law change of variable, the integral in the left hand side of (6.34) can be rewritten in terms of the incomplete beta function $B_z(a,b) \equiv \int_0^z t^{a-1}(1-t)^{b-1}dt$. Doing so we finally get that

$$\bar{x} = \pm\left(\frac{c_0^{\frac{1-n}{2}}}{2(n+1)^n}\right)^{\frac{1}{n+1}}\left[B_{\frac{2}{(n+1)c_0}\bar{\rho}^{1+1/n}}\left(\frac{1}{n+1},\frac{1}{2}\right) - B_{\frac{2}{(n+1)c_0}}\left(\frac{1}{n+1},\frac{1}{2}\right)\right] \tag{6.35}$$

This relation looks complicated but is in fact simply in the form $f(\bar{\rho}) = \bar{x}$, so all that is left to do is invert the first beta function in the right hand side (the inverse Beta function can be evaluated to arbitrary numerical precision in Mathematica for instance) and we may have $\bar{\rho}$ explicitly as a function of $\bar{x}$. But for the present discussion, let us only explicit the thickness. Let's call $\bar{x}_t$ the smallest $\bar{x}$ for which $\bar{\rho}$ vanishes, which is the natural way of defining the thickness of the slab. Since $\gamma > 1$ we have $n > 0$ and thus $\bar{\rho}(\bar{x}_t)^{\frac{n+1}{n}} = 0$ without singularity. Now since $B_0(a, b) = 0$ by definition of this function, relation (6.35) gives (getting rid of $\pm$ because $\bar{x}_t > 0$)

$$\bar{x}_t = \left( \frac{c_0^{\frac{1-n}{2}}}{2(n+1)^n} \right)^{\frac{1}{n+1}} B_{\frac{2}{(n+1)c_0}} \left( \frac{1}{n+1}, \frac{1}{2} \right) \tag{6.36}$$

Finally, the simple result we may keep in mind is that for the particular but common case of a flat central profile, $\bar{\rho}'(0) = 0$. The thickness is then simply given by

$$\boxed{\bar{x}_t = \sqrt{\frac{\gamma - 1}{2\gamma}} B \left( \frac{\gamma - 1}{\gamma}, \frac{1}{2} \right)} \tag{6.37}$$

(Thickness of a $\gamma > 1$ Self-Gravitating Slab)

where now $B$ is the ordinary beta function.

## 6.4 Baryonic Structures Embedded in Dark Matter

In the cosmological context, baryons are not purely self-gravitating, but are often embedded in Dark Matter. Describing the equilibrium system as a bi-fluid, we have that the gravitational potential satisfies the following Poisson equation, rather than (6.2),

$$\Delta \Phi_0 = 4\pi G \left( \rho_0 + \rho_0^d \right) \tag{6.38}$$

where $\rho_0$ is the equilibrium profile of baryons as before, and $\rho_0^d$ is a chosen equilibrium profile of the Dark Matter fluid. The hydrostatic equilibrium equation remains unchanged. Then the Lane Emden equations, (6.23) for $\gamma \neq 1$ and (6.26) for $\gamma = 1$, acquire a right hand side, namely

$$\begin{cases} \Delta\theta + L_\gamma^{-2}\, \theta^{\frac{1}{\gamma-1}} = -L_\gamma^{-2}\, \dfrac{\rho_0^d}{\rho_c} & \text{for } \gamma > 1 \\ \Delta\theta + L_1^{-2}\, e^{\theta} = -L_1^{-2}\, \dfrac{\rho_0^d}{\rho_c} & \text{for } \gamma = 1 \\ \Delta\theta - L_\gamma^{-2}\, \theta^{\frac{1}{\gamma-1}} = L_\gamma^{-2}\, \dfrac{\rho_0^d}{\rho_c} & \text{for } \gamma < 1 \end{cases} \tag{6.39}$$

In section 6.3 we have been exploring the self-gravitating regime, corresponding to $\rho_0 \gg \rho_0^d$. But given the overall matter content of the Universe, with about five times more Dark Matter than baryonic matter, it is relevant[1] to study the opposite regime, namely $\rho_0 \ll \rho_0^d$. This limit corresponds to neglecting the second term in the left hand side of these equations. Therefore in this limit, the Lane-Emden equation becomes a Poisson equation, namely

$$\Delta\theta = \pm L_\gamma^{-2}\, \frac{\rho_0^d}{\rho_c} \tag{6.40}$$

with a minus sign for $\gamma \geq 1$ and a plus otherwise, and where $L_\gamma$ is given by (6.21) or (6.25) according to whether $\gamma = 1$ or not. For illustration, let us explicit two solutions of (6.40), one in each of the geometries of interest, and for simple Dark Matter profiles. Indeed, the dynamics of Dark Matter is in essence collisionless, and is best treated in a kinetic approach. In the fluid description adopted here, we are reduced to considering effective equilibrium profiles. Numerous studies of numerical cosmological simulations show that a remarkably good fit to the profiles of spherical Dark Matter halos is the so-called 'NFW profile' (Navarro et al., 1996). Many alternatives exist though, in particular because of its cusp (e.g. Merritt et al., 2006; Hjorth et al., 2015). Similar studies for filaments and walls are more rare yet. For walls I will use a simple model proposed in Wadekar & Hansen (2015) and for filaments I will use an NFW type profile, to illustrate the effect on the baryon density of a cusp in the Dark Matter profile. The ambition of this section is not to be exhaustive and build many physical models of walls and filaments. The point is to expose two examples which have the huge advantage of being analytical and particularly simple. They may constitute interesting toy models to start discussing stability. Indeed, having at hand very simple analytical models for the equilibrium is necessary given the complexity of the full equations governing the perturbations, as we will see in chapter 8.

[1] Note however that, despite the relevance of this idea, it is not obvious that the background always shapes the profile as such, as Harford & Hamilton (2011) argue.

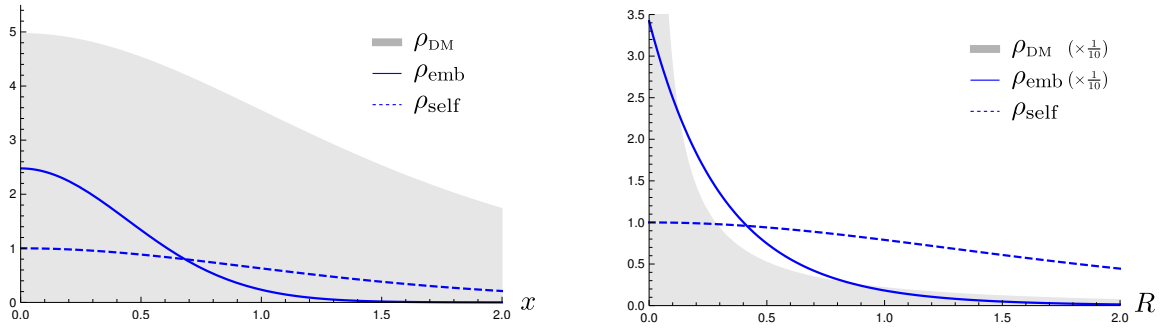


Figure 6.2: Density profiles in the isothermal case, comparing the self-gravitating and the embedded situations, in the planar (left panel) and cylindrical (right panel) cases. In order for this comparison to make sense, these plots are such that the total mass ($\int_0^\infty \rho dx$ in the planar case and $\int_0^\infty \rho r dr$ in the cylindrical case) is the same in both situations, i.e. the dashed blue curve represents a given self-gravitating structure, and the continuous blue curve represents the profile of the *same amount* of baryons but modified by the presence of Dark Matter, with profile represented by the gray area. Note that two curves on the right panel are shrinked by a factor 10 to make the plot more readable. Here $\xi = 5$ for the reason given in the text.

**Wall** In planar geometry, working with nondimensionalized length $\bar{x} \equiv x/L_\gamma$, we obtain

$$\theta'' = \pm \frac{\rho_0^d}{\rho_c}. \tag{6.41}$$

For illustration, let us consider a simple model for the Dark Matter background, namely a core with a power-law cutoff (Wadekar & Hansen, 2015)

$$\rho_0^d(x) = \rho_c^d \left(1 + \left(\frac{x}{L_d}\right)^2\right)^{-\frac{3}{2}}. \tag{6.42}$$

with central density $\rho_c^d$ and scale height $L_d$. Then equation (6.41) can be solved and gives

$$\boxed{\begin{cases} \bar{\rho}(\bar{x}) = \left[1 + \xi - \xi\sqrt{1 + \left(\frac{L_\gamma}{L_d}\bar{x}\right)^2}\right]^{\frac{1}{\gamma-1}} & \text{for } \gamma > 1 \\ \bar{\rho}(\bar{x}) = \exp\left[\xi\left(1 - \sqrt{1 + \left(\frac{L_\gamma}{L_d}\bar{x}\right)^2}\right)\right] & \text{for } \gamma = 1 \\ \bar{\rho}(\bar{x}) = \left[1 - \xi + \xi\sqrt{1 + \left(\frac{L_\gamma}{L_d}\bar{x}\right)^2}\right]^{\frac{1}{\gamma-1}} & \text{for } \gamma < 1 \end{cases}} \tag{6.43}$$

where

$$\xi \equiv \left(\frac{L_d}{L_\gamma}\right)^2 \frac{\rho_c^d}{\rho_c}. \tag{6.44}$$

An integration constant has been removed imposing $\rho_0'(0) = 0$ in the shown solutions. The isothermal expression should be compared to its self-gravitating counterpart (6.27).

**Filament** In cylindrical geometry, working with nondimensionalized radius $\bar{R} \equiv R/L_\gamma$, equation (6.40) reads

$$\frac{1}{\bar{R}}\left(\bar{R}\theta'\right)' = \pm \frac{\rho_0^d}{\rho_c}. \tag{6.45}$$

A way of getting some feeling of this expression is to consider the following simple Dark Matter model

$$\rho_0^d(R) = \frac{\rho_c^d}{\frac{R}{L_d}\left(1 + \frac{R}{L_d}\right)^\beta}, \tag{6.46}$$

inspired from the universal 'NFW' profiles of spherical halos. However, it turns out that the calculations in the $\beta = 2$ case are particularly simple, so that to lighten further the illustration, I will here only explicit

this case. Note that the profile is then really an NFW profile elongated in the longitudinal direction, and the solutions of (6.45) are

$$\boxed{\begin{cases} \bar{\rho}(\bar{R}) = \left[1 - \xi \ln\left(1 + \frac{L_\gamma}{L_d}\bar{R}\right)\right]^{\frac{1}{\gamma-1}} & \text{for } \gamma > 1 \\ \bar{\rho}(\bar{R}) = \left(1 + \frac{L_\gamma}{L_d}\bar{R}\right)^{-\xi} & \text{for } \gamma = 1 \\ \bar{\rho}(\bar{R}) = \left[1 + \xi \ln\left(1 + \frac{L_\gamma}{L_d}\bar{R}\right)\right]^{\frac{1}{\gamma-1}} & \text{for } \gamma < 1 \end{cases}} \tag{6.47}$$

where $\xi$ is also given by (6.44). The isothermal expression should be compared to its self-gravitating counterpart (6.28). Look at the isothermal case. We see that close to the center ($R \ll L_d$) the profile plummets as $\sim 1 - \xi\frac{R}{L_d}$. How steep is this in our context? Consider the total mass per unit length $m_\infty \equiv \int_0^\infty \rho_0 r dr$, and the same for Dark Matter noted as $m_\infty^d$. With the expressions of the Dark Matter profile (6.46) and of the self-gravitating one (6.28), it is easy to show that the parameter $\xi$ governs the relative quantity of Dark versus baryonic matter since we have

$$\xi = 4\frac{m_\infty^d}{m_\infty}. \tag{6.48}$$

Now, since in the cosmological context there is typically five times more Dark than baryonic matter, $\xi \sim 20$ is a relevant value. Therefore the profile in the embedded case is extremely steep. Figure 6.2 shows these profiles in the isothermal case, comparing the self-gravitating and the embedded situations in the planar and cylindrical cases.

The expressions above may constitute very useful toy models to manipulate the equations on the perturbations that we are going to derive in the following chapters.

# Chapter 7

# Spectral Theory

Equilibrium configurations such as those discussed in the previous chapter may be stable or unstable. In the latter case, the fate of the system is in great part dictated by the first stages of evolution of the perturbations which drive it away from its initial state and lead it towards fragmentation. The fragmentation of self-gravitating sheet-like and filamentary structures may in principle occur through many different instabilities. In the cosmological context, thermal, Rayleigh-Taylor, Kelvin-Helmholtz, etc., may play a role in the denser environments of massive haloes (e.g. Kereš & Hernquist, 2009). In the more dilute environment of the filamentary cosmic web, gravity is the universal actor at play. Gravitational instability of sheet-like structures has been explored by several authors since the seminal work of Ledoux (1951), essentially in the context of the ISM. Most of these studies, if not all, concentrated on the gravitational instability of equilibria configuration with an isothermal equation of state (e.g. Ledoux, 1951; Simon, 1965b), pressure confined (e.g. Elmegreen & Elmegreen, 1978; Miyama et al., 1987a,b; Narita et al., 1988), including rotation (e.g. Safronov, 1960; Simon, 1965a; Narita et al., 1988; Burkert & Hartmann, 2004) and magnetic fields (e.g. Strittmatter, 1966; Kellman, 1972, 1973; Langer, 1978; Nakano & Nakamura, 1978; Tomisaka & Ikeuchi, 1983; Nakano, 1988). Studies that consider deviations from isothermality include Goldreich & Lynden-Bell (1965) who obtained stability criteria for pressure bounded, uniformly rotating polytropic sheets. The fragmentation of cylindrical filaments was first studied by Chandrasekhar & Fermi (1953) in the magnetized, isothermal and incompressible case and has been since then the object of careful attention of many authors including, in addition to those mentioned above, notably Ostriker (1964a), and more recently Breysse et al. (2014) and Freundlich et al. (2014a) for instance. Most these studies, if not all, approach the problem with the usual procedure of analyzing the system of linearized equations in the so-called primitive variables (see section 7.1.1 below). In the present work, we will adopt a different approach. We will study the onset of gravitational instability in the frame of spectral theory, in the force operator formalism introduced below, and notably derive the full wave equation satisfied by the displacement vector (cf. chapters 8 and 9).

As discussed at the beginning of chapter 6, in order to understand the evolution of matter in the Universe, a detailed analysis of instabilities *in stratified media* is essential. When on the contrary an equilibrium is stable, perturbations oscillate about the equilibrium state. Understanding the occurrence and evolution of such waves represents complementary information that helps understand instabilities. But it is also important to study waves per se, as they can play fundamental dynamical roles, essentially by carrying energy, the importance of which cannot be underestimated in physics. I have presented in chapter 2 the general equations governing the dynamics of self-gravitating, possibly magnetized fluids, and in chapter 6 the various physically interesting equilibrium states in the astrophysical context. The purpose of this chapter is to introduce general tools for stability analyses.

Ultimately, I wish to understand gravitational fragmentation of magnetized structures in full generality, because it is of great importance in the astrophysical context, where magnetized structures are omnipresent. However, including magnetic fields in cosmological structures is not necessary in a first approach, because cosmological magnetic fields are far too weak to play any dynamical role. Thus, the dynamics of the cosmic web is essentially hydrodynamical. Also, as we will see, even without magnetic fields, studying gravitational fragmentation is already quite involved. Hence, it would seem normal to leave considerations on magnetic fields for future work only. Yet, I will not do so, for two simple reasons. First, the tools I propose to use to tackle the question of gravitational fragmentation (even hydrodynamical only) are based on the works of plasma physicists, who developed them primarily to study the stability of plasmas in tokamaks for fusion research. Therefore, in this manuscript, discussing magnetic fields will serve as the example to follow, and generalize in some aspects. Second, as we will see, because I will adapt the description to that used by plasma physicists, my work and results derived in the hydrodynamical case will be ideally formulated to naturally incorporate magnetic fields in the description. My goal of describing magnetized gravitational fragmentation will thus be at reach in a rather close future, though still as a prospect for the present work.

We will proceed as follows. In section 7.1, I will present the general tools necessary for stability analyses, belonging to the realm of *spectral theory*. I will provide a brief overview of their scope, to give the reader

a flavor of their amazing extent, but also in order to situate where the specific approach I will adopt in this manuscript fits in, namely that of the eigenvalue problem formulation in the force operator formalism. Then in section 7.2, I will show how this method is applied to study magnetized structures without gravity, in the frame of ideal MHD. In the light of this, we will be ready to focus on waves and instabilities due to gravitation, without magnetic field. In section 7.3, we will discuss the general features of the problem, in preparation to chapter 8, in which we will delve into a thorough analysis of the particular example of a planar stratification, i.e. to study the stability of cosmic walls.

## 7.1 Generalities

In section 7.1.1, first I will present the most natural and common approach to study gravitational fragmentation, namely the linearization of the fluid equations in terms of the so-called primitive variables. Then I will justify that it is extremely advantageous to rather work in terms of what is called the Lagrangian displacement vector, and to perform the stability analysis in the frame of spectral theory, reformulating the problem as an *eigenvalue problem*. In sections 7.1.2, 7.1.3 and 7.2, I summarize, in my own words and adapted to the present purpose, a certain number of points developed in the book of Goedbloed & Poedts (2004). This will introduce the reader to the tools that I used in my own work, and will also be the opportunity to assess its scope, and to help foresee the promising results it will later lead to. Then, from section 7.3 to the end of the manuscript, unless mentioned otherwise explicitly, the rest is the work that I have done myself.

### 7.1.1 Governing Equations

#### a) Linearization with the primitive variables

Consider a magnetized, self-gravitating, static structure at equilibrium, i.e. suppose that we have found a set of time-independent functions $\{\rho_0(\vec{r}), \vec{v}_0(\vec{r}) = \vec{0}, p_0(\vec{r}), \vec{B}_0(\vec{r}), \phi_0(\vec{r})\}$ satisfying the set of equations (2.32). We are interested in assessing how this system reacts to a given small amplitude perturbation. Following the usual procedure, we do so by considering that the variables[1] $\rho, \vec{v}, p, \vec{B}$ and $\phi$, are in the form

$$\left\{\begin{array}{rcccl} \rho(\vec{r},t) & = & \rho_0(\vec{r}) & + & \rho_1(\vec{r},t) \\ \vec{v}(\vec{r},t) & = & \vec{0} & + & \vec{v}_1(\vec{r},t) \\ p(\vec{r},t) & = & p_0(\vec{r}) & + & p_1(\vec{r},t) \\ \vec{B}(\vec{r},t) & = & \vec{B}_0(\vec{r}) & + & \vec{B}_1(\vec{r},t) \\ \phi(\vec{r},t) & = & \phi_0(\vec{r}) & + & \phi_1(\vec{r},t) \end{array}\right. \tag{7.1}$$

where quantities with the subscript 1 constitute initially small deviations from the equilibrium quantities, marked with subscript 0, i.e. that $|\rho_1| \ll \rho_0$, $|p_1| \ll p_0$, $|\vec{B}_1| \ll |\vec{B}_0|$ and $|\phi_1| \ll |\phi_0|$. Note that there is a subtlety for $\vec{v}_1$ since we are considering a static background $\vec{v}_0 = \vec{0}$ and that $|\vec{v}_1|$ cannot be smaller than 0. A relevant quantity to compare it to would be the local speed of sound (subsonic perturbations), but we shall not try to be more rigorous on that point here, and we will simply assume $|\vec{v}_1|$ to be 'small enough' to be considered as a first order quantity.

Plugging expressions (7.1) in the set of equations (2.32), keeping only first order terms, and simplifying the resulting equations using the fact that the equilibrium quantities satisfy (2.32), we are left with the following set of linearized equations:

$$\left\{\begin{array}{ll} & \text{Linearized:} \\ \partial_t \rho_1 + \vec{\nabla}\cdot(\rho_0\vec{v}_1) = 0 & \text{(Mass conservation)} \\ \rho_0\partial_t\vec{v}_1 = -\vec{\nabla}p_1 + \vec{j}_1\times\vec{B}_0 + \vec{j}_0\times\vec{B}_1 - \rho_1\vec{\nabla}\phi_0 - \rho_0\vec{\nabla}\phi_1 & \text{(Momentum Conservation)} \\ \vec{j}_1 = \frac{1}{\mu_0}\vec{\nabla}\times\vec{B}_1 & \text{(Ampère's law)} \\ p_1 = c_a^2\rho_1 & \text{(Closure Relation)} \\ \partial_t\vec{B}_1 = \vec{\nabla}\times\left(\vec{v}_1\times\vec{B}_0\right) & \text{(Induction Equation)} \\ \Delta\phi_1 = 4\pi G\rho_1 & \text{(Poisson Equation)} \end{array}\right. \tag{7.2}$$

I will give more details on the meaning of the terms in the momentum conservation in the next section, where I expose again this set of equations but in the form that will be suited for the subsequent analysis, namely equation (7.29).

[1] These variables are referred to as 'primitive' to contrast with the other variable, $\vec{\xi}$, that we will later use instead, and which is, in a sense, more 'sophisticated'.

**Switching-off convection** Let me give a precision on the closure relation above. In the linearization procedure, we have assumed that the equilibrium *and* the perturbed fluids satisfy the same set of equations (2.32), and in particular that the perturbed fluid remains a polytrope of exponent $\gamma$, identical to the one of the equilibrium, i.e. that $p_0 = \kappa\rho_0^\gamma$ and $p = \kappa\rho^\gamma$. Then, when linearizing, we have

$$p = \kappa\rho^\gamma = \kappa(\rho_0 + \rho_1)^\gamma \simeq \kappa\rho_0^\gamma(1 + \gamma\frac{\rho_1}{\rho_0}) \tag{7.3}$$

since $\rho_1 \ll \rho_0$, so that identifying with $p = p_0 + p_1$ and using the definition of the adiabatic speed of sound (6.6), we have

$$\boxed{p_1 = c_a^2\rho_1} \tag{7.4}$$

(Closure Relation for Perturbations – No convection)

As I will detail in section 9.2, by doing so we are preventing the advent of convective instability and of oscillations called g-modes. Allowing for different polytropic exponents, a more general equation of state, used notably in stellar physics, is given by relation (9.12). By adopting (7.4) we are avoiding the additional complications of g-modes and convection, which is a good thing since the priority of this manuscript is to study acoustic waves (p-modes in the stellar physics vocabulary) and their unstable counterpart, gravitational fragmentation, which matters the most in the context of the cosmic web.

**Other form of the Linearized Poisson equation** As for the equilibrium state, it is fruitful to think about the perturbations related to gravity both in terms of gravitational potential $\phi_1$ and acceleration $\vec{g}_1$. In the set of equations (7.2) I have explicited the linearized Poisson equation for the potential. For the acceleration, linearizing (2.30) gives

$$\boxed{\vec{\nabla}\cdot\vec{g}_1 = -4\pi G\rho_1}. \tag{7.5}$$

(Linearized Poisson Equation for $\vec{g}_1$)

Now, note that the gravitational potential $\phi_1$ is a scalar, so that one equation ($\Delta\phi_1 = 4\pi G\rho_1$) is sufficient, but $\vec{g}_1$ is a vectorial quantity so that, as such, the scalar relation (7.5) alone is not constraining enough to define it fully. The information missing in (7.5) is that the gravitational acceleration is a gradient ($\vec{g}_1 = -\vec{\nabla}\phi_1$) and is thus irrotational. Hence, to keep the same amount of information as when working with $\phi_1$, we must add the constraint

$$\vec{\nabla}\times\vec{g}_1 = \vec{0}. \tag{7.6}$$

In this manuscript, I will often privilege a description in terms of the gravitational fields $\vec{g}_0$ and $\vec{g}_1$ rather that the potentials $\phi_0$ and $\phi_1$ because, in my opinion, it makes the equations look simpler and thus easier to manipulate, as it avoids additional gradient operators.

Finally, note that equation (7.5) may also be written in integral form[2] as

$$\vec{g}_1 = -G\int \rho_1(\vec{r'})\frac{\vec{r}-\vec{r'}}{|\vec{r}-\vec{r'}|^3}d^3r', \tag{7.7}$$

or, in a form exhibiting the integral form of $\Phi_1$,

$$\vec{g}_1 = -\vec{\nabla}\Phi_1 \text{ where } \Phi_1 = -G\int\frac{\rho_1(\vec{r'})}{|\vec{r}-\vec{r'}|}d^3\vec{r'}, \tag{7.8}$$

which will constitute another point of view and other ways of formulating the problem, as for instance in section 7.3.

### b) A first approach to gravitational fragmentation

Let us for now focus on gravitation. Linearizing the equations making use of the primitive variables $\rho, \vec{v}, p$ and $\phi$, as we are doing so far, is the approach followed in every Cosmology textbook. Ignoring magnetic fields in (7.2) and considering the closure relation $p_1 = c_a^2\rho_1$, perturbations are governed by the linearized mass conservation, linearized Poisson equation and the following momentum conservation

$$\rho_0\partial_t\vec{v}_1 + \vec{\nabla}\left(c_a^2\rho_1\right) + \rho_1\vec{\nabla}\phi_0 + \rho_0\vec{\nabla}\phi_1 = \vec{0}. \tag{7.9}$$

[2]Omitting surface terms, the discussion of which is out of my scope here. For their analysis in the stellar case, see Cox (1980) and Smeyers & Van Hoolst (2010) for instance.

**A historic milestone** Among the results J. Jeans derived in his works on gravitational instability in the early twentieth century (Jeans, 1902), the best-known is what is now called the Jeans criterion. To derive it, let us consider the simplest equilibrium density profile possible, namely a homogeneous profile $\rho_0 =$ constant at rest. Note that this profile is *not* a solution of the equilibrium equations of a self-gravitating fluid (hydrostatic equilibrium and Poisson equation as discussed in chapter 6). The trick is to still manipulate the perturbation equations considering that the density $\rho_0$ does not depend on position, despite its conflict with the equilibrium equations. Doing so is now known as the 'Jeans swindle' (see for instance Binney & Tremaine, 2008). In this case, we get rid of the term $\vec{\nabla}\phi_0$ in (7.9) and treat $\rho_0$ and $c_a^2$ as mere constants. Then, taking the divergence of (7.9) and making use of the linearized mass conservation and Poisson equations, we obtain the following equation on $\rho_1$ only

$$\boxed{\partial_t^2 \rho_1 - c_a^2 \Delta \rho_1 - 4\pi G \rho_0 \rho_1 = 0}. \tag{7.10}$$

(Wave Equation – Jeans Swindle)

This equation is a type of *wave equation*, because of the presence of the d'Alembert[3] operator $c_a^{-2}\partial_t^2 - \Delta$. It governs the behaviour of density perturbations in this medium, that is, in the stable regime, of acoustic waves, and in the unstable regime, of gravitational fragmentation. Now, due to our assumptions, all coefficients are constant here, so that we may Fourier transform with respect to all variables (spatial and temporal). We may thus consider plane wave solutions

$$\rho_1 \propto e^{i(\vec{k}\cdot\vec{r} - \omega t)}. \tag{7.11}$$

Inserting these in the above wave equation yields the following dispersion relation

$$\boxed{\omega^2 = c_a^2 k^2 - 4\pi G \rho_0 = c_a^2 \left(k^2 - k_J^2\right)} \tag{7.12}$$

(Jeans Dispersion Relation)

where the (homogeneous) Jeans wavenumber is defined as

$$\boxed{k_J \equiv \sqrt{\frac{4\pi G \rho_0}{c_a^2}}}. \tag{7.13}$$

(Jeans Wavenumber)

From this, we can see that perturbations with a wavenumber $k$ greater than $k_J$ (i.e. small wavelengths) have a real angular frequency ($\omega^2 > 0$), corresponding to an oscillatory behaviour, while for $k$ smaller than $k_J$ (i.e. large wavelengths), perturbations grow exponentially with time ($\omega^2 < 0$), resulting in gravitational fragmentation of the equilibrium, homogeneous medium of density $\rho_0$. This result is known as 'Jeans criterion'.

It is enlightening to reformulate this criterion in terms of timescales. The characteristic timescale corresponding to gravitational attraction is the so-called free fall time

$$t_{\mathrm{ff}} \equiv \frac{1}{\sqrt{4\pi G \rho_0}}, \tag{7.14}$$

which is apparent in the right hand side of the equilibrium Poisson equation for instance, and the characteristic timescale of sound propagation is the time a sound wave takes to travel a distance $k^{-1}$, namely

$$t_{\mathrm{s}} \equiv \frac{1}{k c_a}. \tag{7.15}$$

The key point is that sound propagation is not instantaneous (while, as mentioned before, in our Newtonian framework gravitation is instantaneous), which is why $t_{\mathrm{s}}$ depends on the scale $k$ considered, and which is why for perturbations of large extent, pressure, mediated by sound waves, does not have time to compensate the gravitational infall of matter into the potential well generated by the overdensities. For small wavelengths on the contrary, pressure may balance gravity, resulting in simple oscillations. The wavenumber for which both times are equal, $t_{\mathrm{s}} = t_{\mathrm{ff}}$, is the Jeans wavenumber, marking the transition between oscillatory and exponential behaviour.

**Stratified media: Intuitively** But how do perturbations evolve (waves and gravitational fragmentation) in realistic media, which are not homogeneous, but stratified?

[3] More precisely, this is called a Klein-Gordon equation, in which the Jeans wavenumber (cf. below) acts as the mass parameter. Physically, it is interesting to thus see the competition between gravitational attraction of the background and pressure (quantified by the Jeans wavenumber) as an inertia of the perturbation (like mass in the particle physics context), and hence acoustic waves behave differently than in the absence of gravity.

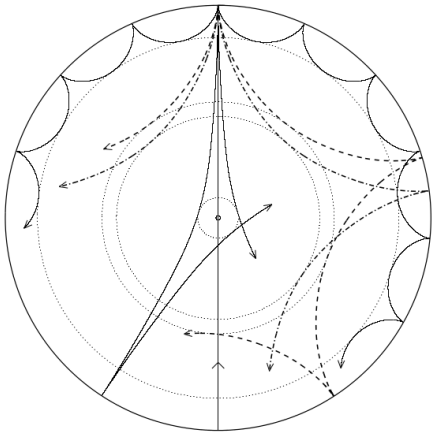

Figure 7.1: Schematic cross-section of the solar interior, in which the propagation of 'rays of sound' is represented, i.e. acoustic waves in the small wavelength limit, in analogy with geometrical optics. The curves ending with an arrow represent the direction perpendicular to wave fronts. As they go deeper towards the solar interior, they are bent by the increase in speed of sound due to the temperature stratification, until they reach a turning point (the collection of which forms the dotted circles) where they are totally refracted and start propagating towards the surface. At the surface the waves are totally reflected because the density gradient there is very steep. The various curves represent various modes, of different wavelengths. (Source: Figure 3 of İbanoğlu, 2000)

*Waves* — First, let us focus on the behaviour of acoustic waves. Naturally, waves in stratified media have long been a subject of study, for example in terrestrial contexts, such as seismology, atmospheric physics and oceanography, but also in the astrophysical context to understand stars for example, as their oscillations are not only a key to figuring out their dynamics but also to probe remotely from Earth their internal structure. Thanks to these researches, we are inheriting an abundant knowledge of the effects of stratification on the evolution of waves. For instance, just like light rays are bent by spatially varying refractive indices in temperature-stratified media (such as in a desert, a beach or a road heated by the sun), small wavelength acoustic waves may be described in terms of ray theory, with analogous behaviours. In stars for instance, the radial temperature gradient due to the central heating gives rise to the beautiful rosette-like shapes of the wave fronts of p-modes (i.e. acoustic waves) represented in figure 7.1.

Another physical process is at play in stratified media when they are subject to gravity, namely f-modes and Rayleigh-Taylor instability. To illustrate this, let us consider a piecewise-homogeneous fluid, i.e. a fluid composed of two homogeneous parts of different densities, lying one on top of the other. When the surface separating the two media is perfectly horizontal, that configuration is at equilibrium. If the upper fluid is lighter than the lower one, then this equilibrium is stable because a volume element from the upper fluid that is brought downwards in the denser fluid will be pushed back by buoyancy. The corresponding oscillations correspond to f-modes at the surface of stars for example. If on the contrary the upper fluid is denser, then the equilibrium is unstable and a slight perturbation of the separatrix will be amplified by gravity which will invert the ordering of the two media, the denser one taking the place of the lighter medium at the bottom. This is the so called Rayleigh-Taylor instability. Now, interpreting a continuously stratified medium as a collection of such interfaces with infinitesimally varying densities, we expect gravity in a stratified medium to either induce internal oscillations, when the density decreases with altitude, or an instability in the opposite case.

Many other phenomena may occur in complex situations, and my ambition is not to try and review them all here. Instead, let me mention a last point that is of great importance, notably in the study undertaken in this manuscript. From the aforementioned physical contexts, we are taught how much *boundaries* matter, and not only locally at the boundaries themselves, but they may impact the evolution of the whole structure. For instance, the behaviour of internal waves in the ocean depends on its depth, and similarly in atmospheres where the wavelength becomes comparable to the local density scale height, waves are reflected, leading to regions of mode trapping.

In light of this short discussion, we may already build up an intuition of what may happen in the cosmological context. Filaments of the cosmic web may act as waveguides, inducing a privileged direction for the propagation of waves, and thus redistribute anistropically the energy, along their longitudinal direction, i.e. towards the nodes. While in stars modes are trapped and have the trajectories illustrated in figure 7.1, in cylinders they are not trapped longitudinally so that they will have helicoidal trajectories instead. But cosmological filaments are not infinitely long. They are bounded by clusters. Therefore we may expect modes of longitudinal wavelength much smaller than the intercluster distance to behave qualitatively differently than those with a longitudinal wavelength greater than this length. Similarly, in the radial direction, the

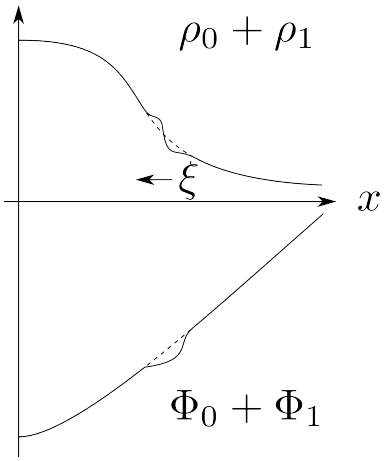


Figure 7.2: In dashed lines are sketches of a typical equilibrium density profile $\rho_0$ and its corresponding gravitational potential $\Phi_0$. In the presence of a small perturbation $\xi$, a little amount of matter is displaced from its equilibrium position, modifying slightly the density and potential profiles to respectively $\rho_0 + \rho_1$ and $\Phi_0 + \Phi_1$ (the continuous lines). The problem addressed in this part of the manuscript may then be stated as follows: Under certain conditions, to be determined, density perturbations induce potential well perturbations that may lead to the fragmentation of the global structure.

length scale associated with the stratification due to the density profile must delimit two different regimes for the behaviour of waves, with long wavelengths being stationary, as opposed to short wavelengths. These behaviours depend on how structured the filament is, since it most likely depends on how steep the density profile in the radial direction is, and on the relative density and size of the clusters it connects in the longitudinal direction. Therefore, it will strongly depend on the cosmological epoch and the scale of the considered filament. We also get a feeling that a Dark matter background, which may steepen equilibrium density profiles as we have seen in section 6.4, will also modify the behaviour of perturbations.

*Gravitational fragmentation* — The aforementioned considerations neglect, for legitimate reasons in their respective contexts, the following fact. An acoustic wave is essentially nothing but a succession of overdense and underdense regions, therefore, as represented in figure 7.2, *a wave propagating in a stratified medium modifies the gravitational potential well of the global structure within which it propagates.* More precisely, we may intuitively distinguish two processes:

(i) The overdensities constituting the wave will tend to fall into the overall potential well dictated by the global structure, i.e. '$\rho_1$ falls into $\Phi_0$', and the name 'Cowling' will be associated with this aspect in the following,

(ii) the overdensities constituting the wave generate potential wells too, and this local perturbation of the potential well affects the entire distribution of matter, i.e. '$\rho_0$ falls into $\Phi_1$', and the name 'Jeans' will be associated with this aspect in the following. This corresponds to the local growth of overdensities, hence to the gravitational fragmentation of the global structure.

Note that, in fact, one may think of an additional phenomenon: The overdensity may fall into the potential well it generates itself i.e. '$\rho_1$ falling into $\Phi_1$'. This corresponds to the self-gravity of the perturbation, just like the equilibrium profile $\rho_0$ is stemming from self-gravitation. However this effect is neglible because it is of second order.

*Orders of magnitude* — Let us now take a glimpse at the numerical values of the Jeans length in various structures of astrophysical and cosmological interest, and compare them with the relevant lengths involved. To do so, let us consider the following very simple estimate of the Jeans length: By definition $\lambda_J \equiv \frac{2\pi}{k_J} = \sqrt{\frac{\pi c_a^2}{G\rho}}$ and, for an ideal gas of Hydrogen, the speed of sound is given by $c_a^2 = \gamma \frac{k_B T}{m}$ where $\gamma = 5/3$ and $m$ is the proton mass. We then get

$$\lambda_J = \sqrt{\frac{\pi \gamma k_B T}{G m^2 n}}. \tag{7.16}$$

In a spherically stratified structure, like a star, perturbations may not be of arbitrary length: the wavelength of perturbations cannot exceed the perimeter of the star. Considering a sun-like star, with typical central volumic mass $\bar{\rho}_c \sim 10\ \mathrm{g\,cm^{-3}}$ and thus typical density about the surface $\bar{\rho}_s \sim 0.1\ \mathrm{g\,cm^{-3}}$ where the longest perturbation may be present, composed only of protons and with typical internal temperature $10^6$

K, we obtain

$$\lambda_J = 2 \times 10^6 \text{ km } \left(\frac{T}{10^6 \text{K}}\right)^{1/2} \left(\frac{n}{10^{23} \text{ cm}^{-3}}\right)^{-1/2}. \tag{7.17}$$

This value is of the order of the Solar perimeter. Therefore, perturbations in stars always have wavelengths shorter than the Jeans length, so that these objects do not fragment gravitationally but oscillate about their equilibrium configuration. This was to be expected since we know by experience that typical stars are gravitionally stable. Their lifetime is dictated by the amount of fuel they have to maintain nuclear fusion and not by gravitational instability. Having said that, note that this value of the Jeans length is *of the order* of the wavelength of the lowest order perturbations. Therefore, we may expect the lowest order perturbations to oscillate differently, in a manner to be defined precisely, than those with wavelengths significantly smaller than the Jeans length, since they oscillate with wavelengths close to those of the unstable regime.

A cylindrically stratified structure however is fundamentally different since one of its dimensions, the longitudinal one, has an infinite extent or, at least, an extent much longer than the other two dimensions. Perturbations of arbitrary (almost) wavelength may thus be present and fragmentation should, a priori, always be able to occur. In reality of course, structures like cosmological filaments have a finite extent, namely the distance separating the clusters that the filament interconnects. This is typically several Mpc long. The same applies to plane stratified structures, which even have two a priori unlimited directions. In reality, cosmic wall have typically dimensions (transverse to the stratification) of the order of the radius of cosmic voids, namely larger than a few tens of Mpc. These lengths should again be compared to the Jeans length. To get an idea, let us consider a homogeneous and isotropic universe in which the density depends on redshift as $\bar{n} \simeq 2 \times 10^{-7}(1+z)^3$ cm$^{-3}$, and the gas temperature depends on redshift as $T \propto (1+z)^2$, so that the Jeans length in the intergalactic medium decreases with redshift (increases with time) basically as $\lambda_J \propto (1+z)^{-1/2}$. During the Dark Ages, the intergalactic medium was quite cold, with temperature of the order of tens of Kelvins (e.g. Loeb & Furlanetto, 2013; Mesinger, 2016). Reionization then heated it up to roughly $T \sim 10^4$ K. Now, considering intergalactic values just before Reionization occured (say at $z \sim 9$, Planck Collaboration, 2016), we obtain

$$\lambda_J = 11 \text{ kpc } \left(\frac{T}{30\text{K}}\right)^{1/2} \left(\frac{n}{10^{-4} \text{ cm}^{-3}}\right)^{-1/2}. \tag{7.18}$$

In other words, voids, walls and filaments could have had typical sizes larger than the Jeans lengths during the Dark Ages, and may in principle have been subject to gravitational fragmentation.

Finally, note that with values more relevant for the interstellar medium, this simple estimate of the Jeans length yields (references values are those of the Cold Neutral Medium of the ISM Lequeux et al., 2005)

$$\lambda_J = 37 \text{ pc } \left(\frac{T}{10^2\text{K}}\right)^{1/2} \left(\frac{n}{30 \text{ cm}^{-3}}\right)^{-1/2}. \tag{7.19}$$

This falls precisely in the range of lengths scales of structures observed in the ISM, which is a sign that gravitational instability plays a major role in structure formation, and stresses the importance of fully understanding this processes.

The above intuitive discussion complemented with some orders of magnitude is an important start, but one may not conclude on the possibility of fragmentation directly from this, because the Jeans criterion (7.12) is derived from the study of the fragmentation of homogeneous equilibria. Let us now investigate precisely how this occurs in stratified media.

**Stratified media: Formally** The ultimate goal of my study is to identify where precisely the phenomena that we have discussed intuitively above appear in the formalism, in order to assess precisely the role they play in the structuring of the Universe at its largest scales. To do so, let us now look for the generalization of the wave equation (7.10), governing the dynamics of density perturbations $\rho_1$ around an arbitrary equilibrium density profile $\rho_0(\vec{r})$. Let us again take the partial time derivative of (2.13), the divergence of (7.9), and subtract them. This yields

$$\partial_t^2 \rho_1 - (\vec{\nabla}\rho_1 \cdot \vec{\nabla}\phi_0 + \vec{\nabla}\rho_0 \cdot \vec{\nabla}\phi_1) - (\rho_1 \Delta\phi_0 + \rho_0 \Delta\phi_1) - \Delta\left(c_a^2 \rho_1\right) = 0. \tag{7.20}$$

As such, this equation is already rather involved. But to get an equation for $\rho_1$ only, we still have to get rid of $\phi_1$. The difficulty comes from the fact that the gradient of $\phi_1$ intervenes while $\phi_1$ is linked to $\rho_1$ through its Laplacian only (the linearized Poisson equation (7.5)), so that the $\vec{\nabla}\rho_0 \cdot \vec{\nabla}\phi_1$ term requires further differentiation and manipulations. It is possible to do so, but the equation gets humongous and this procedure does not allow us to follow the meaning of the various steps. Also, in terms of content, the system studied here is in essence very simple: no convection, no rotation, no magnetic field, no flow, etc. Adding these ingredients would require a lot of additional work and ingenuity.

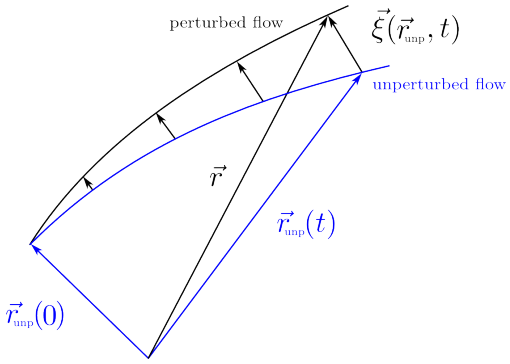


Figure 7.3: At a given time $t$, the displacement vector $\vec{\xi}$ is the difference between the position vector $\vec{r}$ of a fluid element of the perturbed fluid and the position vector $\vec{r}_{\rm unp}$ of that fluid element if the fluid were unperturbed (adapted from Frieman & Rotenberg, 1960).

Instead of trying to climb this mountain alone, I propose to follow the steps taken by researchers from another field, namely plasma physics. In great part motivated by the need to study the stability of tokamaks, plasma physicists already developed very powerful tools to analyze waves and instabilities in stratified media, of various geometries, in a most rigorous and systematic way. *My ambition is to study gravitational fragmentation in stratified media, having in mind the cosmic web, precisely in the line of their works.*

For instance, while in the homogeneous case above, we 'simply' have to consider plane wave solutions (7.11), how may we obtain information on the stability of the system, and on the properties of its fragmentation, when dealing with the more involved inhomogeneous case, governed by an equation that (7.20) gives a hint of the complexity? Also, how should one deal with geometric effects, when considering cylindrically stratified media such as in cosmic filaments? What is the importance and the role played by boundary conditions, a discussion which is of course absent in the homogeneous case? As we shall see, spectral theory (section 7.2) will be a very useful tool to help us probe the stability of such systems and answer these questions, and many others.

### c) Linearization with the Lagrangian displacement vector $\vec{\xi}$

The first step to match our approach of gravitational fragmentation to the techniques used by plasma physicists, is to use the same variable as they do. So far we have linearized the system of equations (2.32) in terms of the primitive variables $\rho, \vec{v}, p, \vec{B}$ and $\phi$ (or $\vec{g}$). In fact, it turns out to be extremely powerful to adopt a description making use of the so-called *Lagrangian displacement vector* $\vec{\xi}$, i.e. to perform a transformation called the Lagrangian reduction (Goedbloed & Poedts, 2004). This new variable is more fundamental in the sense that all the perturbed primitive quantities above may be expressed in terms of $\vec{\xi}$ alone, so that $\vec{\xi}$ carries all the information in itself.

Figure (7.3) represents intuitively what the displacement vector $\vec{\xi}$ is, in the most general case in which the unperturbed fluid is moving. The vector field $\vec{\xi}$ is defined by the relation

$$\vec{r} = \vec{r}_{\rm unp} + \vec{\xi}(\vec{r}_{\rm unp}, t) \tag{7.21}$$

where $\vec{r}$ is the position of fluid elements of the perturbed fluid, while $\vec{r}_{\rm unp}$ is the position of fluid elements of the unperturbed fluid. In other words, $\vec{\xi}$ *tells where the fluid elements are with respect to where they would be if the fluid were not perturbed.* It is a Lagrangian quantity in the sense that it is defined by following the fluid elements, as opposed to the Eulerian way of describing fluids, in which the flow field is described from fixed locations in space and through which the fluid flows. Historic milestones introducing the importance of this vector field are Bernstein et al. (1958) in the static case, and Frieman & Rotenberg (1960) in the presence of a stationary background flow.

To make use of $\vec{\xi}$ in practice, we need to relate it to the velocity flow $\vec{v}_1$. The main subtlety in doing so is that the primitive variables above are defined in the Eulerian description, while $\vec{\xi}$ is Lagrangian. Now, in the present manuscript I will work in the case of static equilibria (with only a brief presentation of what flows may modify in chapter 10), and we will admit that in this case the link between the Eulerian velocity perturbation $\vec{v}_1$ and the Lagrangian displacement vector $\vec{\xi}$ is simply

$$\boxed{\vec{v}_1 = \partial_t \vec{\xi}} \tag{7.22}$$

(Lagrangian Displacement Vector – Static Background)

In our context, the vector $\vec{\xi}$ is thus simply the time primitive of the velocity $\vec{v}_1$. For a more general and precise definition with the related derivations, see for instance section 12.2.2 of Goedbloed et al. (2010).

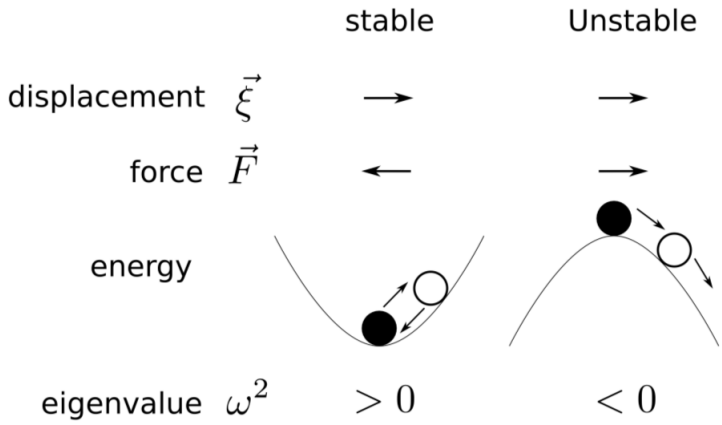


Figure 7.4: Intuitively, an equilibrium is stable if, when volume elements are displaced from their equilibrium position, the force acting on them brings them back to their initial position, otherwise the equilibrium is unstable. In a description based on the concept of energy, this corresponds to being at the bottom of a potential well (stable) or the top of a potential hill, and in a normal mode analysis terminology, stability is given by the sign of the eigenvalue $\omega^2$ (adapted from Goedbloed & Poedts, 2004).

Let us now try to get a sense of the physical meaning of the Lagrangian reduction we are presently undertaking.

(i) Linearizing in terms of the primitive variables consists in saying that when a system initially at equilibrium undergoes a small perturbation, each of the variables $\rho, \vec{v}, p, \vec{B}$ and $\phi$, separately, is (weakly) modified. However these quantities do not evolve independently, and the challenge consists in finding how these quantities may have been modified in a consistent way. Formally, this corresponds to solving a set of equations. Intuitively, if we perturb a given physical quantity, the system rearranges itself through a cascade of events so that it returns to an equilibrium configuration in the stable case. For example, if the magnetic field, for some reason, gets a little bit different here, then pressure gets adjusted, and thus density varies as well, etc.

(ii) In the description using the displacement vector, the first step will be to express all these physical primitive quantities in terms of $\vec{\xi}$ only[4]. Therefore, in this description, we will be able to tell directly what the magnetic field, the density etc. are equal to, given how the fluid elements are displaced by the perturbation. Thus, the problem will be reduced to telling where the fluid elements are, i.e. determining *how the fluid elements move* in the system in reaction to the perturbation. Formally, this will correspond to solving the equation governing $\vec{\xi}$ (see the eigenvalue problem of equation (7.28) below), and *only then* will we be able to deduce the behaviour of the physical quantities. This approach is thus more fundamental than the previous one in the sense that, once we have solved for $\vec{\xi}$, we know virtually everything about the system.

These two approaches are thus very different, but which is best? As always, it all depends on the answers we are looking for, i.e. the precise questions we are asking. An approach such as based on the wave equation (7.20) on $\rho_1$ for example would 'only' tell us how the density evolves. But this may be sufficient in certain situations. Hence, this primitive approach may still be interesting when it turns out to be simpler and sufficient. I will come back to this comment in section 9.3, but until then I will focus on using the Lagrangian displacement vector, which is the most powerful tool.

Let us now explore how to study the stability of a system when perturbations are described in terms of $\vec{\xi}$. This will provide the reader with a global picture of what can be done, and will be the opportunity to set the frame in which the work I will then present, about gravitational fragmentation, fits in.

### 7.1.2 Stability: Intuitively

There are at least two essential ways of analyzing the dynamics of systems: reasoning in terms of *forces*, using essentially Newton's laws, and reasoning in terms of *energy*, with Euler-Lagrange, Hamilton, or Hamilton-Jacobi's equations. Historically these two viewpoints correspond to respectively Newton's and Liebniz's legacies. Of course, adopting one or the other yields the same results, but depending on the answers we are looking for and depending on the situation, one approach may turn out to be more convenient than the other. As far as linear stability studies are concerned, these two viewpoints are summarized (i) intuitively speaking in figure 7.4 and (ii) formally speaking in figure 7.5. The latter will be discussed in more details in the next section.

[4] cf. equation (7.22) for $\vec{v}_1$, which comes from the definition of $\vec{\xi}$, and then respectively (7.30) for $\rho_1$, (7.31) for $p_1$, (7.32) for $\vec{B}_1$ and (7.34) for $\vec{g}_1$, which come from the physics governing the system, i.e. from the conservation laws.

Intuitively, if one perturbs an equilibrium state by displacing a volume element from its position $\vec{r}$ to a position $\vec{r}+\vec{\xi}$, two situations may occur: (i) the local forces acting on the volume element bring it back towards its initial position ($\vec{\xi}$ and $\vec{F}$ in opposite directions in figure 7.4), or (ii) they take it away from its initial position ($\vec{\xi}$ and $\vec{F}$ in the same direction in figure 7.4). The first situation corresponds to a *stable* equilibrium, the other one to an *unstable* equilibrium. Using the energetic description, stable situations correspond to minima of the potential energy and unstable situations to maxima[5].

Note that in fact, one may think of other possibilities, which we will not consider in this manuscript, but that are interesting to keep in mind. For instance, once displaced, the volume element may come back towards its equilibrium position, auguring stability, but with a restoring force that provides it with enough energy for it to leave again this position, thus transiting rather than actually settling back. This may occur several times, resulting in oscillations around the original position but with increasing amplitude, and ending up in an instability. The restoring force has been 'too efficient', and this phenomenon is thus rightly called *overstability*.

Another interesting subtlety, is that of *$\sigma$-stability*. As always in physics, what is relevant is to compare processes with one another. In non trivial systems, many phenomena are in competition, and an equilibrium may be in the absolute unstable, as described previously, but if the characteristic timescale of the instability is longer than the other timescales of relevance in the problem, then this instability will not have time to develop, and we would in that sense be dealing in practice with stability. In thermonuclear confinement for instance, one is interested in equilibria stable *only long enough* to obtain fusion. The $\sigma$ in the expression '$\sigma$-stability' corresponds to the maximum instability growth rate one allows. This extension to the concept of stability, of great importance for experimental setups, was introduced and formalized in Goedbloed & Sakanaka (1974). See section 6.5.3 of Goedbloed & Poedts (2004) for more details, in particular on how the energy principle (cf. below) is then modified.

### 7.1.3 Stability: Formally

We are interested in the analysis of the evolution of linear perturbations, for which various approaches are possible, as summarized in figure 7.5. The point is that depending on the aim of the study, one will not use the same tools. We may distinguish three aims, namely determining:

(I) the full dynamics of the perturbations $\vec{\xi}(\vec{r},t)$,

(II) the growth rates of the various unstable modes, in a normal mode analysis, and we will be particularly interested in the most unstable mode since it will be the one dictating the fate of the system,

(III) stability criteria, to tell simply whether an equilibrium is stable or not.

These are ordered by decreasing amount of information, but also of difficulty. In this section 7.1.3 I am going to introduce these three points one after the other, presenting them each time by first adopting the 'force viewpoint' (paragraphs a) ) and then the 'energy viewpoint' (paragraphs b) ). Among all these approaches, in this manuscript I will focus on *determining the spectrum $\{\omega^2\}$ in the eigenvalue problem approach of the force operator formalism i.e. on paragraph* (II) a) below, as indicated by the green frames in figure 7.5.

#### (I) Full dynamics: $\vec{\xi}(\vec{r},t)$

**a) Equation of motion** Using the Lagrangian displacement vector in the set of governing equations (7.2), the linearized momentum conservation has the form

$$\rho_0 \partial_t^2 \vec{\xi} = \vec{F}\left(\vec{\xi}\right), \tag{7.23}$$

where I will explicit and discuss the vector $\vec{F}$ only in equation (7.29) of the next paragraph, because in this manuscript we will not use the equation of motion in the form (7.23) but in its temporal Fourier transform version (7.28). For now, let us only say that the vector $\vec{F}$ is interpreted as the resultant of the forces acting on the considered volume element, i.e. that equation (7.23) is in essence Newton's second law. This is no surprise since it is a rewriting of the momentum conservation. However, the key and subtle point here is that the force $\vec{F}(\vec{\xi})$ is expressed as a function of $\vec{\xi}$ only, so that equation (7.23) is seen as an equation on $\vec{\xi}$ only, i.e. as a kind of *wave equation*. Also, $\vec{F}$ is now interpreted as an operator acting on $\vec{\xi}$, which is why we will refer to this approach as the *force operator formalism*, as opposed to the energy approaches making use of quadratic forms.

[5] Note that we are only considering linear stability here, with infinitesimal displacements, so that we do not consider possible finite jumps from various local minima of the potential.

| | Aim | Force | Energy |
|---|---|---|---|
| (I) | Full dynamics: $\boldsymbol{\xi}(\mathbf{r},t)$ | *Equation of motion:* $\mathbf{F}(\boldsymbol{\xi}) = \rho \dfrac{\partial^2 \boldsymbol{\xi}}{\partial t^2}$ | *Hamilton's principle:* $\delta \int_{t_1}^{t_2} \left( K[\dot{\boldsymbol{\xi}}] - W[\boldsymbol{\xi}] \right) dt = 0$ |
| (II) | Spectrum $\{\omega^2\}$ & eigenf. $\{\boldsymbol{\xi}(\mathbf{r})\}$ | *Eigenvalue problem:* $\mathbf{F}(\boldsymbol{\xi}) = -\rho\omega^2 \boldsymbol{\xi}$ | *Rayleigh's principle:* $\delta \dfrac{W[\boldsymbol{\xi}]}{I[\boldsymbol{\xi}]} = 0$ |
| (III) | Stability & trial $\boldsymbol{\xi}(\mathbf{r})$ | *Marginal equation:* $\mathbf{F}(\boldsymbol{\xi}) = 0$ | *Energy principle:* $W[\boldsymbol{\xi}] \gtrless 0$ |
| | | **Differential eqs.** ('Schrödinger') | **Quadratic forms** ('Heisenberg') |

Figure 7.5: There are essentially two viewpoints to study oscillations and instabilities: One is based on the concept of force and the other on energy. Depending on the amount of information one is looking for, different approaches are appropriate (the three rows, corresponding to items (I), (II) and (III) in the text). As indicated by the green frames, I will focus in this manuscript on the eigenvalue problem approach in the force operator formalism, aiming at determining the spectrum $\{\omega^2\}$ (adapted from figure 6.16 of Goedbloed & Poedts, 2004).

**b) Hamilton's principle** The variational counterpart of the previous equation of motion is the following linearized version of Hamilton's principle (Goldstein, 1980): The evolution of the system from time $t_1$ to time $t_2$ through the perturbation $\vec{\xi}(\vec{r},t)$ is such that the variation of the integral of the Lagrangian vanishes

$$\delta \int_{t_1}^{t_2} L dt = 0 \tag{7.24}$$

where $L \equiv K - W$, with the linearized kinetic energy

$$K\left[\dot{\vec{\xi}}\right] = \frac{1}{2} \int \rho_0 \dot{\vec{\xi}}^* \cdot \dot{\vec{\xi}}\, dV \tag{7.25}$$

and the linearized potential energy

$$W\left[\vec{\xi}\right] = -\frac{1}{2} \int \vec{\xi}^* \cdot \vec{F}\left(\vec{\xi}\right) dV. \tag{7.26}$$

where the symbol $*$ denotes the complex conjugate. Deriving the Euler-Lagrange equation by minimization leads to (7.23): The variational formulation and the differential equation formulation are equivalent.

**(II) Eigenvalue problem: Spectrum $\omega^2$ and eigenfunctions $\hat{\xi}(\vec{r})$**

**a) Normal mode analysis** Because the equilibrium coefficients are time independent, we may Fourier transform equation (7.23) with respect to the time variable and consider normal mode solutions of the form

$$\boxed{\vec{\xi}(\vec{r},t) = \hat{\xi}(\vec{r})\ e^{i\omega t}}. \tag{7.27}$$

(Normal Modes)

The full equation of motion (7.23) then becomes the following *vector eigenvalue problem*

$$\boxed{-\omega^2 \rho_0 \vec{\xi} = \vec{F}\left(\vec{\xi}\right)}, \tag{7.28}$$

(Vector Eigenvalue Problem)

where

$$\boxed{\vec{F}\left(\vec{\xi}\right) = \underbrace{-\vec{\nabla} p_1}_{\text{pressure}} + \underbrace{\vec{j}_1 \times \vec{B}_0 + \vec{j}_0 \times \vec{B}_1}_{\text{magnetic field}} + \underbrace{\overbrace{\rho_1 \vec{g}_0}^{\text{Cowling}} + \overbrace{\rho_0 \vec{g}_1}^{\text{Jeans}}}_{\text{gravity}}}. \tag{7.29}$$

First, notice that with equation (7.28), the link between the second and fourth row in the table of figure (7.4) gets clear: The sign of $\omega^2$ dictates whether the force applied on the displaced volume element is in the same or opposite direction as the displacement $\vec{\xi}$ itself.

Second, when expressed in terms of the primitive variables $\rho_1, p_1, \vec{j}_1, \vec{B}_1$ and $\vec{g}_1$, the right hand side is naturally interpreted as the resultant of the forces applied on the volume element. It consists of three parts. The pressure part, which induces acoustic waves, due to the compressibility of the medium. The magnetic field part, which modifies the behaviour of acoustic waves by inducing anisotropy, but also additional pressure. It also gives rise to purely magnetic waves, named Alfvén waves. Finally, the gravitational part, which also modifies the behaviour of acoustic waves, and studying precisely how is the main objective of this part of the manuscript. As highlighted in equation (7.29) and anticipated page 72, we will distinguish two contributions to this gravitational part, namely what I will hereafter call

(i) the Cowling term $\rho_1\vec{g}_0$,

(ii) and the Jeans term $\rho_0\vec{g}_1$.

I will use this terminology because, in the stellar community, it is common to do the so-called *Cowling approximation* (Cowling, 1941) which consists in keeping only the term $\rho_1\vec{g}_0$ out of the two gravitational terms. The Cowling term is the one which may give rise to the Rayleigh-Taylor instability and to convection. In Cosmology, on the contrary, it is often expedient to keep only the $\rho_0\vec{g}_1$. The Jeans term is the one which may give rise to the Jeans gravitational instability, i.e. to gravitational fragmentation, which is the very reason of the effort made in this manuscript to explore it and understand it as well as possible in stratified media.

Third, equation (7.28) is now expressed as an *eigenvalue problem* (where $\omega^2$ is the *eigenvalue*), so that the right hand side is now seen as a function of $\vec{\xi}$ only. We thus need to express all the primitive variables in terms of $\vec{\xi}$. We may do so using the governing equations (7.2). It is in these forms that we are going to manipulate the equations in the rest of this manuscript.

The linearized mass conservation gives

$$\boxed{\rho_1 = -\vec{\nabla}\cdot\left(\rho_0\vec{\xi}\right)}, \tag{7.30}$$

(Density Perturbation)

our choice of closure relation gives

$$\boxed{p_1 = -c_a^2\vec{\nabla}\cdot\left(\rho_0\vec{\xi}\right)}, \tag{7.31}$$

(Pressure Perturbation)

the linearized induction equation gives

$$\boxed{\vec{B}_1 = \vec{\nabla}\times\left(\vec{\xi}\times\vec{B}_0\right)}, \tag{7.32}$$

(Magnetic Field Perturbation)

the linearized Ampère's law gives

$$\boxed{\vec{j}_1 = \vec{\nabla}\times\left(\vec{\nabla}\times\left(\vec{\xi}\times\vec{B}_0\right)\right)}, \tag{7.33}$$

(Current Density Perturbation)

and finally, inverting the linearized Poisson equation[6] (7.5) we obtain

$$\boxed{\vec{g}_1 = G\int\vec{\nabla}\cdot\left(\rho_0\vec{\xi}\right)\frac{\vec{r}-\vec{r}'}{|\vec{r}-\vec{r}'|^3}d^3r'}\,. \tag{7.34}$$

(Gravitational Acceleration Perturbation)

We will discuss the last relation especially in section (7.3).

[6] To be complete, this expression contains surface terms too, cf. section 7.51.

**Tracking the MHD waves** In the plasma literature, it is shown that, when neglecting the $\vec{g}_1$ term i.e. in *ideal MHD working in the Cowling approximation*, equation (7.28) describes *three waves* only[7]: the *slow* magneto-acoustic wave, the *Alfvén* wave and the *fast* magneto-acoustic wave. What happens when the $\vec{g}_1$ term is taken into account? As briefly mentioned in section 2.4, in the Newtonian framework considered here, gravity is instantaneous and the linearized Poisson equation is an additional constraint, but not a proper evolution equation. Therefore when considering the full system of equations, not in the Cowling approximation, we do not expect additional waves (gravitational waves as in a general relativistic treatment). We are thus going to *track how the three MHD waves are modified by gravity.*

**Road map** In section 7.2 we will focus on the magnetic terms of the force operator, switching-off gravity, in order to get acquainted with the way plasma physicists analyze equation (7.28). Then, with this background, we will focus on the gravitational terms, switching-off magnetic fields. First, in section 7.3, we will discuss general features of the eigenvalue problem in this case. Then, in chapter 8 we will explore fully this problem in the particular case of a plane stratified structure. This will be physically relevant for the modeling of the sheets of the cosmic web, but also it will turn out to be methodologically absolutely indispensable because of the complexity of the general problem. This work will ease the generalization to cylindrically symmetric stratifications (filaments of the cosmic web) as discussed in chapter 9. It will also show the way to follow to combine magnetic fields and gravity, which is however left for future work.

**Analogy with Quantum Mechanics** There is a formal analogy between the analysis of the MHD spectrum and that of quantum mechanical systems. It is beyond the scope of this manuscript to go into details on it, but note that the force operator approach corresponds to the Schrödinger picture, with a description exploiting differential equations based on the eigenvalue problem $H\psi = E\psi$, while the variational approach corresponds to the Heisenberg picture, with a description exploiting quadratic forms based on the matrix elements of the Hamiltonian. This is the reason why Schrödinger and Heisenberg are mentioned in figure 7.5. The interested reader may have a look at chapter 6 of Goedbloed & Poedts (2004) for more information. This analogy is also the root of the following crucial property.

**Self-adjointness of the force operator: Eigenvalues $\omega^2$ are real** A key property of the force operator $\vec{F}$, or rather of $\rho_0^{-1}\vec{F}$, is *self-adjointness.* Formally, the operator $\rho_0^{-1}\vec{F}$ is said to be self-adjoint when

$$\text{for all } \vec{\xi} \text{ and } \vec{\eta}, \qquad \int \vec{\eta}^{\,*} \cdot \vec{F}\left(\vec{\xi}\right) dV = \int \vec{F}\left(\vec{\eta}^{\,*}\right) \cdot \vec{\xi}\, dV \tag{7.35}$$

where the symbol $*$ denotes the complex conjugate. As such, the origin of this definition may seem obscure, but it is in fact natural when considering the full mathematical framework of linearized ideal MHD, discussing it in terms of Hilbert space, defining an inner product and a norm for the MHD displacements, in analogy with Quantum Mechanics, where the terminology 'Hermitian' is sometimes used instead of 'self-adjoint'. The interested reader may have a look for instance at section 6.2.2 of Goedbloed & Poedts (2004). For our purpose here, we only need to keep in mind, and benefit from, two points about this property: First, physically self-adjointness is associated with energy conservation, and second, when $\rho_0^{-1}\vec{F}$ is self-adjoint, then we are guaranteed that *the eigenvalues $\omega^2$ are real.* This immensely reduces the difficulty of the analysis, because the spectrum is then reduced to the real axis only. This is why the ideal MHD spectrum, which we will discuss in section 7.2, is represented as a simple line in figure 7.6 below.

The fact that the eigenvalues $\omega^2$ are real remains true when adding gravity (e.g. Cox, 1980), which will greatly simplify the analysis in section 7.3 and the following chapters, and also when considering convection (9.2). However, when considering resistivity (which is far beyond the scope of this work, so the reader is invited to delve into Goedbloed et al., 2010, to learn about this aspect), $\omega^2$ is a complex quantity, so that the spectrum has to be discussed in the full complex plane. The analysis then involves many tools from the theory of functions of a complex variable, and is much more elaborate than the present discussion, which constitutes the first, necessary, step to go that far.

Finally, note that self-adjointness depends on the boundary conditions imposed on the system. This fact is intuitive since even in ideal MHD where no dissipation occurs, energy may come in or out from the interfaces of the system, in which case energy is not conserved. In Goedbloed & Poedts (2004), the authors present six different models of plasmas: three relevant to laboratory plasmas and three others relevant to the astrophysical context. Each is characterized by different boundary conditions. The simplest of them, called the 'rigid walls' model, consists in imposing that the displacement field vanishes at the boundaries (cf. for instance equation (8.13) below). In this case, it can be proved that the general force operator (7.29) is self-adjoint. To lighten the discussion, we will consider those simple boundary conditions in this manuscript[8].

[7] It is so because we are dealing with a background state that is at rest. When adding flow, as introduced in chapter 10, each of these three waves splits up into two, one backward and one forward. And also, it can be shown that because we are adopting a Lagrangian description, in terms of the displacement vector $\vec{\xi}$, we are not taking into account a seventh wave, namely the Eulerian entropy wave, but which is marginal ($\omega^2 = 0$) in this context. For more details see section 5.2 of Goedbloed & Poedts (2004) and section 13.1.3 of Goedbloed et al. (2010).

[8] Finally, on the self-adjointness of the force operator, and thus on the *reality* of $\omega^2$, it is interesting to note that some

**b) Rayleigh-Ritz's principle** The energetic counterpart of the eigenvalue problem approach with the force operator is the Rayleigh-Ritz's principle. It may be stated as follows. Eigenfunctions $\vec{\xi}$ of the operator $\rho_0^{-1}\vec{F}$ make the Rayleigh quotient

$$\Lambda\left[\vec{\xi}\right] = \frac{W\left[\vec{\xi}\right]}{I\left[\vec{\xi}\right]} \tag{7.36}$$

stationary, and the eigenvalues $\omega^2$ are the stationary values of $\Lambda$, i.e. $\delta\Lambda = 0$. Here $I\left[\vec{\xi}\right] \equiv \frac{1}{2}\int \rho_0 \vec{\xi}^* \cdot \vec{\xi}\, dV$. The article of Hasan & Sobouti (1987) is an interesting example of mode analysis using this principle in MHD.

**(III) Stability criteria**

**a) Marginal Equation** Restricting ourselves to boundary conditions which leave the force operator self-adjoint, we know that the eigenvalues $\omega^2$ are real. Therefore the transition between stable and unstable regimes must occur when $\omega^2 = 0$. This is called the marginal frequency. Setting $\omega^2 = 0$ in equation (7.28) yields the *marginal equation*

$$\vec{F}\left(\vec{\xi}\right) = \vec{0}. \tag{7.37}$$

This equation should be seen as an equation on the governing parameters of the system (external magnetic field applied, gravitational field in which the system is embedded, etc.). Indeed, the idea is to find the set of parameters such that solutions of (7.37) exist which satisfy the imposed boundary conditions. Then, since these parameters correspond to the marginal frequency $\omega^2 = 0$, these parameters delimit the stable and unstable regions in parameter space. A general criterion for stability is thus obtained. For examples adopting this approach, see for instance Ledoux (1951) and Miyama et al. (1987a).

**b) Energy principle** Another approach to establish simple stability criteria is as follows. If one can find a *single* displacement field $\vec{\xi}$ such that

$$W\left[\vec{\xi}\right] < 0, \tag{7.38}$$

then the system is unstable, as illustrated on the right of figure (7.4). The important point here is that we only need to find one particular function $\vec{\xi}$ to conclude that the system is unstable. Such a function is thus called a trial function. There is at the present no general way to find such a function. However, an idea is for instance to notice that the linearized potential energy $W\left[\vec{\xi}\right]$ given by (7.26) contains $\vec{\nabla}\cdot\vec{\xi}$ terms, so that considering an incompressible displacement field, for which this quantity vanishes, $W\left[\vec{\xi}\right]$ greatly simplifies. Then sometimes relations on the governing parameters which render $W\left[\vec{\xi}\right]$ negative appear clearly. A simple illustrative example of this method can be found in section 6.5.4 of Goedbloed & Poedts (2004). In practice, it turns out that it is often much quicker to conclude on the instability of a given configuration using the Energy principle, rather than through the study of the marginal equation. Note however that, to prove that the system is stable, one would have to prove that $W\left[\vec{\xi}\right] > 0$ for *all* displacements $\vec{\xi}$.

I will not discuss further the energetic approach, since in the rest of this manuscript I will adopt the eigenvalue problem approach, looking for the spectrum of the system, as highlighted in figure 7.5. But both viewpoints are important to keep in mind, because they are complementary and both can be found in the literature (cf. references mentioned in the introduction of chapter 7 for instance).

## 7.2 Ideal MHD

Let us now reveal the waves and instabilities contained in equation (7.28) when gravity is switched-off to focus on magnetic fields.

### 7.2.1 Vector Eigenvalue Problem

In ideal MHD, without gravity, the force operator (7.29) reads:

$$\vec{F}\left(\vec{\xi}\right) = -\vec{\nabla}p_1 + \vec{j}_1 \times \vec{B}_0 + \vec{j}_0 \times \vec{B}_1. \tag{7.39}$$

stability studies do report complex-valued $\omega$s (e.g. Freundlich et al., 2014b, who analyze self-gravitating, non-rotating filaments, linearizing the system of perturbed equations in primitive variables). The origin of this complexity, whether physical or an artefact, in those cases is unclear at this point, but may reside in the chosen formal approach and the assumptions made.

Then, inserting these expressions in relation (7.28), we find that the vector eigenvalue problem in ideal MHD has the following explicit expression:

$$\boxed{-\rho_0\omega^2\vec{\xi} = \vec{\nabla}\left(c_a^2\vec{\nabla}\cdot\left(\rho_0\vec{\xi}\right)\right) + \left(\vec{\nabla}\times\left(\vec{\nabla}\times\left(\vec{\xi}\times\vec{B}_0\right)\right)\right)\times\vec{B}_0 + \left(\vec{\nabla}\times\vec{B}_0\right)\times\left(\vec{\nabla}\times\left(\vec{\xi}\times\vec{B}_0\right)\right)}. \quad (7.40)$$

(Vector Eigenvalue Problem – Ideal MHD)

This expression is quite involved, in the sense that it is composed of intertwined $\vec{\nabla}$ operators and vector products which makes it pretty nonintuitive. However, it remains in essence rather simple in the sense that this is just the expression of various geometric effects, because the magnetic field distinguishes the various spatial directions, inducing anisotropy in the system, but it is not a conceptual complication. What makes this eigenvalue problem even technically relatively simple is that the force operator (together with reasonable boundary conditions) is *self-adjoint* as we have seen above, but also linear (in $\vec{\xi}$) and *differential*. Both these properties considerably reduce the difficulty of the analysis. As we will see in the next section, when adding gravity in the system, the governing operator is not differential anymore, but integro-differential. This MHD eigenvalue problem is also quite intricate because it contains a huge amount of information. Indeed, a wave equation such as (7.10) is a scalar equation, describing the evolution of scalar waves. Equation (7.40) describes the evolution of a vector field, so that it contains also the information on the polarisation of the waves (linear, circular) for instance.

Just like rotating an object enables to reveal parts of it which were initially out of sight, reformulating a physics problem in various forms is most generally very rewarding. In the present case, we are dealing with a vector eigenvalue problem. This has the advantage of being linear in $\omega^2$, which is essential in demonstrating general results such as the self-adjointess of the force operator. Also, in this form, each term may be interpreted physically as a force in Newton's second law, as the very name 'force operator' reminds us. But this description has the disadvantage of being vectorial, so that as such the various components of $\vec{\xi}$ are described through their complicated coupling. A first enriching way of reformulating the problem consists in deriving from (7.40) an equation governing one of the components of $\vec{\xi}$ only, say $\xi_x$ (in a Cartesian description, as below), and study it independently[9]. The resulting equation is called the MHD wave equation. As we will see, this transformation is extremely valuable because the entire structure of the spectrum can be read in its coefficients, while this is invisible in the vector formulation. Now, as we will see, the cost of turning to a scalar (wave) equation, is that $\omega^2$ will be distributed all over the coefficients in the equation. The problem will thus be reduced to a scalar but non-linear eigenvalue problem.

### 7.2.2 Wave Equation

Since the works I will present later on gravitation will be in great part done considering a planar stratification (chapter 8), I will now detail the analysis of the MHD wave equation in this geometry. In section 9.1, we will discuss another one-dimensional stratification, but that has a cylindrical symmetry. Here, the absence of curvature effects greatly simplifies the analysis but keeps the essential of the physics.

**Planar stratification** Consider a medium that is stratified in one direction only, say the $x$ direction. This one dimensional stratification is assumed to be planar, hence the use of cartesian coordinates $x$, $y$ and $z$. The equilibrium density and pressure are functions of $x$ only:

$$\rho_0 = \rho_0(x) \text{ and } p_0 = p_0(x). \quad (7.41)$$

Let us consider a magnetic field confined to plane layers perpendicular to the stratified direction $x$, but whose components vary along the stratification, namely

$$\vec{B} = B_y(x)\hat{y} + B_z(x)\hat{z}. \quad (7.42)$$

Now, thanks to the translation invariance along the $y$ and $z$ directions, we can consider plane waves in these directions, so that the most general expression of $\vec{\xi}$, from the decomposition (7.27), is

$$\vec{\xi} = \left[\hat{\xi}_x(x)\ \hat{x} + \hat{\xi}_y(x)\ \hat{y} + \hat{\xi}_z(x)\ \hat{z}\right] e^{i(k_y y + k_z z - \omega t)}. \quad (7.43)$$

Quantities with a hat, other than unit vectors, depend on $x$ only. Inserting this expression into (7.40), it is possible to derive an equation on the $\hat{\xi}_x$ component only, the scalar wave equation. Because the MHD part of the force operator is not the priority of this manuscript but only its results matter here, I am not going to explicit this derivation. We are anyway going to follow similar steps in chapter 8 so that this would

[9] In this process, the other two components of $\vec{\xi}$ can be expressed as functions of $\xi_x$ only, so that we may, if needed, recover the full expression of $\vec{\xi}$ once the equation on $\xi_x$ is solved. Therefore no information is lost, so this can really be seen as a reformulation of the vector problem.

be redundant. The interested reader may find the MHD derivation in section 7.3.2 of Goedbloed & Poedts (2004).

First of all, let us define the two local (due to their $x$-dependence) speeds that appear in the following analysis, respectively the Alfvén speed and the speed of sound:

$$\begin{cases} b(x) \equiv \frac{B}{\sqrt{\rho_0}} \\ c(x) \equiv \sqrt{\gamma \frac{p_0}{\rho_0}}. \end{cases} \tag{7.44}$$

Formally, they are the most natural speeds one can define on dimensional grounds, given the physical parameters involved. Physically we are familiar with the speed of sound, while the other one is the speed associated with the propagation of purely magnetic waves, called Alfvén waves. They are analogous to the waves travelling along guitar strings, where the magnetic field lines act as strings. In essence, the Alfvén speed is vectorial since $\vec{B}$ is a vector, but given the stratification considered, only this scalar Alfvén speed intervenes here.

**Wave equation** The wave equation, first derived[10] by Goedbloed (1971), and which we will hereafter refer to as the *MHD wave equation*, reads

$$\boxed{\left(\frac{N}{D}\hat{\xi}_x'\right)' + Q\ \hat{\xi}_x = 0} \tag{7.45}$$

(Wave Equation – Ideal MHD)

where the numerator $N$ contains three *continua* of the spectrum $\{\omega^2\}$ (the fast is peculiar, cf. discussion below)

$$\boxed{N(x;\omega^2) = \rho_0(b^2+c^2)[\omega^2 - \omega_A^2(x)][\omega^2 - \omega_S^2(x)]} \tag{7.46}$$

with

$$\begin{cases} \omega_A^2(x) = \frac{(k_y B_y + k_z B_z)^2}{\rho_0} & \text{(Alfvén continuum)} \\ \omega_S^2(x) = \frac{c^2}{b^2+c^2}\omega_A^2 & \text{(slow magneto-sonic continuum)} \\ \omega_F^2(x) = \infty & \text{(fast magneto-sonic continuum)} \end{cases} \tag{7.47}$$

and the denominator $D$ contains two *turning point frequencies*

$$\boxed{D(x;\omega^2) = [\omega^2 - \omega_{s0}^2(x)][\omega^2 - \omega_{f0}^2(x)]} \tag{7.48}$$

with

$$\begin{cases} \omega_{s0}^2(x) = \frac{1}{2}(k_y^2+k_z^2)(b^2+c^2)\left[1 - \sqrt{1 - \frac{4c^2}{(k_y^2+k_z^2)(b^2+c^2)^2}\omega_A^2}\right] & \text{(slow turning point)} \\ \omega_{f0}^2(x) = \frac{1}{2}(k_y^2+k_z^2)(b^2+c^2)\left[1 + \sqrt{1 - \frac{4c^2}{(k_y^2+k_z^2)(b^2+c^2)^2}\omega_A^2}\right] & \text{(fast turning point)} \end{cases} \tag{7.49}$$

and finally

$$Q(x;\omega^2) = \rho_0(\omega^2 - \omega_A^2). \tag{7.50}$$

The explicit expressions (7.47) and (7.49) are given here only for the sake of completeness. I will not discuss in this manuscript the details of the physics behind these frequencies, but only make use of the techniques developed using them. The expressions which will matter for the following are that of the numerator (7.46) and the denominator (7.48), independently of the full expressions of the frequencies they contain.

**Boundary conditions** The differential equation (7.45) is of second order and thus solving it requires specifying two boundary conditions. The simplest of boundary conditions, called the 'rigid walls', consists in imposing that the displacement along $x$ vanishes at $x = 0$ and at the surface $x = x_t$, that is

$$\hat{\xi}_x(0) = \hat{\xi}_x(x_t) = 0. \tag{7.51}$$

As mentioned in section 7.1.3, the self-adjointess of the force operator, and thus the real or complex nature of the eigenvalues $\omega^2$, depends on the choice of boundary conditions. The advantage of such simple conditions is that the force operator is indeed self-adjoint.

[10] To be precise, in this article the author takes gravity into account, but in the Cowling approximation only, the discussion of which is left for the next chapter.

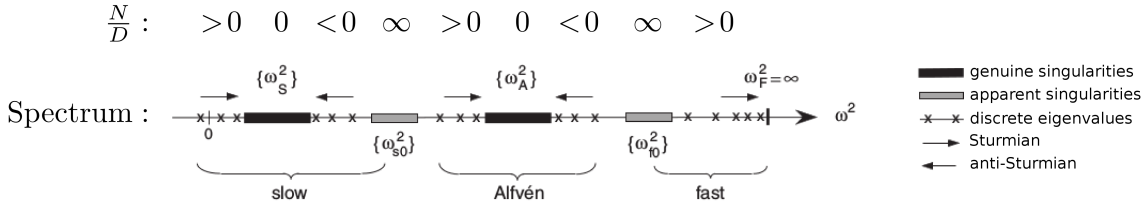


Figure 7.6: Typical structure of the ideal MHD spectrum without flow. The spectrum is confined to the real axis, and composed of (i) three continuous spectra (slow, Alfvén and fast: the black boxes) originating from genuine singularities in the wave equation, (ii) two ranges of turning point frequencies (slow and fast: the gray boxes) originating from apparent singularities in the wave equation, and (iii) a discrete spectrum (the various sets of crosses) originating from the boundary conditions. The monotonicity (Sturmian or anti-Sturmian) of the discrete sub-spectra is revealed by the oscillation theorem, which states that it is given by the sign of $N/D$ in the wave equation (upper line in the figure). Adapted from figure 7.18 of Goedbloed & Poedts (2004).

### 7.2.3 Spectrum

It is out of the scope of this manuscript to delve into rigorous demonstrations about the structure of the spectrum. Instead, I am now going to state the result and give some of the key points that help getting a feeling of where it comes from.

**The result:** *The ideal MHD spectrum may be represented by figure 7.6*, i.e. it is contained in the *real axis*, and composed of various *continuous ranges of values* (the black and grey boxes) surrounded by *discrete values* (the crosses).

**The ideas behind this result:** First of all, as mentioned in section 7.1.3, the fact that the spectrum belongs to the real axis rather than the full complex plane, and is thus simply represented as a line, is due to the *self-adjointness* of the force operator, which guarantees that the eigenvalues $\omega^2$ are real.

The rest of the structure essentially comes from two key properties of differential equations: (i) Their singularities, giving rise to the continuous ranges, and (ii) the imposed boundary conditions, giving rise to the discrete parts.

#### (i) Singularities

In the theory of ordinary differential equations in the complex plane $\mathbb{C}$ (e.g. Bender & Orszag, 1978), the points of $\mathbb{C}$ are classified into ordinary points, at which the equation's coefficients are analytic functions, and singular points, at which some coefficient has a singularity. Various types of singularities exist, the precise study of which is crucial because it indicates the appropriate technique to use to analyze the nature of the solution around such points. In the context of stability analysis, this gives various stability criteria. For the purpose of the present discussion, I will just mention the following *intuitive* argument[11]. Consider a general $n^{\text{th}}$ order ordinary differential equation

$$\sum_0^n a_i(x) y^{(i)}(x) = 0. \tag{7.52}$$

At a point $x_s$ where the coefficient of the highest order term vanishes ($a_n(x_s) = 0$), this equation becomes 'locally' of order $(n-1)$. Similarly, at a point $x_s$ where the coefficient of the lowest order term vanishes ($a_0(x_s) = 0$), the order of the equation also decreases by one, because it then becomes an equation in the variable $y'$, of the $(n-1)^{\text{th}}$ order. Now, we may also encounter situations where singular points exist such that $a_i(x_s) \to \infty$ for some $i \in \{0..n\}$. Obviously, such points deserve special attention too. Thus, in other words, it is intuitive that the solutions of a differential equation are fundamentally different if the equation is solved on an interval $[a, b]$ on which the coefficient of either the highest or the lowest order term vanishes, or at least one of the coefficient diverges at one point (at least) in $[a, b]$.

The procedure to analyze wave equations such as (7.45) is thus to examine their singularities. The factors $N$ and $D$ defined respectively in (7.46) and (7.48) have clearly been written in a form that optimizes this procedure.

[11] As the following of the manuscript will show, determining the nature of the singularities will be somewhat subtle.

**Genuine singularities: The continuous spectrum** Equation (7.45) becomes singular ($N \to 0$) when $\omega^2 \to \omega_A^2(x)$ or $\omega^2 \to \omega_S^2(x)$. Hence solutions with eigenvalues $\omega^2 \in \{\omega_A^2(x)\}$ and $\omega^2 \in \{\omega_S^2(x)\}$ have 'something particular'. Let me mention that it can be shown that they correspond to solutions that are non square-integrable. The slow magneto-sonic $\omega_S^2(x)$ and the Alfvén $\omega_A^2(x)$ frequencies are thus called *genuine singularities*, and the ranges of frequencies $\omega_A^2(x)$ and $\omega_S^2(x)$ constitute what is called the *continuous spectrum*. For completeness, we will admit that there is in fact a third continuum, that is 'formal' in the sense that the values of its frequencies are infinite. This is the fast magneto-sonic continuum mentioned in (7.47).

**Apparent singularities: Turning point frequencies** Similarly, 'something particular' clearly happens ($D \to 0$) when $\omega^2 \to \omega_{s0}^2(x)$ or $\omega^2 \to \omega_{f0}^2(x)$. It can be shown that solutions with eigenvalues $\omega^2 \in \{\omega_{s0}^2(x)\}$ and $\omega^2 \in \{\omega_{f0}^2(x)\}$ present cancellations in their series expansion which leaves them finite, so that these solutions are fundamentally different from those belonging to the continuous spectrum. Therefore, the frequencies $\omega_{s0}^2(x)$ and $\omega_{f0}^2(x)$ are called *apparent frequencies*, by opposition to the genuine ones, and the ranges $\{\omega_{s0}^2(x)\}$ and $\{\omega_{f0}^2(x)\}$ are not continuous spectra but are called ranges of *turning point frequencies*. The origin of the latter denomination is soon going to be clear (cf. paragraph (ii) below): They are zones in the spectrum separating the three continuous spectra, because of the following ordering[12] which is true at each position in the plasma slab:

$$0 \leq \omega_S^2(x) \leq \omega_{s0}^2(x) \leq \omega_A^2(x) \leq \omega_{f0}^2(x) \leq \omega_F^2(x) = \infty, \tag{7.53}$$

They are also delimiting different monotonicities in the discrete spectrum (i.e. anti-Sturmian behaviour on their left, Sturmian on their right).

### (ii) The discrete spectrum: Boundary conditions

The discussion above did not require specifying the boundary conditions with which the differential equation is being solved. In physics, boundary conditions are paramount. The best known and simplest example is that of a vibrating string.

Consider a string that is being shaken. Intuitively, we know that the perturbation will travel along the string, and will be reflected back once it meets a fixed point. If both ends of the string are fixed points, the travelling wave will interfere with its counterpropagating sibling so that only perturbations whose wavelength is a multiple of the internode distance will remain and will form a standing wave. A very important feature is that the frequency at which each mode oscillates is directly linked to the number of nodes the standing wave contains, and in particular in this case the larger the number of nodes, the higher the frequency of the oscillation. This increase of the frequency with the number of nodes is called a *Sturmian* behaviour.

Formally, what happens is that the differential equation governing the oscillations of the string is a wave equation. One can solve it to derive its general solution, but not all these solutions satisfy the required boundary conditions. Therefore only a certain set of solutions is relevant to the physical problem posed, and thus only certain frequencies may exist in the system. More generally, the study of the behaviour of solutions of a differential equation with respect to the parameters present in its coefficients belongs to the realm of *spectral theory* in Mathematics. Let us have a glimpse on an important example, namely that of a so-called *Sturm-Liouville problem*[13]. It is fundamental because it is simple, omnipresent in physics in general, and also because basically the crux of the present study is to generalize it to the more complicated differential equations we are going to face. Consider the following real, second-order non-singular differential equation, called a classical Sturm-Liouville equation (e.g. Al-Gwaiz, 2008):

$$L[y;\alpha] = 0 \tag{7.54}$$

where

$$L[y;\alpha] \equiv \frac{d}{dx}\left[P(x)\frac{dy}{dx}\right] - [Q(x) - \alpha R(x)]y. \tag{7.55}$$

The parameter $\alpha$ is called the eigenvalue of the differential operator $L$, and the functions $P$ and $R$ are assumed to be strictly positive, ensuring in particular that this equation is non-singular. The domain associated with this equation is the interval $a \leq x \leq b$, and the boundary conditions are

$$y(a) = y(b) = 0. \tag{7.56}$$

Under these assumptions, the following theorem can be demonstrated:

— *Sturm's oscillation theorem* —
Let $y_1$ and $y_2$ be two functions satisfying respectively $L[y_1;\alpha_1] = 0$ and $L[y_2;\alpha_2] = 0$, and suppose that both vanish at a point $x = x_0$. Let $x_1$ be the zero of $y_1$ closest to $x_0$. Then, if $\alpha_2 > \alpha_1$, then $y_2$ vanishes at a point $x_2 < x_1$. The function $y_2$ is then said to oscillate faster.

[12] This ordering also justifies the terminology 'slow' and 'fast' for the magneto-acoustic waves.
[13] This is at the origin of the terminology 'Sturmian' mentioned.

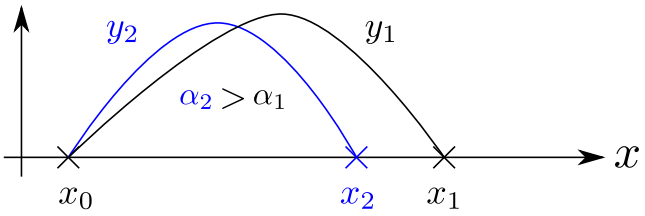


Figure 7.7: Sturm's oscillation theorem: The larger the parameter $\alpha$ in the Sturm-Liouville equation (7.54), the faster the solution $y$ oscillates.

This theorem is illustrated in figure 7.7. Now, if $x_0$ and $x_1$ correspond to the boundaries $a$ and $b$ on which the boundary conditions are imposed, then $\alpha_1$ is an eigenvalue for instance. Thus, it is clear from this theorem that, the larger the eigenvalue, the more nodes the eigenfunction possesses. Such a behaviour is called *Sturmian*. In problems in which the opposite is true, i.e. when the eigenvalue is smaller as the number of nodes increases, the behaviour is called *anti-Sturmian*.

Having this in mind, let us reinspect the wave equation (7.45). It *looks like* the Sturm-Liouville equation (7.54), because it is the same differential operator. However the eigenvalue $\alpha$ in (7.54) appears only linearly, while the eigenvalue $\omega^2$ in (7.45) is distributed throughout the coefficients in a much more complicated, non-linear manner! For this reason, the ideal MHD eigenvalue problem is often referred to as a non-linear Sturm-Liouville problem. An important step forward has been made by Goedbloed & Sakanaka (1974) who generalized Sturm's oscillation theorem to the far more general MHD eigenvalue problem. It may be stated as follows:

— *Goedbloed-Sakanaka's oscillation theorem* —
If $x_0$ and $x_1$ are two consecutive zeros of the function $\xi_1$ satisfying the MHD wave equation (7.45) for $\omega^2 = \omega_1^2$, then the solutions $\xi_2$ of the MHD wave equation for $\omega^2 = \omega_2^2$ oscillate faster than $\xi_1$ if $\omega_2^2 > \omega_1^2$ and $N/D > 0$ (Sturmian), and slower if $N/D < 0$ (anti-Sturmian).

This is a very general and non trivial result. It shows how the gaps between the genuine and apparent singularities in the spectrum (the black and grey boxes in figure 7.6) are filled. It was not obvious at all from the intricate distribution of the eigenvalue parameter $\omega^2$ in the MHD wave equation that these various gaps would be filled by discrete sets of eigenvalues that are *monotonic* (i.e. either Sturmian or anti-Sturmian), and above all that the monotonicity is simply *directly given by the sign of* $N/D$, as illustrated by the upper line in figure 7.6. We could not hope for a simpler result, which makes it so powerful. The collection of these discrete sets of eigenvalues is called the *discrete spectrum*.

All these results belong to the wide field of spectral theory in Mathematics. However, so far, I have not found in the literature references that could generalize Goedbloed-Sakanaka's oscillation theorem for the fourth order wave equations we will be dealing with in the next chapter, explicited in section 8.2.4. Examples of papers that deal with the stability of spherically symmetric stellar equilibrium models with respect to small adiabatic Lagrangian perturbations from the mathematical point of view are Beyer (1995) and Beyer & Schmidt (1995), which is the closest to the question of interest in this manuscript that I have found. The authors say that they are the first in the mathematics community to work on these aspects.

### 7.2.4 Stability analysis

This spectral theory approach is not only crucial to gain a fundamental understanding of the structure of the spectrum per se, but it is also of practical interest, fortunately. Powerful tools to study the stability of a system from a wave equation such as (7.45) have been developed. For instance, the point in identifying singularities such as those mentioned above, is that it provides us with the physical locations where it is relevant to perform a local analysis. Indeed, in a non-singular differential equation, the whole solution is fully constrained by the boundary conditions imposed on the edges of the interval on which we are solving it, while on the contrary, positions at which a singularity occurs, i.e. points $x_s$ satisfying $\omega_S^2(x_s) = \omega^2$ or $\omega_A^2(x_s) = \omega^2$ in the case of equation (7.45), split the interval into two independent parts. The stability of the system then depends on what is happening locally at position $x_s$. The procedure consists in performing a Frobenius expansion (Bender & Orszag, 1978) around those points. This may provide local stability criteria such as Suydam's criterion for instance (Suydam, 1958).

Another key information provided by the details of the spectrum, i.e. understanding it up to the monotonicity of the discrete spectrum, is to identify the fastest growing unstable mode, which is the one that will in principle determine the fate of the system. In the present ideal MHD case, the ordering (7.53) tells us that all singularities are positive. Therefore the unstable part of the spectrum is only discrete. It also tells us that the continuum closest to zero, i.e. to marginal stability where the transition from stability to instability

occurs, is the slow continuum. And finally, thanks to the Goedbloed-Sakanaka theorem, we know that the discrete modes on the left of that continuum are Sturmian. Therefore, we know that the fastest growing unstable mode, if it exists, is the $n = 1$ of the discrete sub-spectrum associated with the slow continuum. It is represented by the little cross on the far left of the spectrum in figure 7.6.

Finally, expliciting the wave equation as in (7.45) also enables us to study the short-wavelength waves by deriving local dispersion relations. I will detail this approach in sections 8.1.4 and 8.2.6 of chapter 8.

## 7.3 Gravitation

In section 7.2 we have learnt how to analyze the equation of motion (7.28) when pressure and magnetic fields are present. In the same lines let us now reveal the waves and instabilities contained in equation (7.28) when the magnetic field is switched-off to focus on gravity, which is the heart of our concern.

### 7.3.1 Vector Eigenvalue Problem

Let us now consider the force operator (7.29), this time turning gravity back on and switching off magnetic fields, namely

$$\vec{F}(\vec{\xi}) = -\vec{\nabla}p_1 + \rho_1\vec{g}_0 + \rho_0\vec{g}_1. \tag{7.57}$$

With expressions (7.30) of $\rho_1$, (7.31) of $p_1$ and (7.34) of $\vec{g}_1$, we may express it explicitly in terms of $\vec{\xi}$, so that from now on, instead of the MHD vector eigenvalue problem (7.40), we will focus on the gravitational vector eigenvalue problem

$$\boxed{-\rho_0\omega^2\vec{\xi} = \vec{\nabla}\left(c_a^2\vec{\nabla}\cdot\left(\rho_0\vec{\xi}\right)\right) - \vec{\nabla}\cdot\left(\rho_0\vec{\xi}\right)\vec{g}_0 + \rho_0 G\int\vec{\nabla}\cdot\left(\rho_0\vec{\xi}\right)\frac{\vec{r}-\vec{r}'}{|\vec{r}-\vec{r}'|^3}d^3r'}. \tag{7.58}$$

(Vector Eigenvalue Problem – Full Gravity)

In the following, I will call 'Full Gravity' cases in which *both* the Cowling term $\rho_1\vec{g}_0$ and the Jeans term $\rho_0\vec{g}_1$ are taken into account, as opposed to the Cowling approximation in which the Jeans term is neglected, or to the Jeans swindle in which the Cowling term is set to zero.

The eigenvalue problem (7.58) looks pretty involved per se. The MHD case gave the same impression, but we then got the pleasant surprise of ending up with a wave equation which was not obscure at all and rather compact, from which the spectrum could be read directly. We are thus all the more encouraged to look for the wave equation corresponding to the above gravitational vector eigenvalue problem.

As for the MHD case, the force operator is linear in $\vec{\xi}$, but it is now *integro-differential* while it was only differential before. Similar non local wave equations appear for example in the domain of continuum mechanics when treating deformations with discontinuities, especially fractures, leading to an approach called *peridynamics*. The peridynamic theory is based on integral equations. For recent mathematical results on this, see e.g. Beyer et al. (2016). Here, because of the integral part in the vector eigenvalue equation, in order to derive the corresponding scalar wave equation, we will have to *differentiate*, and not only *combine*, as in the MHD case, the various components of the vector eigenvalue problem. For this reason, the differential wave equation on $\hat{\xi}_x$ (planar case) or $R\hat{\xi}_R$ (cylindrical case) will turn out to be of *fourth order*.

Now, working in the Cowling approximation consists in getting rid of the term which contains the integral, so that the force operator becomes differential again, and the wave equation in this case is of second order only, as in ideal MHD, and with much simpler coefficients than in the full gravity case, as we will see in chapter 8. For this reason, working in the Cowling approximation *greatly* simplifies the analysis. This will be very useful for our purpose, because it will be simple enough for some exact solutions to be found, which I will then use as the starting point to solve the full problem perturbatively.

However, we must be cautious with this approximation, because in a sense it misrepresents the problem. Indeed, as we have seen, a particularly important feature of a differential equation is the coefficient in front of its highest order term. But since in the Cowling approximation we are eliminating the highest order term, by going from a fourth to a second order equation, we are necessarily 'qualitatively' altering the spectrum. In fact, in Goedbloed et al. (2010), the authors study the spectrum of inhomogeneous plasmas, with resistivity, i.e. beyond the ideal MHD case mentioned above. The outcome is that resistivity increases the order of the wave equation, just like gravity does for us here, so that the singularities due to the vanishing of the coefficients in front of the highest derivatives disappear. The consequence is that *the continua split up into discrete modes*. The same may also happen when generalizing the ideal MHD spectrum by including gravity, but only by doing it fully, and not only in the Cowling approximation. Finally, note another qualitative difference appearing in this approximation: Given the order of the wave equations, the full gravity case will require four boundary conditions while in the Cowling approximation only two are needed.

### 7.3.2 Cowling vs Jeans

Since the Jeans term is the one that significantly complicates the analysis, it is legitimate to try and find a criterion, hopefully simple, to determine in which configurations the Jeans term is negligible, and thus the simple analyses and results obtained in the Cowling approximation are valid. To do so, let me first stress what is really meant by 'Cowling approximation'.

**What is meant by 'Cowling approximation'** In the literature, it is always written that the Cowling approximation consists in neglecting the perturbation of the gravitational potential $\Phi_1$. I find important to emphasize that just saying so is a little short cut, because implicitly the authors have in mind that the Cowling approximation in fact consists in neglecting $\Phi_1$ *in the linearized momentum conservation equation.* Indeed, the stage in the calculation at which we set $\Phi_1$ to zero matters. For example if we set $\Phi_1 = 0$ in equation (7.20) (and use the unperturbed Poisson equation $\Delta\Phi_0 = 4\pi G\rho_0$), we obtain:

$$\partial_t^2\rho_1 - \vec{\nabla}\rho_1\cdot\vec{\nabla}\Phi_0 - 4\pi G\rho_0\rho_1 - \Delta p_1 = 0, \tag{7.59}$$

while if we *first* use the linearized Poisson equation $\Delta\Phi_1 = 4\pi G\rho_1$ and *then* neglect $\phi_1$ (and use the unperturbed Poisson equation), we obtain

$$\partial_t^2\rho_1 - \vec{\nabla}\rho_1\cdot\vec{\nabla}\Phi_0 - 8\pi G\rho_0\rho_1 - \Delta p_1 = 0, \tag{7.60}$$

which brings a factor 2 of difference in the third term. This example is also the opportunity to make the following comments. First, this reminds us that the Cowling approximation is in essence a(n arbitrary) truncation in the information we are carrying, and not a certain regime of the dynamics. Also, the factor 2 here is not meaningless. In fact, it keeps appearing in the calculations, prosaically as $1+1=2$, translating the fact that the equilibrium and the linearized Poisson equations are formally exactly the same. In practice, this may be less benign than it looks, because it sometimes brings in confusion when one performs the calculations trying to track the separate role of the Cowling and the Jeans terms (cf. the discussion with the $\epsilon_C$ and $\epsilon_J$ parameters in section 8.3), or may even turn out to be misleading when one tries to recover results derived in the Jeans or Cowling approximations for consistency checks.

**Cowling vs Jeans** Let us discuss two points that will help us get an intuition of where and when the Cowling or Jeans terms prevail.

First, an intuitive discussion about the domain of validity of the Cowling approximation can be found for example in Cox (1980). The argument simply consists in saying that Fourier transforming the linearized Poisson equation on the potential, i.e. replacing the Laplacian $\Delta$ by $-k^2$, where $k$ is the wavenumber, we find that $\Phi_1$ is proportional to $k^{-2}$ and thus that $\Phi_1$ goes to zero as $k$ goes to infinity[14]. The author then concludes that the Cowling approximation should be a good approximation *for 'high order modes'*, i.e. for perturbations of small wavelength. This is indeed what is observed in numerical resolutions of the full system of equations in stellar physics.

Another fact stemming from the formal identity of the equilibrium and the perturbed Poisson equations is that the vector $\vec{g}_0$ may be written like $\vec{g}_1$ in the integral form (7.7), by replacing subscripts 1 by subscripts 0. Therefore, another way of expliciting the force operator (7.57) is

$$\vec{F} = -\vec{\nabla}p_1 - G\int[\underbrace{\rho_0(\vec{r'})\rho_1(\vec{r})}_{\text{Cowling}} + \underbrace{\rho_0(\vec{r})\rho_1(\vec{r'})}_{\text{Jeans}}]\frac{\vec{r}-\vec{r'}}{|\vec{r}-\vec{r'}|^3}d^3\vec{r'}. \tag{7.61}$$

This form is very interesting because it exhibits the very different nature of the Cowling and Jeans terms, and helps giving a hint of their ordering for a given equilibrium density profile and a given density perturbation. For instance, we see that at a given position $\vec{r}$, what matters in the Cowling term is the whole equilibrium profile $\rho_0$ (since it is integrated over) but only the local density perturbation $\rho_1$. It is the precise reverse for the Jeans term, so that for spatially rapidly varying perturbations, the alternance of positive and negative values of $\rho_1(\vec{r'})$ in the integral may render the Jeans term neglible. This thus exhibits the fact that the Jeans term will play a role essentially for *long spatial extent perturbations.* In directions in which the perturbation may be Fourier transformed, namely $y$ and $z$ in the planar case considered in chapter 8, this amounts to *long wavelength* perturbations. For directions with stratification, $x$ in the planar case, this amounts to saying that we do not expect instability in this direction for short perturbations[15], but that we may find instabilities when considering the full general perturbations.

[14] To be a little more precise, because his discussion happens in the context of stellar pulsations, Cox (1980) shows that $|\Phi_1| \propto \left[k^2 + \frac{l(l+1)}{r^2}\right]^{-1}$, where $k$ is the radial wavenumber and $l$ is the spherical harmonic order, so that in spherical systems, what is meant by 'high order mode' is large $k$ and/or large $l$.

[15] Therefore we do not expect WKB dispersion relations to reveal instabilities in the directions of stratification.

Now, my ambition is to determining the full spectrum of the force operator (7.29), i.e. that I would like to generalize figure 7.6 by taking gravity fully into account. The first step, that we are currently undertaking, is to determine the equivalent of figure 7.6 without magnetic field. To do so, in light of the MHD case, I have derived the wave equation corresponding to (7.58), in a planar and then in a cylindrical stratification. I will expose the details of these calculations in chapter 8 and briefly show my results in chapter 9.

# Chapter 8

# Stability of Cosmic Walls

The purpose of this chapter is to study the competition between pressure and gravity in the evolution of perturbations in a *planar stratification*, because it is relevant to study the stability of cosmic walls. I also decomposed the investigation of the eigenvalue problem (7.58) by first focusing on a planar stratification because curvature in cylindrical symmetry, relevant for cosmic filaments, adds a couple more subtleties that are all the better figured out once the planar case is clear. We will regularly focus on two particular planar stratifications (cf. chapter 6), namely a fluid embedded in a uniform gravitational field, essentially because it will turn out to be a non-trivial simple example very convenient for the calculations and constituting an interesting first approach to model some environments of physical interest, but also a self-gravitating slab, relevant to model cosmic walls.

We will proceed as follows. First we will study the effect of the background stratification on perturbations, by studying the spectrum in the Cowling approximation. Then we will include the effect of perturbations on the background itself by considering both the Cowling and Jeans terms in the force operator, with the aim of tracking gravitational fragmentation. We will explore this 'full gravity' case in two ways: first by deriving the wave equation and then by rewriting the equations matricially.

## 8.1 In the Cowling Approximation

Let us now work in the Cowling approximation and go through the derivation of the wave equation. We will solve the problem exactly, i.e. exhibit the full spectrum, in the case of a fluid embedded in a uniform gravitational field and in the case of a self-gravitating slab.

### 8.1.1 Vector Eigenvalue Problem

Without magnetic field, in the Cowling approximation, the force operator (7.29) reads:

$$\vec{F}\left(\vec{\xi}\right) = -\vec{\nabla}p_1 + \rho_1\vec{g}_0 \tag{8.1}$$

and the vector eigenvalue problem (7.58) becomes

$$\boxed{-\omega^2\rho_0\vec{\xi} = \vec{\nabla}\left(c_a^2\vec{\nabla}\cdot\left(\rho_0\vec{\xi}\right)\right) - \vec{\nabla}\cdot\left(\rho_0\vec{\xi}\right)\vec{g}_0}. \tag{8.2}$$

(Vector Eigenvalue Problem – Cowling Approximation)

### 8.1.2 Wave Equation

**Planar stratification** As in the previous chapter, thanks to the translation invariance along $y$ and $z$, we can consider plane waves in these directions, so that the most general expression of $\vec{\xi}$ is in principle given by (7.43) again. However now, contrary to the magnetic case before in which $\vec{B}$ was inducing a difference between the $y$ and $z$ directions, in the present case there is no preferred horizontal direction in the system, since gravity is in the $x$ direction (it is precisely the source of the stratification). Therefore there is no loss in generality if we rotate the coordinate system in order to take $k_z = 0$. We will thus consider from now on

$$\vec{\xi} = \left[\hat{\xi}_x(x)\ \hat{x} + \hat{\xi}_y(x)\ \hat{y} + \hat{\xi}_z(x)\ \hat{z}\right] e^{i(k_y y - \omega t)}. \tag{8.3}$$

**Wave equation** One way to continue would be to directly insert this expression in the vector eigenvalue problem (8.2) and combine the components to find the equation on $\hat{\xi}_x$ only. Now in fact, it will be very convenient to work with the variable

$$\boxed{\psi \equiv \rho_0 \hat{\xi}_x} \tag{8.4}$$

rather than $\hat{\xi}_x$, and most importantly, in order to keep track of the physical meaning of each equation, let us instead start one step backwards, as follows.

With the expression (8.3) of the displacement vector, the linearized mass conservation (7.30) reads

$$\rho_1 = \hat{\rho}_1(x)\ e^{i(k_y y - \omega t)} \tag{8.5}$$

where

$$\hat{\rho}_1(x) = -\psi' - \rho_0 i k_y \hat{\xi}_y. \tag{8.6}$$

Quantities with a hat, other than unit vectors, depend on $x$ only. Similarly, the components of the linearized momentum conservation $\rho_0 \partial_t \vec{v}_1 = -\omega^2 \rho_0 \vec{\xi} = \vec{F}$ with the force operator (8.1) read

$$\begin{cases} -\rho_0 \omega^2 \hat{\xi}_x = -c_a^2 \hat{\rho}_1' + \hat{\rho}_1 (\hat{g}_0 - (c_a^2)') \\ -\rho_0 \omega^2 \hat{\xi}_y = -i k_y c_a^2 \hat{\rho}_1 \\ -\rho_0 \omega^2 \hat{\xi}_z = 0. \end{cases} \tag{8.7}$$

Let us consider $\omega^2 \neq 0$. I will discuss the physical interpretation of this in the paragraph 'Taking a little hindsight' below in this section. The third equation above states that $\hat{\xi}_z = 0$, which is consistent with the fact that we rotated the axes for the dynamics to occur only in the $x$ and $y$ directions. Now, combining (8.6) and the second equation of (8.7), we can isolate $\hat{\rho}_1$ in order to express it as a function of $\psi$ only. This results in

$$\hat{\rho}_1 = -\frac{\omega^2}{\omega^2 - \omega_y^2} \psi', \tag{8.8}$$

where we introduced the frequency

$$\boxed{\omega_y^2(x) \equiv k_y^2 c_a^2(x)} \tag{8.9}$$

which corresponds to the Lamb frequency in stellar physics. Clearly, in this expression, we have assumed $\omega^2 \neq \omega_y^2$. This is done in the same spirit as in the ideal MHD case detailed in section 7.2, in which we first derived 'carelessly' the wave equation (7.40), and only later discussed the singularities that appear for particular values of $\omega^2$. Also, we remind the reader that although the $y$ direction here seems to play, through $\omega_y^2$, a particular role compared to $z$, this is simply due to the choice of coordinates, as stated earlier in the expression of $\vec{\xi}$: what physically matters here is that the $y$ direction corresponds to a direction transverse to the stratification.

Finally, we may insert the expression of $\hat{\rho}_1$ from (8.8) into the first equation of (8.7) to get the equation governing $\psi$:

$$\psi'' - \frac{1}{c_a^2} \left( g_0 - \frac{\omega^2 (c_a^2)'}{\omega^2 - \omega_y^2} \right) \psi' + \frac{\omega^2 - \omega_y^2}{c_a^2} \psi = 0. \tag{8.10}$$

From the definition (8.4) of $\psi$, we may finally obtain the equation governing $\hat{\xi}_x$. Using the hydrostatic equilibrium relation $\rho_0 g_0 = c_a^2 \rho_0'$, we may even rewrite it in the same form as the MHD wave equation, namely

$$\boxed{\left( \frac{N}{D}\ \hat{\xi}_x' \right)' + Q\ \hat{\xi}_x = 0} \tag{8.11}$$

(Wave Equation – Cowling Approximation)

where here

$$\begin{cases} N(x) = c_a^2 \rho_0 \\ D(x;\omega^2) = \omega^2 - \omega_y^2 \\ Q(x;\omega^2) = \rho_0 + (\frac{c_a^2 \rho_0'}{D})' - \frac{g_0 \rho_0'}{D}. \end{cases} \tag{8.12}$$

Note that if we were looking for the full expression of $\vec{\xi}$ (e.g. if boundary conditions were defined on other components than the $x$ one, or if we wanted at the end the full velocity vector), then once we have solved the equation for $\psi$, as in the two examples below, we may use the second equation of (8.7) together with (8.8) to deduce $\hat{\xi}_y$. As for the $z$ component, it is simply equal to zero here by construction.

**Boundary conditions** As discussed in section 7.2.3, the choice of boundary conditions is crucial as they strongly affect the discrete spectrum and thus the possible instabilities in the system. A thourough discussion of this is left for future work. For a discussion in the stellar case, see Cox (1980) and Smeyers & Van Hoolst (2010) for instance, and for models suited to other astrophysical contexts, see section 4.6.3 of Goedbloed & Poedts (2004) for instance. Let us here consider the simplest, 'rigid wall' conditions

$$\hat{\xi}_x(0) = \hat{\xi}_x(x_t) = 0 \tag{8.13}$$

where $x = 0$ corresponds to the center of the slab, and $x = x_t$ corresponds to its thickness (in this case, a truncated thickness, because the exponential atmosphere has an infinite extent in principle – see chapter 6). For smaller and smaller wavelength perturbations, boundary conditions matter less and less, and solutions can then be taken as plane-wave like (cf. section 8.2.6).

**Taking a little hindsight** This is an appropriate moment to assess the scope of what we are describing in this chapter, by anticipating works that I will mention in chapter 9 and 10.

Let us look at the eigenvalue parameter in equation (8.11). Only $\omega^2$ appears, and not $\omega$. This comes from the fact that we do not consider any flow here ($\vec{v}_0 = \vec{0}$). Indeed, for that reason, there is no distinction between backward and forward directions, so that all waves are degenerate. Backward and forward waves are undistinguishable, which is at the origin of the squaring of $\omega$'s (Goedbloed et al., 2010).

Also, recall that to derive equation (8.11), we have assumed $\omega^2 \neq 0$. The solutions we are then getting, namely the discrete spectrum (8.23) or (8.32) below, correspond to acoustic waves (called p-modes in the stellar physics community). But the $\omega^2 = 0$ modes are physically important: they are modes driven by buoyancy. They are vanishing here only because we deliberately 'switched off' convection through our assumption on the perturbed fluid (cf. section 9.2). Once we modify this assumption, the dependence in $\omega^2$ in equation (8.11) is more involved, and the quantization imposed by boundary conditions results in a quadratic equation in $\omega^2$ rather than linear, so that solutions similar to (8.23) and (8.32) remain (p-modes, but modified by buoyancy), but the additional solution becomes non zero, corresponding either to g-modes in the stable case, or convection in the unstable case.

### 8.1.3 Spectrum

Let us now study the spectrum. We will obtain the equivalent of figure 7.6 but for this hydrodynamical situation in which we have made the Cowling approximation. We are seeking two things: (i) The singularities, which give rise to the continuous spectrum and the turning points ranges, and (ii) the discrete spectrum.

#### (i) Singularities

What are the singularities of the wave equation (8.11) and of which nature are they?

**Naïve answers** First, based on the argument that I presented about the general differential equation (7.52), which states that the points where the coefficient of either the lowest or highest order term vanished were key, it is tempting to say that the wave equation (8.10) contains $\omega_y^2$ as an apparent singularity because it is present on the lowest order term. However, one may argue that in this equation when $\omega^2 \to \omega_y^2$, the coefficient in front of $\psi'$ diverges... It is then tempting to first multiply the wave equation (8.10) by $(\omega^2 - \omega_y^2)^2$ in order to get rid of all the denominators, and then, observing that the highest order coefficient is proportional to $\omega^2 - \omega_y^2$, conclude that the frequency $\omega_y^2$ is in fact genuine... And the same reasoning can be applied with equation (8.11).

Second, another similar observation could be made. From the previous derivation, one may easily obtain an equation on $\rho_1$ rather than on $\psi$, and deduce the following wave equation:

$$\hat{\rho}_1'' + \left(2\frac{(c_a^2)'}{c_a^2} - \frac{g_0}{c_a^2}\right)\hat{\rho}_1' + \frac{\omega^2 - \omega_y^2 + (c_a^2)'' - g_0'}{c_a^2}\hat{\rho}_1 = 0. \tag{8.14}$$

It is now very tempting, in view of the lowest order coefficient, to conclude that there is only one singularity, the frequency $\omega_y^2 - (c_a^2)'' + g_0'$, and that it is apparent.

Consequence: Depending on how we write the wave equation and with which variable, we seem to be lead to different conclusions...

**What is happening?** This remark is the opportunity to warn the reader about two very important aspects.

First, the choice of variable (here $\psi$, $\hat{\xi}_x$ or $\rho_1$) is not without significance. Indeed, the operator intervening in the eigenvalue problem formulated in one or the other variable is different, therefore the corresponding spectrum is not necessarily the same for each of them. I will come back to this point in section 9.3.

Second, fortunately Goedbloed & Poedts (2004) have already treated this question, i.e. they studied the MHD wave equation, as detailed in the previous section, but they also considered gravity, *in the Cowling approximation only* though, as we are doing in this section. We may therefore take advantage of their works for the present question. The outcome is that they show that $\omega_y^2$ remains the fast magneto-acoustic apparent frequency. The ideal MHD singularities are unaffected by gravity, in the Cowling approximation. The point I want to stress here is that the simple correspondences 'numerator vanishes $\leftrightarrow$ genuine singularity' and 'denominator vanishes $\leftrightarrow$ apparent singularity' is proper to the MHD wave equation (7.45) written in the Sturm-Liouville form only. Now, the aim of the present work is to study how gravity modifies the spectrum *beyond* the Cowling approximation. As we will see, the wave equation will not be of the simple Sturm-Liouville form. For this reason, at this stage of my investigations, I shall be cautious when drawing conclusions about the nature of the singularities that will appear in the complicated wave equation we will obtain.

**Experience gained** a) Which variable? In this manuscript, I aim at generalizing the MHD spectrum detailed in section 7.2. Therefore I will focus on the equations governing the variable $\vec{\xi}$ and its components. However, in the hydrodynamical case, the variable $\psi$ will be a very convenient (and even *extremely* convenient, cf. equation (8.59)) variable to lighten the intermediate calculations. And the variable $\rho_1$ may be interesting to answer some simpler questions, but I will not focus on it here and refer the reader to the relevant discussion in chapter 9.

b) Which approach? I am still convinced that addressing the question of gravitational fragmentation as a spectral problem and to learn from the MHD literature is essential. However, as we can see here, the MHD and the gravity problems being fundamentally different, we still have some work in front of us to adapt the techniques developed by plasma physicists to our context.

c) To answer the initial question of this section: The only singularity in the present case is the frequency $\omega_{f0}^2 = c_a^2 k_y^2$, which is apparent, constituting a range of turning point frequencies since $c_a^2$ depends on $x$ in general.

### (ii) The discrete spectrum

What is the discrete spectrum? The good news is that we may explicit it entirely in two physically interesting cases: an isothermal fluid in a uniform external gravitational field (i.e. the exponential atmosphere) and an isothermal self-gravitating slab. Both are isothermal models, so that we are eliminating the effects of the stratification of the speed of sound. Physically, we are thus avoiding complicated trajectories of acoustic waves, and formally $c_a^2$ is a mere constant, which is why the wave equation greatly simplifies, up to having simple analytical solutions. Indeed, in this case equation (8.10) reads

$$\psi'' - \frac{g_0}{c_a^2}\psi' + \frac{\omega^2 - \omega_y^2}{c_a^2}\psi = 0 \tag{8.15}$$

that we are now going to solve in the two aforementioned models.

**Uniform external gravitational field ($g_0 = g_{\text{ext}}$)** Recall from section 6.2 that in this case the atmosphere has an exponential profile (equation (6.16)):

$$\rho_0(x) = \rho_c \; e^{-x/L_{\text{ext}}} \tag{8.16}$$

where

$$L_{\text{ext}} \equiv -\frac{c_a^2}{g_{\text{ext}}}. \tag{8.17}$$

The power of this model is its simplicity and handiness, as equation (8.15) now has constant coefficients so that its solutions are well known. The solutions of the differential equation $y'' + by' + cy = 0$ are given by the roots of its characteristic polynomial $x^2 + bx + c$, and the nature of its solutions depends on the sign of the discriminant $\Delta = b^2 - 4c$. In our case we have

$$\Delta = \frac{g_{\text{ext}}^2}{c_a^4} - 4\frac{\omega^2 - \omega_y^2}{c_a^2}, \tag{8.18}$$

hence the following solutions:
For $\Delta > 0$ solutions are exponential (spatially)

$$\psi(x) = c_1 \; \exp\left(\left(\frac{g_{\text{ext}}}{c_a^2} + \sqrt{\Delta}\right)\frac{x}{2}\right) + c_2 \; \exp\left(\left(\frac{g_{\text{ext}}}{c_a^2} - \sqrt{\Delta}\right)\frac{x}{2}\right), \tag{8.19}$$

for $\Delta = 0$ they read

$$\psi(x) = (c_1 x + c_2)\, e^{\frac{g_{\text{ext}}}{c_a^2}\frac{x}{2}}, \tag{8.20}$$

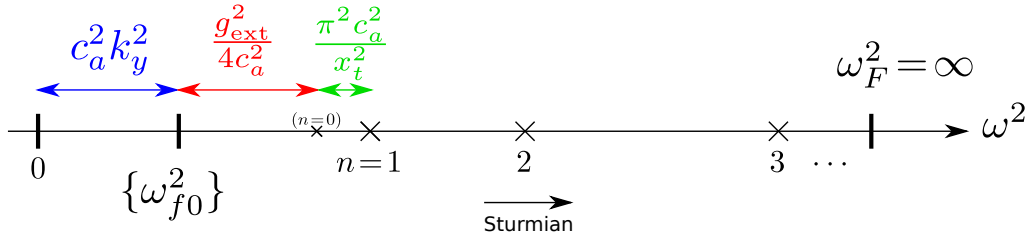


Figure 8.1: The explicit spectrum (8.23) of the exponential atmosphere, in the spirit of figure 7.6. Because this case corresponds to an isothermal atmosphere, $c_a^2$ is position independent, so that the turning point frequency range is only the singleton $\{\omega_{f0}^2\} = \{c_a^2 k_y^2\}$. This is not representative of general inhomogeneous media, for which singular frequencies are non trivial ranges of values. The Alfvén and slow continua, and the slow turning point frequency range are not represented because they are all equal to 0 and are gathered at the origin of the spectrum.

and for $\Delta < 0$ they are oscillatory (spatially)

$$\psi(x) = e^{\frac{g_{\rm ext}}{c_a^2}\frac{x}{2}} \left\{ c_1 \cos\left(\sqrt{|\Delta|}\frac{x}{2}\right) + c_2 \sin\left(\sqrt{|\Delta|}\frac{x}{2}\right) \right\} \tag{8.21}$$

where $c_1$ and $c_2$ are constants determined by boundary conditions. The purely exponential solutions correspond to regions where waves have spatially damped amplitudes, while the oscillatory solutions exhibit discrete locations (specific values of $x$) where the wave ampitudes are exactly zero. In addition, from the discussion in 7.2.3, we expect the corresponding eigenvalues to be quantized due to boundary conditions. Indeed, let us now explicit the $\Delta < 0$ case. The boundary condition (8.13) at $x = 0$ imposes $c_1 = 0$, and the one at $x = x_t$ then imposes that

$$\boxed{\sin\left(\frac{x_t \delta}{2}\right) = 0} \quad \text{where} \quad \delta \equiv \sqrt{4\frac{\omega^2 - \omega_y^2}{c_a^2} - \frac{g_{\rm ext}^2}{c_a^4}}. \tag{8.22}$$

(Quantization Condition – Uniform External $g_{\rm ext}$, Isothermal, Cowling Approximation)

The argument inside the sine function thus must be a multiple of $\pi$, so that the modes are quantized according to

$$\boxed{\omega_n^2 = c_a^2 \left(\frac{n^2\pi^2}{x_t^2} + k_y^2\right) + \frac{g_{\rm ext}^2}{4c_a^2}} \tag{8.23}$$

(Discrete Spectrum – Uniform External $g_{\rm ext}$, Isothermal, Cowling Approximation)

where $n \in \mathbb{N}^*$ ($n \neq 0$ since $\Delta$, and thus the argument of the sine function above, are assumed non zero here). This constitutes the discrete spectrum of the Exponential Atmosphere model. The purpose of section 8.3.3 will be to find the discrete spectrum but without making the Cowling approximation. The generalization of the quantization condition (8.22) is then much more involved. Indeed, already in the limit of a 'small enough' density atmosphere it is given by equation (8.144), and if in addition the boundaries are 'far', it is reduced to the relation (8.151) which generalizes (8.23). The expressions 'small enough' and 'far' will be defined precisely in the corresponding section.

**Self-gravitating slab** The previous model is interesting in cases in which an exterior gravitational field is fixed, as for example in the atmosphere of a planet or for a fluid embedded in, and dominated by, Dark Matter. However, in the Universe, many fluids are self-gravitating, and $g_0$ is determined self-consistently rather than being imposed. I will now derive in this case the explicit discrete spectrum of p-modes, in the Cowling approximation, as we just did for the exponential atmosphere. I have not found this in the literature yet so, to the best of my knowedge, the spectrum I obtain below is a new result.

The equations governing the equilibrium were detailed in chapter 6, and for a self-gravitating planar isothermal atmosphere, the density profile is given by (6.27), and from this expression one may easily get with (6.19) that the gravitational acceleration reads

$$g_0 = -2\frac{c_a^2}{L}\tanh\left(\frac{x}{L}\right) \tag{8.24}$$

with the characteristic length scale[1]

$$L^2 \equiv 2\frac{c_a^2}{\omega_c^2} \tag{8.25}$$

[1]It is a slightly different definition from $L_1$ given by (6.25) to avoid carrying $\sqrt{2}$ factors in the following.

where $\omega_c^2 \equiv 4\pi G\rho_0(0)$. To clarify the discussion, let us work again with the dimensionless variable $\bar{x} \equiv \frac{x}{L}$. Equation (8.15) then reads

$$\psi'' + 2\tanh\bar{x}\ \psi' + a\psi = 0 \tag{8.26}$$

where now the derivatives are with respect to $\bar{x}$, and where

$$a \equiv 2\frac{\omega^2 - \omega_y^2}{\omega_c^2}. \tag{8.27}$$

The good surprise is that equation (8.26) has two very simple linearly independant analytic solutions. Their nature depends on the value of $a$: For $a < 1$ they are exponential (spatially)

$$\psi_\pm = \frac{e^{\pm\sqrt{1-a}\ \bar{x}}}{\cosh\bar{x}} \tag{8.28}$$

and for $a > 1$ they are oscillatory (spatially)

$$\psi_\pm = \frac{e^{\pm i\sqrt{a-1}\ \bar{x}}}{\cosh\bar{x}}. \tag{8.29}$$

Let us for now consider the case $a > 1$, which corresponds to high frequencies

$$\omega^2 > \omega_y^2 + \frac{\omega_c^2}{2}. \tag{8.30}$$

The solutions are $\psi = A\psi_+ + B\psi_-$, where the rigid walls boundary conditions (8.13) fix the coefficients $A$ and $B$. The condition at the center $\bar{x} = 0$ imposes $A = -B$ and that at the boundary $\bar{x} = x_t/L$ leads to $\sin\left(\sqrt{a-1}\ x_t/L\right) = 0$ and thus to the quantization

$$\sqrt{a-1}\frac{x_t}{L} = n\pi \tag{8.31}$$

with $n \in \mathbb{N}^*$ since $x_t \neq 0$ and $a \neq 1$. Finally, using the definitions of $L$ (8.25) and $a$ (8.27), we may explicit the discrete spectrum, equivalent of (8.23) for the exponential atmosphere but for a self-gravitating fluid:

$$\boxed{\omega_n^2 = c_a^2\left(\frac{n^2\pi^2}{x_t^2} + k_y^2\right) + \frac{\omega_c^2}{2}}. \tag{8.32}$$

(Discrete spectrum – Self-Gravitating, Isothermal, Cowling Approximation)

**Comments on the discrete spectra (8.23) and (8.32)** Given the choice of our closure relation (section 7.1.1), we cannot have convection in this system, and since we got rid of the Jeans term (section 7.1.3), we cannot have gravitational fragmentation. Hence, the only other gravitational instability we could have in principle is the Rayleigh-Taylor instability. However, as we can see, in both cases here the spectrum is confined to the positive real axis $\omega^2 > 0$, so that we do not have any instability. In fact, finding a Rayleigh-Taylor instability here would have been rather absurd since the density profiles of these two atmospheres are decreasing with $x$. Thus, the denser layers lie always below the lighter ones, and it makes sense that the greater the stratification, the greater the density difference between adjacent layers, and the more restoring the force is. Therefore, the stratification has naturally a stabilizing effect with respect to the Rayleigh-Taylor instability.

We can also see that the stratification induces an offset. In the literature, the $\omega_{n=0}^2(k_y = 0)$ frequency is called the *acoustic cut-off frequency*. In the exponential atmosphere it is equal to

$$\omega_{\text{cut}}^2 = \frac{g_{\text{ext}}^2}{4c_a^2} \tag{8.33}$$

and in the self-gravitating slab to

$$\omega_{\text{cut}}^2 = \frac{\omega_c^2}{2}. \tag{8.34}$$

Intuitively this comes from the fact that, at a given frequency, short wavelength waves evolve in a medium that is roughly homogeneous, because their wavelength is shorter than the density profile length scale, and thus they propagate. For long enough wavelength waves on the contrary, the profile appears as extremely steep, acting as a wall, so that these are stationary.

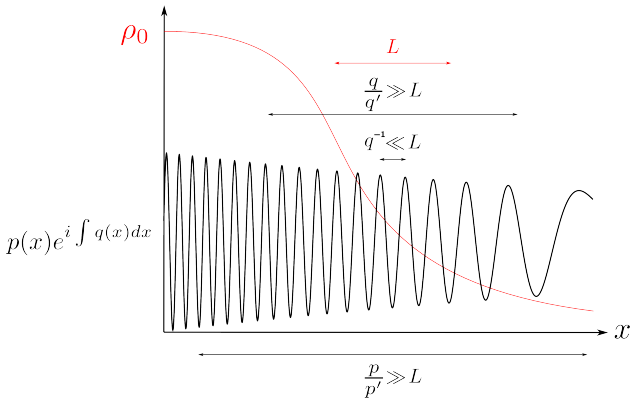


Figure 8.2: Illustration of the shape required for the solution $\xi = pe^{i\int qdx}$ to be locally looking like a plane wave: (i) The local 'wavenumber' $q(x)$ around position $x$ should be large compared to the local gradient, estimated as $1/L$ where $L$ is the characteristic length of the equilibrium profile, for the medium to 'appear' as almost homogeneous for the perturbation, (ii) the amplitude function $p(x)$ has to vary slowly enough ($\frac{p'}{p}$ of the order or smaller than $\frac{1}{L}$) for the amplitude of the perturbation to be approximately constant, and (iii) $q(x)$ should not vary too fast either ($\frac{q'}{q}$ of the order or smaller than $\frac{1}{L}$) to have a well defined wavenumber at position $x$.

### 8.1.4 Local analysis: WKB dispersion relations

When studying waves and instabilities in homogeneous media, the wave equation has constant coefficients, so that we may look for solutions of the form $\rho_1 \propto e^{i(\vec{k}\cdot\vec{r}-\omega t)}$ which results in a dispersion relation, as we have done in chapter 7 to derive Jeans dispersion relation (7.12). In an inhomogeneous medium however, plane waves are clearly not solutions, but intuitively it is clear that an inhomogeneous medium can be seen as *locally* homogeneous so that we should be able to derive dispersion relations for waves of *large enough* wavenumber. In the literature, most authors (e.g. Smeyers & Van Hoolst, 2010; Binney & Tremaine, 2008) perform such local stability analyses by plugging plane waves solutions of the above form, thus reducing the differential equation or system to an algebraic one, and then neglecting terms that are small because the wavenumber is assumed to be large, for example in cylindrical systems by considering that $|k|R \gg 1$. Authors like (e.g. Goedbloed, 1984; Keppens et al., 1993) however, use in their works a similar but quite different technique to study local waves in stratified media. Both are referred to as 'WKB dispersion relations', named after Wentzel–Kramers–Brillouin who popularized the use of solutions of the form (8.35) as they used it in Quantum Mechanics. Note however that we are not going to perform a 'proper' formal WKB analysis, which consists in determining approximate solutions to differential equations in which the highest order coefficient is multiplied by a small parameter. The literature on this subject is humongous, but I would advise the very clear Holmes (2013) for instance. But in essence, this 'proper' WKB method also relies on the idea of looking for solutions of differential equations close to the exponential form, which is the solution in the case in which coefficients are constant. The method consists in the following. Let us look for solutions of the form

$$\xi_x = pe^{i\int qdx}, \tag{8.35}$$

where $p$ and $q$ are two real functions of $x$. As illustrated in figure 8.2, the function $p$ monitors how the envelope of the solution varies, while $q$ corresponds to how fast the solution oscillates spatially. In order for the solution to be close to a plane wave, we should require that $p$ and $q$ change slowly with respect to position $x$ but the phase in (8.35) must vary fast. Translating these two requirements in the equation governing the solution, we will obtain a constraint on $q$, which we may then interpret as the local dispersion relation and $q$ as the local 'wavenumber' in the $x$ direction (quotation marks because the solution is not rigorously a plane wave in the stratified case).

Let us first repeat the approach adopted in works such as Goedbloed (e.g. 1984); Keppens et al. (e.g. 1993). Since these are studies of MHD, their governing equation is the MHD wave equation (7.45), which is of the Sturm-Liouville form $(f\hat{\xi}_x')' + g\hat{\xi}_x = 0$. In order to later generalize this method to fourth order equations (cf section 8.2.6), let us now rearrange this equation and write it as

$$A_2\hat{\xi}_x'' + A_1\hat{\xi}_x' + A_0\hat{\xi}_x = 0. \tag{8.36}$$

where

$$\begin{cases} A_2 = 1 \\ A_1 = \frac{f'}{f} \\ A_0 = \frac{g}{f}. \end{cases} \tag{8.37}$$

Plugging in solution (8.35) and identifying real and imaginary parts gives

$$\begin{cases} -q^2 + A_0 + \frac{p'}{p} A_1 + \frac{p''}{p} = 0 \\ 2\frac{p'}{p} + \frac{q'}{q} + A_1 = 0. \end{cases} \tag{8.38}$$

Now, let us call $L$ the characteristic length of the equilibrium profile, so that we have the correspondence

$$\frac{d}{dx} \leftrightarrow \frac{1}{L} \tag{8.39}$$

and

$$\begin{cases} \frac{p''}{p} \sim \frac{1}{L^2} \\ \frac{p'}{p} \sim \frac{1}{L} \\ A_1 \sim \frac{1}{L}. \end{cases} \tag{8.40}$$

The idea is then to work in the limit of 'high order modes' in which

$$\frac{1}{L} \ll q \tag{8.41}$$

so that we may do a perturbative expansion. The $\frac{p''}{p}$ and $\frac{p'}{p} A_1$ terms in the first equation of (8.38) are thus of second order, so that this equation gives, up to first order,

$$\boxed{-q^2 + A_0 = 0} \tag{8.42}$$

(Local Dispersion Relation – 2nd order equation)

where second and higher derivatives in the expression of $A_0$ are neglected. Now, the whole point of looking for a solution of the WKB form (8.35) is to interpret $q$ as the local wavenumber in the $x$ direction, so that equation (8.42) is interpreted as the local dispersion relation, and to emphasize this interpretation we will hereafter use the notation $k_x$ instead of $q$. Also, note that the second equation of (8.38) gives a constraint on $p$, which does not affect the equation on $q$ so we do not need it in this case.

Now, coming back to the problem at hand in this section, the governing equation[2] on $\hat{\xi}_x$ is (8.36) with

$$\begin{cases} A_2 = 1 \\ A_1 = \frac{\rho_0'}{\rho_0} \\ A_0 = \frac{\omega^2 - \omega_y^2}{c_a^2} + \frac{\rho_0''}{\rho_0} - \left(\frac{\rho_0'}{\rho_0}\right) \end{cases} \tag{8.43}$$

but we neglect the last two terms in $A_0$ as mentioned above, so that the WKB dispersion relation gives

$$\omega^2 = c_a^2 \left(k_x^2 + k_y^2\right). \tag{8.44}$$

In this local dispersion relation, modes along $x$ are not quantized: $k_x$ is a continuous variable. However, for a slab of finite thickness, the only modes that satisfy the boundary conditions are those whose half of the wavelength fits in the slab an integer number of times. This means that for a slab with edge at $x = x_t$ we have[3] $n\lambda_x/2 = x_t$, so that $k_x = \frac{n\pi}{x_t}$. Now since (8.44) is valid in the limit of large wavenumbers, we may thus write

$$\omega^2 = c_a^2 \left(\frac{n^2\pi^2}{x_t^2} + k_y^2\right) \tag{8.45}$$

but keeping in mind that $n$ is 'large' here. This dispersion relation matches the discrete spectrum (8.32) deduced previously, in the limit of large $n$ for which the contribution of the constant cut-off frequency becomes negligible. It is important for consistency to recover this, because the previous analysis which leads to (8.32) determined completely the spectrum, so that it must contain the result of this local analysis. At this point, this local analysis is not of great interest since we have been able to solve the problem exactly first. But in what follows, we will not be able to derive the full spectrum as easily, so that simple relations such as (8.42) will bring us valuable information.

## 8.2 Wave Equation formulation

I am now going to derive from the full vector eigenvalue problem (7.58) the corresponding wave equation, i.e. we are going to generalize the wave equation (8.11) we deduced in the Cowling approximation. To the best of my knowledge, all that follows is new in the literature.

[2] This corresponds to equation (8.15) where we have used the hydrostatic equilibrium (6.1) which in the planar case reads $g_0 = c_a^2 \frac{\rho_0'}{\rho_0}$.

[3] And not $2x_t$, though the slab spans between $-x_t$ and $+x_t$, because we have imposed boundary conditions such that the displacement vanishes at $x = x_t$ and $x = 0$.

### 8.2.1 Wave equation

For clarity, I will decompose this derivation in 5 steps.

**Step 1: Expression of $\vec{g}_1$** We are going to follow the same steps as in section 8.1. The only difference is that we now have the vector $\vec{g}_1$ in the linearized momentum conservation, i.e. we consider the 'full gravity' version of the force operator (7.57). Using the same expression (8.3) for the displacement vector, the linearized mass conservation (7.30) reads again

$$\rho_1 = \hat{\rho}_1(x)\, e^{i(k_y y - \omega t)} \quad \text{where} \quad \hat{\rho}_1(x) = -\psi' - \rho_0 i k_y \hat{\xi}_y, \tag{8.46}$$

and therefore we see that all quantities, other than $\vec{g}_1$, in the momentum conservation equation are proportional to $e^{i(k_y y - \omega t)}$, so that this equation ensures that we may write $\vec{g}_1$ as

$$\vec{g}_1 = [\hat{g}_{1x}(x)\hat{x} + \hat{g}_{1y}(x)\hat{y} + \hat{g}_{1z}(x)\hat{z}]\, e^{i(k_y y - \omega t)}. \tag{8.47}$$

Here again quantities with a hat, other than unit vectors, depend on $x$ only. Then, the constraint (7.6) on $\vec{g}_1$, stating that it is irrotational, links its components to each other according to

$$\begin{cases} \hat{g}_{1x} = \left(\frac{\hat{g}_{1y}}{ik_y}\right)' \\ \hat{g}_{1z} = 0 \end{cases} \tag{8.48}$$

which will greatly simplify the rest of the derivation.

**Step 2: Rewriting Momentum conservation** Now, the linearized momentum conservation $\rho_0 \partial_t \vec{v}_1 = -\omega^2 \rho_0 \vec{\xi} = \vec{F}$ with the force operator (7.57), projected onto the three directions, reads

$$\begin{cases} -\rho_0 \omega^2 \hat{\xi}_x = -c_a^2 \hat{\rho}_1' + \hat{\rho}_1(\hat{g}_0 - (c_a^2)') + \rho_0 \hat{g}_{1x} \\ -\rho_0 \omega^2 \hat{\xi}_y = -i k_y c_a^2 \hat{\rho}_1 + \rho_0 \hat{g}_{1y} \\ -\rho_0 \omega^2 \hat{\xi}_z = 0. \end{cases} \tag{8.49}$$

As before, let us consider $\omega^2 \neq 0$, so that the third equation ensures that $\hat{\xi}_z = 0$. Combining (8.46) and the $y$-component of (8.49), we can isolate $\hat{\rho}_1$, and get

$$\hat{\rho}_1(x) = -\frac{\omega^2}{\omega^2 - \omega_y^2}\psi' + \rho_0 k_y^2 \mathcal{G}_y, \tag{8.50}$$

where, for convenience in the derivation of this section, I introduce

$$\mathcal{G}_y \equiv \frac{1}{\omega^2 - \omega_y^2}\frac{\hat{g}_{1y}}{ik_y}. \tag{8.51}$$

Plugging (8.50) in the $x$-component of (8.49), and using (8.48), we obtain

$$\boxed{\mathcal{G}_y' = -\frac{c_a^2}{\rho_0(\omega^2 - \omega_y^2)}\left[\psi'' - \frac{1}{c_a^2}\left(g_0 - \frac{\omega^2 (c_a^2)'}{\omega^2 - \omega_y^2}\right)\psi' + \frac{\omega^2 - \omega_y^2}{c_a^2}\psi\right]}. \tag{8.52}$$

(Rewriting Momentum Conservation)

Note that we recover the wave equation (8.10) of the Cowling approximation, as we should, by setting the left hand side to zero, i.e. $\hat{g}_{1y} = 0$. But equation (8.52) is not closed because there are two variables for one equation only. The complementary information we have not added yet is of course the linearized Poisson equation.

**Step 3: Rewriting Poisson equation** With (8.48), the linearized Poisson equation (7.5) becomes

$$\left(\frac{\hat{g}_{1y}}{ik_y}\right)'' - k_y^2\left(\frac{\hat{g}_{1y}}{ik_y}\right) = -4\pi G \hat{\rho}_1. \tag{8.53}$$

Now, in order to combine it with equation (8.52), it is best to rewrite it using the variable $\mathcal{G}_y$. Using (8.50) and (8.51) we obtain

$$\boxed{\mathcal{G}_y'' - 2\frac{(\omega_y^2)'}{\omega^2 - \omega_y^2}\,\mathcal{G}_y' - k_y^2 \frac{\omega^2 - \omega_G^2}{\omega^2 - \omega_y^2}\,\mathcal{G}_y = 4\pi G \frac{\omega^2}{(\omega^2 - \omega_y^2)^2}\psi'}. \tag{8.54}$$

This step is crucial because it is exactly when the key frequency $\omega_G^2$ appears, namely[4]

$$\boxed{\omega_G^2(x) = \omega_y^2 - \frac{(\omega_y^2)''}{k_y^2} - \omega_0^2} \tag{8.55}$$

(Singular Frequency – Full Gravity)

where $G$ stands for 'gravitational', and let us recall the definitions $\omega_y^2(x) \equiv k_y^2 c_a^2(x)$ (cf. equation (8.9)) and $\omega_0^2(x) \equiv 4\pi G\rho_0(x)$ (cf. equation (6.3)). We will discuss it in the next section, but note already that its importance stems from the fact that it will end up as the singular frequency of the highest degree term of the final (fourth order) wave equation. We can already see at this stage, before the long calculations that follow, that it is indeed going to play a significant role. Indeed, to get the equation on $\psi$ only, we are going to plug (8.52) into (8.54). But note that (8.52) gives $\mathcal{G}_y'$ while (8.54) contains $\mathcal{G}_y$, so that we will need to have to differentiate (8.54) one more time. This is what makes the final equation of fourth order, *unless* the term containing $\mathcal{G}_y$ in (8.54) actually vanishes, which happens precisely when $\omega^2 = \omega_G^2$. In this case, we do not have to differentiate once more, so that the order of the resulting equation will be of one order less. This gives a feeling that the highest order term of the final equation must be proportional to $\omega^2 - \omega_G^2$ since this frequency lowers the equation by one order.

**Step 4: Equation on $\psi$** Isolating $\mathcal{G}_y$ from (8.54) and differentiating gives an equation in which only $\mathcal{G}_y'$ intervenes, and all that is left to do is to insert the expression of $\mathcal{G}_y'$ from (8.52) to end up with an equation on $\psi$ only, namely

$$\sum_{i=0}^{4} B_i \psi^{(i)} = 0 \tag{8.56}$$

where all the coefficients $B_i$ depend on $x$ and are parameterized by $\omega^2$. Their full expressions are the following (with $\Omega_G \equiv \omega^2 - \omega_G^2$):

$$\begin{cases}
B_4 = \Omega_G \\
B_3 = \Omega_G \left[3\frac{(c_a^2)'}{c_a^2} - 3\frac{\rho_0'}{\rho_0}\right] - \Omega_G' \\
B_2 = \Omega_G \left[\frac{\omega^2+\omega_0^2-2g_0'}{c_a^2} + 3\frac{(c_a^2)''}{c_a^2} - 4\frac{\rho_0'}{\rho_0}\left(\frac{(c_a^2)'}{c_a^2} - \frac{\rho_0'}{\rho_0}\right) - \frac{\rho_0''}{\rho_0} - 2k_y^2\right] \\
\quad - \Omega_G' \left[2\frac{(c_a^2)'}{c_a^2} - 2\frac{\rho_0'}{\rho_0}\right] \\
B_1 = \Omega_G \left[\frac{\rho_0'}{\rho_0}\left(-\frac{2\omega^2+\omega_0^2}{c_a^2} - 3\frac{(c_a^2)''}{c_a^2} + 6\frac{\rho_0''}{\rho_0} - 6\left(\frac{\rho_0'}{\rho_0}\right)^2 + 3k_y^2\right) - \frac{\rho_0'''}{\rho_0} - 3\frac{(c_a^2)'}{c_a^2}\left(\frac{\rho_0''}{\rho_0} - 2\left(\frac{\rho_0'}{\rho_0}\right)^2 + k_y^2\right)\right] \\
\quad + \Omega_G' \left[2\frac{(c_a^2)'}{c_a^2}\frac{\rho_0'}{\rho_0} + \frac{\rho_0''}{\rho_0} - 2\left(\frac{\rho_0'}{\rho_0}\right)^2 + k_y^2\right] \\
B_0 = \Omega_G \left[\frac{\omega^2}{c_a^2}\left(-\frac{\rho_0''}{\rho_0} + 2\left(\frac{\rho_0'}{\rho_0}\right)^2 - k_y^2\right) + k_y^2\left(-\frac{\omega_0^2}{c_a^2} - 3\frac{(c_a^2)''}{c_a^2} + 3\frac{\rho_0'}{\rho_0}\frac{(c_a^2)'}{c_a^2} + \frac{\rho_0''}{\rho_0} - 2\left(\frac{\rho_0'}{\rho_0}\right)^2 + k_y^2\right)\right] \\
\quad + \Omega_G' \left[\frac{\rho_0'}{\rho_0}\frac{\omega^2}{c_a^2} + k_y^2\left(2\frac{(c_a^2)'}{c_a^2} - \frac{\rho_0'}{\rho_0}\right)\right].
\end{cases} \tag{8.57}$$

Equation (8.56) is the full equation governing $\psi$, of which equation (8.10) is only an approximation obtained in the Cowling approximation.

**Step 5: The wave equation on $\hat{\xi}$** Finally, to get the equation on $\hat{\xi}_x$ only, we simply have to use the definition $\psi = \rho_0\hat{\xi}_x$ and differentiate it up to four times. Using Leibniz's rule, it is direct to show that by writing the wave equation as

$$\boxed{\sum_{i=0}^{4} A_i \hat{\xi}_x^{(i)} = 0} \tag{8.58}$$

(Wave Equation – Full Gravity)

the coefficients $A_i$ can be expressed in terms of the $B_i$s according to

$$\begin{pmatrix} A_0 \\ A_1 \\ A_2 \\ A_3 \\ A_4 \end{pmatrix} = \rho_0 \begin{pmatrix} 1 & \frac{\rho_0'}{\rho_0} & \frac{\rho_0''}{\rho_0} & \frac{\rho_0'''}{\rho_0} & \frac{\rho_0^{(4)}}{\rho_0} \\ 0 & 1 & 2\frac{\rho_0'}{\rho_0} & 3\frac{\rho_0''}{\rho_0} & 4\frac{\rho_0'''}{\rho_0} \\ 0 & 0 & 1 & 3\frac{\rho_0'}{\rho_0} & 6\frac{\rho_0''}{\rho_0} \\ 0 & 0 & 0 & 1 & 4\frac{\rho_0'}{\rho_0} \\ 0 & 0 & 0 & 0 & 1 \end{pmatrix} \begin{pmatrix} B_0 \\ B_1 \\ B_2 \\ B_3 \\ B_4 \end{pmatrix}. \tag{8.59}$$

[4] Of course, one may eliminate $k_y^2$, writing $\omega_G^2 = \omega_y^2 - (c_a^2)'' - \omega_0^2$, but the form given here is how it naturally appears, and is such that the comparison with its cylindrical generalization (9.6) is transparent. And in the latter case, the analogue of $k_y$ is position dependent so that we may not simplify like here.

Equation (8.58) with coefficients (8.59) is the full equation governing $\hat{\xi}_x$, of which the simple equation (8.11) is only an approximation obtained in the Cowling approximation.

**Comments** First of all, while we did anticipate that the order of the wave equation would be higher than in the Cowling approximation, the finding now is that the problem is also far more complex because of the length of the coefficients. However, confronted with the complexity of this wave equation, one should be all the more rejoiced by the spectral theory approach. Indeed, it is particularly pleasant to see that the highest order term is very simple, and that at the same time, this is what matters the most. As mentioned in section 7.2, in order to study the stability, the key is to focus on the positions at which the singularity occurs, i.e. in our case the positions $x_s$ for which $\omega^2 = \omega_G^2(x_s)$. I have already started exploring this. It is clearly very promising, but the techniques developed in the plasma literature I have been learning from cannot be directly used because the equation here is of fourth order. Some more little steps are required, but the way to proceed is clear and left for future work. To stress this point, let me mention two quotes from two very important articles. In Ledoux (1950) the author comments on the work of Pekeris (1938) who derived a similar equation, saying "il est conduit à une équation différentielle du quatrième ordre aux coefficients extrêmement compliqués[5]", and does not pursue in this direction (neither does he in Ledoux & Walraven, 1958). Similarly, Goldreich & Lynden-Bell (1965) state that they could "end up with an equation for $\phi_1$ (of fourth order). However [they] did not find the result very enlightening so [they] shall not repeat it [in their paper]". My point is that studying the equation through its singularities is a way of having potentially simple information from a complicated equation. Note that the equations mentioned in these two articles are on other variables than the Lagrangian displacement vector, so they do not end up with the same singularity $\omega_G^2$ as I exhibit here. We will come back to the importance of the choice of variable in section 9.3, but as we discussed in section 7.1.1 the Lagrangian displacement vector is a very fundamental variable, from which the others may be derived, so it is an improvement to work with it as in this manuscript.

Secondly, the steps 4 and 5 are in essence simple, since they are just a matter of bookkeeping. Relation (8.59) gives a hint of how convenient the intermediate step 4 is. Look at the expression of $A_0$ for instance. It is a linear combination of *all* the $B_i$'s, so if one tries to compute directly the wave equation on $\hat{\xi}_x$, the calculation is particularly difficult. In the Cowling approximation, step 4 to 5 occurred from equation (8.10) to (8.11), which did not make this variable seem necessary. Having said that, note that unfortunately, in the perspective of future works, this convenient variable is relevant here only because we are dealing with a simple situation, in which the background is static, without any magnetic field and rotation, etc. Indeed, $\rho_0\vec{\xi}$ does not appear as a natural variable anymore already in the more general force operator (7.29) because of the magnetic terms. Thus, obtaining equation (8.58) with coefficients (8.59) is in fact absolutely necessary, be it only for the sake of reference when later generalizing to non-static magnetized situations.

Thirdly, I will show in section 8.2.3 that by exploiting the equilibrium relations fully, we can fortunately rewrite the coefficients $B_i$ and $A_i$ in a much more handy way, which is why I do not develop further the expression of the $A_i$'s above. They will remain far more involved than in the Cowling approximation, but will fit in two lines.

### 8.2.2 A new singular frequency $\omega_G^2$

**A New Singular frequency $\omega_G^2$** The wave equation (8.58) presents a *singular frequency*, analogous to those found in the MHD wave equation (7.45). So far, despite my efforts, I have not found the mention of such a frequency in the literature. It is in that sense that I qualify it as 'new' here, and not because it would be a new continuum. Indeed, as mentioned in section 7.2, adding the Jeans term does not add any new wave because the Poisson equation is not an evolution equation (no gravitational waves!). Therefore this singularity can only correspond to one of the MHD singularities exposed in section 7.2, and since the magnetic field is put to zero here, there is no other choice than stating that

$$\omega_G^2 \textit{ is the generalization of the fast singularity } \omega_{f0}^2$$

which takes into account the fact that acoustic waves themselves modify the gravitational potential they propagate into, so that they propagate in a potential well different from the one of the equilibrium configuration. This statement is also consistent with the fact that $\omega_G^2$ is equal to $\omega_y^2$ (which is $\omega_{f0}^2$ in this context) plus terms that are due to gravity, since the derivatives in the $(\omega_y^2)''/k_y^2$ term are clearly stemming from the stratification, and the $4\pi G$ factor hidden in $\omega_0^2$ directly comes from Poisson's equation. Therefore in the limit of vanishing gravity, we recover the classical fast singularity.

**Nature of this singularity** Having said that, a striking fact appears: the fast singularity in the MHD wave equation has been demonstrated to be an *apparent* singularity, which was 'intuitive' because this singularity occurs in the *denominator* of the highest order term of the MHD wave equation. But the $\omega_G^2$ singularity on the contrary occurs at the *numerator* of the wave equation here! In that sense it *looks* genuine.

[5] "he ends up with a fourth order differential equation with very complicated coefficients"

However, as I pointed out in section 8.1.3, the form in which we write the wave equation matters. At the present, I can not tell the true nature of the singularity in equation (8.58) because it is not yet in the same form as the MHD wave equation.

Something very enlightening, that I am planning to do, would be actually to include a magnetic field. Indeed, one of the outcomes of MHD spectral theory studies is that, paradoxically, studying the HD spectrum is harder than studying its MHD generalization. In fact, the hydrodynamical case contains degeneracies which bring in confusions. When a magnetic field is included, the equations are lengthier, but the degeneracies are lifted, and the equations become easier to interpret. In the same spirit, I am convinced that adding a magnetic field here would help interpreting the spectrum in this 'Full Gravity' situation, by analysing how all the MHD singularities are modified and generalized.

**Information on stability** As one can see in the ordering (7.53), the singularities of the MHD wave equation are only *positive* frequencies. So far, since I have been essentially exploring the MHD literature in which those singularities are positive, I have seen very few references mentioning what happens in systems in which the singularities extend to the negative part of the spectrum. The rare authors who mention this possibility suggest that the analysis would then be more complicated (e.g. Lifschitz, 1989; Freidberg, 2014). The important point is that in many cases that I have explored, i.e. for relevant $\rho_0$ and $c_a^2$ profiles as those from chapter 6, part of the range of frequencies $\omega_G^2(x)$ belongs to the *negative* domain of the real axis. This is clearly the sign of instability, but in a sense that deserves to be spelled out. For instance, an extremely important piece of information provided by expression (8.55) is the singular point $x_s$ for which $\omega^2 = \omega_G^2(x_s)$, about which a local analysis must be performed.

### 8.2.3 The Three Important (inverse) Length Scales: $k_\rho$, $k_\mathrm{J}$ and $k_y$

The coefficients $B_i$ contain the quantities $(\rho_0, \rho_0', \rho_0'', \rho_0''')$ and $(c_a^2, (c_a^2)', (c_a^2)'', (c_a^2)''')$, and the $A_i$s too, with $A_0$ containing $\rho_0^{(iv)}$ in addition[6]. Therefore, as such, it seems that the system contains many different characteristic length scales of which, for instance, $L_1 \equiv \frac{\rho_0}{\rho_0'}$, $L_2 \equiv \sqrt{\frac{\rho_0}{\rho_0''}}$, etc., and similarly with $c_a$. This, however, is not correct. I am now going to show that the derivatives of $\rho_0$ and those of $c_a$ are not independent of each other. In fact, the system is fully described by exactly three length scales only: two characterize the stratification along $x$ of the equilibrium state ($k_\rho$ and $k_\mathrm{J}$ below), and one characterizes the perturbation along the transverse direction to the stratification (namely $k_y$).

**Equilibrium relations** In a plane stratified medium, the hydrodynamic equilibrium (6.1) and the equilibrium Poisson equation (6.2) may be rewritten respectively

$$\left\{ \begin{array}{l} g_0 = -c_a^2 k_\rho \\ g_0' = -\omega_0^2 \end{array} \right. \tag{8.60}$$

where I introduce the local gradient $k_\rho$ defined as

$$\boxed{k_\rho(x) \equiv -\frac{\rho_0'}{\rho_0}}. \tag{8.61}$$

(Local Gradient)

For convenience, I add a minus sign in this definition to ensure that $k_\rho > 0$ in physical situations, in which $\rho_0$ is a decreasing function of $x$. The other crucial length is given by the local Jeans wavenumber $k_\mathrm{J}$ defined as

$$\boxed{k_\mathrm{J}^2(x) \equiv \frac{\omega_0^2}{c_a^2}} \tag{8.62}$$

(Local Jeans Wavenumber)

These two length scales are the most natural in the context of gravitational fragmentation in stratified media: We are already familiar with the Jeans length (7.13) in the homogeneous case which is the fundamental length governing the transition between stability and instability, and the local gradient surely plays an important role since it is the length characterizing the steepness and thus the 'importance' of the stratification, whose effect we are precisely trying to assess.

Written in the form of system (8.60), the equilibrium is strikingly simple to handle. Plugging the first in the second directly gives

$$\frac{(c_a^2)'}{c_a^2} k_\rho + k_\rho' = k_\mathrm{J}^2. \tag{8.63}$$

[6]The dependence on $(c_a^2)'''$ is hidden in the factors $\Omega_G' = -k_y^2 (c_a^2)' + (c_a^2)''' + \omega_0 \frac{\rho_0'}{\rho_0}$ that I have left this way to make the expression (8.57) a little bit more compact.

In addition, given that for a polytrope $c_a^2 = \kappa\gamma\rho_0^{\gamma-1}$ (cf. equation (6.6)), we obtain $\frac{(c_a^2)'}{c_a^2} = (1-\gamma)k_\rho$. It is then easy to combine these relations to express the quantities present in the $B_i$ and $A_i$ coefficients in terms of $k_\rho$, $k_{\rm J}$ and $k_y$ only, as promised:

• Derivatives of $c_a^2$:

$$\left\{\begin{array}{lcl} c_a^2 & = & \kappa\gamma\rho_0^{\gamma-1} \\ \frac{(c_a^2)'}{c_a^2} & = & (1-\gamma)k_\rho \\ \frac{(c_a^2)''}{c_a^2} & = & (1-\gamma)k_{\rm J}^2 \\ \frac{(c_a^2)'''}{c_a^2} & = & (\gamma-1)k_\rho k_{\rm J}^2 \end{array}\right. \tag{8.64}$$

• Derivatives of $\rho_0$:

$$\left\{\begin{array}{lcl} \frac{\rho_0'}{\rho_0} & \equiv & -k_\rho \\ \frac{\rho_0''}{\rho_0} & = & (2-\gamma)k_\rho^2 - k_{\rm J}^2 \\ \frac{\rho_0'''}{\rho_0} & = & (2\gamma-3)(2-\gamma)k_\rho^3 + (7-3\gamma)k_\rho k_{\rm J}^2 \\ \frac{\rho_0^{(4)}}{\rho_0} & = & (3\gamma-4)(2\gamma-3)(2-\gamma)k_\rho^4 + (7-3\gamma)k_{\rm J}^4 \\ & & + (2-\gamma)(12\gamma-23)k_\rho^2 k_{\rm J}^2 \end{array}\right. \tag{8.65}$$

**Intuition may be deceiving** Here is a first very important consequence of this. As discussed in chapter 6, typical equilibrium profiles are flat in their center ($x \sim 0$). Therefore intuitively, it is reasonable to think that since the slab is locally homogeneous, perturbations behave as they would in a homogeneous Universe, satisfying the usual Jeans criterion for instance. However, look at relations (8.65). Doing the 'Jeans swindle' (cf. chapter 7) consists in setting the quantities on the left hand side to zero, but in fact, because $k_{\rm J}^2$ is finite as $x \to 0$, the right hand side of $\rho_0''/\rho_0$ and of $\rho_0^{(4)}\rho_0$ does not vanish in this limit! Therefore the equation governing the evolution of the perturbations is *not* the one deduced doing the 'Jeans swindle', even in this region where the profile is flat. Physically this is stemming from the fact that gravity is not local, and the lesson is that the whole profile may matter, even locally.

### 8.2.4 Rewriting the wave equation simply

We are now ready to rewrite (8.58) in a compact form, bringing its expression back to a 'humanly' tractable size.

**Isothermal fluid** For an isothermal equation of state, the frequency (8.55) reads

$$\omega_G^2 = \omega_y^2 - \omega_0^2 \tag{8.66}$$

and the coefficients of the wave equation become

$$\boxed{\left\{\begin{array}{l} A_4^{\rm IS} = c_a^2\ (\omega^2 - \omega_G^2) \\ A_3^{\rm IS} = -c_a^2 k_\rho(\omega^2 - \omega_y^2) \\ A_2^{\rm IS} = (\omega^2 - \omega_G^2)(\omega^2 - 2\omega_y^2 - 2\omega_0^2) - c_a^2 k_\rho^2 \omega_0^2 \\ A_1^{\rm IS} = k_\rho(\omega_y^2 + 2\omega_0^2)(\omega^2 - \omega_y^2) \\ A_0^{\rm IS} = -k_y^2\left[(\omega^2 - \omega_G^2)(\omega^2 - \omega_y^2) - c_a^2 k_\rho^2 \omega_0^2\right] \end{array}\right.} \tag{8.67}$$

(Wave Equation – Full Gravity, Isothermal)

The superscripts 'IS' here stand for 'Isothermal Self-gravitating'. Indeed, this is valid for a self-gravitating fluid only because we have used the equilibrium Poisson equation to derive it.

**Polytropic fluid** For a general polytropic equation of state, the frequency (8.55) reads

$$\omega_G^2 = \omega_y^2 - (2-\gamma)\omega_0^2 \tag{8.68}$$

and the coefficients of the wave equation become

$$\boxed{\left\{\begin{array}{lcl} A_4 & = & A_4^{\rm IS} + (1-\gamma)\ c_a^2\omega_0^2 \\ A_3 & = & A_3^{\rm IS} + (1-\gamma)\left[3\omega^2 - 2\omega_y^2 + 3(2-\gamma)\omega_0^2\right] c_a^2 k_\rho \\ A_2 & = & A_2^{\rm IS} + (1-\gamma)\left[\omega_0^2\left(4\omega^2 - 5\omega_y^2 + (4-3\gamma)\omega_0^2\right)\right. \\ & & \left. + c_a^2 k_\rho^2\left((1-2\gamma)\omega_y^2 + (3-2\gamma)\omega_0^2\right)\right] \\ A_1 & = & A_1^{\rm IS} - (1-\gamma)\left[3\omega^2 - 2\omega_y^2 + (8-3\gamma)\omega_0^2\right]\omega_y^2 k_\rho \\ A_0 & = & A_0^{\rm IS} - (1-\gamma)\left[\omega_0^2\left(4\omega^2 - 4\omega_y^2 + 3(2-\gamma)\omega_0^2\right)\right. \\ & & \left. + c_a^2 k_\rho^2\left((1-2\gamma)\omega_y^2 + (3-2\gamma)\omega_0^2\right)\right] k_y^2 \end{array}\right.} \tag{8.69}$$

I chose to express these $A_i$ coefficients in the above form, namely as 'the isothermal self-gravitating coefficients plus additional terms', having in mind the following idea. The isothermal self-gravitating case is the simplest. In the Cowling approximation, the wave equation may be solved exactly as we have seen in the previous section. In addition, as we will see next, we can find solutions of the full wave equation pertubatively starting from the solution in the Cowling approximation. In the full polytropic case however, even the density profile cannot be expressed analytically, and $k_\rho$ is linked to $k_\mathrm{J}$ in the non trivial way (8.63). Therefore, there is little hope of having as many possibilities of finding analytical solutions of (8.69) in the general case. However, as usually, it is extremely enlightening to solve equations considering various regimes. In the present case, I think that a promising way to study the effect of the temperature stratification (because after all, the isothermal case $\gamma = 1$ is pretty limited physically speaking) is to solve the wave equation is the nearly isothermal limit, i.e. for $\gamma \simeq 1$. Formally, the idea is to study (8.69) manipulating $1-\gamma$ as a small parameter and solve it using perturbative methods about the isothermal solution.

**With an external background** So far, the fluid has been considered as self-gravitating. But in many astrophysical and cosmological situations, fluids are not isolated. Let us therefore now briefly explore the case in which the fluid is embedded in an other fluid of density $\rho_\mathrm{ext}$. The hydrostatic equilibrium (6.1) retains its form, namely $-\vec{\nabla}p_0 + \rho_0\vec{g}_0 = \vec{0}$, but now the equilibrium gravitational field is that due to the *total* matter density, so that it is governed by the following Poisson equation

$$\vec{\nabla}\cdot\vec{g}_0 = -\left(\omega_0^2 + \omega_\mathrm{ext}^2\right), \tag{8.70}$$

where $\omega_\mathrm{ext}^2 \equiv 4\pi G\rho_\mathrm{ext}$, rather than (6.2). Therefore, the equilibrium state is modified, and thus the equilibrium relations (8.64) and (8.65) intervening in the evolution of perturbations are modified too. It is straightforward to show, in the lines of what we have done above, that in this case the following new terms appear:

• Derivatives of $c_a^2$:

$$\left\{\begin{array}{lcl} c_a^2 & : & 0 \\ \frac{(c_a^2)'}{c_a^2} & : & 0 \\ \frac{(c_a^2)''}{c_a^2} & : & (1-\gamma)k_{J\mathrm{ext}}^2 \\ \frac{(c_a^2)'''}{c_a^2} & : & (\gamma-1)k_{\rho\mathrm{ext}}k_{J\mathrm{ext}}^2 \end{array}\right. \tag{8.71}$$

• Derivatives of $\rho_0$:

$$\left\{\begin{array}{lcl} \frac{\rho_0'}{\rho_0} & : & 0 \\ \frac{\rho_0''}{\rho_0} & : & -k_{J\mathrm{ext}}^2 \\ \frac{\rho_0'''}{\rho_0} & : & \left[3(2-\gamma)k_\rho + k_{\rho\mathrm{ext}}\right]k_{J\mathrm{ext}}^2 \\ \frac{\rho_0^{(4)}}{\rho_0} & : & \Big[6(2\gamma-3)(2-\gamma)k_\rho^2 + (13-6\gamma)k_\mathrm{J}^2 \\ & & \quad + 3(2-\gamma)k_{J\mathrm{ext}}^2 + 4(\gamma-2)k_{\rho\mathrm{ext}}k_\rho - \frac{\rho_\mathrm{ext}''}{\rho_\mathrm{ext}}\Big]k_{J\mathrm{ext}}^2 \end{array}\right. \tag{8.72}$$

with $k_{J\mathrm{ext}}^2 \equiv \omega_\mathrm{ext}^2/c_a^2$.

Now, in principle, when linearizing the equations, both fluids (of density $\rho_0$ and $\rho_\mathrm{ext}$) are perturbed and are coupled through the linearized Poisson equation $\vec{\nabla}\cdot\vec{g}_1 = -4\pi G\left(\rho_1 + \rho_{1\mathrm{ext}}\right)$. However, it is out of the scope of this manuscript to consider this bi-fluid approach. It may though be very interesting and important, but it is left for future work. For now, I will neglect the perturbations of the background fluid[7] by considering that $\rho_{1\mathrm{ext}} \ll \rho_1$. This assumption decouples the evolution of the perturbations of both fluids, so that the perturbation equations are identical to the self-gravitating ones, and the only changes with respect to the previous derivation concern the equilibrium relations, given by (8.71) and (8.72).

Let us look at the modifications in the isothermal case. This gives

$$\omega_G^2 = \omega_y^2 - \omega_0^2 \tag{8.73}$$

[7]It is tempting to think that the case considered here is physically motivated by the fact that in most cosmological environments dark matter dominates the density budget and the gravitational potential in which baryons evolve. But there is no reason a priori that if $\rho_0 \ll \rho_{0\mathrm{ext}}$, then $\rho_{1\mathrm{ext}} \ll \rho_1$. So my feeling about this model is that it is an interesting case in which, *for some reason*, the background fluid is stiff. Note also that in reality, in the cosmic web, the dark matter density distribution contains non linear substructures (e.g. Schneider et al., 2010) into which cold baryonic gas may fall. I do not include those in my analysis precisely because my aim is to investigate whether the gas may fragment gravitationally on its own.

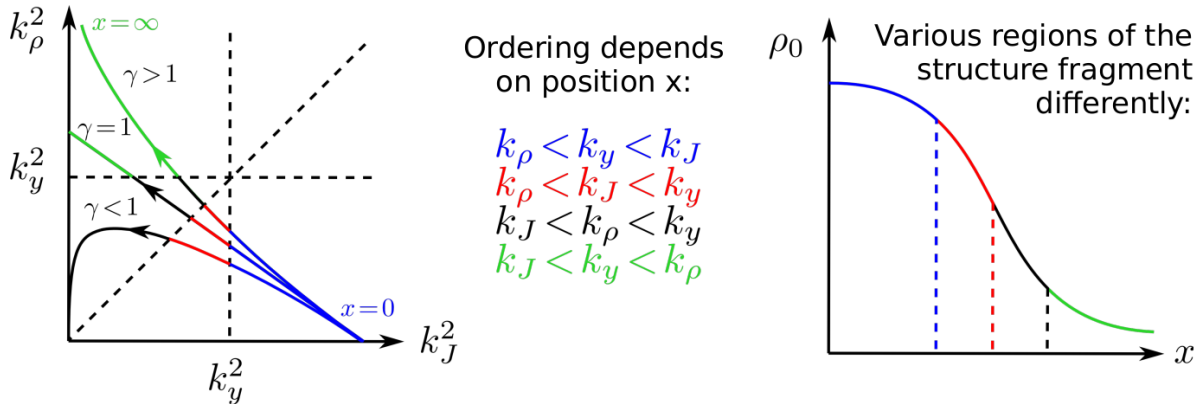


Figure 8.3: The ordering of the three length scales depends on the position $x$ in the slab. Left: Sketch of typical equilibrium density profiles for $\gamma > 1, = 1$ and $< 1$ in the parameter space $(k_\mathrm{J}^2, k_\rho^2)$. Curves are parametrized by position $x$, increasing from right to left. Middle: Color coding for the various orderings. Right: Sketch of a typical equilibrium density profile. As we see from the left and middle panels, depending on the wavenumber $k_y$ of the perturbation along $y$, we expect perturbations to behave differently in various regions in the slab along $x$.

and

$$\boxed{\begin{cases} A_4 = A_4^{\mathrm{IS}} \\ A_3 = A_3^{\mathrm{IS}} \\ A_2 = A_2^{\mathrm{IS}} - 3\left(\omega^2 - \omega_G^2\right)\omega_{\mathrm{ext}}^2 \\ A_1 = A_1^{\mathrm{IS}} + \left(3(\omega^2 - \omega_G^2)k_{\rho\mathrm{ext}} - 2\omega_0^2 k_\rho\right)\omega_{\mathrm{ext}}^2 \\ A_0 = A_0^{\mathrm{IS}} + \left((\omega^2 - \omega_G^2)(k_y^2 - \frac{\rho_{\mathrm{ext}}''}{\rho_{\mathrm{ext}}}) + k_{\rho\mathrm{ext}}\omega_0^2 k_\rho\right)\omega_{\mathrm{ext}}^2 \end{cases}} \tag{8.74}$$

(Wave Equation – Full Gravity, Isothermal, With External Background)

where $k_{\rho\mathrm{ext}} = -\frac{\rho_{\mathrm{ext}}'}{\rho_{\mathrm{ext}}}$. We can see that the coefficients $A_3$ and $A_4$ are not modified compared to the isothermal case and thus neither is $\omega_G^2$. This stems from the fact that the potential is assumed to stay fixed, and thus does not intervene in the linearized Poisson equation (7.5), which is what makes the equation of fourth order, and only modifies the equilibrium profile.

Equations (8.67), (8.69) or (8.74) are the starting point to build physical models of perturbed walls and filaments, with the equilibrium profiles detailed in chapter 6. These are left for future work, but obviously a lot of interesting physics is in sight.

### 8.2.5 Ordering of the length scales in the slab

Now, in addition, the lengths $k_\rho$ and $k_\mathrm{J}$ are not independent. Indeed, with relation (8.63), one can show that

$$\frac{dk_\rho^2}{dx} = 2k_\rho k_\rho' = 2k_\rho((\gamma-1)k_\rho^2 + k_\mathrm{J}^2) \tag{8.75}$$

and

$$\frac{dk_\mathrm{J}^2}{dx} = (\gamma-2)k_\rho k_\mathrm{J}^2, \tag{8.76}$$

so that, considering $k_\rho^2$ as a function of $k_\mathrm{J}^2$ rather than of $x$, the ratio of these two relations gives

$$\frac{dk_\rho^2}{dk_\mathrm{J}^2} = 2\frac{\gamma-1}{\gamma-2}\frac{k_\rho^2}{k_\mathrm{J}^2} + \frac{2}{\gamma-2} \tag{8.77}$$

which is a first order linear differential equation of the form

$$y' = \alpha\frac{y}{x} + \beta \tag{8.78}$$

for a function $y(x)$. I solve it imposing as the boundary condition that the density profile is flat at $x = 0$, so that $k_\rho^2(k_{\mathrm{J}0}^2) = 0$ where $k_{\mathrm{J}0}^2 \equiv k_\mathrm{J}^2(x=0)$. This results in

$$\boxed{k_\rho^2 = \frac{2}{\gamma}k_\mathrm{J}^2\left[\left(\frac{k_\mathrm{J}^2}{k_{\mathrm{J}0}^2}\right)^{\gamma/(\gamma-2)} - 1\right]} \tag{8.79}$$

(Link between $k_\rho$ and $k_\mathrm{J}$)

Thanks to this relation, we can study exactly, i.e. depending on the position $x$ in the slab, the ordering of the three length scales $k\rho$, $k_\mathrm{J}$ and $k_y$ appearing in the wave equations (8.67), (8.69) and (8.74). This is paramount because in different regions of the slab where they are differently ordered, in principle the coefficients $A_i$ will change qualitatively, and so will the evolution of the perturbations. Now, representing these orderings in the three dimensional space $(k_\rho^2, k_\mathrm{J}^2, k_y^2)$ would be rather complicated. Instead, I propose a more efficient way of visualizing this, by considering a projection on the $(k_\rho^2, k_\mathrm{J}^2)$ plane for a given $k_y^2$. This plane is then composed of six different regions, delimited by the dashed lines in the left of figure 8.3, corresponding to the six possible orderings of these three lengths, so that no information is lost.

The left of figure 8.3 is a schematic plot of relation (8.79). Curves are parametrized by position $x$, with $x$ increasing from right to left. On the right of that same figure, I schematically represent a typical density profile, with colors indicating regions in the slab with different orderings of the three characteristic lengths. It is interesting to notice for example that at the outskirt of the slab ($x \to \infty$) there is a qualitative change of the behaviour of perturbations for $\gamma > 1$ and $\gamma < 1$. But one has to keep in mind that for equilibria with $\gamma > 1$, physics requires us to truncate such profiles, cf. chapter 6. Therefore the curve corresponding to $\gamma > 1$ is in practice truncated at some position $x_t$.

### 8.2.6 Local analysis: Generalizing WKB dispersion relations

The outcome of our analysis of the ordering of the three length scales $k_\rho, k_\mathrm{J}$ and $k_y$ is that the evolution of perturbations may be qualitatively different in various regions of the slab. This prompts us to study the local behaviour of perturbations in the slab, in the same lines as we did in section 8.1.4. However, despite all my efforts, I did not find in the literature a proper generalization of this method to fourth order equations. Therefore, I propose the following derivation to do so. It is not highly rigorous in the sense that the orderings used to neglect terms might not be satisfied in some cases, but given the complexity that a fourth order equation represents and in particular a non trivial one as the above wave equation, this study is an important exploratory phase. I would rather see the dispersion relations below as educated guesses which may later be compared with numerical resolutions. In fact, this is the spirit of Blokland et al. (2005) for instance, dealing with second order equations, who study a posteriori the validity of their WKB dispersion relation by comparing it to a numerical solution. They find that their prediction is in excellent agreement, even in a region where the approximation should a priori be failing. Actually, the fact that WKB approximations tend to be surprisingly good even well beyond their strict domain of validity is a general feature (Holmes, 2013).

Plugging the same WKB form (8.35) for $\hat{\xi}_x$ in the wave equation (8.58) and identifying real and imaginary parts gives the equivalent of the system of two equations (8.38) of the second order case. Now this system is much more involved and contains up to fourth order derivatives, but with the correspondence $\frac{d}{dx} \leftrightarrow \frac{1}{L}$ we will consider them as negligible for large $L$, and conserve only terms of order zero and one. We are then left with

$$\begin{cases} A_4 q^4 - 3A_3 \left(\frac{p'}{p} + \frac{q'}{q}\right) q^2 - A_2 q^2 + A_1 \frac{p'}{p} + A_0 = 0 \\ -2A_4 q^2 \left(2\frac{p'}{p} + 3\frac{q'}{q}\right) - A_3 q^2 + A_2 \left(2\frac{p'}{p} + \frac{q'}{q}\right) + A_1 = 0. \end{cases} \tag{8.80}$$

For $A_4 = A_3 = 0$ and $A_2 = 1$ we recover (8.38), without its second order term, as we should. Now, recall that the $A_i$s depend on $x$. Thus, in these two equations, depending on the region in the slab, some terms are much smaller or much bigger than others. More precisely, a general feature of the wave equation (8.58) is that coefficients with odd indices ($A_3$ and $A_1$) contain only odd powers of $k_\rho$, while coefficients with even indices ($A_4$, $A_2$ and $A_0$) contain only even powers of $k_\rho$, and thus in particular terms independent of $k_\rho$. Therefore, depending on $k_\rho$ the ordering between the terms in (8.80) varies. We will distinguish two regimes, namely a 'flat regime' corresponding to regions where $k_\rho$ is extremely small, and a 'steep regime' where it is not.

**(i) The 'flat regime'** It corresponds to regions of the slab in which $k_\rho$ is small, i.e. the density profile is locally flat, typically at its center ($x \ll L$) and outskirts ($x \gg L$). In this case we may treat coefficients $A_1$ and $A_3$ as first order terms since they are proportional to $k_\rho$. After getting rid of second order terms, the first equation of (8.80) becomes $A_4 q^4 - A_2 q^2 + A_0 = 0$. We then interpret $q$ as the local 'wavenumber' in the $x$ direction, so that we will hereafter use the notation $k_x$ instead of $q$, and call this constraint the *'flat dispersion relation'*:

$$\boxed{A_4 k_x^4 - A_2 k_x^2 + A_0 = 0.} \tag{8.81}$$

('Flat' Local Dispersion Relation)

Note that the second equation in (8.80) constrains the function $p$ but we do not need this information in this regime. Let us now look at this relation in the three situations of which we derived the wave equations in section 8.2.4.

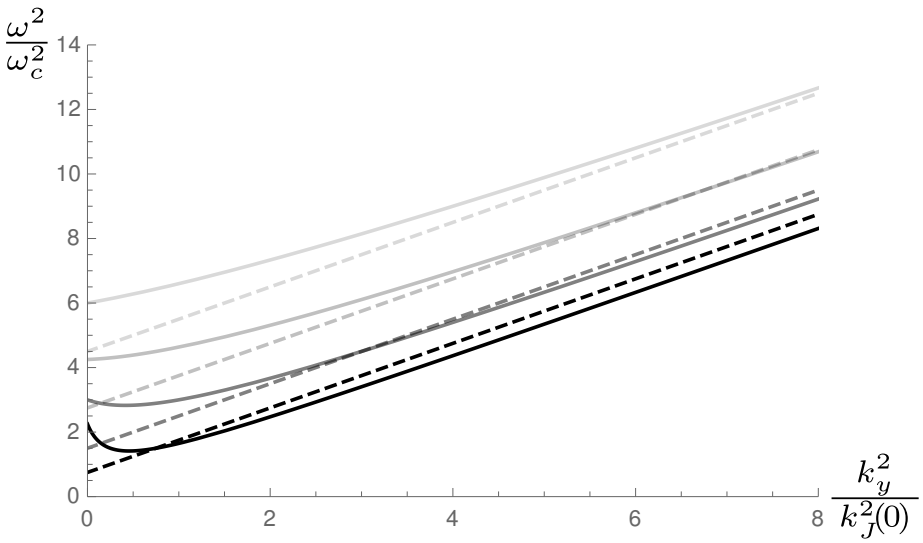


Figure 8.4: Diagnostic diagram, i.e. $\omega^2$ as a function of $k_y^2$, in the central region of an isothermal self-gravitating slab. The angular frequencies $\omega^2$ are normalized by $\omega_c^2 = \omega_0^2(x = 0)$ and $k_y$ is normalized using the central Jeans wavenumber $k_J(0)$. In dashed lines I show the spectrum in the Cowling approximation given by expression (8.32). In continuous lines is the spectrum using the 'flat' WKB dispersion relation (8.82), where the $x$-wavenumber is quantized as $k_x = \frac{n\pi}{x_t}$ to enable a comparison. The first four modes $n = 1, 2, 3, 4$ are shown here (the lighter the color, the higher the mode), and the thickness of the slab $x_t$ is chosen such that $k_J(0)x_t = 2\pi$ simply to make this plot more readable. The shift between these two sets of curves is due to the Jeans term: We see that for high $k_y$ the Jeans term has a destabilizing effect, while it stabilizes for low $k_y$.

**a) Isothermal** The wave equation of an isothermal self-gravitating slab is (8.67), and in such a profile, $k_\rho \to 0$ as $x \to 0$. Therefore, in the central region of the slab, the relevant local dispersion relation is (8.81) and it gives

$$\omega^2 = c_a^2(k_x^2 + k_y^2) + \frac{2k_x^2}{k_x^2 + k_y^2}\omega_c^2 \tag{8.82}$$

where $\omega_c^2 = \omega_0^2(x = 0)$. The continuous lines in figure 8.4 represent these solutions, with units of length given by the Jeans wavenumber at the center $k_J(0)$, i.e. by $L$ (up to a $\sqrt{2}$ factor, cf. definition (8.25)). These solutions are compared to the exact spectrum (8.32) we obtained in the Cowling approximation in order to visualize the effect of the Jeans term on the spectrum. Because the latter is discrete, in the same lines as in section 8.1.4, we quantize the modes from relation (8.82) in figure 8.4 to perform the comparison. By construction, we expect this dispersion relation to be valid for $k_x$ larger than $1/L$ since we have been working under the assumption $qL \gg 1$. In the plot (8.4) we should therefore in principle[8] be cautious with the black curve which corresponds to low $k_x$, but the others are directly reliable. There is no restriction on $k_y$ however, so we may trust the plot (8.4) on the full range $k_y$, for large enough $k_x$. We see in these plots that as $k_y$ goes to infinity, the correction due to Jeans vanishes. We recover the idea anticipated in section 7.3.2 that the Cowling approximation in good for high order modes. It is also interesting to observe that for small $k_y$ the predicted eigenvalues are higher than in the Cowling approximation. The Jeans term thus tends to take $\omega^2$ away from the negative values, and in that sense has a stabilizing effect. This comes as a surprise based on the intuition from the usual Jeans criterion in homogeneous media that the long wavelengths are the unstable ones.

**b) Polytropic** From equation (8.69), the flat local dispersion relation at the center reads

$$\omega^2 = c_a^2(k_x^2 + k_y^2) + \frac{2k_x^2}{k_x^2 + k_y^2}\omega_c^2 + 3(\gamma - 1)\omega_c^2. \tag{8.83}$$

The fact that there is a qualitative change of behaviour in the evolution of the perturbations for $\gamma$ greater or smaller than 1 was already anticipated in chapter 6, where we noted that the gradient of the speed of sound

[8] As stated above, WKB approximations are often very good approximations even beyond their strict domain of validity, so that the precautions taken here may turn out to be unnecessary. Comparison with a numerical resolution (e.g. with a shooting method Goedbloed & Poedts, 2004) will give this answer.

changes sign at $\gamma = 1$. More precisely, it is instructive to rewrite the force operator (7.57), using (7.4), as

$$\vec{F}(\vec{\xi}) = -c_a^2 \vec{\nabla}\rho_1 + \rho_1 \vec{g}_0^{\text{eff}} + \rho_0 \vec{g}_1 \tag{8.84}$$

where the spatial dependence of the speed of sound acts locally as an effective gravitational field:

$$\vec{g}_0^{\text{eff}} \equiv \vec{g}_0 - \vec{\nabla} c_a^2 = [g_0 + (\gamma - 1) k_\rho c_a^2]\ \hat{x}. \tag{8.85}$$

The second equality stems from the equilibrium relations (the second relation in (8.64)). Recalling that $g_0 < 0$ and $k_\rho > 0$, we can see that when $\gamma < 1$, the absolute value of this effective local gravitational field is greater than $|g_0|$. Intuitively we may say that this favors the mixing of adjacent layers of the stratified fluid, as discussed in chapter 7, and thus the term $3(\gamma - 1)\omega_c^2$, which does not appear in the isothermal case, may be interpreted as the signature of a Rayleigh-Taylor instability.

**c) External Background** Considering a profile flat at the center, which is not necessarily the case when an external background exists (cf. chapter 6), we have

$$\omega^2 = c_a^2(k_x^2 + k_y^2) + \frac{2k_x^2}{k_x^2 + k_y^2}\omega_c^2 + \frac{(3k_x^2 + k_y^2)\omega_{\text{c,ext}}^2 - (\omega_{\text{c,ext}}^2)''}{k_x^2 + k_y^2} \tag{8.86}$$

where $\omega_{\text{c,ext}}^2$ and $(\omega_{\text{c,ext}}^2)''$ are the values of $\omega_{\text{ext}}^2$ and $(\omega_{\text{ext}}^2)''$ at $x = 0$. The minus sign seems to indicate a destabilizing effect. However, consider the Taylor expansion of the density profile about $x = 0$. Since the profile is decreasing with $x$, and it is flat at the center (for this relation to be valid), the linear term in the expansion is null, and the second term, given by the second derivative, has to be negative in order for $\rho(x)$ to indeed be smaller than its value at $x = 0$. Hence in fact relation (8.86) states that such profiles have only a stabilizing effect.

**(ii) The 'steep regime'** It corresponds on the contrary to regions in which $k_\rho$ is large, typically in regions $x \sim L$. Then in this regime, in the first equation of (8.80), we still expect the terms $-3A_3\left(\frac{p'}{p} + \frac{q'}{q}\right)q^2$ and $A_1\frac{p'}{p}$ to be small compared to the others because we are in the limit of small $(qL)^{-1}$. But now, in the second equation, the terms $-A_3q^2$ and $A_1$ will be the dominant ones. Hence, at their leading order, the equations of the system (8.80) become in this regime

$$\begin{cases} A_4q^4 - A_2q^2 + A_0 = 0 \\ -A_3q^2 + A_1 = 0 \end{cases} \tag{8.87}$$

and thus the first equation is not decoupled from the second anymore. Also, in this regime $A_3 \neq 0$ so that we may combine these two equations to get what we may call the *'steep dispersion relations'*

$$\boxed{A_4A_1^2 - A_3A_2A_1 + A_3^2A_0 = 0} \tag{8.88}$$

and

$$\boxed{-A_3q^2 + A_1 = 0}. \tag{8.89}$$

('Steep' Local Dispersion Relations)

Note that these are indeed dispersion relations, even the first one which does not contain $q$, because the $A_i$s contain $\omega^2$ and $k_y^2$. Unfortunately, at this stage I do not have time to pursue their analysis, but they look particularly interesting because they show signs of instability. If fragmentation occurs in these regions far from the center, blobs forming there will fall into the background gravitational potential and angular momentum may be induced if various blobs merge at the center with different impact parameters.

## 8.3 Matrix formulation

So far, we have reformulated the vector eigenvalue problem into a one-dimensional wave equation, constituting another point of view that brought us important information. The good news is that we may reformulate the problem in a third way, namely in matrix form, which will reveal yet more information. The wave equation is of fourth order and has very large coefficients. As we will see, reformulated in matrix form, the problem will be lighter, and will enable us to naturally find explicit solutions in a perturbative approach. Finally, a matrix form is most adapted for numerical resolutions, and also from the analytical point of view, many tools from linear algebra may be used, for example discussions on the eigenvalues of the governing matrix. Unfortunately, such discussions are beyond the scope of this manuscript, but from the experience of other fields of physics, it is clear that such a formulation is potentially a mine of information from which very simple and powerful results can be derived.

### 8.3.1 Matrix formulation

In order to lighten the derivation and focus on the ideas I want to develop, I will present this section in the isothermal case only. Therefore the frequency $\omega_y^2$ is a constant here, and one can have the simple exponential atmosphere and the self-gravitating slab profiles in mind when $\rho_0$ coefficients appear.

**Tracking the Cowling and Jeans terms** As we have seen in the previous section, when deriving the wave equation the calculations were long. We saw also that the Cowling and Jeans terms have important similarities, due to the fact that the equilibrium and linearized Poisson equations are formally identical. Therefore, when combining the Poisson and the momentum conservation equations, after a few manipulations it becomes difficult to distinguish coefficients stemming from the Cowling or the Jeans term, while it would be useful for the interpretations. To keep track of the origin of the numerous terms that appear, I decided to place artificially two factors, $\epsilon_{\rm C}$ and $\epsilon_{\rm J}$ in the force operator according to

$$\vec{F}\left(\vec{\xi}\right) = -\vec{\nabla}p_1 + \epsilon_{\rm C}\rho_1\vec{g}_0 + \epsilon_{\rm J}\rho_0\vec{g}_1. \tag{8.90}$$

The Cowling approximation then corresponds to $(\epsilon_{\rm C}, \epsilon_{\rm J}) = (1, 0)$ while the Jeans approximation is $(\epsilon_{\rm C}, \epsilon_{\rm J}) = (0, 1)$. Now, while this is an interesting idea per se, in practice it is far less obvious to perform than it seems, because the coefficient $\epsilon_{\rm C}$ prevents some simplifications to occur when using the hydrostatic equilibrium... The outcome is that tracking the Cowling term (and thus switching on and off the Jeans approximation at any time) is far too costy. I will therefore put $\epsilon_{\rm C} = 1$. Keeping track of the Jeans term with the coefficient $\epsilon_{\rm J}$ however, does not induce any additional difficulty, and as we will see, it will turn out to be sufficient for our purpose here.

**Governing matrix equation** Let us rewrite the two main equations which lead us to the wave equation in the previous section, namely the momentum conservation (8.52) and Poisson equation (8.54):

$$\left\{\begin{array}{l} \epsilon_{\rm J}\frac{\rho_0}{c_a^2}\hat{g}_{1x} + \psi'' + k_\rho\psi' + \frac{\omega^2-\omega_y^2}{c_a^2}\psi = 0 \\ \hat{g}_{1x}'' + \frac{\epsilon_{\rm J}\omega_0^2}{\omega^2-\omega_y^2+\epsilon_{\rm J}\omega_0^2}k_\rho\hat{g}_{1x}' - k_y^2\frac{\omega^2-\omega_y^2+\epsilon_{\rm J}\omega_0^2}{\omega^2-\omega_y^2}\hat{g}_{1x} - \frac{4\pi G\omega^2}{\omega^2-\omega_y^2}\psi'' - \frac{4\pi G\omega^2}{\omega^2-\omega_y^2}\frac{\epsilon_{\rm J}\omega_0^2}{\omega^2-\omega_y^2+\epsilon_{\rm J}\omega_0^2}k_\rho\psi' = 0, \end{array}\right. \tag{8.91}$$

where I have used in addition the hydrostatic equilibrium in the form $g_0 = -c_a^2 k_\rho$, cf. relations (8.60). Any ordinary differential equation of order $n$ can be rewritten as a system of $n$ first order equations. For example consider $y'' + ay' + by = 0$. As is well known, the trick is to put $y_1 \equiv y$ and $y_2 \equiv y'$, and rewrite this equation as

$$\begin{pmatrix} 1 & 0 \\ 0 & 1 \end{pmatrix} U' + \begin{pmatrix} 0 & -1 \\ b & a \end{pmatrix} U = 0 \text{ where } U = \begin{pmatrix} y_1 \\ y_2 \end{pmatrix}, \tag{8.92}$$

the first line being the definition of $y_2$ and the second line is really the differential equation. Here we have two second order differential equations that we transform in such a way, and thus transform the system into a single $(4 \times 4)$ matrix first order differential equation. Using the vector

$$\boxed{V \equiv \begin{pmatrix} \psi \\ \psi' \\ \hat{g}_{1x} \\ \hat{g}_{1x}' \end{pmatrix},} \tag{8.93}$$

we now rewrite (8.91) matricially as

$$\begin{pmatrix} 1 & 0 & 0 & 0 \\ 0 & 1 & 0 & 0 \\ 0 & 0 & 1 & 0 \\ 0 & -\frac{4\pi G\omega^2}{\Omega_y} & 0 & 1 \end{pmatrix} V' + \begin{pmatrix} 0 & -1 & 0 & 0 \\ \frac{\Omega_y}{c_a^2} & k_\rho & \epsilon_{\rm J}\frac{\rho_0}{c_a^2} & 0 \\ 0 & 0 & 0 & -1 \\ 0 & -\frac{4\pi G\omega^2}{\Omega_y}\frac{\omega_0^2 k_\rho}{\Omega_{G\epsilon}}\epsilon_{\rm J} & -k_y^2\frac{\Omega_{G\epsilon}}{\Omega_y} & \frac{\omega_0^2 k_\rho}{\Omega_{G\epsilon}}\epsilon_{\rm J} \end{pmatrix} V = 0. \tag{8.94}$$

The matrix on the left is very easy to invert: one just needs to change the sign in the only non diagonal term. Multiplying on the left by this inverse matrix, we have

$$\boxed{\begin{array}{c} \dfrac{dV}{dx} = A(x)V \\ \\ \text{where} \\ \\ A(x) = \begin{pmatrix} 0 & 1 & 0 & 0 \\ -\frac{\omega^2-\omega_y^2}{c_a^2} & -k_\rho & -\epsilon_{\rm J}\frac{\rho_0}{c_a^2} & 0 \\ 0 & 0 & 0 & 1 \\ -\frac{4\pi G\omega^2}{c_a^2} & -\frac{4\pi G\omega^2}{\omega^2-\omega_y^2+\epsilon_{\rm J}\omega_0^2}k_\rho & k_y^2-\epsilon_{\rm J}k_{\rm J}^2 & -\frac{\epsilon_{\rm J}\omega_0^2}{\omega^2-\omega_y^2+\epsilon_{\rm J}\omega_0^2}k_\rho \end{pmatrix}. \end{array}} \tag{8.95}$$

The matrix $A$ contains one singularity, because of the possibly vanishing denominators. Once $\epsilon_J$ is set back equal to one, as it should, it corresponds to the frequency $\omega^2 = \omega_G^2$ given by (8.55), as it appears in the denominators. This is how the singular frequency of the wave equation appears in this matricial approach.

Now, the important point to notice is that to derive (8.95) we *only* used the hydrostatic equilibrium, and *not* the Poisson equation of the equilibrium state. Therefore this equation is valid for *any* isothermal atmosphere, be it the exponential atmosphere, the self-gravitating slab, or a slab embedded in an external non-uniform background.

### 8.3.2 Solutions

We can now take advantage of the literature dealing with matrix differential equations, from the mathematics community naturally, for example Tracy (2016), but also from many other fields of physics, for example formally this potentially vanishing denominator is like propagators in Quantum Field Theory. We know that in the most general case, in which the coefficients of $A(x)$ depend on $x$, there is no easy general rule to solve the problem. However, in the simplest case in which the matrix $A$ has *constant coefficients*, the problem can be solved making use of the matrix exponential $\exp xA$, as we shall see in the next section. There are several ways of analysing the solutions of (8.95) using for example Dyson series or Magnus expansions. One way of expliciting formally the solution is (Aslangul, 2011)

$$V(x) = \left[\mathbb{1} + \int_0^x dx_1 A(x_1) + \int_0^x dx_1 \int_0^{x_1} dx_2 A(x_1)A(x_2) + \dots\right] V(0) \tag{8.96}$$

where the $n^{\text{th}}$ term is $n$ integrals of the product of $n$ matrices $A$ evaluated at different positions. To use this formula, one should better change the basis and work with the following vector $V$ instead of (8.93)

$$\begin{pmatrix} \psi \\ \hat{g}_{1x} \\ \psi' \\ \hat{g}'_{1x} \end{pmatrix} \tag{8.97}$$

because in this case the matrix $A$ has the form

$$\begin{pmatrix} 0 & 1 \\ B & C \end{pmatrix} \tag{8.98}$$

where the two upper blocks are simply 0 and the identity matrices, while $B$ and $C$ are not trivial. The point is that this block shape eases greatly the calculation of products of $A$, which is the essential complication of formula (8.96). But in fact, the problem with this expansion is that there is no reason a priori for the terms to be ordered, so that truncating even at a high order does not guarantee that the approximation is good.

Instead, I propose to proceed as follows. Define the parameter[9]

$$r_0(x) \equiv \epsilon_J \frac{\omega_0^2(x)}{\omega^2 - \omega_y^2}, \tag{8.99}$$

so that matrix $A$ may be expressed as

$$A = \begin{pmatrix} 0 & 1 & 0 & 0 \\ -\frac{\omega^2-\omega_y^2}{c_a^2} & -k_\rho & -\frac{\omega^2-\omega_y^2}{4\pi G c_a^2} r_0 & 0 \\ 0 & 0 & 0 & 1 \\ -\frac{4\pi G\omega^2}{c_a^2} & -\frac{4\pi G\omega^2}{\omega^2-\omega_y^2}\frac{k_\rho}{1+r_0} & \frac{\omega_y^2-(\omega^2-\omega_y^2)r_0}{c_a^2} & -\frac{r_0}{1+r_0}k_\rho \end{pmatrix}. \tag{8.100}$$

Now, consider the full case where $\epsilon_J = 1$. The interesting thing with this formulation is that whenever $r_0$ becomes extremely small, this is formally as if $\epsilon_J = 0$, i.e. this corresponds to situations in which the dynamics is governed by the Cowling approximation, and as we have seen in section 8.1, we can solve the problem in this case. Therefore, in order to find explicit solutions beyond the Cowling approximation, we are going to perform a perturbative expansion in the small parameter $r_0$, which is indeed small when the density is small.

Here is another way of stating this. The singular frequency $\omega_G^2$, exhibited in section 8.2.2, is equal to $\omega^2 - \omega_y^2 + \epsilon_J\omega_0^2$ because we are considering an isothermal fluid. The $\omega^2 - \omega_y^2$ term corresponds to the usual sound waves, i.e. those computed without taking into account the effect of the perturbation itself on the background, while the $\epsilon_J\omega_0^2$ term is the correction to this neglect (the $\epsilon_J$ parameter shows that it directly

[9] As in the sections about the wave equation, we are working with $\omega^2 \neq \omega_y^2$ and discussing singularities later.

comes from the Jeans term). Thus, the parameter $r_0$ is simply the measure of the relative importance of the contribution of the Jeans term. When we are here going to perform an expansion in $r_0$, it means that we are going to study the correction induced by perturbations on the background but for a wealky dense medium.

Finally, the importance of working with the vector (8.93), instead of (8.97) for instance, is that as we will see, what will matter in this approach is the matrix exponential of $A$ which has a simple form with this vector while it does not with the other.

### 8.3.3 Revisiting and completing the analysis of the exponential atmosphere

Solving equation (8.95) perturbatively about the solution from the Cowling approximation is possible both in the exponential atmosphere and the self-gravitating slab models that we have solved in section 8.1. However I will only focus on the exponential atmosphere here, because it lightens the calculations while presenting all the aspects of the method.

#### a) General expression

In the exponential atmosphere case

$$r_0 = r_c e^{-\frac{x}{L_0}} \tag{8.101}$$

where $r_c$ is the dimensionless and $x$-independent parameter

$$r_c \equiv \epsilon_{\mathrm{J}} \frac{\omega_c^2}{\omega^2 - \omega_y^2}. \tag{8.102}$$

Because the density profile $\rho_0(x)$ is decreasing, $|r_0(x)| \leq |r_c|$ for all $x$. Therefore, for a given choice of parameters such that $|r_c| < 1$, we may develop, at any position $x$, the expression of $A(x)$ given by (8.100) in powers of $r_c$ using the identity $(1+x)^{-1} = \sum_{n=0}^{\infty}(-1)^n x^n$, valid for $|x| < 1$. Doing so yields

$$A(x) = A_0 + r_c e^{-\frac{x}{L_0}} A_1 + \sum_{n=2}^{\infty} r_c^n e^{-n\frac{x}{L_0}} A_{n\geq 2} \tag{8.103}$$

where the $A_i$ are the following *constant* matrices:

$$A_0 = \begin{pmatrix} 0 & 1 & 0 & 0 \\ -\frac{\omega^2-\omega_y^2}{c_a^2} & -k_\rho & 0 & 0 \\ 0 & 0 & 0 & 1 \\ -\frac{4\pi G\omega^2}{c_a^2} & -\frac{4\pi G\omega^2}{\omega^2-\omega_y^2}k_\rho & k_y^2 & 0 \end{pmatrix}, \tag{8.104}$$

and

$$A_1 = \begin{pmatrix} 0 & 0 & 0 & 0 \\ 0 & 0 & -\frac{\omega^2-\omega_y^2}{4\pi G c_a^2} & 0 \\ 0 & 0 & 0 & 0 \\ 0 & \frac{4\pi G\omega^2}{\omega^2-\omega_y^2}k_\rho & -\frac{\omega^2-\omega_y^2}{c_a^2} & -k_\rho \end{pmatrix}, \tag{8.105}$$

and

$$A_{n\geq 2} = (-1)^n k_\rho \begin{pmatrix} 0 & 0 & 0 & 0 \\ 0 & 0 & 0 & 0 \\ 0 & 0 & 0 & 0 \\ 0 & -\frac{4\pi G\omega^2}{\omega^2-\omega_y^2} & 0 & 1 \end{pmatrix}. \tag{8.106}$$

The matrix $A_0$ is the matrix one obtains in the Cowling approximation, for $r_0 = 0$. The upper right block is the null matrix because in this case the equation of motion is decoupled from the linearized Poisson equation, and we recover the fact that the equation is of second order only. Let us look for solutions $V$ of the form (Holmes, 2013)

$$V(x) = V_0(x) + r_c V_1(x) + \mathcal{O}\left(r_c^2\right), \tag{8.107}$$

$V_0$ being the solution in the Cowling approximation. In terms of initial conditions this imposes, to first order in $r_c$, that

$$V(0) = V_0(0) + r_c V_1(0). \tag{8.108}$$

Then plugging these linearized expressions (8.103) and (8.107) of $A$ and $V$ in equation (8.95) leads to zeroth order in $r_c$

$$\boxed{\frac{dV_0}{dx} = A_0 V_0}, \tag{8.109}$$

(Constraint on the $0^{\text{th}}$ order)

and to first order in $r_c$

$$\boxed{\frac{dV_1}{dx} = A_0 V_1 + A_1 V_0 e^{-\frac{x}{L_0}}}. \tag{8.110}$$

(Constraint on the $1^{\text{st}}$ order)

The pleasant property of the exponential atmosphere model is that $A_0$ has *constant coefficients*, so that these two equations may be solved explicitly.

The solution of (8.109) reads

$$V_0(x) = e^{xA_0} V_0(0) \tag{8.111}$$

where $e^{xA_0}$ is the matrix exponential of $A_0$ (explicit expression (8.130) derived below), and $V_0(0)$ is the initial condition vector for $V_0$, not to be confused with $V(0)$, both being linked by relation (8.108).

Equation (8.110) constitutes an inhomogeneous problem, i.e. with a source term. Namely, consider an equation of the form

$$\frac{dU}{dx} = BU + f(x) \tag{8.112}$$

with a given constant matrix $B$, a given $x$-dependent vector $f(x)$, and a given initial condition $U(0)$. Its solution is given by (e.g. Tracy, 2016)

$$U(x) = e^{xB} U(0) + e^{xB} \int_0^x e^{-sB} f(s) ds. \tag{8.113}$$

Now equation (8.110) corresponds to (8.112) with $U \equiv V_1$, $B \equiv A_0$ and $f(x) \equiv A_1 V_0(x) e^{-\frac{x}{L_0}}$. Finally using (8.111) in this expression of $f(x)$ we obtain

$$V_1(x) = e^{xA_0} V_1(0) + e^{xA_0} \int_0^x e^{-sA_0} A_1 e^{sA_0} V_0(0) e^{-\frac{s}{L_0}} ds. \tag{8.114}$$

Here too, beware of the initial conditions: $V_1(0)$ is the initial condition vector for $V_1$, not to be confused with $V(0)$, both being linked by relation (8.108). All that is left to do now is to plug in (8.107) the expressions of $V_0(x)$ and $V_1(x)$ just deduced. Doing so, we shall use the initial condition (8.108), in particular to replace the $V_0(0)$ vector in (8.114) by $V(0)$, since we are working up to order one in $r_c$. We obtain

$$\boxed{V(x) = e^{xA_0} \left[ \mathbb{1} + r_c \int_0^x Z_1(s) ds \right] V(0)} \tag{8.115}$$

(Solution up to $1^{\text{st}}$ order in $r_c \ll 1$)

where

$$\boxed{Z_1(s) \equiv e^{-\frac{s}{L_0}} \left( e^{-sA_0} A_1 e^{sA_0} \right)}. \tag{8.116}$$

The identity matrix corresponds to the Cowling approximation, and the second part is the correction induced by the Jeans term. This result is valid in the 'Cowling dominated' regime $r_c \ll 1$. The first exponential in (8.116) is the usual exponential function while the others are matrices. Hence facing that expression, the first thing to do is to check whether the matrices $A_1$ and $e^{sA_0}$ commute. If so, we would have[10] in the integrand $e^{-sA_0} e^{sA_0} = e^{-sA_0 + sA_0} = \mathrm{Id}$ and thus the expression of $V_1$ would be greatly simplified. Unfortunately it is not the case.

What does this development at higher orders look like? At order two, the same procedure yields

$$V(x) = e^{xA_0} \left[ \mathbb{1} + r_c \int_0^x dx_1 Z_1(x_1) + r_c^2 \left[ \int_0^x dx_1 \int_0^{x_1} dx_2 Z_1(x_1) Z_1(x_2) + \int_0^x dx_1 Z_2(x_1) \right] \right] V(0) \tag{8.117}$$

and in fact all orders are a sum of products of the generalization of (8.116), namely

$$Z_n(s) \equiv e^{-\frac{ns}{L_0}} \left( e^{-sA_0} A_n e^{sA_0} \right). \tag{8.118}$$

Hence we may get the solution not only for $r_c \ll 1$ but for $r_c < 1$ by increasing the order of the development, if needed. Note that this infinite expansion is very different from the formal solution (8.96) because now the terms are ordered, with respect to the parameter $r_c$, while in (8.96) we do not control a priori the amount of information lost when stopping the development at a finite order.

[10] This is not a trivial statement per se, since in general $e^A e^B \neq e^{A+B}$, but it is the case when $A$ and $B$ commute. Here the matrices $-sA_0$ and $sA_0$ clearly commute.

**b) Revisiting the Cowling case**

Expression (8.118) shows that the *only* information needed to have the solution for $r_c < 1$ is the exponential of the matrix $xA_0$, for all $x > 0$, i.e. to find the solution in the Cowling approximation given by (8.111). Let us now explicit it. We have

$$xA_0 = x \begin{pmatrix} 0 & 1 & 0 & 0 \\ -\frac{\omega^2-\omega_y^2}{c_a^2} & -k_\rho & 0 & 0 \\ 0 & 0 & 0 & 1 \\ -\frac{4\pi G\omega^2}{c_a^2} & -\frac{4\pi G\omega^2}{\omega^2-\omega_y^2}k_\rho & k_y^2 & 0 \end{pmatrix}. \tag{8.119}$$

The determinant of a block triangular matrix is simply the product of the determinant of its diagonal blocks. Therefore the characteristic polynomial of $xA_0$, namely $P(\lambda) \equiv |xA_0 - \lambda \mathbb{1}|$, is directly given by

$$P(\lambda) = \left(\lambda^2 + xk_\rho\lambda + x^2\frac{\omega^2-\omega_y^2}{c_a^2}\right)\left(\lambda^2 - x^2k_y^2\right). \tag{8.120}$$

The eigenvalues of $xA_0$ are the roots of $P(\lambda)$. For the first two, we recover as in section (8.15), the need to discuss the sign of the discriminant

$$\Delta \equiv x^2\left(k_\rho^2 - 4\frac{\omega^2-\omega_y^2}{c_a^2}\right). \tag{8.121}$$

When $\Delta > 0$, the two additional eigenvalues are distinct and real,

$$\lambda_{1,2}(x) = \frac{x}{2}\left(-k_\rho \pm \sqrt{k_\rho^2 - 4\frac{\omega^2-\omega_y^2}{c_a^2}}\right), \tag{8.122}$$

when $\Delta < 0$ they are distinct and complex,

$$\lambda_{1,2}(x) = \frac{x}{2}\left(-k_\rho \pm i\sqrt{4\frac{\omega^2-\omega_y^2}{c_a^2} - k_\rho^2}\right), \tag{8.123}$$

and when $\Delta = 0$ they are real and degenerate

$$\lambda_{1,2}(x) = -\frac{xk_\rho}{2}. \tag{8.124}$$

The last two roots are clearly given by

$$\lambda_{3,4}(x) = \pm xk_y. \tag{8.125}$$

It is out of the scope of this manuscript to discuss the stability of the system in view of the eigenvalues of matrix $A$, but as we see here the eigenvalues are position dependent, in a trivial way in this simple example, but which gives a hint that in more general cases they may have different signs in the various regions of the slab or atmosphere. The positions at which such inversions occur are surely of importance to characterize the evolution of the system.

**The $\Delta < 0$ case** All four eigenvalues are distinct, so that we know that $xA_0$ is diagonalizable, which is very enjoyable since the exponential of a diagonalizable matrix is easy to compute. We have

$$xA_0 = PD(x)P^{-1} \tag{8.126}$$

where $D$ is the diagonal matrix composed of the eigenvalues $\lambda_i$ above, and $P$ is composed of the eigenvectors. The important point is that it is block triangular

$$P = \begin{pmatrix} P_1 & 0 \\ P_2 & P_3 \end{pmatrix} \tag{8.127}$$

so that its inverse is simply given by

$$P^{-1} = \begin{pmatrix} P_1^{-1} & 0 \\ -P_3^{-1}P_2P_1^{-1} & P_3^{-1} \end{pmatrix} \tag{8.128}$$

and the computation of the matrix exponential, according to

$$e^{xA_0} = Pe^{D(x)}P^{-1}, \tag{8.129}$$

is also greatly simplified by this fact. These computations finally result in

$$\boxed{e^{xA_0} = \begin{pmatrix} E_1 & 0 \\ E_2 & E_3 \end{pmatrix}} \tag{8.130}$$

where

$$E_1(x) = e^{-\frac{k_\rho}{2}x}\begin{pmatrix} \cos\left(\frac{x\delta}{2}\right) + \frac{k_\rho}{\delta}\sin\left(\frac{x\delta}{2}\right) & \frac{2}{\delta}\sin\left(\frac{x\delta}{2}\right) \\ -\frac{2}{\delta}\frac{\omega^2-\omega_y^2}{c_a^2}\sin\left(\frac{x\delta}{2}\right) & \cos\left(\frac{x\delta}{2}\right) - \frac{k_\rho}{\delta}\sin\left(\frac{x\delta}{2}\right) \end{pmatrix} \tag{8.131}$$

and

$$E_2(x) = E_{2,1}\; e^{k_y x} + E_{2,2}\; e^{-k_y x} + E_{2,3}\; e^{\frac{x}{2}(b+i\delta)} + E_{2,4}\; e^{\frac{x}{2}(b-i\delta)} \tag{8.132}$$

where $E_{2,i}$ are simply *constant* matrices, depending on the parameters $\delta$, $k_y$ and $k_\rho$ in a non-trivial way which is not enlightening to explicit here, and

$$E_3(x) = \begin{pmatrix} \cosh(k_y x) & \frac{1}{k_y}\sinh(k_y x) \\ k_y \sinh(k_y x) & \cosh(k_y x) \end{pmatrix} \tag{8.133}$$

where we put

$$\delta \equiv \sqrt{4\frac{\omega^2-\omega_y^2}{c_a^2} - k_\rho^2}, \tag{8.134}$$

which is well defined since we are exploring the $\Delta < 0$ case here. These expressions may look involved, but they are in essence simple. Since trigonometric functions, hyperbolic or not, are only exponentials, the matrix $e^{xA_0}$ is really only a linear combination of exponentials. Thus we are sure that expressions like (8.115), and even at all orders with (8.118), can be easily computed fully though I must admit it is pretty lengthy to do.

Finally, it is important to notice that with the expression (8.130) of $e^{xA_0}$ we recover, as we should, the Cowling solution. It corresponds to the first component of (8.111), namely

$$\psi(x) = a_1(x)\;\psi(0) + a_2(x)\;\psi'(0) \tag{8.135}$$

where

$$\begin{cases} a_1(x) = e^{-\frac{k_\rho}{2}x}\left[\cos\left(\frac{x\delta}{2}\right) + \frac{k_\rho}{\delta}\sin\left(\frac{x\delta}{2}\right)\right] \\ a_2(x) = e^{-\frac{k_\rho}{2}x}\frac{2}{\delta}\sin\left(\frac{x\delta}{2}\right). \end{cases} \tag{8.136}$$

One can easily check that this expression is indeed exactly the expression (8.21) that we obtained without this matrix formulation, once the integration constants $c_1$ and $c_2$ are expressed in terms of $\psi(0)$ and $\psi'(0)$, by evaluating (8.21) and its derivative at $x = 0$.

### c) The discrete spectrum

To get the discrete spectrum we need to consider $\psi$ and impose the boundary conditions[11]. With the expressions (8.105) of $A_1$ and (8.130) of $e^{xA_0}$ plugged into the expression (8.115) of $V(x)$, we have that $\psi$ can be written as

$$\boxed{\psi(x) = a_1\;\psi(0) + a_2\;\psi'(0) + r_c\left\{b_1\;\psi(0) + b_2\;\psi'(0) + b_3\;\hat{g}_{1x}(0) + b_4\;\hat{g}'_{1x}(0)\right\}} \tag{8.137}$$

($\psi(x)$ beyond the Cowling approximation)

where the first two terms are the Cowling solution (8.135), and the $b_i(x)$ are the first order corrections. The latter coefficients are in essence simple, since they are just integrals of exponentials, but are very lengthy (e.g. $b_2$ below in (8.141)). Rather than expliciting them in the general case which will not be very enlightening, let us choose boundary conditions which will simplify greatly the calculations, but still induce a non vanishing correction to the Cowling case to be interesting for the present discussion. We will also choose the same boundary conditions on $\psi$ as in section 8.1 so that we may directly compare our results to it.

**Illustrative example** Let us consider here the three following conditions ($\psi'(0)$ being left arbitrary)

$$V(0) \equiv \begin{pmatrix} \psi(0) \\ \psi'(0) \\ \hat{g}_{1x}(0) \\ \hat{g}'_{1x}(0) \end{pmatrix} = \begin{pmatrix} 0 \\ \psi'(0) \\ 0 \\ 0 \end{pmatrix} \tag{8.138}$$

together with the following fourth condition imposed at the boundary $x = x_t$

$$\psi(x_t) = 0 \tag{8.139}$$

[11] Recall that $\hat{\xi}_x$ is proportional to $\psi$ so that with the boundary conditions we are going to consider shortly, we may use $\psi$ rather than $\hat{\xi}_x$ to determine the discrete spectrum.

in order to be able to compare with the previous study of section 8.1. These now yield the quantization condition

$$\boxed{a_2(x_t) + r_c b_2(x_t) = 0}, \tag{8.140}$$

keeping in mind that in the Cowling approximation this condition was (8.22) which is indeed $a_2(x_t) = 0$. In this simple case the only remaining coefficient to be computed is $b_2(x)$, and thanks to the numerous zeros in the matrices $A_1$ and $e^{xA_0}$ entering the calculation, the *only* terms remaining to compute are

$$b_2(x) = -\frac{\omega^2 - \omega_y^2}{4\pi G c_a^2}\left\{e_{11,1}(x)\int_0^x e^{-\frac{s}{L_{\text{ext}}}} e_{12,1}(-s)e_{12,2}(s)ds + e_{12,1}(x)\int_0^x e^{-\frac{s}{L_{\text{ext}}}} e_{22,1}(-s)e_{12,2}(s)ds\right\} \tag{8.141}$$

where $e_{ij,n}$ denotes the element at the $i^{\text{th}}$ row and $j^{\text{th}}$ column of the matrix $E_n$ in expression (8.130). Performing these integrations, we obtain

$$\begin{aligned} b_2(x) \;=\; & \tfrac{1}{\delta}\tfrac{\omega^2}{\omega^4-\omega_\rho^2\omega_y^2} e^{-k_\rho x}\left\{\left(\omega^2-\omega_y^2\right)\tfrac{\delta}{k_y}\sinh\left(k_y x\right) + \tfrac{\delta}{k_\rho}\omega_\rho^2\cosh\left(k_y x\right)\right. \\ & +\tfrac{1}{2}\tfrac{\delta}{k_\rho}\cos\left(\tfrac{x\delta}{2}\right)\left[\left(\omega^2-2\omega_\rho^2\right)e^{\frac{k_\rho x}{2}} - \omega^2 e^{-\frac{k_\rho x}{2}}\right] \\ & \left.-\tfrac{1}{2}\sin\left(\tfrac{x\delta}{2}\right)\left[\left(5\omega^2-2\omega_y^2-2\omega_\rho^2\right)e^{\frac{k_\rho x}{2}} + \left(\omega^2-2\omega_y^2\right)e^{-\frac{k_\rho x}{2}}\right]\right\} \end{aligned} \tag{8.142}$$

where

$$\omega_\rho^2 \equiv c_a^2 k_\rho^2. \tag{8.143}$$

We may finally rewrite the quantization condition (8.140) explicitly, in the as-symmetric-as-possible form

$$\boxed{\begin{aligned} \sin\left(\tfrac{x_t\delta}{2}\right) + \tfrac{r_c}{4}\tfrac{\omega^2}{\omega^4-\omega_\rho^2\omega_y^2}e^{-\frac{k_\rho x_t}{2}}\left\{\tfrac{\delta}{k_y}\right. & \left[\left(\omega^2-\omega_y^2+\tfrac{k_y}{k_\rho}\omega_\rho^2\right)e^{k_y x_t} - \left(\omega^2-\omega_y^2-\tfrac{k_y}{k_\rho}\omega_\rho^2\right)e^{-k_y x_t}\right. \\ & \left.\left. -\left(5\omega^2-2\omega_y^2-2\omega_\rho^2\right)e^{\frac{k_\rho x_t}{2}} + \left(\omega^2-2\omega_y^2\right)e^{-\frac{k_\rho x_t}{2}}\right]\sin\left(\tfrac{x_t\delta}{2}\right) \\ & +\tfrac{\delta}{k_\rho}\left[\left(\omega^2-2\omega_\rho^2\right)e^{\frac{k_\rho x_t}{2}} - \omega^2 e^{-\frac{k_\rho x_t}{2}}\right]\cos\left(\tfrac{x_t\delta}{2}\right)\Big\} = 0. \end{aligned}} \tag{8.144}$$

(Full quantization condition – Low density Atmosphere ($r_c \ll 1$))

At first sight it seems that there is a divergence for $k_y \to 0$ because of the $\frac{\delta}{k_y}$ factor. In fact, if expressed as sinh and cosh as in formula (8.142), we can see that since $\sinh\left(k_y x\right)/k_y \to x$ as $k_y \to 0$ , there is no such divergence. Similarly, another divergence seems to appear: the overall factor contains the denominator $\omega^4 - \omega_\rho^2\omega_y^2$, which seems to indicate that $\omega^2 = \omega_\rho\omega_y = k_\rho k_y c_a^2$ is a singularity. But recall that this derivation was made in the $\Delta < 0$ case given by (8.121), so that[12] we have in particular $\omega^2 > k_y k_\rho c_a^2$. While this is not a singularity that can be reached, it is interesting to note that the closer $\omega^2$ is to $k_y k_\rho c_a^2$, the more significant the correction becomes.

Does the Jeans term have a stabilizing or destabilizing effect, i.e. are the eigenfrequencies $\omega_n^2$ larger or smaller than those deduced in the Cowling approximation? In fact, what the richness of formula (8.144) tells us is that we cannot answer simply this question. Indeed, the sign of the correction due to the Jeans term may vary from one system to another since it depends on $x_t$ and on $k_\rho$. Also, the Jeans term does not stabilize all perturbations in the same way since the correction depends on $k_y$. Finally, the fact that the parameter $k_y x_t$ matters is yet another evidence, as in figure 8.3, that what happens (size and growth rate of clumps forming) perpendicularly to the stratification is very much affected by what happens in the direction of the stratification.

Expression (8.144) is complicated and contains a lot of information. It deserves a long and thorough study dedicated to it, for example by analyzing the various regimes it nicely exhibits, governed by parameters $k_\rho x_t$, $\delta x_t$ and $k_y x_t$. This is left for future work, but in order to get a first feeling of the content of this relation and of how one may explore it, let us now consider the physically interesting limit in which the boundaries may be considered as 'far', as illustrated in figure 8.5.

**Far Boundaries: The $k_\rho x_t \gg 1$ limit** Distributing the $e^{-\frac{k_\rho x_t}{2}}$ factor in front of the bracket in (8.144), we can see that this expression may be simplified greatly in the regime $k_\rho x_t \gg 1$. Without doing a rigorous[13] Taylor expansion, we may say that the exponential factors will suppress other terms so that what remains is

$$\sin\left(\frac{x_t\delta}{2}\right) + \frac{r_c}{4}\frac{\omega^2}{\omega^4-\omega_\rho^2\omega_y^2}\left[-(5\omega^2-2\omega_y^2-2\omega_\rho^2)\sin\left(\frac{x_t\delta}{2}\right) + \frac{\delta}{k_\rho}(\omega^2-2\omega_\rho^2)\cos\left(\frac{x_t\delta}{2}\right)\right] = 0. \tag{8.145}$$

[12] Indeed, $\Delta < 0$ is equivalent to $\frac{\omega^2}{c_a^2} - k_y^2 - \frac{k_\rho^2}{4} > 0$, but since $\frac{\omega^2}{c_a^2} - k_y^2 - \frac{k_\rho^2}{4} = \frac{\omega^2}{c_a^2} - k_y k_\rho - (k_y - \frac{k_\rho}{2})^2$ and that $(k_y - \frac{k_\rho}{2})^2 \geq 0$, we have $\frac{\omega^2}{c_a^2} - k_y k_\rho > 0$.

[13] My precaution in the formulation comes from the fact that $\delta$ contains $k_\rho x_t$, and the competition of the $e^{k_y x_t}$ factor has to be assessed properly. At this point I will just say the $k_y$ has to be small enough, leaving the rest for future work.

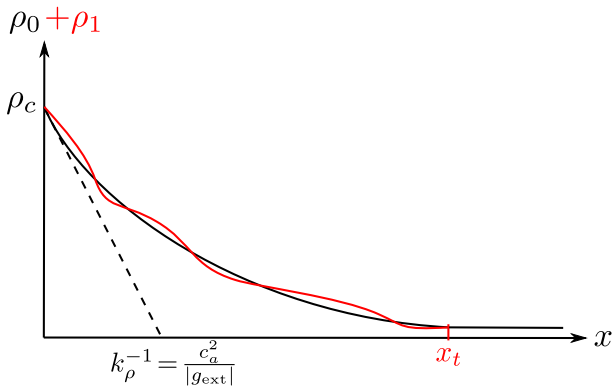


Figure 8.5: Illustration of a perturbed exponential atmosphere in which the boundary $x = x_t$, corresponding to the distance after which the perturbation is vanishing, may be considered as far ($k_\rho x_t \gg 1$), as explored in the text. In black is the equilibrium density profile, and in red the perturbed one. The dashed line recalls that the steepness of such an exponential atmosphere is governed by the speed of sound in the medium $c_a$ and the value of the gravitational field $g_{\rm ext}$ imposed (directed from right to left in this illustration).

Because of the $e^{k_y x_t}$ factor, we should also consider this relation to be valid for $k_y \ll k_\rho$, which is anyway the regime of interest since we expect the Jeans term to be negligible for perturbations of small wavelengths. Now, the great property of relation (8.145) is that it is a linear combination of sines and cosines, thus it is in fact simply a phase-shifted sine. Indeed, using the exponential forms of sine and cosine gives the identity

$$a\sin x + b\cos x = \sqrt{a^2+b^2}\sin(x+\varphi) \tag{8.146}$$

the phase being given by

$$\varphi = \arctan\frac{b}{a} \tag{8.147}$$

for $a > 0$. Then the quantization condition simply reads

$$x + \varphi = n\pi \tag{8.148}$$

while it was $x = n\pi$ in the Cowling approximation. In this case this gives explicitly (still at first order in $r_c$, using in particular the fact that $\arctan\epsilon \sim \epsilon$ for $\epsilon \ll 1$)

$$\boxed{\frac{x_t\delta}{2}\left[1+\frac{1}{2}\frac{r_c}{k_\rho x_t}\frac{\omega_n^2\left(\omega_n^2-2\omega_\rho^2\right)}{\omega_n^4-\omega_y^2\omega_\rho^2}\right]=n\pi.} \tag{8.149}$$

(Quantization – Low density ($r_c \ll 1$), Far Boundaries ($k_\rho x_t \gg 1$), Large y-wavelength ($k_y \ll k_\rho$))

Note that for $r_c = 0$ we do recover, as we should, the discrete spectrum deduced in the Cowling approximation

$$\frac{x_t\delta}{2} = n\pi, \tag{8.150}$$

and we see that the corrective term (with respect to Cowling) goes as $\omega^{-2}$ as $\omega^2 \to \infty$ (do not forget the $\omega^2$ dependence in $r_c$), showing that the higher the frequency, the better the Cowling approximation. Equation (8.149) is an equation on $\omega_n^2$, which is involved since $\delta$ contains $\omega_n^2$. Assuming that the solution will be only slightly modified with respect to the Cowling case, let us solve it perturbatively, in $(k_\rho x_t)^{-1} \ll 1$ now, by putting $\omega_n^2 = \omega_{n,0}^2 + (k_\rho x_t)^{-1}\omega_{n,1}^2$ where $\omega_{n,0}^2$ is the discrete spectrum in the Cowling case (8.23), and solving for $\omega_{n,1}^2$. The discrete spectrum may finally be explicited as

$$\boxed{\omega_n^2 = \omega_{n,0}^2\left[1+\frac{16\pi G\rho_c}{c_a^2k_\rho^2}\frac{4\pi^2n^2}{k_\rho^3x_t^3}\frac{7-\frac{4\pi^2n^2}{k_\rho^2x_t^2}}{\left(1+\frac{4\pi^2n^2}{k_\rho^2x_t^2}\right)^3}\right]} \tag{8.151}$$

(Discrete Spectrum – Low density ($r_c \ll 1$), Far Boundaries ($k_\rho x_t \gg 1$), Large y-wavelength ($k_y \ll k_\rho$))

where we have used $k_y \ll k_\rho$ to be consistent with the assumptions made. Now the dependence on $n$ is explicit. For large $n$, the correction goes as $n^{-2}$, which is consistent with the idea that the Cowling approximation is better for high order modes (cf. section 7.3.2). Finally, we anticipated above that unfortunately

we cannot draw a general rule on the stabilizing effect of the Jeans term, and this is an example of this fact since the sign of the correction depends on the mode. Modes with $n$ greater than the floor of $\sqrt{7}k_\rho x_t/2\pi$ are destabilized by the Jeans term (negative contribution) while others are stabilized (positive contribution). However, this number marking the transition is large since we are in the 'far boundaries' regime, and since the value of the correction is smaller as $n$ increases, this destabilization will be small. Hence, in this analysis, valid for modes with small $k_y$, we are led to the conclusion that the Jeans term essentially has a stabilizing effect. It is interesting to see that from our local analysis represented in figure 8.4 we observe the same trend for small $k_y$. Whether this is a general feature remains to be assessed.

# Chapter 9

# Further Ongoing Works

Clearly, a lot can still be explored further already in what I have presented so far. But I have also explored two other paths, constituting two important generalizations: (i) cylindrical geometry in order to explore the stability of cosmic filaments and (ii) taking buoyancy fully into account in order to explore the importance of this physical process, which is paramount in stellar dynamics. After presenting them, I will finally mention key interrogations brought by the experience gained through the above analysis and that must be tackled to go further to optimize the approach.

## 9.1 Stability of Cosmic Filaments

**Cylindrical symmetry** Now that we have explored the plane symmetric equilibria, relevant to model cosmic walls and sheets, it is natural to focus on cylindrically symmetric ones, relevant to model cosmic filaments. In the following, the notation will be standard, by denoting the radial, azimuthal and longitudinal coordinates respectively $R, \theta$ and $z$, and their corresponding unit vectors $\hat{R}, \hat{\theta}$ and $\hat{z}$. This stratification is still one dimensional, but several very important differences arise due to the particular geometry. The differential operators entering the force operator now contain $\frac{1}{R}$ factors, which make the $R = 0$ positions (constituting the $z$ axis) particular points, and therefore necessitate great attention. This was to be expected, comparing the planar and cylindrical equilibrium states in chapter 6 already. In terms of variables, working with $R\hat{\xi}_R$ will thus often be more convenient. Also, one always has to keep in mind that the unit vectors are position dependent, which may be tricky in some situations. Finally, the two dimensions transverse to the stratification are fundamentally different: the longitudinal direction $z$ has an infinite extent, while the azimuthal $\theta$ direction is closed. For this reason, in the decomposition (9.2) of the displacement vector $\vec{\xi}$ below, the wavenumber $k_z$ associated with $z$ is a continuous variable, like $k_x$ and $k_y$ in the planar case, while the number $m$ associated with $\theta$ is quantized. This makes the cylindrical symmetry particularly interesting because it is thus really intermediate between the spherical (both transverse dimensions are closed) and the planar (no closed dimension) symmetries.

**The displacement vector** We now have the two following properties.

(i) Due to the translation invariance in $t$, $z$ and $\theta$ of the equilibrium state, we may Fourier transform in these variables, so that the most general displacement vector may be written as

$$\vec{\xi} = \hat{\xi}\, e^{i(m\theta + k_z z - \omega t)} \tag{9.1}$$

but beware of this notation: since unit vectors in cylindrical coordinates depend[1] on $R$ and $\theta$, we have $\hat{\xi}(R, \theta, z)$ and *not* $\hat{\xi}(R)$ even though its components depend on $R$ only:

$$\hat{\xi}(R, \theta, z) = \hat{\xi}_R(R)\hat{R} + \hat{\xi}_\theta(R)\hat{\theta} + \hat{\xi}_z(R)\hat{z}. \tag{9.2}$$

(ii) Due to the cylindrical symmetry of the equilibrium system, the gravitational acceleration is radial so that $\nabla\Phi_0$ is parallel to $\hat{R}$. Thus it does not appear in the $\theta$ and $z$ components of the equation of motion (7.23), which may be written, in the absence of magnetic fields:

$$\begin{array}{lll} \rho_0 \frac{\partial^2 \xi_\theta}{\partial t^2} & = -\frac{1}{R}\partial_\theta p_1 - \rho_0 \frac{1}{R}\partial_\theta \Phi_1 & = -\frac{1}{R}\partial_\theta \left(p_1 + \rho_0 \Phi_1\right) \\ \rho_0 \frac{\partial^2 \xi_z}{\partial t^2} & = -\partial_z p_1 - \rho_0 \partial_z \Phi_1 & = -\partial_z \left(p_1 + \rho_0 \Phi_1\right). \end{array} \tag{9.3}$$

The second set of equalities stems from the cylindrical symmetry of the equilibrium density ($\partial_\theta \rho_0 = 0$ and $\partial_z \rho_0 = 0$). From these two equations, it is clear that applying $\partial_z$ to the first, and $\partial_\theta$ to the second,

[1] More precisely, the only non zero derivatives are $\partial_\theta \hat{R} = \hat{\theta}$ and $\partial_\theta \hat{\theta} = -\hat{R}$

we have the following identity

$$\frac{\partial^2}{\partial t^2}\left(\partial_z \xi_\theta - \frac{1}{R}\partial_\theta \xi_z\right) = 0 \tag{9.4}$$

everywhere and at any time. Then, given the above decomposition of $\vec{\xi}$ we obtain

$$\hat{\xi}_\theta = \frac{m}{R}\frac{1}{k_z}\hat{\xi}_z. \tag{9.5}$$

Needless to say that this relation greatly simplifies the calculations. In fact, it is not surprising to have a universal relation between the non radial components, because in essence this system is still one-dimensional: the stratification is only along $R$, just like it was only along $x$ in the planar situation. And indeed, this relation was deduced solely from the fact that the equilibrium depends on $R$ only.

**Wave equation** Then, following the same steps as I have taken in the planar case of chapter 8, I have arrived at the wave equation, equivalent of equation (8.58), expressed using the variable $\chi \equiv R\hat{\xi}_R$. It is a fourth order differential equation whose highest order term has the singularity

$$\boxed{\omega_G^2 = \omega_\perp^2 - \frac{1}{R}\frac{(\omega_\perp^2)'}{k_\perp^2} - \frac{(\omega_\perp^2)''}{k_\perp^2} - \omega_0^2} \tag{9.6}$$

(Singular Frequency – Cylindrical)

which corresponds to (8.55) in the planar case, and where

$$k_\perp^2 = \frac{m^2}{R^2} + k_z^2 \tag{9.7}$$

corresponds to $k_y^2$ in the planar case, i.e. to the wavenumber in the direction transverse to the stratification which is now the radial direction. But note that there is a crucial difference between $k_y$ and $k_\perp$ here: $k_\perp$ is a function of $R$. Therefore, while the steps to follow to reach the wave equation are really the same as for the planar case detailed previously, the fact that the gradient operator brings in $1/R$ terms and that $k_\perp^2 = k_\perp^2(R)$, every time we differentiate, the number of terms increases compared to the planar case. In the end, the wave equation in the cylindrical case is of the form 'the planar coefficients plus terms involving $1/R$ and $k_\perp$', thus making the coefficients *roughly twice longer*...! The point of this remark is to insist on the methodological importance of having started this discussion with the planar case, which turns out to be a necessity. Once the planar case is well understood, the cylindrical case appears far simpler since one then has only to focus on the additional terms induced by geometry.

In Goedbloed & Poedts (2004) the authors study MHD instabilities in cylindrically symmetric stratifications (in the Cowling approximation), because a tokamak or an accretion disc of large radius can be described, in a first approximation, as being straight. Without discussing the details, let me simply show what cylindrical symmetry changes to the MHD wave equation (7.45) we discussed earlier. It becomes of the form[2]

$$\frac{d}{dR}\left(\frac{N}{RD}\frac{d\chi}{dR}\right) + Q\chi = 0. \tag{9.8}$$

The point I want to stress is that position $R = 0$ plays a special role: it is a singularity of the wave equation! However, the authors insist that this singularity is of *completely different nature* from the physical singularities associated with the two continuous spectra, the slow $\{\omega_S^2(R)\}$ and the Alfvén $\{\omega_A^2(R)\}$ ranges. This distinction is subtle and important. In fact, it may also be confusing, as in the literature 'singularity' may not always be used in the same sense. Finally, note that the ordering of the apparent and genuine singularities remains valid, at every radius $R$, but another important difference compared to the planar case is that no matter how small the inhomogeneity, the slow turning point frequencies overlap the slow continuum and the fast turning point frequencies overlap the (formal) fast continuum, because of the geometrical singularity $R = 0$. In the hydrodynamical context of interest here, I have not reached that level of detail yet, but what is already worth noticing is that the $R = 0$ singularity appears in the singular frequency $\omega_G^2$, with possibly a negative sign... A lot of interesting physics is within sight.

## 9.2 Buoyancy: g-modes and convection

Buoyancy is a key ingredient to understand the dynamics of stars, because it gives rise to convection, but is also important because it gives rise to oscillations (g-modes, cf. figure 9.1) which, when they are observed, will constitute a probe of stellar interiors. How about in the cosmological context? The importance of the convective zone in stars is that it redistributes the energy very efficiently. In the pristine cosmic web, in which magnetic fields are extremely weak, convection may play a non neglible role[3].

[2] Goedbloed & Poedts (2004) call it a generalized Hain-Lüst equation after Hain & Lüst (1958).

[3] Note that the importance of convection in the intracluster gas of galaxy clusters has been studied by several authors. See for instance Chandran & Dennis (2006) and Gupta et al. (2016), and references therein.

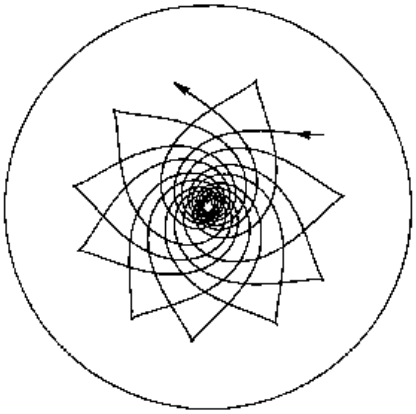

Figure 9.1: Cross section of the solar interior: This figure is complementary to figure 7.1 which represented acoustic oscillations, called p-modes. In this case the buoyancy-driven oscillations are represented, called g-modes. Continuous lines represent the direction orthogonal to wave fronts. As we can see, these modes propagate in the center of the star, on the contrary to p-modes which propagate close to the surface, which is why detecting g-modes would constitute a probe of the sun's interior (from Gough et al., 1996). What would such oscillations look like in a cosmic filament, and what dynamical role may they play?

**Closure relation for perturbations** As discussed in section 2.3, in order to close the infinite hierachy of equations resulting from taking the various moments of the Boltzmann equation, one needs to add a closure relation. Usually the purpose of this relation is to close the equation governing the second moment of the distribution function, i.e. the energy equation. The closure thus usually consists in making an assumption on the third moment of the distribution function, namely the heat flow. The relevance of a closure relation thus depends on the timescales of the processes involved. For instance for fast dynamical processes, i.e. faster than heat conduction, an adiabatic (isentropic) closure is relevant, while for slow processes, temperature gradients do not exist and an isothermal closure is appropriate.

Here, let us consider that the timescales of the perturbations, i.e. the oscillation period if stable and growth time if unstable, are sufficiently short so that no heat is exchanged between neighbouring fluid elements. Then the evolution of the perturbations may be considered as *adiabatic*. In this case, using the laws of Thermodynamics, it can be shown (cf. e.g. Thompson, 2006) that the equation expressing the absence of heat $\delta Q = 0$ becomes the following relation between the Lagrangian variation of pressure $\delta p$ and the Lagrangian variation of density $\delta\rho$:

$$\boxed{\frac{\delta p}{p_0} = \gamma_{\rm ad}\frac{\delta\rho}{\rho_0}} \tag{9.9}$$

(Adiabatic Fluctuations)

where, in general $\gamma_{\rm ad} \neq \gamma$ the polytropic exponent from the polytropic equation of state (6.4) of the equilibrium. Equation (9.9) is written in terms of Lagrangian perturbations $\delta\rho$ and $\delta p$. Let us rewrite it in the Eulerian variables $\rho_1$ and $p_1$. The link between the two descriptions is given by (cf. e.g. Cox, 1980)

$$\begin{aligned}\delta\rho &= \rho_1 + \vec{\xi}\cdot\vec{\nabla}\rho_0\\ \delta p &= p_1 + \vec{\xi}\cdot\vec{\nabla}p_0.\end{aligned} \tag{9.10}$$

Now, defining the speed of sound

$$c_{\rm ad}^2 \equiv \gamma_{\rm ad}\frac{p_0}{\rho_0}, \tag{9.11}$$

which is different from the speed $c_a^2 \equiv \gamma\frac{p_0}{\rho_0}$ defined in the equilibrium state (6.6) because $\gamma_{\rm ad} \neq \gamma$ in general, expression (9.9) may be rewritten

$$\boxed{p_1 = c_{\rm ad}^2\rho_1 + \gamma_{\rm ad}\ p_0\ \vec{\xi}\cdot\vec{A}} \tag{9.12}$$

(Closure relation – With convection)

where the vector

$$\vec{A} = \frac{\vec{\nabla}\rho_0}{\rho_0} - \frac{\vec{\nabla}p_0}{\gamma_{\rm ad}\ p_0} = \left(1 - \frac{\gamma}{\gamma_{\rm ad}}\right)\frac{\vec{\nabla}\rho_0}{\rho_0} \tag{9.13}$$

is a well known quantity in stellar physics, linked to the Brunt-Väisälä frequency as $N^2 \equiv -Ag_0$ which gives the timescale associated with buoyancy (frequency of oscillations or growth rate of convective instability). The second equality is valid in the case of a polytrope of exponent $\gamma$ and indicates that stability depends on the ordering between $\gamma$ and $\gamma_{\rm ad}$. Convective instability is governed by the so-called Schwarzschild criterion, illustrated in figure 9.2.

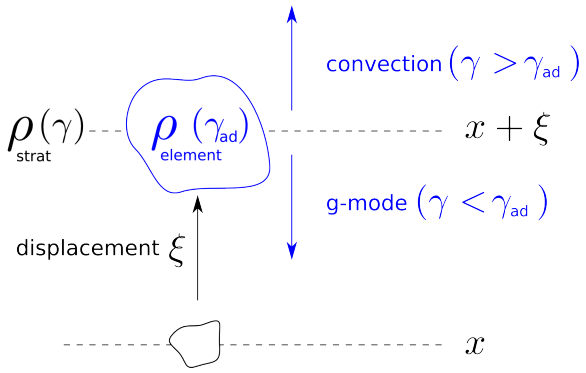


Figure 9.2: Consider a plane stratified medium, whose layers are labeled by the variable $x$. The density profile of this stratification is $\rho_{\text{strat}}$, and is governed by the parameter $\gamma$. Consider a volume element that belongs to the layer at position $x$ when at equilibrium. It is displaced by some perturbation to the layer at position $x + \xi$. The density $\rho_{\text{element}}$ of the volume element evolves according to a law governed by the parameter $\gamma_{\text{ad}}$, which reflects how efficient the heat transfers are on the typical timescale of this displacement. When the volume element is in its equilibrium position, the buoyancy it undergoes is counterbalanced by gravity which is why it remains at position $x$ in the absence of perturbations. However, once displaced, it is in a new environment in which the forces acting on it do not necessarily balance anymore. Three cases are possible: (i) $\gamma = \gamma_{\text{ad}}$ so that the volume element remains at $x + \xi$, and the atmosphere is said to be convectively neutral, (ii) $\gamma > \gamma_{\text{ad}}$ so that buoyancy moves the volume element towards upper layers, giving rise to convection and (iii) $\gamma < \gamma_{\text{ad}}$ so that the volume element is brought back towards its equilibrium position, giving rise to oscillations, the g-modes, as in figure 9.1.

## 9.3 Refining the question and the approach

It is a general feature that questions bring more questions, but fortunately the additional questions help framing and answering the initial ones. In the present case, the question was (cf. section 1.3): **How does gravitational instability occur in stratified media?** What was already clear from the beginning is that in terms of objectives, this question can already be subdivided into more questions such as: Under which conditions may fragmentation occur, i.e. for a given model of filament for instance, which ranges of parameters give rise to instability? What are the sizes of the clumps resulting from this fragmentation? What are their growth rates? Etc. But what was not obvious, and that comes out as one of the main outcomes of the analysis performed in this manuscript, is that to facilitate answering these questions *the choice of variable seems to be essential.*

**Which variable?** In section 7.1.1, we already discussed in general terms the difference between the displacement vector and the primitive variables as we performed the Lagrangian reduction: The displacement vector is more fundamental and contains all the information about all perturbed quantities. We later pointed out, in section 8.1.3, that the equations governing different variables are fundamentally different, and chose to privilege $\vec{\xi}$. A point that I did not discuss extensively here because it is beyond our scope, is boundary conditions, but we may already get a feeling that the choice of variables will also matter in this respect. Despite all this, it may seem like the choice of variable is just a matter of convenience, i.e. of choosing the right tool to reach the answer to our question faster or in a simpler way, just like it is naturally more adapted to work with cylindrical coordinates to describe a cylindrically symmetric system for instance. The fragmentation of a structure does not physically depend on how we describe it! But in fact, in Goedbloed & Poedts (2004) and Goedbloed et al. (2010) the authors show that the choice of variable to describe perturbations has heavy consequences because with one or the other, *we do not describe the same phenomena.* For instance, they point out differences between primitive variables and $\vec{\xi}$: one description is Eulerian while the other is Lagrangian, but what is more subtle and crucial is the fact that in a description with $\vec{\xi}$, one misses a mode, namely the entropy mode, and also this description may not be generalized to dissipative plasmas (see e.g. in their section 12.2.1). These two descriptions are thus not equivalent, and are more than mere changes of variables. Hence, the relevant analogy is not choosing cylindrical coordinates to describe a cylindrically symmetric system, but it is rather like the fact that a lot of information is lost when describing a plasma as a fluid rather than kinetically for instance, as we saw in chapter 2. Now, discarding some information may be a good thing, as long as we get rid of the unnecessary one and that we keep track of what we left behind. For example, in Goedbloed & Poedts (2004) and Goedbloed et al. (2010), the authors argue that ignoring the entropy mode is all the better for their purpose.

We see that we clearly need to specify the role and meaning of the variable we use. For the present question of gravitational fragmentation, which is the most relevant choice? I have not seen so far in the literature discussions on these aspects, for example comparisons of the various approaches adopted in the

works mentioned in the introduction of chapter 7. At this point, I observe that various authors use various variables: Pekeris (1938) worked with the divergence of the displacement vector $\vec{\nabla}\cdot\vec{\xi}$, Goldreich & Lynden-Bell (1965) and Elmegreen & Elmegreen (1978) privilege the perturbed potential $\phi_1$, Ledoux & Walraven (1958) a convenient potential for homogeneous equilibria $\phi_1+p_1/\rho_0$ and Breysse et al. (2014) the displacement itself $\vec{\xi}$ for example. It is particularly interesting, and intriguing, to note that Elmegreen & Elmegreen (1978) derived an equation on $\phi_1$ only, of fourth order, but which does not present a singular frequency like the $\omega_G^2$ that we obtain in the present manuscript. My understanding at this stage on this point is that the perturbed potential may not be the most suited variable since even if the system becomes clumpy, the potential, being a global quantity, is only weakly affected and it may be that no sign of instability appears in the equation governing it. However, so far I did not find references performing comparisons of the scopes and results obtained with these various approaches. In the same spirit, I am not sure at this stage of what exactly $\rho_0\vec{\xi}$, rather than $\vec{\xi}$, physically corresponds to. Is it really just a convenient change of variable, or does it have a profound physical meaning? Interestingly this variable is not natural in more general situations, e.g. when magnetic field is included, which is why I suppose it is not common in the literature. Finally, how does this translate in the spectral approach to gravitational fragmentation adopted in this manuscript? Depending on the variable we choose, the governing operator is different, so the spectrum is a priori not the same, and intriguing results might perhaps appear (as hinted at in the footnote page 80)...

**Focusing on $\rho_1$** Following the steps of the ideal MHD literature, I have explored gravitational fragmentation using the displacement vector, which seems a great idea since it is a most fundamental variable. But could it be that this represents too much information, and that working with $\rho_1$ for instance is sufficient? And indeed, in section 7.1.1, this is the choice we have made in our 'first approach to gravitational fragmentation'. Studying the evolution of the perturbed density $\rho_1$ seems physically like the variable relevant for our purpose, since we are interested in the formation of dense clumps. Now, as opposed to when we were in section 7.1.1, thanks to the journey we have undertaken, we may reformulate the problem in terms of spectral theory and benefit from all the tools associated with it. Let us look at the wave equation (7.20) as an eigenvalue problem for $\rho_1$. First we need to explicit $\phi_1$ as a function of $\rho_1$ by using the integral form (7.8). Then, considering temporal normal modes $\rho_1=\hat{\rho}_1 e^{i\omega t}$, and using Poisson equation, we obtain

$$-\omega^2\hat{\rho}_1=\mathcal{W}(\hat{\rho}_1) \tag{9.14}$$

where the operator $\mathcal{W}$ satisfies

$$\mathcal{W}(\hat{\rho}_1)=\Delta\left(c_a^2\hat{\rho}_1\right)+8\pi G\rho_0\hat{\rho}_1-\vec{g}_0\cdot\vec{\nabla}\hat{\rho}_1+\vec{\nabla}\rho_0\cdot G\int\hat{\rho}_1\frac{\vec{r}-\vec{r}'}{|\vec{r}-\vec{r}'|^3}d^3r'. \tag{9.15}$$

This is a *scalar eigenvalue problem* in which the eigenvalue $\omega^2$ intervenes *linearly*. Indeed, contrary to the eigenvalue problem (7.58) we focused on, we are now dealing with the scalar variable $\rho_1$, rather than the vectorial $\vec{\xi}$. The problem (9.14) is thus a priori much simpler! However, the operator $\mathcal{W}$ does not have a simple physical interpretation of each term as the force operator $F$ has. Also, it contains less information than the vectorial one (7.58). For instance the pressure term $\Delta(c_a^2\rho_1)$ in (9.15) contains the information on the fact that wave fronts are deviated by the stratification of the speed of sound, but the pressure term $\Delta(c_a^2\vec{\nabla}\cdot(\rho_0\vec{\xi}))$ in (7.58) not only contains this information, but also informs us on the polarisation of the waves. As mentioned above, this loss of information may be an advantage, since the vectorial description may be too much for a statement on stability in simple cases. However, for a more general treatment of gravitational fragmentation, including magnetic field, convection, and most importantly for the cosmological context, including flow, it is probably more appropriate to pursue the analysis in the line of the ideal MHD literature, in terms of $\vec{\xi}$, in order to benefit from the *huge* amount of results already obtained in very complex systems.

# Chapter 10

# Prospects

In this thesis, I have focused on two major questions of Cosmology and Astrophysics: The origin of cosmological magnetic fields (part I) and the advent of gravitational instabilities (Jeans, Rayleigh-Taylor and convection) in the Cosmic Web (part II). The structuring of the Universe is fascinating, but obviously also very challenging. The underlying physics is extremely rich and numerous phenomena occur simultaneously, in a complex interplay. The numerical approach nowadays developed by many authors may embrace them collectively but the analytical approach really helps disentangling the role of each process. It is fundamental to develop toy models to explore these processes, first separately one by one, and then to study their interplay and assess whether they hamper or enhance each other.

Already at this stage, with the work I have presented here, a lot of interesting and practical results can be derived in the short term.

**Explicit stability conditions.** – Using equations (8.67), (8.69) or (8.74), we may analyze the stability of given physical models with respect to gravitational instabilities. For starters, we may use the equilibrium toy models from chapter 6 for instance, since they present the huge advantage of being analytical and simple, as well as physically motivated. We may then construct many interesting models of various cosmological environments and, increasing the refinement little by little, investigate their implications on the structuring of the Universe. As mentioned in chapter 8, one way to derive local stability criteria such as Suydam's criterion is to perform Frobenius expansions. However, in order to be able to draw definite conclusions such as those derived in Goedbloed & Poedts (2004) for instance, which deal with second order equations, we need a profound understanding of fourth order differential equations. The higher the degree of the equation, the larger the number of independent solutions, so that one cannot simply transpose the aforementioned works to the present case. Fortunately, many of the necessary tools are detailed in Bender & Orszag (1978) for example. Another very promising path to follow is to pursue the matrix formulation that I exposed in section 8.3. There surely is a lot that could be understood from the analysis of the eigenvalues of $A_0$ for example.

In any case, a necessary discussion, that I have kept to a minimum in this manuscript, is that of boundary conditions, which we know may completely change stability properties. To model the cosmic web and protogalaxies, a countless number of boundary conditions may be relevant given the high diversity of these environments. In chapter 6, I have shown how to compute the thickness of self-gravitating polytropes, and in our stability analysis here we have essentially considered the rigid walls boundary conditions. Accounting for the vast variety of environments present in the cosmic web, and getting representative examples, requires a thorough, dedicated study. A very good starting point is to make choices inspired from other fields, e.g. from the theoretical models of interstellar clouds and those from stellar physics (e.g. Goldreich & Lynden-Bell, 1965; Cox, 1980). Reference Goedbloed & Poedts (2004) also present interesting astrophysically relevant boundary conditions (cf. their models IV-VI of closed or open coronal magnetic loops, and stellar wind outflows).

**Expliciting singular modes.** – In this manuscript, we have discussed and explicited discrete and continuous spectra, i.e. eigenfrequencies, but the modes that we have explicited corresponded only to the discrete parts, the eigenmodes. What are the modes corresponding to the continuous spectrum? Here is a very brief overview of some historical key moments of research on this topic. In 1946, L. Landau performed a proper treatment of the linearized Vlasov–Poisson equations by means of the Laplace transform of the initial value problem, i.e. of plasma oscillations in a kinetic description (Landau, 1946). He showed that singularities give rise to damping of the plasma oscillations, a phenomenon now called Landau damping. Later, N. van Kampen proved that the same result can be obtained with a normal mode analysis, but using Dirac $\delta$-functions (Van Kampen, 1955), showing that these equations have a continuous spectrum of singu-

lar normal modes, now known as Van Kampen modes, and referred to as 'improper' eigenmodes because they are distributions rather than regular functions. Because these analyses were performed in the kinetic description, this damping was thought to be restricted to the microscopic picture. However, the study of a fluid model, namely the electrostatic oscillations in inhomogeneous cold plasmas, by Barston in 1964 by means of singular normal modes *à la* Van Kampen and later by Sedláček in 1971 with a Laplace transform *à la* Landau (Barston, 1964; Sedláček, 1971), showed that a macroscopic description may also lead to dissipationless damping, which is due to inhomogeneity in ordinary space while in the Landau damping case it is due to inhomogeneity in the velocity space. The point is that damping of initial perturbations occurs in conservative systems with a continuous spectrum through redistribution over the different continuum modes. For more information, see chapters 10 and 11 of Goedbloed & Poedts (2004), or for example Balbinski (1984) in which the author exhibits the 'eigenfunctions' of the continuum for a differentially rotating perfect fluid, and argues that indeed they represent a physical perturbation despite their singular form. In light of these studies, an important step following the work in this manuscript will be to derive explicitly the singular modes relevant in cosmological situations.

So far our stability analysis focused on walls and filaments at rest, without magnetic field and considering essentially one fluid only. Let me now briefly underline the ingredients that I think are the most important to add, little by little, in the description to bring it closer to realistic astrophysical and cosmological environments, and give elements as to how to proceed.

**Expansion.** – In the cosmological context, a major element to consider is the expansion of the Universe. Its impact on the fragmentation of filaments will surely be of great importance, but it may be quantitatively and qualitatively different at various epochs. For instance, we may expect the expansion to play an important role in all three principal directions of early filaments, since they are not strongly bound yet, while in a later filament one or two directions may have detached from the global expansion (the 'turn around'). Also, in the Standard Model of Cosmology, expansion is radically different in the matter dominated era and in the dark energy dominated era, so early and late filaments also evolve in different global frameworks. It will be very fruitful to compare the results obtained with this spectral theory approach with works tackling gravitational instability with expansion such as Lacey (1989) for instance who locally analyses the evolution of perturbations in a collapsing, nearly pressure-free spherical or planar background.

**Dark matter.** – The second unescapable element to consider for modeling cosmological structure formation is dark matter, which is dominant at those scales. As discussed in chapter 1, cosmological numerical simulations show that the dark matter cosmic web has a lot of substructure, and also that baryons in filaments are clumpy too, inducing an intermittent accretion onto the nodes (galaxies and clusters) of the web. To what extent is the clumpiness of the gas inside filaments due to the clumpiness of the underlying dark matter? To answer this question, we may develop two approaches. First the structured dark matter background may be treated as a fixed external potential which breaks the assumed axisymmetry of the baryonic fluid equilibrium. We may then evaluate how this affects the fragmentation of baryons compared to the case, which I have detailed in this manuscript, of the fragmentation of baryons in an axisymmetric external potential. Another approach consists in treating the dark matter background as a second fluid. However, while a fluid description is relevant for baryons, the dark matter component has a subtler dynamics, because of its collisionless nature, and in principle requires a kinetic description. This requires identifying physically motivated effective closure relations to legitimate an effective fluid description of the dark component too. Various approaches to do so can be found in the literature, with discussions on their respective validity. Such a bi-fluid approach will then help uncover the dynamical channels through which baryons and dark matter affect each other's behaviours in cosmological filaments.

**Magnetic field.** – In many astrophysical environments, magnetic fields clearly play a major role, and they may also be important in the formation of protogalaxies. Fortunately, given that the approach adopted in this manuscript is inspired from plasma physics, it is natural and relatively straightforward to include magnetic fields in the description. Also, as mentioned in section 8.2.2, one of the outcomes of research in MHD is that, paradoxically at first sight, studying the MHD case turns out to be simpler than exploring the HD case. Indeed, this more general case lifts degeneracies and thus alleviates possible confusions and misunderstandings. In that spirit, I am convinced that adding magnetic fields to the above study on gravitational instability will also help understand better the latter.

**Flows.** – While adding magnetic fields in the description is probably not absolutely necessary in the cosmological context (because of their weak strengths at those scales) but is certainly crucial to describe astrophysical situations, an element that we have discarded in this manuscript, and that is of the utmost importance for both Cosmology and Astrophysics, is *flows*.

Physically, we may distinguish two broad classes of cosmological filaments because the environments in which filamentary structures evolve in the early Universe and late Universe are in many aspects radically different. For example, late times filaments are well defined, with rather sharp profiles and clearly delimited by the nodes that they interconnect, which is not the case in the early stages. Indeed, as discussed in chapter 1, dark matter decouples much earlier than baryons so that, at Recombination, baryons are rather homogeneously distributed but evolve in an already formed web-like gravitational landscape due to the dark matter field which started structuring itself much earlier (at matter-radiation equality, essentially). Consequently, accretion on filaments is very different in the Universe early on vs at late times. Late filaments may be seen as the intersection of several walls or sheets, along which matter flows onto the filaments (e.g. Cautun et al., 2014). Late filaments are thus fed with matter in a much more anisotropic manner than early ones. That may induce azimuthal flows because the walls that feed them do not intersect edge-on but have a relative non zero impact parameter. In addition, we expect longitudinal flows along late filaments due to the gravitational attraction of the clusters they interconnect. Typically, we may expect flows to be essentially azimuthal in the middle of filaments where the attraction of clusters at both ends roughly balances, while they would be longitudinal in the vicinity of each cluster. I think that this will be a very important element to take into account in the modeling of structure formation.

Formally, how does the spectral problem change when including flows? The book by Goedbloed et al. (2010) is dedicated to this question. Here are briefly the key points that change with respect to the static case. Firstly, with flow the equilibrium states are different from those presented in chapter 6. But most interestingly, while stationary equilibria require more equations to be satisfied than the simple hydrostatic and Poisson equations of the static case, more solutions are permitted because there is then more freedom in the choice of the density, pressure and magnetic field profiles[1]. Secondly, the presence of a background flow also radically modifies the behaviour of perturbations. The most important additional features are that the eigenfrequencies are Doppler shifted, the Kelvin-Helmoltz instability may now arise and, in the presence of geometrical curvature effects, the centrifugal acceleration plays a major role. The crucial point is that the very simple relation (7.22) between $\vec{v}_1$ and $\vec{\xi}$ does not hold anymore, and now involves the background flow velocity. This is intuitively clear since the perturbed flow differs from the unperturbed one, as illustrated in figure 7.3. The consequence of this is that the general vector eigenvalue problem (7.28), at the heart of the present study, now has the following form, first derived by Frieman & Rotenberg (1960):

$$\vec{G}(\hat{\xi}) - 2\omega U\hat{\xi} + \omega^2\rho_0\hat{\xi} = \vec{0} \tag{10.1}$$

where the generalized force operator is such that

$$\vec{G}(\hat{\xi}) \equiv \vec{F}(\hat{\xi}) + \vec{\nabla}\cdot(\hat{\xi}\rho_0\vec{v}_0\cdot\vec{\nabla}\vec{v}_0 - \rho_0\vec{v}_0\vec{v}_0\cdot\vec{\nabla}\hat{\xi}) \tag{10.2}$$

where $\vec{F}$ is the force operator of the static case, and the Doppler-Coriolis shift operator is

$$U \equiv -i\rho_0\vec{v}_0\cdot\vec{\nabla} \quad . \tag{10.3}$$

As expected, we recover the static spectral equation (7.28) in the absence of background flow ($\vec{v}_0 = \vec{0}$). As we have seen in this manuscript, taking gravity fully into account greatly complexifies the analysis, but what keeps things relatively simple still is that the force operator is self-adjoint, and thus the eigenvalues are real. The important point is that here $\rho_0^{-1}\vec{G}$ and $\rho_0^{-1}U$ are also *self-adjoint* (for appropriate choices of boundary conditions), *but* the eigenvalue problem does not only involve $\omega^2$ linearly as in the static case, but it now involves $\omega$ *non-linearly*. This is what makes the eigenvalues $\omega$ *complex*. The spectrum is thus not restricted to the simple real axis anymore, but spans regions in the $(\Re(\omega), \Im(\omega))$ plane. However, it turns out that the eigenvalues cannot be in arbitrary places in the complex plane, but lie on well defined particular locations, called paths. The continuous spectra belong to the paths, and monotonicity theorems for the discrete spectrum, generalizing the Goedbloed-Sakanaka theorem presented in chapter 7, are proven to exist along those paths. Thanks to these studies, we now have a deep understanding of the MHD spectral problem including stationary flows as in the static case detailed in chapter 7. Note however that this is still an active field of research among plasma physicists themselves. For example the authors in Goedbloed et al. (2010) point out that 'Surprisingly [...] this more general theory [including background flow] remains underdeveloped', and they fight against the current and common misconception that if the spectrum is complex it is because the operator governing the spectral problem is *not* self-adjoint, while in fact, as I just mentioned, the operators are still self-adjoint, but the key is that the eigenproblem in $\omega$ is quadratic[2]. Also, finally, most of the literature treats 'only' stationary flows. A more general theory is yet to come.

These studies were performed in the Cowling approximation. An important step forward will be now to generalize these very powerful tools to study gravitational instability including flows to assess the possibility

[1] It may seem paradoxical that adding a constraint increases the number of solutions. A nice analogy to convince ourselves that this is indeed not necessarily the case is the following. Instead of one ball on a hill as in figure 7.4, consider two balls on opposite sides of the hill. As such, the balls roll down the hill, so that this is clearly not a stable equilibrium. However, if the two balls are attached together by a wire, i.e. we add a constraint, then an infinite number of stable solutions now exist.

[2] See also details and discussion in Goedbloed (2011).

of clumps forming along the cosmic web. It will be very interesting and important to then compare these with works dealing with similar problems such as Welter (1982) for instance who examines gravitational instabilities in shock-compressed gas layers.

**Turbulence, dissipation, thermal instability, etc.** – Modeling structure formation is an almost endless, fascinating game, but energetic considerations are too essential to be left aside. For example, another important feature that should be discussed in terms of epochs is the gas temperature and metallicity. It is crucial as it governs the existing radiative cooling channels so that cooling efficiency varies a lot with redshift. Hence, fragmentation by thermal instability, which we know is crucial in interstellar environments, will greatly vary in relevance, efficiency and size of subsequent clumps from one cosmological epoch to another (e.g. pre-reionization vs post-reionization). I think that delving into these energy considerations is important, but probably at a second stage, once the ingredients evoked above are already taken into account properly. As a hint on how to take into account dissipative effects, we may turn once again to the book of Goedbloed et al. (2010) which shows how to incorporate resistivity in the spectral analysis.

**More references.** – Two authors, other than Goedbloed & Poedts (2004) and Goedbloed et al. (2010), that really tackle the question of the Mathematics of the spectrum of adiabatic oscillations are M. Takata and H. R. Beyer (we mentioned the latter in section 7.2.3). For instance, Takata (2012) explores the spectrum with an approach adapted from geoseismology using wedge products. However these authors focus on stars, i.e. spherically symmetric objects, thus working with spherical harmonics, and do not discuss gravitational instability with their viewpoints.

**More analogies.** – On physical grounds, analogies between the IGM and the ISM are paramount because the physics of these environments is fundamentally the same. From the formal point of view, it is now clear that the parallel between linearized ideal MHD and Quantum Mechanics, both dealing with finding the spectrum of linear self-adjoint operators in Hilbert spaces, is extremely fruitful (Goedbloed & Poedts, 2004). For the question of gravitational fragmentation, I would add three analogies that I think should be worth exploring: *(i) Electrostatics:* The formal analogy between electrostatics and gravity is well known. The only fundamental difference between them is that pure dipole or quadrupole gravitational potentials cannot arise as in the electrostatic case since there is no gravitational analogue of negative charge (e.g. Binney & Tremaine, 2008). However, as far as perturbations are concerned, the density field entering the Poisson equation is $\rho_1$ which *can* be negative in contrast to the density $\rho_0$. Therefore, this analogy may be extremely fruitful to build up intuition on how perturbations evolve, and also to use all the formal tools developed in this field, or even maybe to build up an experimental set up where gravity is modeled by electric fields. There is no screening effect for gravitation since mass is positvie, while having two oppositely charged species in plasmas gives rise to the concept of Debye length, so could it be relevant and useful to define a gravitational Debye length in the evolution of perturbations? *(ii) Peridynamics:* As briefly mentioned in section 7.3, a field from which I believe a lot can be learnt is the peridynamics theory, which has its roots in studies of elasticity. Indeed, it deals with integral equations and non local wave equations, so that a lot of formal tools relevant for wave equations like (7.58) governing $\vec{\xi}$ or (9.14) governing $\rho_1$ could be transferred. *(iii) Quantum to Classical transition:* The fundamental constant $\hbar$ 'monitors the power' of quantum effects in quantum theory, in the sense that one recovers classical mechanics when taking the formal limit $\hbar \to 0$ of quantum mechanics, i.e. the Hamilton-Jacobi equation from the Schrödinger equation. Now since in the force operator (7.57) the parameter $4\pi G$ is in factor of the gravitational terms, it may be enlightening, or at least interesting, to look at pressure waves as the 'classical' limit of the full regime, the combination of the Cowling and Jeans terms giving rise to the 'quantum' regime, in which the effects due to the fundamental constant $4\pi G$ become important. Beyond a mere curiosity, this idea can be interesting in practice, by looking for solutions of the propagation of acoustic waves in the WKB form[3] using $4\pi G$ as $\hbar$ when studying the quantum to classical transition.

So far I have presented ideas of extensions to the work presented in part II only. For the problematic of the origin of cosmological magnetic fields of part I, I foresee the following.

**Evolution of Cosmological Magnetic Fields.** – As we have seen in chapter 3, most magnetogenesis models operate very early in the History of the Universe. But in order to compare predictions with observations we need to model properly the evolution of those fields once generated, beyond a simple dilution $B \propto a^{-2}$ due to the expansion as presented in chapter 2. As we have seen in chapter 2, cosmological magnetic fields are frozen-in in the cosmological plasma. This is actually the basic reason why it is difficult to generate a large scale magnetic field, but it also has two interesting consequences in our problem: firstly, once

[3] I here mean the genuine WKB approach for finding approximate solutions to a differential equation for which the highest order term contains a small parameter, not the WKB-type dispersion relations discuted in the previous chapter.

a magnetic field is created we know that it will not disappear by diffusion, and secondly, since the magnetic fields will be following the fate of matter, the study of the evolution of magnetic fields can be reduced in great part to the study of the evolution of matter throughout the large scale structure formation. Having said that, the evolution of matter is already complex, therefore computing the evolution of cosmic magnetic fields will not be an easy task, but at least we have a solid track to follow. Concretely speaking, the induction equation (2.16) governs the evolution of magnetic fields in a given velocity field $\vec{v}$. Taking the latter to be the cosmological velocity field, this gives us the means to link the statistical properties of cosmological magnetic fields to those of the flows at the largest scales given by the Standard Model of Cosmology. Also, it may be necessary to decompose this work in epochs, scales and geometries, similarly to what we have done in the present manuscript, and treat the linear and non-linear regimes separately.

What is certain is that there is still a lot of rich science to be explored at this level. In fact, it might be necessary to refine the description of the IGM. Indeed, because of its low collisionality, the MHD model may not be the most appropriate (e.g. Falceta-Gonçalves & Kowal, 2015). Alternatives to this description exist. For example Freidberg (2014) presents two of them (in the context of tokamaks): kinetic MHD, which is the most reliable and physically motivated description but it is particularly difficult to manipulate, and the double adiabatic MHD (the so-called Chew-Goldberger-Low approximation, Chew et al., 1956), a *collisionless fluid* model, which is much more tractable, but that is unfortunately not physically motivated. In his book, Freidberg shows that, in a sense, the ideal MHD and the double adiabatic models are two fluid models which bracket the most difficult kinetic MHD model (cf. e.g. MHD stability comparison theorems in his section 10.6). This justifies the importance of studying ideal MHD and double adiabatic MHD, despite their (relative) simplicity.

All in all, there is still a lot of fascinating physics within reach. On the one hand, these researches will help us better understand what numerical astrophysicists and cosmologists call the subgrid physics, and take into account in effective and realistic ways these complicated effects still unreachable numerically because of the necessarily limited dynamical ranges. On the other hand, this study is relevant and essential both for high and low redshift environments. For lower redshifts and large scales, aside from giving us clues as to how fresh matter is funnelled into galaxies and galaxy clusters to sustain their star formation activity accross cosmic times, it will provide valuable hints on how intergalactic gas and magnetic fields are distributed in the cosmic web in the prospect of future telescopes like *Athena* (its current science working group 1.4 is dedicated to "the missing baryons and the warm-hot intergalactic medium") and the SKA (it will be the first telescope capable of directly mapping the IGM gas in the cosmic web, see e.g. Wilcots, 2004, and the origin of cosmic magnetic fields is one of its main drivers, as stressed by the activities of its "Cosmic Magnetism" science working group). For higher redshifts and smaller scales, it will help us understand whether the pristine IGM was prone to fragmentation, and enable us to determine the state of matter (size of clumps, their temperature, density, etc.) as it fell into the forming core of protogalaxies which is crucial to determine their subsequent evolution. Such information on the local physics of the first stars and first galaxies will then bring valuable insight to the modeling of the Epoch of Reionization itself.

# Bibliography


Al-Gwaiz, M. A. 2008, Sturm-Liouville Theory and its Applications (London: Springer)

Alonso, D., Salvador, A. I., Sanchez, F. J., et al. 2015, Monthly Notices of the Royal Astronomical Society, 449, 670

Ando, M., Doi, K., & Susa, H. 2010, The Astrophysical Journal, 716, 1566

André, P. 2015, in Lessons from the Local Group, ed. K. Freeman, B. Elmegreen, D. Block, & M. Woolway (Cham: Springer International Publishing), 73–83

André, P., Di Francesco, J., Ward-Thompson, D., et al. 2014, in Protostars and Planets VI, ed. T. H. H. Beuther, R. Klessen, C. Dullemond (University of Arizona Press), 27–52

Angrick, C., & Bartelmann, M. 2010, Astronomy and Astrophysics, 518, 9

Aslangul, C. 2011, Des mathématiques pour les sciences - Concepts, méthodes et techniques pour la modélisation, Collection Licence Maîtrise Doctorat (De Boeck)

Aubert, D., Deparis, N., & Ocvirk, P. 2015, Monthly Notices of the Royal Astronomical Society, 454, 1012

Balbinski, E. 1984, Monthly Notices of the Royal Astronomical Society, 209, 145

Bally, J., Langer, W. D., Stark, A. A., & Wilson, R. W. 1987, The Astrophysical Journal, 312, L45

Barrau, A., & Grain, J. 2011, Relativité générale – Cours et exercices corrigés (Dunod)

Barston, E. M. 1964, Annals of Physics, 29, 282

Beck, A. M., Hanasz, M., Lesch, H., Remus, R.-S., & Stasyszyn, F. A. 2013, Monthly Notices of the Royal Astronomical Society, 429, L60

Beck, R. 2011, in 25th Texas Symposium on Relativistic Astrophysics (Texas 2010), ed. F. A. Aharonian, W. Hofmann, & F. M. Rieger, AIP Conference Proceedings, 117–136

Bender, C. M., & Orszag, S. A. 1978, Advanced Mathematical Methods for Scientists and Engineers (McGraw-Hill)

Bernardeau, F. 2007, Cosmologie: des fondements théoriques aux observations, Savoir actuels (EDP Sciences)

Bernet, M. L., Miniati, F., Lilly, S. J., Kronberg, P. P., & Dessauges-Zavadsky, M. 2008, Nature, 454, 302

Bernstein, I. B., Frieman, E. A., Kruskal, M. D., & Kulsrud, R. M. 1958, Proceedings of the Royal Society of London Series A, 244, 17

Bertone, S., Vogt, C., & Enßlin, T. 2006, Monthly Notices of the Royal Astronomical Society, 370, 319

Beyer, H. R. 1995, Journal of Mathematical Physics, 36, 4792

Beyer, H. R., Aksoylu, B., & Celiker, F. 2016, Journal of Mathematical Physics, 57, 062902

Beyer, H. R., & Schmidt, B. G. 1995, Astronomy and Astrophysics, 296, 722

Biermann, L. 1950, Zeitschrift für Naturforschung A, 5, 65

Binney, J., & Tremaine, S. 2008, Galactic dynamics, 2nd edn. (Princeton University Press)

Blokland, J. W. S., van der Swaluw, E., Keppens, R., & Goedbloed, J. P. 2005, Astronomy and Astrophysics, 444, 337

Bonafede, A., Vazza, F., Bruggen, M., et al. 2013, Monthly Notices of the Royal Astronomical Society, 433, 3208

Bourke, T. L., Braun, R., Fender, R., et al., eds. 2015, Advancing Astrophysics with the Square Kilometre Array – Vol. I (Dolman Scott Ltd for SKA Organisation), available at https://www.skatelescope.org/books/

Brandenburg, A., & Subramanian, K. 2005, Physics Reports, 417, 1

Breysse, P. C., Kamionkowski, M., & Benson, A. 2014, Monthly Notices of the Royal Astronomical Society, 437, 2675

Bromm, V. 2013, Reports on Progress in Physics, 76, 112901

Brüggen, M. 2013, Astronomische Nachrichten, 334, 543

Burkert, A., & Hartmann, L. 2004, The Astrophysical Journal, 616, 288

Carilli, C., & Barthel, P. 1996, Astronomy and Astrophysics Review, 7, 1

Carilli, C. L., & Taylor, G. B. 2002, Annual Review of Astronomy and Astrophysics, 40, 319

Cautun, M., van de Weygaert, R., Jones, B. J. T., & Frenk, C. S. 2014, Monthly Notices of the Royal Astronomical Society, 441, 2923

Chabrier, G., ed. 2009, Structure Formation in Astrophysics (Cambridge University Press)

Chandran, B. D., & Dennis, T. J. 2006, The Astrophysical Journal, 642, 140

Chandrasekhar, S., & Fermi, E. 1953, The Astrophysical Journal, 118, 116

Chew, G. F., Goldberger, M. L., & Low, F. E. 1956, Proceedings of the Royal Society A: Mathematical, Physical and Engineering Sciences, 236, 112

Chuzhoy, L. 2004, Monthly Notices of the Royal Astronomical Society, 350, 761

Cole, S., Percival, W. J., Peacock, J. A., et al. 2005, Monthly Notices of the Royal Astronomical Society, 362, 505

Cowling, T. G. 1941, Monthly Notices of the Royal Astronomical Society, 101, 367

Cox, J. P. 1980, Theory of stellar pulsation (Princeton University Press)

Daly, R. A., & Loeb, A. 1990, The Astrophysical Journal, 364, 451

Dekel, A., Sari, R., & Ceverino, D. 2009a, The Astrophysical Journal, 703, 785

Dekel, A., Birnboim, Y., Engel, G., et al. 2009b, Nature, 457, 451

Dodelson, S. 2003, Modern Cosmology (Academic Press)

Doi, K., & Susa, H. 2011, The Astrophysical Journal, 741, 93

Dolag, K., Bartelmann, M., & Lesch, H. 2002, Astronomy and Astrophysics, 387, 383

Donnert, J., Dolag, K., Lesch, H., & Müller, E. 2009, Monthly Notices of the Royal Astronomical Society, 392, 1008

Durrer, R., & Neronov, A. 2013, The Astronomy and Astrophysics Review, 21

Durrive, J.-B., & Aubert, D. 2016, in preparation, Astronomy and Astrophysics

Durrive, J.-B., & Langer, M. 2015, Monthly Notices of the Royal Astronomical Society, 453, 345

Durrive, J.-B., & Langer, M. 2016, to be submitted, Astronomy and Astrophysics

Durrive, J.-B., Tashiro, H., Langer, M., & Sugiyama, N. 2016, to be submitted, Astronomy and Astrophysics

Eckert, D., Jauzac, M., Shan, H., et al. 2015, Nature, 528, 105

Elmegreen, B. G., & Elmegreen, D. M. 1978, The Astrophysical Journal, 220, 1051

Ensslin, T. A., Biermann, P. L., Kronberg, P. P., & Wu, X.-P. 1997, The Astrophysical Journal, 477, 560

Falceta-Gonçalves, D., & Kowal, G. 2015, The Astrophysical Journal, 808, 65

Federrath, C. 2016, Monthly Notices of the Royal Astronomical Society, 457, 375

Fenu, E., Pitrou, C., & Maartens, R. 2011, Monthly Notices of the Royal Astronomical Society, 414, 2354

Feretti, L., Giovannini, G., Govoni, F., & Murgia, M. 2012, The Astronomy and Astrophysics Review, 20, 54

Fialkov, A. 2014, International Journal of Modern Physics D, 23, 1430017

Fletcher, A. 2010, in ASP Conference Series, Vol. 438, The Dynamic Interstellar Medium: A Celebration of the Canadian Galactic Plane Survey, ed. R. Kothes, T. L. Landecker, & A. G. Willis (Astronomical Society of the Pacific), 197–210

Fletcher, A., Beck, R., Shukurov, A., Berkhuijsen, E. M., & Horellou, C. 2011, Monthly Notices of the Royal Astronomical Society, 412, 2396

Freidberg, J. P. 2014, Ideal MHD (Cambridge University Press)

Freundlich, J., Jog, C. J., & Combes, F. 2014a, Astronomy and Astrophysics, 564, A7

Freundlich, J., Jog, C. J., Combes, F., & Anathpindika, S. 2014b, in SF2A-2014: Proceedings of the Annual meeting of the French Society of Astronomy and Astrophysics, ed. J. Ballet, F. Martins, F. Bournaud, R. Monier, & C. Reylé (Société Française d'Astronomie et d'Astrophysique), 325–328

Fridman, A. M., & Polyachenko, V. L. 1984a, Physics of Gravitating Systems I (Berlin, Heidelberg: Springer Berlin Heidelberg)

—. 1984b, Physics of Gravitating Systems II (Berlin, Heidelberg: Springer Berlin Heidelberg)

Frieman, E., & Rotenberg, M. 1960, Reviews of Modern Physics, 32, 898

Furlanetto, S. R., & Loeb, A. 2001, The Astrophysical Journal, 556, 619

Furlanetto, S. R., Zaldarriaga, M., & Hernquist, L. 2004, The Astrophysical Journal, 613, 1

Gheller, C., Vazza, F., Favre, J., & Brüggen, M. 2015, Monthly Notices of the Royal Astronomical Society, 453, 1164

Gnedin, N. Y., Ferrara, A., & Zweibel, E. G. 2000, The Astrophysical Journal, 539, 505

Goedbloed, H. 2011, Magnetohydrodynamic Spectroscopy: Unraveling the dynamics of plasma on all scales from the laboratory to the Universe, oral presentation at the workshop "Advanced Magnetohydrodynamics" held at the Lorentz Center, 11–15 April, slides available on-line at https://www.lorentzcenter.nl/lc/web/2011/441/info.php3?wsid=441

Goedbloed, J. P. 1971, Physica, 53, 412

—. 1984, Physica D Nonlinear Phenomena, 12, 107

Goedbloed, J. P., Keppens, R., & Poedts, S. 2010, Advanced Magnetohydrodynamics (Cambridge University Press)

Goedbloed, J. P., & Sakanaka, P. H. 1974, Physics of Fluids, 17, 908

Goedbloed, J. P. H., & Poedts, S. 2004, Principles of Magnetohydrodynamics (Cambridge University Press)

Goldreich, P., & Lynden-Bell, D. 1965, Monthly Notices of the Royal Astronomical Society, 130, 97

Goldstein, H. 1980, Classical mechanics, 2nd edn., Addison-Wesley series in Physics (Addison-Wesley)

Gough, D. O., Leibacher, J. W., Scherrer, P. H., & Toomre, J. 1996, Science, 272, 1281

Govoni, F., & Feretti, L. 2004, International Journal of Modern Physics D, 13, 43

Govoni, F., Murgia, M., Feretti, L., et al. 2005, Astronomy and Astrophysics, 430, L5

Grasso, D., & Rubinstein, H. R. 2001, Physics Reports, 348, 163

Greif, T. H., Johnson, J. L., Klessen, R. S., & Bromm, V. 2008, Monthly Notices of the Royal Astronomical Society, 387, 1021

Gupta, H., Rathor, S., Pessah, M., & Chakraborty, S. 2016, Physics Letters A, 380, 2407

Hain, K., & Lüst, R. 1958, Zeitschrift für Naturforschung A, 13, 936

Hale, G. E. 1908, The Astrophysical Journal, 28, 315

Harford, A. G., & Hamilton, A. J. S. 2011, Monthly Notices of the Royal Astronomical Society, 416, 2678

Harrison, E. R. 1970, Monthly Notices of the Royal Astronomical Society, 147, 279

Hartmann, L. 2002, The Astrophysical Journal, 578, 914

Hasan, S. S., & Sobouti, Y. 1987, Monthly Notices of the Royal Astronomical Society, 228, 427

Haverkorn, M. 2015, in Magnetic Fields in Diffuse Media, ed. A. Lazarian, E. M. de Gouveia Dal Pino, & C. Melioli, Astrophysics and Space Science Library (Springer Berlin Heidelberg), 483–506

Hayes, M., Schaerer, D., Östlin, G., et al. 2011, The Astrophysical Journal, 730, 8

Hjorth, J., Williams, L. L. R., Wojtak, R., & McLaughlin, M. 2015, The Astrophysical Journal, 811, 2

Hobbs, A., Read, J., Power, C., & Cole, D. 2013, Monthly Notices of the Royal Astronomical Society, 434, 1849

Hobbs, A., Read, J. I., Agertz, O., Iannuzzi, F., & Power, C. 2016, Monthly Notices of the Royal Astronomical Society, 458, 468

Hogg, D. W., Eisenstein, D. J., Blanton, M. R., et al. 2005, The Astrophysical Journal, 624, 54

Holmes, M. H. 2013, Texts in Applied Mathematics, Vol. 20, Introduction to Perturbation Methods (Springer New York)

Horedt, G. P. 2004, Astrophysics and Space Science Library, Vol. 306, Polytropes - Applications in Astrophysics and Related Fields (Kluwer Academic Publishers)

Hoyle, F., & Ireland, J. G. 1960, Monthly Notices of the Royal Astronomical Society, 120, 173

İbanoğlu, C., ed. 2000, Variable Stars as Essential Astrophysical Tools, NATO Advanced Science Institutes (ASI) Series C (Dordrecht: Springer Netherlands)

Iwata, I., Inoue, A. K., Matsuda, Y., et al. 2009, The Astrophysical Journal, 692, 1287

Jeans, J. H. 1902, Philosophical Transactions of the Royal Society A: Mathematical, Physical and Engineering Sciences, 199, 1

Kalberla, P. M. W., Kerp, J., Haud, U., et al. 2016, The Astrophysical Journal, 821, 117

Kellman, S. A. 1972, The Astrophysical Journal, 175, 363

—. 1973, The Astrophysical Journal, 179, 103

Kemp, J. C. 1982, Publications of the Astronomical Society of the Pacific, 94, 627

Keppens, R., van der Linden, R. A. M., & Goossens, M. 1993, Sol. Phys., 144, 267

Kereš, D., & Hernquist, L. 2009, The Astrophysical Journal, 700, L1

Kereš, D., Katz, N., Fardal, M., Davé, R., & Weinberg, D. H. 2009, Monthly Notices of the Royal Astronomical Society, 395, 160

Kim, E.-J., Olinto, A. V., & Rosner, R. 1996, The Astrophysical Journal, 468, 28

Klar, J. S., & Mücket, J. P. 2010, Astronomy and Astrophysics, 522, A114

Klypin, A. A., & Shandarin, S. F. 1983, Monthly Notices of the Royal Astronomical Society, 204, 891

Krall, N. A., & Trivelpiece, A. W. 1973, Principles of plasma physics, International Series in Pure and Applied Physics (McGraw-Hill)

Kronberg, P. P. 1994, Reports on Progress in Physics, 57, 325

Kronberg, P. P., Lesch, H., & Hopp, U. 1999, The Astrophysical Journal, 511, 56

Kulsrud, R. M. 2005, Plasma physics for astrophysics, Princeton series in astrophysics (Princeton University Press)

Kulsrud, R. M., Cen, R., Ostriker, J. P., & Ryu, D. 1997, The Astrophysical Journal, 480, 481

Kulsrud, R. M., & Zweibel, E. G. 2008, Reports on Progress in Physics, 71, 046901

Lacey, C. G. 1989, The Astrophysical Journal, 336, 612

Landau, L. 1946, Журнал Экспериментальной и Теоретической Физики, 16, 574, english translation by E. Lifshitz in Journal of Physics (Academy of Sciences of the USSR), 1946, 10, 25.

Langer, M., Aghanim, N., & Puget, J.-L. 2005, Astronomy and Astrophysics, 443, 367

Langer, M., Puget, J.-L., & Aghanim, N. 2003, Physical Review D, 67, 1

Langer, W. D. 1978, The Astrophysical Journal, 225, 95

Ledoux, P. 1950, in IIIe Congrès national des sciences, Bruxelles, 30 mai - 3 juin 1950, Vol. 2 (Liège: Desoer), 133–136

Ledoux, P. 1951, Annales d'Astrophysique, 14, 438

Ledoux, P., & Walraven, T. 1958, in Encyclopedia of Physics / Handbuch der Physik, Vol. 11 / 51, Astrophysics II: Stellar Structure / Astrophysik II: Sternaufbau (Springer Berlin Heidelberg), 353–604

Lequeux, J., Falgarone, E., & Ryter, C. 2005, The Interstellar Medium, Astronomy and Astrophysics Library (Berlin/Heidelberg: Springer-Verlag)

Lifschitz, A. E. 1989, Developments in Electromagnetic Theory and Applications, Vol. 4, Magnetohydrodynamics and Spectral Theory (Dordrecht: Springer Netherlands)

Loeb, A. 2010, How did the first stars and galaxies form? (Princeton University Press)

Loeb, A., & Furlanetto, S. R. 2013, The First Galaxies in the Universe, Princeton Series in Astrophysics (Princeton University Press)

Lyth, D. H., & Liddle, A. R. 2009, The Primordial Density Perturbation – Cosmology, Inflation and the Origin of Structure (Cambridge University Press)

Marinacci, F., Vogelsberger, M., Mocz, P., & Pakmor, R. 2015, Monthly Notices of the Royal Astronomical Society, 453, 3999

Medvedev, M. V., Silva, L. O., & Kamionkowski, M. 2006, The Astrophysical Journal, 642, L1

Mellema, G., Iliev, I. T., Pen, U. L., & Shapiro, P. R. 2006, Monthly Notices of the Royal Astronomical Society, 372, 679

Merritt, D., Graham, A. W., Moore, B., Diemand, J., & Terzić, B. 2006, The Astronomical Journal, 132, 2685

Mesinger, A., ed. 2016, Astrophysics and Space Science Library, Vol. 423, Understanding the Epoch of Cosmic Reionization (Cham: Springer International Publishing)

Mishustin, I. N., & Ruzmaĭkin, A. A. 1972, Soviet Journal of Experimental and Theoretical Physics, 34, 233

Mitchell, N. L., Vorobyov, E. I., & Hensler, G. 2013, Monthly Notices of the Royal Astronomical Society, 428, 2674

Miville-Deschênes, M.-A., Martin, P. G., Abergel, A., et al. 2010, Astronomy and Astrophysics, 518, L104

Miyama, S. M., Narita, S., & Hayashi, C. 1987a, Progress of Theoretical Physics, 78, 1051

—. 1987b, Progress of Theoretical Physics, 78, 1273

Mizuno, A., Onishi, T., Yonekura, Y., et al. 1995, The Astrophysical Journal, 445, L161

Mo, H., van den Bosch, F. C., & White, S. D. M. 2010, Galaxy Formation and Evolution (Cambridge University Press)

Myers, P. C. 2009, The Astrophysical Journal, 700, 1609

Nakano, T. 1988, Publications of the Astronomical Society of Japan, 40, 593

Nakano, T., & Nakamura, T. 1978, Publications of the Astronomical Society of Japan, 30, 671

Nandra, K., Barret, D., Barcons, X., et al. 2014, *Athena* : The Advanced Telescope for High-Energy Astrophysics, mission proposal summarising The Hot and Energetic Universe science theme, available on-line at http://www.the-athena-x-ray-observatory.eu

Narita, S., Miyama, S. M., Kiguchi, M., & Hayashi, C. 1988, Progress of Theoretical Physics Supplement, 96, 63

Navarro, J. F., Frenk, C. S., & White, S. D. M. 1996, The Astrophysical Journal, 462, 563

Nelson, D., Vogelsberger, M., Genel, S., et al. 2013, Monthly Notices of the Royal Astronomical Society, 429, 3353

Neronov, A., & Vovk, I. 2010, Science, 328, 73

Ostriker, J. 1964a, The Astrophysical Journal, 140, 1529

—. 1964b, The Astrophysical Journal, 140, 1056

Peacock, J. A. 1999, Cosmological Physics (Cambridge University Press)

Peebles, P. J. E. 1980, The large-scale structure of the universe (Princeton University Press)

Peebles, P. J. E. 1993, Principles of Physical Cosmology (Princeton University Press)

Pekeris, C. L. 1938, The Astrophysical Journal, 88, 189

Percival, W. J., Baugh, C. M., Bland-Hawthorn, J., et al. 2001, Monthly Notices of the Royal Astronomical Society, 327, 1297

Peter, P., & Uzan, J. 2013, Primordial Cosmology, 2nd edn., Oxford graduate texts (Oxford University Press)

Petit, P., Jardine, M., & Spruit, H. C., eds. 2014, Magnetic Fields throughout Stellar Evolution (IAU Symposium 302), Proceedings of the International Astronomical Union Symposia and Colloquia (Cambridge University Press)

Planck Collaboration. 2013, Astronomy and Astrophysics, 550, A134

—. 2015a, arXiv:1502.01582, accepted in Astronomy and Astrophysics

—. 2015b, arXiv:1502.01589, accepted in Astronomy and Astrophysics

—. 2015c, arXiv:1502.01594, accepted in Astronomy and Astrophysics

—. 2016, arXiv:1605.03507, accepted in Astronomy and Astrophysics

Press, W. H., & Schechter, P. 1974, The Astrophysical Journal, 187, 425

Priest, E. 2014, Magnetohydrodynamics of the Sun (Cambridge University Press)

Pudritz, R. E., & Kevlahan, N. K.-R. 2013, Philosophical Transactions of the Royal Society A: Mathematical, Physical and Engineering Sciences, 371, 20120248

Pudritz, R. E., & Silk, J. 1989, The Astrophysical Journal, 342, 650

Ramond, P. 2015, Research project report, Magistère de Physique Fondamentale – Université Paris-Sud, Orsay

Rees, M. J. 1987, Quarterly Journal of the Royal Astronomical Society, 28, 197

Rybicki, G. B., & Lightman, A. P. 1986, Radiative Processes in Astrophysics (Wiley), 400

Ryu, D., Kang, H., Hallman, E., & Jones, T. W. 2003, The Astrophysical Journal, 593, 599

Ryu, D., Schleicher, D. R. G., Treumann, R. A., Tsagas, C. G., & Widrow, L. M. 2011, Space Science Reviews, 166, 1

Safronov, V. S. 1960, Annales d'Astrophysique, 23, 979

Saga, S., Ichiki, K., Takahashi, K., & Sugiyama, N. 2015, Physical Review D, 91, 123510

Sánchez Almeida, J., Elmegreen, B. G., Muñoz-Tuñón, C., & Elmegreen, D. M. 2014, The Astronomy and Astrophysics Review, 22, 71

Schlickeiser, R., & Shukla, P. K. 2003, The Astrophysical Journal, 599, L57

Schneider, A., Krauss, L., & Moore, B. 2010, Physical Review D, 82, 063525

Schneider, R. 2012, in AIP Conference Proceedings, Vol. 1480, First Stars IV – From Hayashi to the future, ed. M. Umemura & K. Omukai (American Institute of Physics), 105–112

Schneider, S., & Elmegreen, B. G. 1979, Astrophysical Journal, Supplement Series, 41, 87

Sedláček, Z. 1971, Journal of Plasma Physics, 5, 239

Shaw, J. R., & Lewis, A. 2012, Physical Review D, 86, 043510

Shen, J., Abel, T., Mo, H. J., & Sheth, R. K. 2006, The Astrophysical Journal, 645, 783

Sheth, R. K., Mo, H. J., & Tormen, G. 2001, Monthly Notices of the Royal Astronomical Society, 323, 1

Shiromoto, Y., Susa, H., & Hosokawa, T. 2014, The Astrophysical Journal, 782, 108

Shu, F. H. 1991, The physics of astrophysics. Volume I: Radiation. (University Science Books)

—. 1992, The physics of astrophysics. Volume II: Gas dynamics. (University Science Books)

Silk, J., & Langer, M. 2006, Monthly Notices of the Royal Astronomical Society, 371, 444

Simon, R. 1965a, Annales d'Astrophysique, 28, 625

—. 1965b, Annales d'Astrophysique, 28, 40

Smeyers, P., & Van Hoolst, T. 2010, Astrophysics and Space Science Library, Vol. 371, Linear Isentropic Oscillations of Stars (Berlin, Heidelberg: Springer Berlin Heidelberg)

Sommerfeld, A., & Schur, G. 1930, Annalen der Physik, 396, 409

Springel, V. 2010, Monthly Notices of the Royal Astronomical Society, 401, 791

Springel, V., White, S. D. M., Jenkins, A., et al. 2005, Nature, 435, 629

Strittmatter, P. A. 1966, Monthly Notices of the Royal Astronomical Society, 132, 359

Subramanian, K. 2016, Reports on Progress in Physics, 79, 076901

Subramanian, K., Narasimha, D., & Chitre, S. M. 1994, Monthly Notices of the Royal Astronomical Society, 271, L15

Suydam, B. R. 1958, in Proceedings of the second United Nations international conference on the peaceful uses of atomic energy, Vol. 31 (Geneva: United Nations Publications), 157–159

Takahashi, K., Mori, M., Ichiki, K., & Inoue, S. 2012, The Astrophysical Journal, 744, L7

Takata, M. 2012, in Astronomical Society of the Pacific Conference Series, Vol. 462, Progress in Solar/Stellar Physics with Helio- and Asteroseismology, ed. H. Shibahashi, M. Takata, & A. E. Lynas-Gray, 412

Tashiro, H., & Sugiyama, N. 2006, Monthly Notices of the Royal Astronomical Society, 368, 965

Taylor, A. M., Vovk, I., & Neronov, A. 2011, Astronomy and Astrophysics, 529, A144

Thompson, M. J. 2006, An introduction to astrophysical fluid dynamics (London: Imperial College Press)

Tomisaka, K., & Ikeuchi, S. 1983, Publications of the Astronomical Society of Japan, 35, 187

Tracy, C. A. 2016, Lectures on Differential Equations, lecture notes, Creative Commons license (University of California, Davis)

Tseliakhovich, D., & Hirata, C. 2010, Physical Review D, 82, 083520

Vallée, J. P. 1990, Astronomy and Astrophysics, 239, 57

—. 2011, New Astronomy Reviews, 55, 91

Van de Weygaert, R., & Bond, J. R. 2008, in Lecture Notes in Physics, ed. M. Plionis, D. Hughes, & O. López-Cruz, Vol. 740 (Springer), 409–467

Van Kampen, N. G. 1955, Physica, 21, 949

Vazza, F., Ferrari, C., Brüggen, M., et al. 2015, Astronomy & Astrophysics, 580, A119

Venumadhav, T., Oklopčić, A., Gluscevic, V., Mishra, A., & Hirata, C. M. 2014, arXiv:1410.2250

Wadekar, D., & Hansen, S. H. 2015, Monthly Notices of the Royal Astronomical Society, 447, 1333

Wasserman, I. 1978, The Astrophysical Journal, 224, 337

Weibel, E. S. 1959, Physical Review Letters, 2, 83

Welter, G. L. 1982, Astronomy and Astrophysics, 105, 237

Widrow, L. M. 2002, Reviews of Modern Physics, 74, 775

Widrow, L. M., Ryu, D., Schleicher, D. R. G., et al. 2012, Space Science Reviews, 166, 37

Wilcots, E. 2004, New Astronomy Reviews, 48, 1281, special issue dedicated to "Science with the Square Kilometre Array", ed. C. Carilli & S. Rawlings

Wise, J. H., & Cen, R. 2009, The Astrophysical Journal, 693, 984

Wise, J. H., Demchenko, V. G., Halicek, M. T., et al. 2014, Monthly Notices of the Royal Astronomical Society, 442, 2560

Xu, H., O'Shea, B. W., Collins, D. C., et al. 2008, The Astrophysical Journal, 688, L57

Zackrisson, E., Rydberg, C.-E., Schaerer, D., Östlin, G., & Tuli, M. 2011, The Astrophysical Journal, 740, 13

Zeeman, P. 1897, Philosophical Magazine Series 5, 43, 226

Zeldovich, Y. B. 1970, Astronomy and Astrophysics, 5, 84

# Appendix

# Résumé en français

Lors de ma thèse, je me suis intéressé à deux questions importantes de la cosmologie : l'origine des champs magnétiques cosmologiques et la stabilité des structures baryoniques diffuses dans la toile cosmique. Mon manuscrit est donc naturellement organisé de la façon suivante. Les deux premiers chapitres introduisent respectivement le contexte général et les équations de base utilisées par la suite. Il est donc recommandé de les parcourir quelque soit l'objectif de la lecture. Puis le manuscrit est décomposé en deux grandes parties, chacune des deux problématiques étant abordées l'une après l'autre. Elles peuvent être lues de façon *indépendante*, bien qu'elles soient en soi fortement reliées, car il s'agit de comprendre comment la matière se structure dans l'univers aux grandes échelles. Je détaille ci-dessous le contenu de ces deux parties.

Ces travaux théoriques sont grandement motivés par la perspective des observations actuelles et futures : Les instruments JWST (James Webb Space Telescope), LOFAR (LOw Frequency ARray) et SKA (Square Kilometre Array) pour sonder les Ages Sombres et l'Epoque de la Reionisation, LOFAR et SKA pour le magnétisme cosmique, et Athena et SKA pour la distribution des baryons tièdes dans la toile cosmique. Aussi, comprendre la formation des grandes structures cosmologiques et la formation des galaxies est l'un des grands défis de la cosmologie moderne, dont la principale difficulté est qu'elle nécessite une compréhension de très nombreux phénomènes, interdépendants, fortement non linéaires, et couplant des échelles extrêmement différentes (spatiales et temporelles). Cela rend les études numériques très difficiles, et les cosmologistes numériciens sont obligés d'utiliser des prescriptions pour modéliser simplement, mais sans fondements théoriques précis, la physique opérant aux échelles astrophysiques. La quasi totalité des travaux de ce manuscrit sont analytiques, ce

qui très important pour comprendre pleinement la physique des phénomènes inaccessibles numériquement.

## Partie I : 0rigine des champs magnétiques cosmologiques.

L'Univers semble magnétisé à toutes ses échelles, spatiales et temporelles, y compris les plus grandes. En effet, en complément des observations classiques, depuis quelques années, des observations issues de l'astrophysique des hautes énergies suggèrent qu'une fraction importante du milieu intergalactique est magnétisée. Toutefois, l'origine de ces champs est encore inconnue à l'heure actuelle, malgré les nombreux efforts pour essayer de répondre à cette question. On pense qu'ils ont d'abord été générés avec de très faibles amplitudes, puis qu'ils ont été amplifiés au cours de la formation des structures. Cependant, la turbulence dans les galaxies et les amas de galaxies modifie totalement l'organisation initiale et les propriétés initiales de ces champs, ce qui fait que les champs observés actuellement dans les structures ne nous renseignent pas sur leur(s) origine(s). Il convient donc de s'intéresser aux champs intergalactiques, car eux ont a priori peu évolué et pourraient fournir de précieuses informations sur leur génération.

Dans le chapitre 3, je présente brièvement l'état de l'art des observations actuelles des champs magnétiques dans l'Univers (des échelles astrophysiques aux échelles cosmologiques), puis les différents mécanismes de génération de champs magnétiques cosmologiques proposés dans la littérature actuellement. Il est courant de les classer selon deux catégories, selon la période à laquelle ils opèrent : Les mécanismes opérant (i) dans l'Univers primordial (inflation, transitions de phases électrofaible et quark-hadron, ou au cours de la Recombinaison même) et (ii) après la Recombinaison cosmologique, au cours de la formation des structures (batterie de Biermann lors des chocs ou de la propagation des fronts d'ionisation, instabilités plasma, séparations de charges dues à différentes radiations).

Puis je présente mes travaux sur un modèle particulier de magnétogénèse : Il

est basé sur la photoionisation du milieu intergalactique par les premières étoiles et les premières galaxies apparues dans l'Univers. L'idée de ce modèle avait été proposée en premier par Langer et al. (2005) et ma contribution a consisté à en détailler les calculs en partant de principes fondamentaux (théorie cinétique) et d'ainsi obtenir une expression précise du champs magnétique généré autour d'une source donnée. J'ai aussi étudié les valeurs possibles de ces champs dans divers configurations pertinentes dans le contexte cosmologique.

Les travaux précédents concernent les champs générés autour de sources isolées. Or la Réionisation de l'Univers est un processus global. En collaboration[4] avec Hiroyuki Tashiro et Naoshi Sugiyama (Nagoya, Japon), j'ai alors calculé, de façon analytique également, la densité d'énergie moyenne injectée par ce processus dans le milieu intergalactique au cours de l'Epoque de la Réionisation (chapitre 4). Pour cela, nous avons estimé la répartition statistique des sources (i.e. baryons effondrés) à partir de la répartition de matière noire sous jacente, à l'aide du formalisme de Press-Schechter.

En parallèle, avec Dominique Aubert (Strasbourg, France), j'ai étudié les propriétés du champs généré à travers des simulations numériques (chapitre 5). En effet, les travaux précédents présentent l'avantage d'être des modèles analytiques, permettant de voir explicitement le rôle joué par chaque paramètre, mais avec le désavantage d'être nécessairement simplistes sur certains aspects. L'approche complémentaire numérique nous permet alors d'affiner nos estimations des champs générés, en particulier en considérant des répartitions de matière plus réalistes que dans les modèles précédents.

En somme, nos prédictions sont compatibles avec les observations actuelles, et ce mécanisme a donc dû participer à la magnétisation de l'Univers à ses plus grandes échelles durant le premier milliard d'années de son histoire.

[4]Remarque : j'ai effectué l'ensemble des travaux de ce manuscrit en collaboration avec Mathieu Langer, mon directeur de thèse, également.

# Partie II : Fragmentation gravitationnelle de la toile cosmique.

En combinant arguments théoriques, simulations numériques et observations, les cosmologistes pensent aujourd'hui que la matière noire et la matière baryonique dans l'Univers sont distribuées selon une « toile cosmique », c'est-à-dire un ensemble de nappes (structures bidimensionnelles), dont l'intersection forme des filaments (structures cylindriques), aux croisements desquels se forment des noeuds correspondant aux amas de galaxies. Les baryons s'écoulent le long de ce réseau vers les noeuds. L'accrétion dans les noeuds est donc anisotrope, et il s'avère qu'elle est aussi en partie intermittente. Cela suggère que la matière ne se structure pas uniquement dans les amas, mais aussi dans les filaments, les nappes ou les vides cosmiques. Comprendre précisément à quels endroits et à quelles époques les baryons se fragmentent dans la toile cosmique est crucial car cela a un fort impact sur l'évolution de l'Univers. Par exemple, la façon dont les premières galaxies ont été alimentées en gaz (alimentation intermittente ou non, taux d'accrétion, température, densité, métallicité, etc.) a dû jouer un rôle majeur dans leur évolution ultérieure et donc dans les mécanismes de rétroactions, qui impactent l'évolution de la matière aux plus grandes échelles. Aussi, des galaxies se formant dans un vide, une nappe, un filament ou un amas n'ont pas les mêmes propriétés, et il est donc important de comprendre où et comment elles se forment en prenant en compte l'environnement cosmologique global.

Par ailleurs, dans le contexte cosmologique, la principale instabilité qui structure la matière aux grandes échelles est l'instabilité gravitationnelle. Dans le modèle standard de la Cosmologie, la matière est répartie initialement de façon quasi homogène, et le critère d'instabilité pertinent est le fameux « critère de Jeans ». Seulement, une fois la toile cosmique formée, la matière continue de se structurer mais dans des milieux *stratifiés* (chapitre 6). Dans ce cas, contrairement à ce qui est généralement présupposé, le critère de Jeans n'est plus forcément valide. En fait, il n'y a à l'heure actuelle pas d'étude complète et rigoureuse de l'instabilité gravitationnelle dans les milieux stratifiés, car le problème devient alors extrêmement complexe.

Afin d'essayer de pallier ce problème, durant ma thèse j'ai exploré et adapté la littérature plasma, et en particulier la façon dont les plasmiciens analysent la stabilité des tokamaks, car ce sont aussi des structures cylindriques stratifiées. En m'inspirant des études très complètes et rigoureuses de Goedbloed & Poedts (2004), Goedbloed et al. (2010) et d'articles associés, j'ai alors proposé une nouvelle approche pour étudier l'instabilité de type Jeans, dans le cadre de la théorie spectrale (chapitre 7), afin de comprendre pleinement la façon dont les structures stratifiées de la toile cosmique (nappes et filaments) se fragmentent gravitationnellement (chapitres 8 et 9).

Au cours de mon activité sur ce deuxième sujet, j'ai travaillé dans le contexte cosmologique, mais ces recherches sont également essentielles pour le contexte astrophysique. Dans ce dernier, il faudra toutefois considérer l'influence d'un champ magnétique, et mon approche est idéale pour cela puisqu'elle est directement inspirée de la physique des plasmas. Il sera donc naturel d'ajouter cet élément si important, pour des recherches futures (chapitre 10).

université PARIS-SACLAY | ÉCOLE DOCTORALE PHENIICS

**Title:** Baryonic processes in the large scale structuring of the Universe

**Keywords:** Cosmology, Astrophysics, Cosmic Web, Magnetic Fields

**Abstract:** During my PhD, I have been focusing on two important topics of Cosmology:
(i) Origin of cosmological magnetic fields: Magnetic fields seem ubiquitous in the Universe, present at all scales and all times, probably even in the entire intergalactic medium. Their origin is still unclear, especially on the largest scales. The current paradigm is that they were first generated with extremely weak strengths, and later amplified during structure formation. Because of turbulence, the fields we observe in galaxies and galaxy clusters lost their initial characteristics. However, in less dense regions such as cosmological filaments, sheets or voids, magnetic fields have evolved more mildly. Therefore, intergalactic magnetic fields may still possess a memory of the processes that generated them and hold the key to their origin. I developed analytically a detailed physical model of a natural astrophysical mechanism that generates intergalactic magnetic fields during the first billion year, namely at the time when first stars and galaxies were born. Then, in collaboration with H. Tashiro and N. Sugiyama (Japan), I computed analytically the mean energy density injected in the entire Universe through this mechanism. Independently, in collaboration with D. Aubert (France), I derived the topological and statistical properties of the magnetic field thus generated, using cosmological numerical simulations. This way I demonstrated that this simple, natural photoionization-based magnetogenesis must have created magnetic seed fields with properties a priori perfectly compatible with present day observations.
(ii) Gravitational fragmentation of the cosmic web: Cosmological numerical simulations suggest that the Universe has a web-like structure, the nodes of which are galaxy clusters. These nodes are supplied with matter flowing along the filaments interconnecting them. Part of this accretion occurs intermittently, which indicates that clumps of matter form not only inside clusters themselves, but also either in cosmic voids, walls and/or filaments. I studied gravitational instability in stratified media in the frame of spectral theory, in planar and cylindrical geometries, relevant for cosmic walls and filaments, for isothermal, polytropic, and with and without an external gravitational background (e.g. Dark Matter). I have recasted the problem as an eigenvalue problem in the force operator formalism, and derived the wave equation governing the growth of perturbations. I also studied it in matrix form, which gives complementary information.

**Titre :** Processus baryoniques de la structuration de l'univers à grande échelle

**Mots-clés:** Cosmologie, Astrophysique, Toile Cosmique, Champs magnétiques

**Résumé :** Lors de ma thèse, je me suis intéressé à deux questions importantes de la Cosmologie:
(i) L'origine des champs magnétiques cosmologiques: L'Univers semble magnétisé à absolument toutes ses échelles (spatiales et temporelles), y compris le milieu intergalactique. Mais leur origine est encore inconnue à l'heure actuelle, malgré les nombreux efforts pour essayer de répondre à cette question. On pense qu'ils ont d'abord été générés avec de très faibles amplitudes, puis qu'ils ont été amplifiés au cours de la formation des structures. La turbulence dans les galaxies et les amas de galaxies modifie totalement l'organisation initiale de ces champs, ce qui fait que les champs observés actuellement dans les structures ne nous renseignent pas sur leur origine. Il convient donc de s'intéresser aux champs intergalactiques. J'ai développé analytiquement un modèle de magnétogénèse basé sur la photoionisation du milieu intergalactique par les premières étoiles et les premières galaxies apparues dans l'Univers, il y a environ 13 milliards d'années. Puis, en collaboration avec H. Tashiro et N. Sugiyama (Japon), j'ai calculé de façon analytique la densité d'énergie moyenne injectée par ce processus dans le contexte cosmologique, et en parallèle, en collaboration avec D.Aubert (France), j'ai étudié les propriétés statistiques du champ généré à travers des simulations numériques. Nos prédictions sont compatibles avec les observations actuelles. Ce mécanisme a donc dû participer à la magnétisation de l'Univers à ses plus grandes échelles.
(ii) Fragmentation gravitationnelle de la toile cosmique: Les simulations numériques suggèrent que la matière dans l'Univers est répartie de façon filamentaire, les noeuds de ce réseau étant les amas de galaxies. La matière s'écoule le long de ces filaments. L'accrétion dans les noeuds est donc anisotrope, et il s'avère qu'elle est aussi en partie intermittente. Cela indique que la matière ne se structure pas uniquement dans les amas, mais aussi dans les filaments, voire les nappes ou les vides cosmiques. Je me suis donc intéressé à l'instabilité gravitationnelle dans les milieux stratifiés, par une nouvelle approche, dans le cadre de la théorie spectrale, en m'inspirant de la littérature plasma.